Scale formation and adhesion to mild steels during reheating for hot working.

SERGEANT, D. R.

SCALE FORMATION AND ADHESION TO MILD STEELS DURING REHEATING FOR HOT WORKING

by D.R. SERGEANT, A.C.T. (Sheff)

Thesis submitted to the Council for National Academic Awards for the Degree of Doctor of Philosophy

PREFACE

The work described in this document is submitted for the Degree of Doctor of Philosophy to the Council for National Academic Awards. It was carried out at Swinden Laboratories (The Divisional Research & Development Department of the Special Steels Division of the British Steel Corporation) in the period 1965-1972, during which time a proportion of the working week was devoted exclusively to this project.

During this period the author has attended post graduate lecture courses held at Sheffield Polytechnic on

(1) The mathematics of diffusion

(2) Statistics and the design of experiments.

In addition the author has attended conferences on the oxidation of metals including:

(1) "Reheating for Hot Working" held by the I.S.I. in London in December 1967.

(2) "High Temperature Oxidation of Iron & Steel" held by the I.S.I. and B.I.S.R.A. in London in May 1968.

(3) "The Adhesion and Mechanical Properties of Oxides" held by the C.E.G.B. in Leatherhead in February 1968.

(4) "The Mechanical Properties and Adherence of Scale Layers" held by the European Federation of Corrosion in Düsseldorf in December 1970.

Selected results of this work were presented at some of these.

The author would like to express his appreciation to Dr. K.J. Irvine for permission to submit this thesis and to Dr.'s A. Nicholson and G. Briggs forguidance, interest and helpful discussions during their supervision of the work. Thanks are also gratefully expressed to my colleagues and friends at Swinden Laboratories for the specialist assistance given.

Words can not express my appreciation for the encouragement and the incredible patience which my wife has shown during this time.

The work described herein is to the best of my knowledge original, except where reference is made to others, and no part of it has been submitted for an award at any other college or university.

Project Metallurgist
Bar & Wire
Rotherham Works
B.S.C.

D.R. Sergeant

June 1974

CONTENTS PAGE

1. SYNOPSIS

The literature relating to scale formation and adhesion has been reviewed, with particular reference to the factors which have been found to influence the adherence of scales formed on mild steels during reheating. The methods used to assess scale adhesion and the current thoughts on the mechanism of adherence are also outlined. In addition the practical importance of scale pitting problems and current methods of scale removal are considered.

Laboratory oxidation and scale adhesion tests have been carried out on silicon killed, rimming, semi-killed and a silicon-killed aluminium treated steel under simulated reheating conditions. Temperatures in the range 950°C-1350°C were studied for times of up to three hours in atmospheres simulating the products of combustion of uncleaned coke-oven gas burnt to give 6% free oxygen in the furnace atmosphere.

The oxidation behaviour was studied by metallographic examination of the scale and scale/metal interface and by thermogravimetric techniques.

The amount of oxidation was found to increase rapidly with temperature and only approximately parabolically with time. Deviations from classic oxidation theory are discussed with reference to the structure and composition of the scale and metal/scale interface. Although the amount of oxidation was similar for each steel studied, marked differences were found

in the characteristics of the metal and scale in the metal/scale interface region. In particular the depth of metal/scale entanglement, which increased with temperature and time, varied considerably with steel composition.

Methods of predicting the amount of oxidation and the characteristics of the metal/scale interface region are outlined and shown to give reasonable correlation with practical results.

The effect of reheating times of 1 to 2 hours and temperatures in the range 1050 to 1200°C on scale adhesion have been examined using modifications to a basic apparatus for studying scale adhesion. It has been shown that fracture occurs at the scale/metal interface and consequently the method can be used to study the factors affecting scale adhesion, as distinct from scale cohesion.

The scale adhesion on the aluminium treated steel gave no clear trend with temperature or time, probably because of the precipitation of an aluminium rich phase at the scale metal interface which promoted lack of adhesion. Similar results were obtained with the silicon-killed steel at temperatures below 1150°C, again probably because of the presence of silicon rich phases at the scale metal interface. A decrease in adhesion was found on the rimming steel specimens with increasing temperature in the range 1050 to 1100°C probably because of a planar metal/scale interface and the presence of low melting point sulphur rich liquid phases at the metal surface. In general the scale adhesion was found to increase

with time and temperature above 1100°C because of an increase in the depth of metal/scale entanglement with these factors. The greatest adhesion was found on the silicon-killed steel at the highest temperature studied.

A theory has been proposed based on the observations made and on the results of experiments designed to investigate the mechanism of scale/metal entanglement and whereas nickel enrichment is necessary to form a stable irregular metal/scale interface, the presence of liquid phase markedly influences the growth of the metal/scale entanglement.

2. INTRODUCTION

In most cases the processing of steel involves reheating at some stage for hot working. The oxidation of the steel during the reheating operation can lead to a variety of problems. Not least of these is that resulting from adherent scale being forced into the surface of the product during subsequent hot working and giving rise to surface defects which may either require a costly surface conditioning operation or lead to scrapping of the material.

This work was undertaken to obtain a better understanding of the factors which affect scale adhesion and therefore indicate methods of reducing the 'scale pitting' defect. As part of the programme it was intended to improve a basic technique developed at Swinden Laboratories and to assess its suitability for the study of scale adhesion as distinct from scale cohesion. If this was successful then the method was to be used to

investigate the factors affecting scale adhesion. Concurrently a separate study was to be carried out to investigate the oxidation characteristics of the steels using metallographic and thermogravimetric techniques in order that the results of the scale adhesion exercise could be interpreted. At the time of initiation of this study considerable interest was being shown by a particular works within the company and the materials and variables selected for examination were based on this plant in order that the results should have a specific application.

The variables selected for study were:

(1) Steel composition (as influenced by the method of ingot production used).

(2) Reheating time.

(3) Reheating temperature.

Works experience has indicated that the method of ingot production has an effect on the oxidation/scale adhesion characteristics of mild steels. The materials selected for study include the major methods of conventional ingot production i.e. silicon-killed, balanced (or semi-killed) and rimming. The effect of aluminium (an alternative steel de-oxidising addition) was studied using a silicon-killed steel to which aluminium was added as a grain refining agent. In order to separate the variables of reheating temperature and time isothermal tests were carried out at temperatures in the range 950-1350°C for times of up to 3 hours. These parameters were selected to cover the range of practice used for the reheating of stock from small billets to large slabs. The atmosphere selected was based on the combustion of uncleaned coke oven

gas burnt with approximately 40% excess air.

In the experimental section it is proposed to consider the work carried out under three separate headings, namely,

(a) the oxidation characteristics

(b) the scale adhesion characteristics

(c) Additional work generated by the results of (a) and (b).

3. REVIEW OF PREVIOUS WORK

Increasing effort is being devoted to the influence of scale adhesion on surface defects produced during hot working and recent works have contributed much to the understanding of the mechanisms and the variables which influence scale adhesion.

In this section the available information relating to the formation and adhesion of scale to steel and the current experimental techniques are outlined.

Mild steel may be regarded as an impure iron and it is useful to review the main features of the oxidation of iron as a basis for the work on steel. The oxidation of iron and steel has been the subject of many investigations, and there is a large amount of literature available on this subject, however, what appears to be the most relevant information is summarised below.

3.1 The Oxidation of Iron

Above 570°C three stable oxides form on iron, consisting of an inner layer of wüstite (FeO), an intermediate layer of magnetite (Fe_3O_4), and an outer layer of haematite (Fe_2O_3)[1,2].

At 700°C these phases are in the proportions 95% FeO, 4% Fe_3O_4, 1% Fe_2O_3 and these proportions are essentially independent of time and increasing temperature. The iron-oxygen equilibrium phase diagram (Fig.1) shows the stability ranges of the oxides and it is interesting to note that the stability range of FeO does not include the stoichiometric composition. The oxide is iron-deficient and the defects in the lattice consist of vacant cation sites. Diffusion is thus cationic (Fe^{3+}) via vacant cationic sites although above 850°C diffusion of oxygen through the wüstite also appears to take place[3,4]. However, the observations of Engel and Wever[4] were based on the movement of markers in the FeO layer, and more recent work[5] has shown that the results of marker movement can also be explained in terms of inward creep of the scale layer and a decreasing rate of diffusion of vacancies. In addition Mrowec[6] has shown that the movement of markers in the scale can be explained by a 'dissociative mechanism'[7]. When loss of adhesion occurs at the metal/scale interface, dissociation of the scale is assumed to occur leading to the formation of free oxygen which reacts with the metal surface to form new oxide. In this way, the apparent inward diffusion of the anion in scales having a cation defective lattice can be explained. The dissociation takes place preferentially at grain boundaries in the scale forming micro-cracks and porosity which progresses into the compact layer. When the compact scale layer is entirely consumed the oxidation can take place by inward migration of oxygen and outward diffusion of iron. Both cations and anions diffuse in magnetite but anions (O^{--}) only diffuse[8] through haematite. A model of the oxidation of iron has been put

forward by Hauffe[9] based on the Wagner oxidation theory[10], which explains the formation of the three-layer oxide on iron in terms of the cationic and anionic diffusion and the interactions to produce each layer are shown schematically in Fig.2. After the initial adsorption of oxygen on the iron surface and reaction to produce wüstite studied by Gulbransen[11] the growth of the oxide layers are governed by the diffusion of iron and oxygen and are therefore parabolic[2,3,5,8,12] with time. This can be represented by $w^2 = kt$

where:

w = weight gain/unit area (g/cm^2)

t = time (secs)

k = oxidation rate constant for temperature studied ($g^2cm^{-4}\ sec^{-1}$)

The rate constant k is inversely proportional to the temperature[6] with slight irregularities reported at 620°C, above which the rate controlling step is the diffusion of iron through the wüstite. The activation energy for this reaction has been determined metallographically at 40 500 cal/mole[2] for air oxidation and more recently[12] thermogravimetrically at 46 800 cal/mole for both oxygen and air oxidation. Confirmation of the validity of the Wagner theory to the oxidation of steel has been shown[13] by comparison of calculated and experimentally determined oxidation rate constants.

The diffusion of iron from the metal into the scale results in the formation of vacancies in the metal at the metal/oxide interface. The vacancies may be removed by inward creep of the wüstite[4,14] or maydiffuse into the metal resulting in internal cavitation which can have a marked influence on creep

ductility[15]. With thin specimens vacancies have been found to diffuse through the metal to the opposite surface with the formation of an adherent scale on one surface and a non-adherent scale on the other[16,5]. Adherence can also be maintained by the presence of holes in the metal[17], or by the presence of internal oxides[18] which act as sinks for the vacancies produced by the oxidation reaction.

The presence of stresses in the growing oxide layer has been demonstrated[19] by vapour depositing iron and other metals onto mica strips and subjecting the composite formed to an oxidising environment. Bending of the strips on oxidation was assumed to indicate stresses generated by the oxidation process. The vapour deposit was most probably porous however and the stresses may have been generated in this case by oxidation within pores in the metal. Engel and Wever[4] have confirmed the presence of growth stresses as the oxidation of an iron strip in the form of a helix caused a reduction in the helix diameter. In addition, Maldy[20] has shown the presence of small grains in the metal and oxide at the metal/scale interface of oxidised specimens indicating that the stresses induced at the interface were sufficient to generate dislocation movement and sub-grain formation. Stress at the metal/scale interface may affect the adhesion of the scale and this is important especially during the cooling of small specimens.

The cooling of oxides on iron have been extensively studied[3,21,22], and the precipitation of magnetite in the outer region of wüstite has been observed. On cooling from

temperatures in excess of 570°C pro-eutectoid magnetite is precipitated in the outer, oxygen-rich layer of wüstite (see Fig.1) and below 570°C wüstite becomes unstable and decomposes into magnetite and iron. The reaction is relatively slow and isothermal transformation diagrams have been obtained for FeO[3,21] (see Fig.3), which indicate that the maximum rate of transformation occurs at 480°C and decomposition takes place more readily with increased oxygen contents. The mechanism of transformation below 570°C has been extensively studied[22] by both cooling and reheating wüstite followed by isothermal treatments in each case. Iron is precipitated first in the temperature range 570°C-480°C with an increase in the oxygen content of the surrounding wüstite which eventually decomposes into magnetite and more iron. Below 480°C magnetite is precipitated first with iron enrichment of the wüstite until decomposition is complete with the formation of iron and more magnetite.

During cooling, stresses are set up at the metal/scale interface because of the differential coefficient of expansion of austenite, ferrite and wüstite. On cooling to the temperature of the austenite to ferrite transformation temperature compressive stresses are set up in the wüstite. However, when the underlying metal transforms to ferrite an increase in volume of the metal results (approximately 1%) which may be sufficient to cancel the compressive stresses and leave the wüstite in tension. Further cooling to room temperature results in compressive stresses again being set up in the FeO at the interface. During slow cooling, stresses may also be generated by the precipitation of Fe_3O_4 within the FeO layer.

The scale on pure iron is generally compact and adherent[1,2] with smooth metal/scale interfaces. Non-adherent scales can be produced, depending on the geometry of the specimen used, for example with iron wire heated in air[4] and in such cases an inter-relationship between the adherence and scale formation is also observed. When a gap is formed at the interface during the heating period, and not on cooling because of differential contraction considerations, diffusion of iron ions into the scale from the metal is not possible and the non-adherent wüstite is oxidised to magnetite with a corresponding fall in the oxidation rate. A fissure or crack in this layer allows oxygen access to the metal surface and the reaction to produce FeO is again possible, this is accompanied by an increase in the oxidation rate. In this case, the scale structure depends on the adherence, in other cases the scale structure can influence adhesion, for example Peters and Engel[23] found that alloy elements concentrated in the scale near the scale metal interface have an effect. The interdependence of scale adhesion and scale formation on iron has also been reported by other workers and it is proposed to review the factors which affect scale formation and adhesion concurrently below.

3.2 Factors Affecting Scale Formation and Adhesion to Steel

A large proportion of the work described below is based on metallographic observations on samples cooled to room temperature. These can only differentiate between adherent and non-adherent scales according to the presence of gaps at the interface and some interpretation is necessary to differentiate

between gaps formed at reheating temperatures and those formed on cooling. The main results of some physical methods of assessing the degree of scale adherence are referred to briefly in this section but will be dealt with more fully later.

3.2.1 Steel Composition

Small amounts of impurity elements can affect the scale characteristics quite markedly, Armco iron, which has a low level of impurities has been shown to have a less adherent scale than pure iron for example[1]. A convenient method of classifying the impurity elements[23] is by regard to the free energies of formation of their oxide with that of iron.

3.2.1.1 Alloy Elements Less Noble than Iron

Silicon

The presence of silicon leads to the formation of particles of oxide below the metal surface[24] a phenomenon known as internal oxidation. The particles are rich in SiO_2 and decrease in size with distance from the metal surface. The depth to which they penetrate has been shown to bear a parabolic relationship with time[25]. As the scale-metal interface moves inwards the particles of silica are in effect transported to a zone of higher oxygen potential and combination with wüstite takes place[24,26] to form fayalite (Fe_2SiO_4) particles which remain at the interface at low temperatures. A schematic representation of this process can be seen in Fig.4. If the silicon content is high enough, fayalite can be present as a continuous protective layer at the metal/scale interface with a reduction in the scaling rate. An addition of 1% Si

to iron has been observed to result in a reduction in scaling of 80%[3]. Fayalite forms a eutectic with wüstite which melts at 1177°C[27] and above this temperature the molten eutectic wets the grain boundaries of the wüstite, penetrating in some cases to the scale surface and resulting in an increase in the scaling rate probably because of high oxygen solubility and diffusion rate in the liquid phase.

Silicon has been reported to cause high scale adhesion when measured at high temperatures by Ghosh and Rolls[28] using an impact test, because of the liquid phase cushioning the blow. With room temperature tests however[23], the adherence of the scales on pure iron was markedly reduced with additions of silicon (Fig.5). This was explained by the presence of solidified fayalite/wüstite eutectic at the metal/scale interface.

Chromium

Iron alloys containing chromium also exhibit internal oxides when subjected to reheating under oxidising conditions. The internal oxide particles in this case consist of Cr_2O_3 which appear to obey similar rules as those produced by silicon, at least for small additions of chromium[25,26]. Depletion of chromium in the alloy has also been observed owing to preferential oxidation of the chromium into the scale[29]. Chromium concentrates in the scale in a similar manner to silicon[26,30] and islands of $FeCr_2O_4$ have been observed in the inner wüstite layer. A spinel of iron and chromium oxides can be formed in the magnetite layer. With small additions of chromium to pure iron the oxidation rate increases initially but the amount of oxidation, compared to pure iron, is less for longer periods of oxidation[31]. Increasing chromium content of the material

results in a decreasing oxidation rate[31,32].

Aluminium

For small alloy additions, aluminium has a similar effect on the oxidation characteristics as the above elements[26,30,33]. At a reheating temperature of 850°C in an oxidising atmosphere for example, iron containing 0.017% Al contained traces of an $FeO-Al_2O_3$ spinel at the alloy/oxide interface, whereas an alloy containing 0.1% Al gave a well established interfacial layer of spinel[4]. Aluminium has been reported to decrease the adherence of scales[23] assessed using a cold detachment test (Fig.5). This effect of aluminium has been confirmed recently with a hot bend test by Bateman and Rolls[33] at 950-1050°C for Fe-Al alloys containing 0.1-0.2 Wt% (Table I).

Phosphorus

The presence of 0.05% P in iron has been shown[23] to result in the presence of a dark phase at the metal surface which was assumed to be iron-phosphate and reduced cold scale detachment stress was noted on this alloy when compared with pure iron (Fig.5). Other workers have reported that phosphorus decreases the oxidation rate of iron slightly[32].

Manganese

This element behaves differently to the above elements as manganese oxide forms a solid solution with wüstite[34], hence no concentration occurs and it can also substitute for iron in the magnetite and haematite scale layers[32, 35]. Internal oxidation occurs in iron-manganese alloys, which because of the mutual solubility of iron-manganese oxides has been reported to consist of FeO-MnO particles which also obey a parabolic depth law[36]. During the oxidation of steel, internal

oxidation has been observed to consist of $(Fe/Mn)_2SiO_2$[24] and hence the presence of manganese in fayalite/wüstite eutectics is to be expected, but little effect of manganese on the oxidation rate of an Fe-4% Si alloy[32] or a 13% Mn steel[37] has been found. Manganese (0.15 and 0.62%) has been reported to have little effect on the cold scale adherence of pure iron[23]. (Fig.6).

Carbon

Carbon oxidises preferentially to iron to form gaseous carbon monoxide and this results in a denudation of the underlaying metal in carbon[38]. Thus decarburisation can take place to a considerable depth and has a detrimental effect on the metallurgical properties of the denuded layer. Consequently the subject of decarburisation has received much attention, the greater part of which is not covered by the terms of this review. It is relevant however, that the gaseous evolution of CO is thought to lead to discontinuities (i.e. cracks and blisters) in the scale layer and at the metal surface[39]. The onset of fracture of the scale depends upon the gas pressures developed and the adhesive and cohesive strengths of the scale, and some assessments of this relationship have been attempted [38,40,41].

The gaseous evolution of CO has been put forward to explain the decrease in scale adhesion measured by a hot impact test observed with thick porous scales[28] formed on steel after reheating at high temperatures. (Table 2). Carbon additions to pure iron have been found to decrease the cold scale adherence [23] (Fig.6).

3.2.1.2 Alloy Elements More Noble than Iron

Nickel

Nickel concentrates in the metal at the metal/scale interface owing to selective oxidation of iron. The magnitude of this concentration or enrichment effect is demonstrated by the results of Melford and Duncumb[42], who found areas of metal containing up to 33% nickel in the oxide/metal interface region of a 0.14% Ni steel. Pure iron-nickel alloys containing less than 2% Ni oxidised in dry oxygen at 1000°C produced similar scales as did pure iron[43] and the enrichment in the surface metal was found to be up to 80% Ni. Alloys containing more than 2% Ni exhibited 80-90% nickel enrichment and wüstite was replaced by an iron-nickel oxide spinel as the stable phase in contact with the metal. Marked grain boundary and internal oxidation occurred and void formation was observed behind the large internal oxide particles. This effect of increased internal oxidation beneath an enriched nickel layer has also been observed by other workers[44, 45]. Non-adherent scales have been produced on an Fe-1% Ni alloy oxidised at 800°C under similar conditions[46], at 800°C after cooling to room temperature the oxide layers consisted predominantly of the higher oxides of iron. At 1000°C, adherent scales were produced similar to those on pure iron, but contained a lower proportion of wustite. Inner zones of mixed metal and oxide have frequently been reported in the scale.

Metal particles have been observed in the scales formed on nickel bearing steels in early work by Stead[47] and Pfeil[48] which were shown to be rich in nickel. The particles were found to be present in a zone corresponding to the original

specimen dimensions. It was postulated that the existence of nickel rich particles in the inner oxide layer was explained by the fact that nickel oxide is unstable in iron oxide containing more than 72% iron. Sachs[49] found that depending on the partial pressure of oxygen in the furnace atmosphere and the nickel content of the steel the metal in the oxide may form either a filigree pattern or exist as discreet particles when observed on a transverse metallographic section. In further work[50] he showed that the nickel content of these particles increased with the distance of the metal from the advancing oxide surface. Sachs[50] postulated that the metal particles appeared in the scale by two mechanisms, the preferential oxidation of iron and entrappment of metal in the scale by grain boundary penetration and internal oxidation mechanisms, also the transient solution of nickel in iron oxide could occur, followed by precipitation on suitable metal nuclei. This second feature was considered necessary to explain the growth in size of the metal particles with increasing distance from the metal oxide interface. In later work Sachs[51] examined the mechanism of scale/metal entanglement on low alloy steels in more detail and postulated that the filaments were formed by a process of internal oxidation. As the internal oxides grew they were assumed to result in enrichment of the metal surrounding them, coalescence of these internal spheroids into rods was assumed to take place and when the advancing metal oxide interface approached the enriched filaments of metal they protruded into the scale layer.

Considerable plastic flow was required in the oxide to creep past the filaments and Sachs considered that the presence of a liquid phase in the inner scale layer would assist the flow of the scale. Preferential oxidation of the iron would continue in the filaments as they projected into the iron oxide and they would therefore become enriched in nickel and would shrink in size and would eventually break up into discreet particles further out in the scale layer. This work was concerned mainly with steels having up to 3% nickel but the formation of a metal/scale entangled layer called a contaminated zone was observed by Moreau and Cagnet[24] on mild steels containing residual nickel levels (approximately 0.2%). Nevertheless, nickel enrichments of up to 3% nickel were found in the metal in the oxide layer on the steels. Growth of metal/scale entanglement has also been found by Brown[52] in steels containing from 0.04% to 0.4% nickel at temperatures between 1100°C and 1300°C. At temperatures up to 900°C, however, enrichment of nickel occurred ahead of the advancing interface but no particles were found in the scale layer. Nickel enrichment occurred in the surface grain boundaries at low temperatures, an effect also observed by other workers[53]. It was observed that for oxidation in air the change in behaviour was associated in the change of the scale characteristics. At the lower temperatures the oxide was adherent and compact and the oxide did not contain any metal particles whereas at the higher temperatures a non-adherent scale was found which contained metal particles.

Further experiments[54] were carried out to assess the effects of oxidation under atmospheres of low oxygen partial pressure giving oxidation conditions similar to those found under blisters and non-adherent oxides to evaluate the factors affecting the change from one type of behaviour to the other. However, similar structures were found at 900°C as found in air and a non-adherent and porous scale was formed at 1100°C again similar to that in air. Oxidation in oxygen gave an irregular interface but with few metal particles in the scale at 1100°C and no explanation of this nor of the formation of the entangled zone in air and water vapour hydrogen mixtures and water vapour at 1100°C was advanced. In further work[55] the metal particles observed in the scale were shown by removal of successive layers of metal by polishing to consist of a metal filigree. The mechanism of formation was considered to be by oxide dissociation within pores in the inner scale layer coupled with internal oxidation of the underlying metal. The growth with time of the outer particles (on a transverse section) was explained by the inward creep of the scale and compaction and recrystallisation of the metallic filigree accompanied by oxide dissociation. The differences in behaviour found in the earlier experiments in different atmospheres was explained by considering that oxidising gases could penetrate the pores in the scale layer in atmospheres containing water vapour or CO_2 by redox type reactions as proposed by Rahmel[56].

Wagner[57] has predicted that in the presence of a noble e.g. nickel, and a less noble element, e.g. iron, a uniform scale layer and consequently a planar metal/scale interface

will be stable only if diffusion in the alloy is relatively rapid compared with diffusion in the oxide of the less noble metal.

Thus when the rate controlling step in the oxidation reaction is the diffusion of iron through the enriched layer and not the classical diffusion of iron through the scale, a planar oxide/metal interface will cease to be stable. The development of an irregular metal surface promotes the lateral diffusion of the enriching elements with respect to the direction of oxidation. Hence, with an enriched layer at the metal surface, oxidation can proceed at a faster rate with an irregular metal/scale surface than with planar interface conditions. In a mathematical treatment of this theory Wagner predicts that the length of the metal filaments increase with nickel content and the amount of oxidation, size and spacing of the filaments also increases with time and temperature. The effectiveness of nickel in promoting irregular metal surfaces in mild steel is demonstrated by the results of Brown and Mears[52,54] who found that with nickel contents of 0.04% irregular surfaces resulted and by Maldy[20] who showed that even with nickel contents of 0.02% irregular metal/scale interfaces could be produced.

Nickel has been reported to increase the hot adherence of scale on steel[58,59], and also is said to be a contributory factor in rolled-in scale defects[51]. Small additions of nickel have been shown to decrease the scaling rate compared to pure iron[43,46,52].

Copper

This element also concentrates at the metal surface[58,60,61] owing to preferential oxidation of iron and can lead to precipitation of copper-rich phases at the metal surface. The cold scale adherence on pure iron is decreased at scale formation temperaturesup to 850°C and increased above this temperature by additions of copper[23], (Fig.6). The enrichment of copper has been reported to decrease the oxidation rate of steel at 900°C[58] but above this temperature no effect was found. Liquid copper phases were found at high temperatures which lead to marked grain boundary penetration of copper and surface defects on subsequent hot rolling.

Sulphur

Pronounced sulphur enrichment has been found in the scale on an iron-sulphur alloy containing only 0.003% S[35] oxidised at 800°C. Some grain boundary penetration of sulphides also occurred. Early work[32] suggests that the sulphur exists at the interface as FeS formed by reaction of the MnS in the metal with FeO in the scale at the metal surface. No enrichment of sulphur was found in the scale in this case and it was suggested that volatile sulphur oxides formed and escaped through the scale layer. Sulphur particles have been ooserved in the scale[35,23] but it was not clear if these were formed by diffusion of sulphur or by faulty polishing techniques. Recent work on the oxidation of high sulphur iron-base material (0.099 S) in combusted town and natural gas atmospheres[28] resulted in the formation of wüstite-ferrous sulphide eutectic

at the interface. This phase had a low melting point and caused a marked increase in the scaling rate, and grain boundary penetration.

Increased scale porosity has been noted in high sulphur material which, it was suggested indicated that some of the sulphur may have been oxidised to gaseous sulphur oxides and thus escaped through the scale. This seems unlikely in view of the formation of sulphur phase in the scales by pick-up from the oxidising atmosphere as discussed below, although it should be possible if the dissociation pressure of the liquid phase formed were to exceed the sulphur partial pressure in the atmosphere. High hot scale adherence in this case[28] was thought to be due to a high degree of grain boundary penetration and liquid phases in the scale layer. Sulphur was found to decrease the cold scale adherence of pure iron with oxidation temperatures of 850°C and below, above this higher adhesion resulted[23] (Fig.6).

3.2.2 Oxidising Environment

3.2.2.1 Furnace Atmosphere Composition

According to the classical parabolic oxidation theory[9,10] the oxidation kinetics for compact adherent scales are governed by the diffusion of metal ions through the oxide. Consequently, the oxidation rate should be independent of the furnace atmosphere, providing that there is sufficient oxygen present for wüstite to be a stable phase in contact with iron. This has been confirmed[62] for pure iron at 700°C-950°C in oxygen and argon mixtures but with commercial steels the rate of oxidation depends to a large extent on the composition of the atmosphere[37].

The stoichiometric combustion of fuel oil or gaseous hydro-carbon fuels results in the formation of carbon dioxide, water vapour and nitrogen in the combustion products, if the fuel also contains sulphur, gaseous sulphur compounds will be present. The combustion of such fuels with less than the required amount of air for complete combustion results in the presence of some carbon monoxide, and if excess air is used free oxygen appears in the atmosphere. The atmosphere produced by burning fuel stoichiometrically is often referred to as 'neutral', that containing free oxygen is known as 'oxidising' and that containing free carbon monoxide is called 'reducing' although under commercial reheating conditions all are usually oxidising with respect to iron. The adhesion of scale on steels has been shown to increase slightly as the oxygen content of the furnace atmosphere is decreased in the absence of SO_2[28,33,63,64]. The presence of SO_2 in the atmosphere markedly increases the scale adhesion especially with low oxygen contents[63,64]. Steels heated in atmospheres formed by the combustion of fuel oil were more adherent than those heated in atmospheres produced by burning town's gas (low S) for example[64]. The presence of sulphurous gases in the atmosphere also influences the amount of oxidation obtained.

At 1150°C for example, in the absence of sulphur dioxide, Preece and Riley[37] found that the addition of free oxygen to a neutral atmosphere increased the scaling rate of steel, and the addition of 4% carbon monoxide to the same base atmosphere reduced the scaling rate by approximately 10%. With 0.2% sulphur dioxide in the neutral atmosphere however, the scaling rate increased and the addition of oxygen increased

the scaling rate to a maximum at 1% oxygen. Further additions inhibited the scaling influence of sulphur dioxide and above 5% oxygen the scaling rate was found to be independent of the presence of sulphur dioxide. More recent work by Rolls[65] indicates that sulphur pick-up in the scale increased as the reheating temperature is increased. This effect has also been demonstrated by Nicholson and Murray[58], who also showed that the sulphur content of the scale increased with decreasing oxygen and increasing SO_2 content of the furnace atmosphere. The amount of excess oxygen required to suppress the sulphur pick-up to a low level was also found to increase with temperature to over 8% at 1300°C. Sulphur pick-up in the scale was also noted with an atmosphere containing 4% oxygen and 0.1-0.15% S in the temperature range 1150-1250°C which it was suggested[65], was due to liquid phases in the scale which increased the likelihood of sulphur transport from the atmosphere. The mechanism of transport of sulphur through the oxide layers have recently been reviewed by Tuck[66] and although the exact mechanism is not known, the most likely is thought to be the ingress of gaseous mixtures containing sulphur through small pores or micro-cracks which are being continuously formed and healed.

Sulphur normally forms iron-sulphide in the scale at the metal surface and this forms a low melting point eutectic with wüstite. The presence of this low melting point phase, which is liquid at reheating temperatures, is thought to explain the enhanced scaling rate obtained above[37]. Combination of sulphur can also occur with the elements which concentrate in

the metal surface[67,68,69]. In the case of copper this can be beneficial to some extent and result in the formation of a high melting point sulphide, thus preventing the penetration of low melting point copper down the austenite grain boundaries. In the case of nickel, low melting point nickel sulphide is formed which forms complex eutectics in the scale and results in marked grain boundary penetration.

The presence of water vapour or carbon dioxide can have pronounced effects if non-adherent scales tend to be formed (the non-adherent nature may be due to specimen shape for example, and this will be discussed later). In such cases the introduction of these gases has been shown by Rahmel[56] to accelerate the oxidation of iron. The mechanism suggests that carbon dioxide or water vapour are transported into gaps in the scale where carbon monoxide - carbon dioxide or hydrogen-water vapour gas mixtures are formed, which transfer oxygen from the scale via the gas phase to the metal surface by means of an alternating oxidation and reduction action. Transport of the gases through the scales to the gaps is envisaged via microcracks and inter-connecting pores. In this way gaps formed at the metal surface may be healed and scale adherence maintained. (See Figs.7 and 8).

3.2.2.2. Atmosphere Flow Rate

In laboratory work it is important to be able to eliminate the atmosphere flow rate as a variable, as the rate of delivery of oxygen to the oxidising surface depends on flow rate as well as composition of the atmosphere. Early work[70] on mild steel oxidised in carbon dioxide, steam and air at

1260°C showed that the oxidation rate increased progressively with flow rate until a critical flow rate was reached beyond which the amount of oxidation was unaffected by rate of atmosphere flow. Flow rates of 0.025 m/sec for carbon dioxide and 0.076 m/sec air and 0.117 m/sec for steam were recorded at this critical level. More recent work on mild steel[71] scaled for upto 2 hours at 1100°C in a synthetic atmosphere containing water vapour, oxygen, carbon dioxide and nitrogen, placed this critical level at 1.52-3.05 m/sec. It was pointed out, however, that the concept of 'critical dwell time' (specimen length divided by gas velocity) was a better criteria to take as if too long a time were available for the gas to be in contact with the specimen, depletion of the oxidising constituents could occur. In addition comparison of data from experiments using different sized specimens is possible using this method although the effects of steel composition and furnace atmosphere must also be considered. For synthetic atmosphere simulating burnt town's gas critical dwell times of between 0.06 and 0.13 sec were determined which were approximately one-tenth of the critical speeds required for air or CO_2 or H_2O atmospheres. Further work[72] has shown that flow rate has no effect on the oxidation of mild steel in air at temperatures of 600°C, 800°C and 1000°C using a range of flow rates between 0.05-0.9 m/sec.

3.2.3 Physical Characteristics of Specimen

3.2.3.1 Initial Surface Condition

It has been shown[1] that the adherence of scale is increased if the metal surface is electropolished prior to

oxidation. This was explained by suggesting that the grains of abrasive present in the surface metal layers on mechanically abraded surfaces are removed by the electro-polishing. It was assumed that the grains of abrasive concentrated at the iron-oxide interface and led to an increase in adherence similar to the impurity elements discussed above. The decreased adherence found on abraded samples has been explained[5] by considering the surface oxide layers to be placed under stress by oxide filling cracks in the surface and this view has been supported by the fact that internal stresses have been shown[73] to be less marked in thin oxide layers on finely abraded material than on coarsely abraded. Other work however[2] has shown that sand blasted metal surfaces produced more adherent scales. In addition it was pointed out that textures can be present on as-rolled strip which affect its oxidation rate and presumably the adherence of its scale. In view of the rapid change in the topography as oxidation proceeds with the establishment of irregular metal/scale interfaces and liquid phases in the interface region, it is unlikely that the initial surface condition of the specimen will have a marked influence on the adhesion of scales formed under commercial reheating conditions.

3.2.3.2 Specimen Geometry

The scale on rectangular specimens has been shown to lose adherence at the corners due to restriction of lateral growth or the mutual support which the scale on each side affords for the other, thus restricting the inward flow

of the scale to follow the receding metal surface[1,2,4]. A reduction in the scaling rate thus occurs[4] because of a reduction in the outward flow of iron ions into the scale. For cylindrical specimens the inwards flow of oxide is again restricted and large gaps have been observed on specimens cooled to room temperature at the metal/scale interface. (Fig. 8a). This has been confirmed on small cylindrical specimens by Bruce and Hancock[74] using a vibrational technique; it was demonstrated that the scale formed in air was cracking continuously during growth, and it was pointed out that geometrical factors should be taken into account when assessing the kinetics of oxidation.

Early work[37] in furnace atmospheres containing nitrogen, water vapour, carbon dioxide and oxygen, found little influence of specimen dimensions on the scaling rate. Cylindrical specimens were used with length to diameter ratios of between 0.33 and 10. More recent work[56] has shown that for atmospheres containing water vapour or carbon monoxide, gaseous transport of oxygen across such gaps in the scale is possible as discussed earlier and hence it is doubtful whether the effect of specimen shape is as marked in furnace atmospheres containing water vapour and/or CO_2 (see Fig.8b).

It has been shown[75] that when studying oxidation kinetics it is important to consider the effect of the surface area to volume ratio, (so-called specific area) on the instability of the temperature of the process, as oxidation is an exothermic reaction. Marked temperature rise can be avoided

by the use of specimens of high volume to surface area in order that the temperature rise produced by the initial high rate of oxidation can be dissipated. In addition, the rapid reduction of the specimen dimensions due to oxidation at high temperatures must be taken into account when calculating the oxidation rate and the rate laws applying to oxidation. If this is neglected it can lead to erroneous conclusions about the kinetics of scale growth.

3.2.4 Summary

With conventional steelmaking techniques, elements less noble than iron are removed and such elements are found in commercial steels by design. For example, carbon for strength and manganese to reduce the harmful effects of sulphur. Manganese has been found to have relatively little effect on the scale characteristics but Si and Al which are added to steel to reduce the gaseous evolution of carbon monoxide during solidification (killed and semi-killed steels) have been shown to have pronounced effects. Both form internal oxides and concentrate in the scale at the metal/scale interface. Silicon has been found to increase and aluminium (in large amounts) to decrease hot scale adhesion. Elements more noble than iron are difficult to remove during steelmaking and if large amounts of scrap metal are used in the process elements such as copper and nickel build up in the steel and may reach high levels. Nickel is said to increase the hot scale adherence of steel, because of the irregular interface produced

by enrichment effects. Sulphur is usually maintained at a very low level in steel but high sulphur steels have been found to have liquid sulphur-rich phases in the scale and to exhibit high scale adherence. In general the sulphur content of steels is sufficiently low for this effect to be very small (with the exception of free-cutting steels when sulphur is added to improve the machining properties). However, sulphur can also be absorbed by the scale from the reheating furnace atmosphere. Most conventional furnaces utilise sulphur-bearing hydro-carbon fuels. To minimise the effects of sulphur concentration in the scale the fuel should be burnt with an excess of air to give a minimum of about 5% O_2 in the atmosphere. This combustion also results in H_2O and CO_2 in the furnace both of which maintain the adhesion of the wüstite to the metal during growth. The atmosphere flow rates involved in reheating furnaces are normally high and greatly in excess of the critical level, but there may be stagnant areas in large furnaces. Surfaces reheated in practice will almost always already have an oxide layer and the topography and chemical state of the surface metal will depend on its prior processing. For laboratory studies a reproducible surface finish is usually selected; and although there is some disagreement in the literature as to the effect of surface finish on scale adhesion it may be less important when considering thick scales. A very important aspect of the laboratory study of oxidation kinetics is specimen shape and

size. Specimen edges are known to lead to a pinning effect of the scale and subsequently more oxidation occurs on plane surfaces. Spherical specimens eliminate edges and would also have the optimum specific volume but they are very difficult to prepare. Cylinders are easily prepared to reproducible dimensions and surface finishes but they should be as large as possible to avoid overheating effects and to minimise the change in surface area which occurs during oxidation.

For metallographic study of the oxidation which occurs on the flat faces of large slabs in the laboratory for example, rectangular specimens may be preferred. However, consideration must also be given to the specimen 'specific area' to avoid overheating effects at high temperatures.

3.3 Physical Assessment of Scale Adhesion

3.3.1 Room Temperature Testing

3.3.1.1 Measurement of Adhesion Force [23,76,77]

The room temperature adherence of secondary scale (i.e. scale formed during rolling and subsequent cooling) on rolled plate was assessed[76] by measuring the force required to remove a small area of scale. The scale was removed by attaching a small brass cone to the plate surface with synthetic resin and loading normal to the plate surface in a tensile machine. The scale adhesion was expressed in g/cm^2 of descaled surface. Using this technique it was shown that adhesion values up to 100 g/cm^2 could be obtained on pure

iron, (Fig.7). The adhesion was found to decrease with increased final rolling temperature and scale thickness in the case of unkilled steels. The formation of intermediate layers containing silicate probably explains the lack of variation in the adherence of scale on killed steels. The precipitation of Fe_3O_4 in the wüstite layer during slow cooling (furnace cool) was shown to have no measurable effect on the scale adhesion.

Further work[23] by the same authors using pure iron oxidised isothermally in the temperature range 600-1050°C, with additions of specific elements showed that the addition of elements whose oxides have a higher free energy of formation than FeO resulted in the formation of intermediate layers between the wüstite and the metal and reduced adhesion. Elements whose oxides were soluble in FeO , only slightly reduced the adherence and elements whose oxides had a considerably smaller free energy of formation than FeO precipitated at the interface and increased the adhesion. Carbon was found to decrease the adhesion and the maximum adhesion peak moved to lower temperatures as carbon increases. (See Figs.5 and 6).

Another form of tensile test has been used[77] which is based on the formation of an oxide layer in the space between two adjoining metal specimens. The strength of wüstite, magnetite and hematite grown at low temperatures were reported as 4, >100 and >400 kg/cm^2 (56.9, >1423, >5692 lb/sq.in)

respectively. The author describes the test as a method for determining the strength of scales, but it is similar in principle to the method of Engel and Peters[23] and has therefore been included.

3.3.1.2 Impact by Spherical Indenter[2]

Flat pure iron and Armco iron specimens were reheated in atmospheres of combusted propane, natural gas, town's gas and the product of combustion of fuel oil burnt with an excess and deficiency of air at temperatures in the range 800-1000°C for 2 h. In order to produce an adherent uniform scale layer it was found necessary to sand-blast the metal surface prior to oxidation. After cooling, the scale was subjected to an adherence test similar to that used on enamel coatings on steel. A drop hammer with a spherical head was allowed to fall from a determined height on to the sample which was thus slightly deformed. The area of scale detached from the reverse side of the specimen was taken as an indication of the adherence of the scale.

Under combustion conditions of an air deficiency, no separation of scale could be achieved using this technique. With excess air the scale adherence appeared to reach a maximum at 15% excess air, further additions of air decrease the adherence to a minimum at 30% excess air. The presence of sulphur in the furnace atmosphere (2600 mg/m^3) was found to decrease the cohesion of the scale and assist the exfoliation of the magnetite layer, the adhesion of the wüstite apparently being higher in the presence of sulphur.

3.3.1.3 Tensile Testing[78]

Commercially produced 5 swg hot rolled wire rod with carbon contents of 0.05, 0.09, 0.19 and 0.49% C were mechanically straightened, pickled and polished with 600 grade emery paper. The rods were scaled at 700-900°C for 5 and 20 minutes in air. The air cooled scaled rods were deformed 8% in tension and the scale which spalled off during this deformation was collected and weighed and graded for size. The scale remaining on the rod was removed by a modified iodine extraction technique, and weighed. The weight of adherent scale increased with the time and temperature of oxidation. The proportion of adherent scale increased with the carbon content and decreased as the scale grew thicker. The mechanism of scale spalling during the tensile testing was suggested to be as follows:- a gap or plane of weakness is formed very close to the interface towards the end of oxidation, or more probably during cooling; when the rod is stretched, transverse cracks form in the scale, some of which then falls off; a thin film of oxide remains on the surface together with isolated columns of oxide holding some blocks of thick scale to the adherent film.

3.3.2 High Temperature Testing

3.3.2.1 Hot Bending[33,63,79]

Specimens size 45 mm x 5.5 mm x 4 mm (1.7 in x 0.216 in x 0.158 in) were reheated in commercial forging furnaces, one of which utilised a liquid fuel oil, and the other consisted

of a radiant heat electric muffle furnace. Maximum temperatures in the range 1100-1300°C were used and heating times at these temperatures between 2 and 12 min were used. Bending to an angle of 20-30° was carried out in the furnace and using this method the scale on electrolytic iron, a rimming steel and carbon steels containing 0.2 and 0.7% were all shown[79] to be brittle. However, no attempt was made to determine the amount of scale detached, or that remaining on the metal surface.

The adherence of 0.7% C steels with different contents of residual elements oxidised in atmospheres simulating the combustion of coke oven gas with and without free O_2 and SO_2, and treated at 1050, 1150, 1250°C for up to 2 h was tested by hot bending at different strain rates[63]. The thickest scales exhibited the weakest adhesion (i.e. ratio of non-adherent scale to the total amount formed). Stronger adhesion was shown by thinner scales and those containing liquid phases and 'keyed-on' inner zones. No effect of strain rate was observed, (Fig.9).

A bend test[33] carried out in the treatment furnace was used to assess the adherence (ratio of non-adherent scale to total formed), of pure iron and Fe-Al alloys containing 0.005-0.2 wt % Al. Temperatures of 850-1050°C were used for 0.5 - 2 h in an atmosphere based on combusted town's gas with and without 5% free oxygen. The scales on alloys containing 0.1-0.2% Al oxidised at 950-1050°C were found to be less adherent than on pure iron and alloys containing 0.025% Al and 0.045% Al,

(see Table 1). This was thought to be caused by the presence of aluminium-rich oxidation products at the scale /metal interface.

3.3.2.2 Vibrational Technique

Bruce and Hancock[74] have developed a technique for studying the high temperature oxidation of metals by measuring the changes in natural flexural frequency of a freely suspended specimen. They have shown that such a change can be related to the degree of oxidation and that the oxidation rate was independent of the vibration. Specimens size 152.4 mm x 5.08 mm (6" x 0.2") diameter were used for the vibration experiments and the results were compared with gravimetric results on 1" x 0.2" diameter specimens. Armco iron and mild steel specimens were examined in an air atmosphere at temperatures in the range 500-800°C. Smooth weight gain versus time curves were obtained in each case using the gravimetric technique, whereas discontinuities existed in the change in frequency versus time curves obtained with the vibration technique. It was suggested that such changes in the frequency of the suspended specimen could only have been brought about by cracking of the oxide layer during growth. The results indicated that this cracking was less marked at the higher oxidation temperatures, probably because of increased scale plasticity. By examining the results obtained by subjecting specimens oxidising in the gravimetric vibration apparatus to increasingly severe thermal shocks an assessment

of the scale adherence of the growing oxide layers was made. This technique utilises the differential coefficients of expansion of iron and wüstite to produce circumferential stress at the metal/scale interface which opposes the scale adherence. Thus, if the temperature drop which causes loss of adhesion is known, and this was characterised by a sharp increase in the oxidation rate when the specimens were returned to the oxidising temperature, the stress could be calculated. Using this technique it was found that the adhesion of both Armco iron and a 0.2% C steel increased with increasing temperature and was of the order of 35.2-281.6 kg/cm^2 (500-4000 psi) over the temperature range 600-800°C, (Fig.10). The increased adhesion was thought to be caused either by changing interfacial conditions or by increased plasticity of the oxide with temperature, although only elastic behaviour was assumed in the calculation.

3.3.2.3 Quenching Tests[58]

Small steel specimens were reheated in synthetic atmospheres containing O_2, N_2, H_2O and SO_2, in the proportions commonly found in reheating furnaces, in a laboratory furnace at temperatures in the range 900-1300°C. After reheating under the conditions for up to 6 h the specimens were water quenched. The dried specimens were weighed, descaled using a sodium anhydride bath and re-weighed. The scale removed by descaling was recorded as adherent scale. The amount of adherent scale was found to increase rapidly with temperatures above 1100°C and also to increase with oxidation time. The water vapour and oxygen contents of the furnace atmosphere

had little effect on adherence except insofar as their influence on the SO_2. The presence of the latter in atmospheres of low oxygen content caused an appreciable increase in the amount of adherent scale.

3.3.2.4 Hot Compression Test[59]

Specimens 50.8 x 25.4 x 25.4 mm from a large variety of commercial steels were oxidised for 20 minutes in a furnace heated with town's gas burnt to give 1% oxygen in the furnace atmosphere with a maximum temperature of 1200°C. They were then subjected to a scale adhesion test which consisted of longitudinally upsetting the samples by 25% in a small hand press. The amounts of total and adherent scale were determined by weighing and the percentage of adherent scale calculated, and reported as a scale adhesion index.

The high temperature scale adhesion index ranged from 30 to 76 and the main conclusion was that nickel-steels show a higher adherence index than the chromium steels.

3.3.2.5 Hot impact Tests[28,64]

A hot impact test was used[28] to assess the high temperature adhesion of thick scales formed on 25.4 mm cube samples of iron-base alloys containing 0.1 and 1% C, 0.3 and 3% Si, and 0.01 and 0.1% S, at 1050° and 1250°C. Atmospheres based on combusted natural gas or town's gas were used to give a high and low oxygen potential atmosphere comprising 70% N_2, 20% H_2O, 10% CO_2, with and without 5% O_2. Oxidising

times of up to 4 h were used and the adherence was assessed using a falling weight with insufficient potential energy to deform the sample, and the scale was removed by the shock of the weight striking the sample. When all the scale was retained on the sample it was regarded as strongly adherent (an index of 100%), when all the scale became detached it was considered non-adherent (an index of 0%). This allowed a discrimination to be made between the contrasting adherences of scales differing in thickness and constitution (see Table 2).

Weak scale adhesion was shown by thick porous scales that had become heterogeneous in structure through the evolution of gaseous carbon oxidation products and the loss of liquid phases. Strong scale adhesion, which occurred on the high silicon and sulphur alloys was attributed to the liquid wüstite/fayalite and liquid wüstite/ferrous sulphide eutectics in the scale and sub-scale which cushioned the effect of the impact test stresses. The marked adhesion was not entirely dependent upon the mechanical keying on effect of the intergranular sub-scale penetration which often produced a rough metal/scale interface. It was concluded that liquid phases within the scale probably assisted in crack arrestment and stress absorption near the metal/scale interface thereby maintaining strong scale adhesion.

Other workers[64] investigated the hot scale adherence of carbon and special steels (Ni-Cr-Mo) using a 'hammer test'.

Flat specimens 6.35 mm thick and 50.8 mm wide were oxidised at 1200°C for up to 4 h in atmospheres produced by burning fuel oil, town's gas and mixed fuel oil/town's gas with up to 5% excess air. The specimens were supported on edge in the furnace by recesses in a refractory brick and the adherence of the scale was assessed using a falling weight. A 10.5 kg cylindrical steel weight was allowed to fall from a fixed height onto the hot scaled sample which was held on edge on a solid base with a pair of tongs. The impact of the weight deformed the sample and removed the scale, and the weight of scale remaining was taken as the measurement of adherence.

In general the quantity of adherent scale increased with the time spent at the reheating temperature. With low excess air and fuel oil the quantity of adherent scale was greater than with 30% excess air. This was explained by the presence of low melting point iron oxide/sulphide eutectic at the surface of the metal which caused extensive intergranular penetration of this phase and thus increased the adhesion. Much lower quantities of adherent scale resulted when town's gas was used as the fuel.

3.3.2.6 Hot Detachment Test[80]

A brief investigation has been carried out by Hulley and Rolls of the relationship between scale cohesion and adhesion of a 0.1% C mild steel. An oxide scale was formed by merging the separate growths from the tips of a transversely sectioned tensometer specimen separated by a small gap. Oxidation was carried out in air at 1000 and 1100°C for

up to 16 h. On testing the scale adhesion specimens it was claimed that fracture always occurred at one of the scale/metal joints although no evidence of this was put forward. A peak was detected in the relationship between scale adherence and time after 4½ h oxidation at 1000°C. In addition adhesion values of 73.95 kg/cm^2 and 61.2 kg/cm^2 were obtained at 850°C and 1000°C respectively after 3 h oxidation, (see Fig.11). In separate experiments using specimens oxidised to completion the cohesive strength of the wüstite/magnetite scales formed at 1000°C was 211.2 kg/cm^2 and of the magnetite and hematite scale formed at 1100°C was 176 kg/cm^2. A plastic strain of 5.1% at 1000°C was observed indicating the brittle nature of the scales formed. The slight plastic behaviour observed was thought to be due to a concentric inner shell of wüstite.

3.4 Discussion

3.4.1 Fundamental Consideration

3.4.1.1 Methods of Assessing Scale Adhesion

Metallographic studies on material cooled to room temperature can distinguish between adherent and non-adherent scales and the position of fracture can be readily identified. However, as with all methods based on specimens cooled from the scale formation temperature the results obtained are of little value for assessing the high temperature scale adhesion. The different coefficients of expansion of steel and scale, the phase changes which occur in the scale

(Fe_3O_4 precipitation) and the metal ($\gamma - \alpha$) and the solidification of liquid phase and general decrease in plasticity of the scale render the extrapolation of data obtained on room temperature specimens to higher temperatures impossible.

For fundamental studies of scale adhesion therefore, it is essential that the assessment is carried out at the scaling temperature. This has been done as outlined above but the value of such data is suspect in many cases. The major objection to all the methods examined is that the position of fracture has not been positively identified and therefore scale adhesion and/or scale cohesion may be the actual characteristics determined. This is true for all the methods which rely on a gravimetric determination of the scale/proportion or the of scale non-adherent/adherent after testing.

The parameter used to describe 'scale adhesion' in the hot bend testing[33,63] for example is the amount of non-adherent scale expressed as a fraction of the total scale formed. It is clear that lack of cohesion in the scale layer, resulting in exfoliation of part of the scale over a large area would give exactly the same adherence index as loss of the total layer over a smaller area. The stress system involved in the bending of a composite steel/scale beam with the scale layer varying in plasticity encourages loss of scale cohesion and hence this is not regarded as a very suitable method of studying adhesion. A better method of presenting the results is by recording the amount of adherent scale remaining after testing as used in the quench test[58] and the hammer test[64] as this

is less sensitive to the original scale thickness, although similar results could still be obtained on a specimen showing local loss of adhesion and one with general loss of cohesion. The stress systems involved with the quenching method depend to a large extent on the specimen geometry and the temperature at which scale separation occurs is not known, but it is unlikely that separation occurred before considerable cooling had taken place leading to some of the disadvantages obtained with specimens tested at room temperature. The quench test is therefore not a good method although it has the possibility of determining where fracture occurred as oxidation would not take place even if the temperature of fracture is unknown. The method of edge deformation as used in the hammer test[64] in which a large weight was allowed to fall onto the edge of a thin plate specimen did not appear to be a very selective test probably because the deformation obtained with successive tests would be very difficult to reproduce. However, the less definite trends could be determined depending on the atmosphere conditions used. The deformation obtained would also vary with temperature because of the varying strength of the steel and at longer times because of the decrease in thickness of the specimen. The hot impact test used by Rolls[28] did not use the deformation of the specimen to remove the scale and should therefore have given better results, but the parameter used which was the adherent scale expressed as a percentage of the total scale formed is again very dependent on scale cohesion. The same parameter was used to express the results obtained with the hot compression test[59] which

again was not very selective, although this test was probably representative of commercial forging conditions.

A much more quantitative assessment was made by Hancock and Bruce[74] using the vibration technique with which it was found possible to calculate the scale adhesion. The method used for calculating the adhesion strength, was based on determining the temperature drop necessary to give scale/metal separation. This was said to have occurred when a rapid increase in oxidation of the specimen was observed when returned to the oxidising temperature. However, loss of adhesion can occur with very little change in the oxidation rate if the scale 'blister' formed remained protective. Hence, it is most likely, in view of the rapid oxidation rate obtained, that cracking of the scale layer had also taken place and it is not clear whether scale adhesion or cohesion was being studied and no metallographic evidence of the position of fracture was given. Additional information could be obtained using this apparatus as weight gains caused by oxidation can also be followed by measuring the change in frequency although calibration of the instrument with a thermobalance is advisable. In addition cracking of the scale can be detected during growth, although loss of adhesion and scale cohesion both influence the resonant frequency there is no way of differentiating between them. This method is very complicated and is more useful for examining the properties of growing oxide layers but is not particularly suitable for the study of scale adhesion. In particular, to use this method at higher temperatures would be difficult

because of the introduction of steel transformation stresses. The hot detachment test used by Rolls[80] yields direct quantitative results and should therefore be suitable for fundamental studies. Certain objections can be raised to the method, not the least of which is that once again the position of fracture was not identified. However, the scale cohesion strength was also measured by tensile testing a specimen oxidised to completion and this was found to be much greater than the 'scale adhesion' measured. Consequently, it is likely that this test is actually measuring scale adhesion. However, the growth of scale in the small gap between the two halves of a small steel tensile specimen may lead to compressive stresses set up in the scale which help to maintain adhesion. Conversely, there is the possibility that vacancies produced at one metal/scale interface may diffuse to the other metal/scale interface and result in a non-adherent condition on one surface. In addition, once bridging of the air gap takes place by scale formation the oxidising conditions would vary across the test surfaces because of the variation in effective scale thickness which may lead to rounding of the test surfaces.

Consequently, none of the methods described are considered particularly suitable for fundamental studies of scale adhesion. This is predominantly because the position of fracture has not been determined, although the hot detachment test may give the closest approach to this. Nevertheless,

some useful information can be obtained by examining the results obtained so far.

3.4.1.2 Comparison of Data

The effect of oxidising time and temperature is not at all clear from the results of the various workers A decreasing adhesion with increasing time and temperature was found by methods which assessed the adhesion in terms of the proportion or percentage of adherent scale and this is probably influenced by the increasing scale thickness and lack of scale cohesion discussed earlier. It is significant that the assessments which used the weight of adherent scale as a measure found an increase in adhesion with time and temperature. This was also the finding of the vibration method, although for a much lower temperature range. The results of the other quantitative method, the hot detachment tests, are more confusing as adhesion was found to increase with time to a maximum at $4\frac{1}{2}$ h, but to decrease with temperature, Such behaviour indicates at least, that this test is independent of scale thickness. The detrimental effect of sulphur pick-up from the atmosphere on scale adhesion was indicated by the quench test and the hammer test in atmospheres containing sulphur compounds and a low oxygen level. Using natural gas (sulphur-free) atmospheres the hammer test recorded a much lower level of adhesion for example.

Similar effects of liquid phases were found in the scales containing silicon-rich and sulphur-rich (from the steel) liquid phases. Other effects of steel composition are those

of nickel which increased the adhesion[59] and aluminium which formed brittle particles in the scale and scale/metal interface and caused a decrease in adhesion[33]. The effect of liquid phases was found with methods using the amount of adherent scale[53,64] and the percentage adherent scale[28] and it is thus likely that the effect of liquid phases whether in adhesion or cohesion is large enough to be indicated by relatively insensitive test methods. The effect of nickel must also be marked but has not been correlated, although Sachs[41] postulated from metallographic work that nickel contributes to adhesion. The effect of brittle particles of aluminium is complementary to the low temperature detachment test of Peters and Engell[23] who found that the addition of aluminium decreased the cold scale adhesion.

3.4.1.3 Mechanism of Adhesion

The works described above have shown that the factors which affect scale adhesion are very numerous and complex and it is useful at this stage to examine the mechanisms which have been advanced to explain scale adherence. Much of the work on oxides is devoted to improving the adhesion, and thereby increasing the oxidation resistance and service life of steels used in high temperature structural applications. The mechanisms of scale adherence have been discussed by Stringer[81] and Tylecote[82] and although the 'adherence is desirable' approach has been mainly considered, the discussions

are in part applicable to scales formed during reheating for hot working.

In general the overriding factors influencing the adherence of oxide layers are believed to be those which influence the fracture mechanism at the metal/scale interface in terms of crack nucleation and propagation.

3.4.1.4 Crack Nucleation

Cracks are believed to be initiated by stresses in the scale which are set up during growth. Early work[83] considered the volume ratio of oxide to metal, the Pilling-Bedworth ratio, and suggested that in the cases where this ratio exceeds unity the oxide formed will be in compression, if less than unity tension results. Iron oxidation is in the former category, but the oxidation of iron takes place predominantly by outward diffusion of iron ions through the wüstite[9,10] and hence the volume change does not take place at the metal surface and the scale in this region may not be affected by the Pilling-Bedworth ratio[32]. The difference in lattice spacing has also been considered by Stringer[81] as a source of stress at the metal/scale interface which it was suggested decreased rapidly in the oxide with distance from the metal surface. The existence of stress in growing oxide layers on iron has been demonstrated by the decrease in radius of a helically wound strip during oxidation[4], and further evidence has been put forward by Maldy[20], who found a layer of small grains in the oxide and a narrow layer of polygonised sub-grains in the metal at the surface, indicating that the stress had been sufficient to generate dislocation

movement in the metal. Stress induced during the oxidation of small cylinders of iron has also been observed[74] to result in marked cracking at the scale/metal interface.

Iron diffusion into the scale layer produces a vacancy in the iron lattice at the metal surface[9,10], and condensation of vacancies at the scale/metal interface may cause crack nuclei. These may be removed by inward creep of the scale or the vacancies may diffuse into the metal, as observed by Dunnington et al[16] during the oxidation of thin specimens of iron. In fact the effect was so marked that vacancies produced on one surface of the specimen which had an adherent scale, were able to diffuse to the opposite metal surface which had a non-adherent scale.

3.4.1.5 Crack Propagation

Crack initiation is believed to be virtually unavoidable during oxidation processes and crack propagation is therefore considered by Stringer[81] to be the most important factor governing scale adhesion. This is probably true for oxidation under 'in service' conditions, i.e. low temperatures and relatively brittle scales, but crack initiation may be less readily achieved under reheating conditions with high temperatures and more plastic scales. Nevertheless, in Stringer's opinion, crack propagation depends upon the plasticity of the scale and metal at the metal/scale interface and crack propagation is more difficult in plastic layers. Ductile metal particles and pores in the scale also retard crack propagation. Increased crack propagation is

caused by low plasticity of the scale at the interface and the presence of brittle particles.

The effect of increased plasticity has also been advanced[28,62] to explain the high hot adhesion obtained on specimens containing liquid phases in the scale at the interface. Similar phases have been shown to result in low adherence on scale detachment tests carried out at room temperature when the plasticity of these phases was markedly reduced[23]. This effect of brittle materials has also been observed[33] during hot bend testing Fe-Al alloys. In this case a decrease in the adhesion was associated with the presence of aluminium rich phases at the interface.

3.4.2 Practical Considerations

3.4.2.1 Scale Behaviour during Hot Working

The bulk of steel is conventionally hot worked using forging or rolling. Forging, of the open-die type consists of rapid blows or repeated slow compression and scale removal is not usually a problem, as the slight bulging of the material not in contact with the forming tool surfaces and repeated shock detaches the scale readily. Problems may be encountered with the scale under the tool and also in closed die forging which produces material to closer tolerances and more rigorous inspection standards, because of scale confined within the forging die. Similarly, during rolling, only the scale which enters the roll gap between the metal and the roll is troublesome and this is especially so for wide plate production. The slabs are usually large and require considerable reheating time, and consequently thick scales are

produced. The problem is more acute when the stock is rolled in one operation from slab to finished product size as defective material cannot be dressed and re-rolled.

The limited information available on the mechanical properties of the scale layer indicate that at temperatures in excess of 950°C it has a higher hardness than the underlying metal[84], a low plasticity and a high tensile strength [80,85], thus it is probable that scale entering the roll gap is forced into the metal with little deformation of the scale and can form large defects.

3.4.2.2 Scale Removal

The application of birch brush, or bracken[76,86] has been used to aid scale removal during rolling in the past. Techniques such as 'edge rolling' are also used and in this method the slab is deformed a small amount by passing through the rolls whilst turned on edge thus removing the scale from the larger important faces. Other methods of scale removal in use currently utilise edge rolling and rolls with fluted or nobbled surfaces or more usually high pressure water sprays. The mechanisms of descaling have been suggested[86] as mechanical (e.g. wire brushing) deformation (or edge rolling), deformation-rupture and hydraulic. The deformation rupture model assumes that the enclosed spaces between the rolls and the metal, formed by flutes or brushwood, generate high steam pressures and the areas of contact locally deform the metal and cause cracking of the scale. The hydraulic descaling is considered to consist of the penetration of high pressure water down cracks in the scale

resulting in the generation of high steam pressures which remove the scale. More recent work[87] utilising a single water spray nozzle carried out under laboratory conditions indicated that thermal shock caused fracture normal and parallel to the surface at the metal/scale interface. The fracture parallel to the surface was extended under the action of mechanical vibrations set up by the water jet and further fracture normal to the surface resulted in fragmentation of this scale which was removed by the flow of water. Thin scales, high water pressures, and long times spent in the jet, all led to better scale removal. Commercial descaling, which utilises much higher pressure water was thought to remove the scale mainly by mechanical action similar to that of grit-blasting.

3.4.2.3. Practical Relevance of Tests

It is extremely important, in view of the higher hardness of the scale layer than the metal at hot working temperatures, that as much of the scale layer as possible should be removed. The methods used for assessing scale adhesion may simulate the stress conditions used in hot working and the conditions which cause scale removal in these methods of deformation.

The impact test[28] for example simulates closely the conditions found in a drop-forge, although the deformation would be much greater in practice and the hammer test[64] may give a better approach to the drop forging system. The compression test[59] is similar to a press-forging operation

and the initial stages of rolling although high strain rate rolling may bear more resemblance to the hammer test. The methods may be used to examine the deformation - rupture mechanism of adhesion[86], and can give useful practical results if the amount of adherent scale is taken as the parameter to be studied.

The amount of adherent scale, remaining on slabs of rimming steel and silicon-killed steel after three rolling passes has been determined, for a range of rolling temperatures by Palin[88]. The amount of adherent scale, was found to increase with temperature for each steel with greater amounts of adherent scale remaining on the silicon-killed steel. This practical demonstration of the effect of temperature and liquid phases on scale adhesion correlates with the results of the impact and hammer test and also with the quench test. Hence these methods are to be preferred over the bend-test technique. The vibration method[74] is not considered to be of use for studying high temperature (i.e. reheating temperatures) scale adhesion from the practical point of view because the ($\gamma - \alpha$) transformation may interfere with the results and at least would complicate the calculations. It is most probable that the sensitivity of this technique would be best below 900°C. The hot detachment method[80] did not correlate well with the practical results of Palin[88], although for a different temperature range, but quantitative measurement is obtained. This method is also

sufficiently selective to show a variation in the parameter measured with oxidising time and the results suggest that fracture takes place at or very close to the metal surface and it is therefore considered that the concept of hot detachment is worthy of further development.

3.4.3 Summary

For fundamental studies the methods used to assess scale adhesion have the serious limitation that the position of fracture has not been determined and hence scale cohesion and/or scale adhesion may have been measured.

For practical studies, the impact, hammer and quench tests give some correlation with practical results and may be suitable with refinements to study the amount of adherent scale produced by different treatments.

The hot detachment concept appears to be suitable for both fundamental and practical studies providing that the position of fracture can be determined and good correlation with practical experience can also be obtained.

Although many of the results are confusing, it would appear that scale adhesion is increased with reheating temperature and time, the presence of liquid phases in the scale and mechanical keying-on effects. Brittle particles at the scale/metal interface have been found to decrease the adhesion. The word adhesion is used loosely here as the position of scale fracture has not been identified.

4. ASSESSMENT OF OXIDATION CHARACTERISTICS

The variation in oxidation characteristics with each variable studied are considered in this section in terms of metallographic examination of the scale and scale/metal interface region, and thermogravimetric determinations of the kinetics of oxidation. The investigation into scale adhesion will be considered in a later section .

4.1 Experimental Procedure

Specimens were prepared from 76 mm square billets of commercial steels (Table 3a) in the following way. The billets were forged to 35mm. diameter oversize specimens were turned from these forged bars and were sectioned into cylinders. They were machine ground to 30.48 mm diameter by 25.4 mm high solid cylinders to a standard surface finish of 16 CLA. The rimming steel specimens were prepared in a different way. A rimming steel ingot was obtained and sectioned, the depth of rim was determined by sulphur-printing and the rim removed. This was then forged and specimens prepared in the same way as above.

The specimens were stored immersed in oil, were degreased using carbon tetrachloride, and dried using alcohol before oxidation. They were oxidised in a twin tube horizontal furnace heated by electric resistance elements, (shown in Fig.13). The temperature of the furnace was controlled using a West Guardsman in conjunction with a mercury relay and a variable transformer. In this way control of the specimen temperature was achieved within $\pm 4^{\circ}C$ of the required

temperature. One tube of the furnace was used to pre-heat the atmosphere and the other tube was used to carry out the heat treatment of the specimens. The degreased dried specimen was placed on one of its circular ends in a platinum boat in the furnace at the required temperature. To prevent oxidation during heating up the furnace was flushed with 10L/min of oxygen free nitrogen or high purity argon until the specimen had reached temperature. This was determined by a rare metal thermocouple sheathed in recrystallised alumina placed in close proximity to the specimen. The required furnace atmosphere, which simulated the combustion of uncleaned coke oven gas burnt with approximately 40% excess air (see Table 4), was introduced again at a flow rate of 10L/min. The atmosphere was synthesised using the component gases, nitrogen, oxygen, (as air) and carbon dioxide which were contained under pressure in sealed cylinders and supplied via pressure reduction valves, regulating valves and flow meters to a mixing chamber. Water vapour was introduced by passing the gas mixture produced through a water bath held at a constant temperature and thereafter the transport tube was maintained at approximately 100°C in order that the water vapour did not precipitate out of the gas. Sulphur dioxide was introduced into the gas mixture as close to the furnace as possible and was supplied from a cylinder by a pressure reduction valve and flow meter in a similar way. The oxygen and CO_2 contents of the dry gas mixture were determined using an 'Orsat' apparatus by absorption in solutions

of alkaline pyrogallol and sodium hydroxide respectively. The water content was determined by weighing the water bath and also by absorption using anhydrous calcium chloride. The sulphur dioxide content was determined using a titration technique[89] (see Appendix 1). Specimens were heated at temperatures of 950, 1050, 1150, 1250 and 1350°C for times of $\frac{1}{4}$, 1, $1\frac{1}{2}$ hours in the horizontal tube furnace. Three hour tests were done in a vertical tube furnace with identical furnace tube and with the same synthesised atmosphere as in the horizontal tube furnace but in this case the specimens were suspended on an electro-magnetic continuously recording thermobalance[90] using a platinum suspension wire inserted in small holes drilled in the specimen.

Temperature control was effected by a rare metal thermocouple sheathed in an alumina tube placed in close proximity in a similar manner to above. After oxidation the specimens were air cooled and encapsulated in a cold setting epoxy resin. They were then sectioned into two cylinders and one of these was re-encapsulated under vacuum to fill any pores and cracks in the scale. They were then prepared for metallographic examination by hand grinding on carborundum papers and polished using diamond paste on selvit cloth.

4.2 Results

4.2.1 Metallographic Examination

It is proposed to consider the metallographic results obtained on each steel with reference to the scale layers and to the metal scale interface region in each case.

4.2.1.1 Scale Layers

Multi-layer scales were formed in all cases consisting of a thin layer of Fe_2O_3 a thicker intermediate layer of Fe_3O_4 and a very thick layer of FeO adjacent to the metal. The scales increased in thickness with time (Figs.14-16) and reheating temperature (Figs.17-19) and were very porous. They contained four different types of pore or cavity which were common to all four steels. Two of these occurred predominantly in the wüstite and tended to be lined with a thin layer of magnetite. In one case they tended to be ellipse-shaped with the major axis parallel to the metal surface, and this type occurred in the inner wüstite layer (Fig.20). The second type was confined to the outer wüstite region containing precipitated magnetite and tended to be elongated in a direction normal to the specimens surface. This second type of porosity appeared to be most noticeable at oxidation temperatures of 1150°C in each case (Fig.21). A third type of discontinuity again in the wüstite layer took the form of major cracks or fissures parallel to the metal surface also lined with magnetite. At lower temperatures this type of discontinuity was confined to a single fissure near the metal surface (Fig.22). The number of such fissures increased with increasing oxidation temperature and time (see Figs.14-19), the specimens subjected to high temperatures and long times contained many such parallel cracks giving the wüstite a multi-layer appearance. Finally a large number of angular cavities of various sizes were observed randomly dispersed in the FeO and Fe_3O_4 scale layers and these were not lined

with a higher oxide. In general the amount of porosity in the scales increased with oxidising temperature and time. The wüstite layer contained many cracks some of which were outlined by magnetite and in some cases these were seen to interconnect other types of porosity. Cracks were also noted which penetrated to the scale surface and in these cases they contained haematite as well as magnetite.

Magnetite was precipitated in the FeO in the form of rosettes and cuboids. These tended to be confined to the outer wüstite region in most cases (Fig.20), but in some cases they were evently distributed throughout the wüstite layers separated from the inner wüstite by fissures (Fig.24). Semi-continuous lines of magnetite were also observed in the wüstite layer (Fig.25) often interconnecting cavities in the scale. Magnetite was also found in the inner wüstite layer on the inner surfaces of porosity and discontinuities in the scale, as outlined above.

A layer of discrete particles, darker in colour than the wüstite was observed in the scale at the metal surface on the silicon killed steels at 950°C and the layer became more compact with increased oxidation time (Figs.26 and 27). At 1050°C small amounts of a light coloured liquid phase was also noted in the scale on these steels which was also immediately adjacent to the metal surface. At 1150°C and above a dark liquid phase was observed which wetted the wustite grain boundaries, and appeared to form a eutectic with FeO (Figs.26 and 29). There were also small amounts of a light coloured liquid phase present in the complex eutectic.

The amount of liquid increased with increased oxidation temperature and time and well defined grain boundary networks were observed in the scales on silicon-killed materials at 1150°C (Figs.29(a) and (b)). The amount of this complex eutectic phase was not as great on the aluminium-treated silicon-killed specimen and the penetration of a well defined grain boundary network was not as extensive on this steel.

The dark phase, seen to be liquid at high temperatures was not observed in the scales on the semi-killed and rimming steel specimens. The light-coloured phase was observed however and the scale on the semi-killed steels in general contained more of this constituent than did the scale on the rimming steel. The amount of liquid phases was less than those observed on the silicon-killed steels. They increased in quantity with time and temperature and well defined grain boundary networks were observed in the wüstite layer adjacent to the metal surface at the maximum temperatures studied (Figs.30 and 31).

The irregularity of the metal surface increased with oxidation time and temperature with each steel studied, the results obtained on each steel are outlined separately below.

4.2.1.2 Metal/Scale Interface

Silicon-Killed Steel

At 950°C the surfaces produced were relatively smooth under an almost continuous layer of a dark oxide as described above (Figs.32(a) and 26). Beneath the metal surface in a band immediately adjacent to the metal surface

there were a small number of globular oxides (internal oxidation). The size of these particles increased as the distance from the metal surface decreased. At 1050°C more general oxide penetration of the metal surface was observed and in some cases oxide penetration occurred to a greater depth down prior austenite grain boundaries, (grain boundary oxidation) (Fig.32(b)). The oxide in this grain boundary penetration contained quantities of liquid phases also observed in the inner scale layer at this temperature. Internal oxidation was again present and increased in extent with increasing oxidation time. At 1150°C (Fig.32(c)) the grain boundary penetration by complex eutectics and the extent of internal oxidation increased. Also the surface penetration of oxide became more pronounced and at the metal scale interface an intermediate layer containing mixed metal and scale began to appear (metal scale entanglement). All these effects became more pronounced at 1250°C (Fig.32(d)), and in particular the region of entanglement of scale and metal particles or filaments increased noticeably. The metal in the entangled layer was lighter in colour than the bulk metal and contained no precipitated oxide particles. The amount of liquid phase in the entangled band increased with time and temperature and in most cases liquid phases were seen at the tips of the oxide penetrations into the metal. At 1350°C (Figs.33 and 34) the metal scale entanglement formed an extensive, well-defined layer and the wüstite grain size which was outlined by liquid phases was much finer in the entangled layer than elsewhere. Internal oxidation had increased still further at 1350°C, the depth

of oxidation and the size of the particles being greater. The smaller more deeply seated particles were seen to be single phase and the larger particles near the surface were duplex.

Aluminium-Treated Steel

Similar results were obtained in this case as with the silicon-killed steel examined above. The irregularity of the metal surface increased with time and temperature and the effect of these variables is shown in Figs.35 and 36. At 950°C the metal scale interface was relatively smooth with no metal particles included in the scale, and a layer of fayalite particles was present in the scale at the metal surface (Fig.27). At 1050°C metal particles were noted in the scale layer and small amounts of a liquid phase were observed at the tips of oxide intrusions into the metal (Fig.35(a)). True metal-scale entanglement was only observed at 1250°C and above with this steel (Figs.35 and 36). The depth of the entanglement increased with time and temperature above this temperature and the scale in the entangled band appeared to have a fine grain size outlined by a liquid phase. The metal again appeared lighter in colour in this band and contained no precipitated oxides. Penetration of oxide down austenite grain boundaries was not observed at 950°C at a magnification of 500x for heating times of less than 1½ hours thereafter the depth of grain boundary penetration increased with time and temperature. Internal oxidation was noted in the form of a band of globular oxide particles immediately

below the metal surface at temperatures above 950°C. The depth of internal oxidation increased with time and temperature especially above 1150°C.

Semi-Killed Steel

Similar metal surface features were observed on this steel as with the two steels examined above, and the effect of reheating temperature and time on the interfaces produced is shown in Figs.37 and 38. In this case however the liquid phases seen in the metal scale entangled layer and in the grain boundary penetration consisted only of the light coloured eutectic also observed in the scale on this steel. Grain boundary penetration occurred on all the samples examined and the depth of penetration into the metal increased with increasing time and temperature. Internal oxidation was also noted on this material at all temperatures studied above 950°C and the size of the oxide particles decreased as the distance from the metal surface increased. The depth of internal oxidation again increased with temperature and time.

Rimming Steel

At 950°C relatively smooth interfaces were produced with only very small amounts of oxide penetration after 3 hours. At 1050°C traces of the light yellow phase were observed within the oxide penetration, Fig.39, this increased in amount with oxidation time and after 3 hours at this temperature particles of metal became included in the scale from the metal scale entanglement. After 3 hours at 1150°C the liquid phase could be resolved into a eutectic which appeared at the tips

of the oxide penetrations. Slight metal scale entanglement occurred after $\frac{1}{2}$ hour with metal particles again becoming included in the scale (Fig.39(b)). The amounts of eutectic in the metal scale entanglement increased thereafter with temperature and time (Fig.40). Internal oxidation was not detected using optical metallographic techniques below 1150°C. At 1150°C and above internal oxidation was observed as a band of globular precipitates the size of these precipitates decreased with distance from the metal surface.

In order to make comparisons of the metal scale interface regions possible on the four steels examined, measurements were made of the depth of metal scale entanglement, the depth of grain boundary oxidation, and the depth of internal oxidation at a magnification of 500x for each specimen studied. The mensuration limits employed in this exercise are shown in Fig.41. The results are shown in Figs.42,43 and 44 and all these effects can be seen to increase with time and oxidation temperatures. Samples of each steel oxidised for $1\frac{1}{2}$ hours at 1150°C were examined using an electron-probe micro-analyser (GEC/AEI.SEM2). Particular attention was paid to the metal and scale in the metal scale interface region and the results are shown in Figs.45-48. In all cases enrichment of nickel was detected in the metal in the mixed metal scale zone and the enrichment increased with the distance into the scale. The dark liquid phase seen on the silicon-killed steels was shown to be silicon rich and some sulphur rich oxide was also found in the scales of these materials especially

in the tips of the oxide intrusions. The scales were generally richer in manganese in the case of the aluminium-treated steel. The liquid phases in both rimming and semi-killed steels were found to be sulphur rich. The internal oxidation near the surface of the metal was found to be manganese rich in general and to contain some silicon in the case of the silicon-killed steels.

4.2.2 Oxidation Kinetics

The presentation of thermogravimetric data is usually expressed as the gain in weight due to reaction with oxygen per unit area of original specimen surface with time for each temperature under study. After the oxidation of the specimens used in this investigation however, they were seen to have decreased considerably in size and therefore in surface area. A mathematical treatment was developed to take the decrease in surface area of the specimen as oxidation proceeded into account when presenting the kinetic oxidation data. The method is described in Appendix 2. The results expressed as gain in weight per unit area of 'projected specimen surface' (i.e. assuming a planar metal/scale interface) with time are shown in Figs.49-52. The amount of oxidation increased rapidly with time and temperature for each steel studied.

4.3 Discussion

4.3.1 Scale Layers

The scales formed were typical of those found on commercial steels reheated in oxidising atmospheres[24,39].

Although the porosity of the scales made estimates of the relative proportions of wüstite, magnetite and haematite difficult, the magnetite and haematite layers appeared to be greater than the 4% and 1% of the total scale thickness as reported by Paidassi[1] for scales on pure iron. The porosity, cracks, and the presence of higher oxides of iron in the inner wüstite regions make it unlikely that parabolic oxidation as described by the Wagner[10]/Hauffe[9] mechanism is in operation and this will be dealt with more fully when the kinetics of the oxidation are discussed later.

The angular porosity found on all the scales studied is thought to be the result of mechanical damage during metallographic preparation, although every effort was made to avoid this by the use of double mounting techniques, vacuum impregnation of the scales and by the hand preparation.

The other types of porosity occurring in the FeO all showed well defined magnetite layers on their free surfaces and hence were a product of the oxidation process and were not formed by stresses set up in the scale during cooling. The large fissures parallel to the specimen were probably caused by growth stresses on the cylindrical specimens brought about by the decreasing dimensions of the oxidising specimen[74]. The reasons for the appearance of porosity in the wüstite layer is not clear and has been considered by other workers. Possible mechanisms for pore formation are thought to include, in addition to cavitation by growth stresses; the generation of high carbon monoxide pressures in the scale layer which actually overcomes the local scale adhesion and formation of

a cavity results[41]; the egress of iron ions through the scale and condensation of vacancies on the metal surface[8,9]; Rahmel[56] has shown that pores are present on iron oxidised in atmospheres containing CO_2 or H_2O whereas the scales formed in air or oxygen are compact. Water vapour or carbon dioxide are thought to become entrapped in the pores and stabilise them. Oxidation of the metal beneath the cavity is accomplished by the CO_2 or H_2O and the pore is formed and is taken into the scale layer. The elongated lenticular pores noted at 1150°C may be explained by the dissociation mechanism put forward by other workers[6,7]. It is suggested that dissociation of the wüstite can take place on void formation within the wüstite layer because of the increasing oxygen potential of the scale. The dissociation would be more favourable at grain boundaries in the scale and the presence of columnar grain boundaries would explain this type of porosity.

Cracks observed in the FeO which contain magnetite were probably formed by growth stresses in the scale during oxidation, and the evolution of carbonaceous gases. Many seams of magnetite both continuous and discontinuous are evidence of healing of such cracks and it is probable that the formation and healing of these cracks are taking place continuously as the oxidation proceeds. Cracks not containing the higher oxides of iron were either formed by stresses set up during cooling of the specimen in air or by mechanical damage during metallographic preparation. The layers of discrete particles in the FeO at the metal surface which were only present on

specimens of the silicon-killed steels oxidised at low temperatures probably consisted of the silicon-rich phase fayalite. The formation of such layers has been described by Rahmel[26] as an internal oxidation mechanism. Oxygen dissolved in the metal surface causes dissolved silicon to be oxidised to SiO_2 at some depth below the surface. These small particles grow as the oxidation proceeds and the metal interface advances towards them. Gradually the oxygen potential increases and the silica particles combine with wustite which can now form. The fayalite particles thus formed tend to collect at the interface and become compacted by the inward movement of the scale layer (Figs.26 and 27). Evidence of melting of this phase at 1050°C (Fig.32(b)) would suggest that it is not fayalite as the lowest melting point in the Fe-Si-O system[91] is the wüstite-fayalite eutectic which has a melting point of 1177°C, however, microprobe analysis of this phase at 1150°C indicates that some sulphur and manganese are also present and that the light coloured liquid is also sulphur-rich. According to Olsanskij[91] and Vogel[92] the presence of FeS in the SiO_2-FeO system will lower the melting point appreciably, and evidence of melting at 1050°C was observed. Tholander[27] has suggested that the exothermic reaction of iron with oxygen could locally raise the temperature and cause melting of the scale. It is difficult to visualise how this can occur in thick scales if the oxidation mechanism is controlled by the outward diffusion of iron ions through the wüstite, reaction with oxygen only taking place in the outer scale layers as predicted by

classical theory. However the presence of pores and cracks in the inner wüstite layer containing magnetite is evidence for the existence of oxidising gases in the inner scale layer and hence the direct access of these gases may cause the temperature of the interface zone to be higher than the ambient furnace temperature and cause melting of silicon-rich phases. The larger amounts of the complex liquid phases observed in the high temperature scales formed on the silicon-killed steel compared to the aluminium-treated steels is probably related to the relative silicon contents of these steels (i.e. 0.28% in the silicon-killed steel and 0.18% in the aluminium-treated steel).

The sulphur-rich phases seen in the scales on the semi-killed steel and rimming steels were molten at 1050°C, although according to Hilty and Crafts[93] the Fe-S-O system forms a eutectic at 920°C (Fe-FeO-FeS). There are two possible sources of sulphur in the scale. Firstly, reaction of manganese sulphide in the steel with FeO in the scale to produce MnO and FeS leading to progressive enrichment of FeS in the interface has been suggested[32] and evidence of this has been reported elsewhere[28]. Secondly, sulphur enrichment can occur by the transport of gaseous sulphur-oxides through the scale from the atmosphere and evidence of this has also been advanced[37,67]. The mechanism of transport of sulphur through the scales has been extensively reviewed recently by Tuck[66] and although the exact mechanism is not

known, the most likely was thought to be the ingress of gaseous mixtures containing sulphur through pores in the scale layers. The presence of sulphur in the scales on steels oxidised in atmospheres containing 4% oxygen was noted by Preece[37] even though the addition of this amount of free oxygen suppressed the increased scaling rate obtained with neutral atmospheres. This has since been confirmed by other workers[67,58] who found significant amounts of sulphur on steels heated in atmospheres containing sulphur dioxide. A reduction in the amount of sulphur in the furnace atmosphere also resulted in a reduction in the sulphur in the scale. Evidence of cracks and pores in the scale containing oxidising gases has been observed in this investigation and further evidence for this mechanism will be advanced later. (See Figs. 20, 22-27).

4.3.2 Metal Scale Interfaces

The metal scale entanglement, grain boundary penetration, and internal oxidation, increased rapidly with temperature and approximately parabolically with time in each steel studied (Figs.42-44). The phenomenon of metal scale entanglement observed in each case at temperatures above 1150°C was seen to contain liquid phases in the oxide intrusions into the metal and enrichment of nickel in the metal filaments protruding into the scale layer. This phenomenon has also been observed on commercial steel billets reheated in commercial furnaces and on nickel steels[24,51,52,54,55]. The presence of the entanglement was suggested by Sachs[51] to be the cause of high scale adhesion and rolled in scale defects.

Although the nickel contents of the steels studied by Sachs were very much greater than those used here it is possible that a similar mechanism to that suggested by Sachs was operating. Brown[55] found that the depth of the metal scale entanglement increased with the nickel content and this may explain why the rimming steel had less extensive metal scale entanglement than the other steels examined (0.03% nickel and 0.05% nickel). However, there are differences in the extent of entanglement noted on the steels which have the same nickel content and obviously other factors are involved. Because of the importance of this feature when considering scale adhesion the mechanisms of formation of the metal scale tangled layer will be discussed later. The grain boundary oxide penetrations formed on these steels are not great under these conditions and are very similar in the cases of the silicon-killed steels and the semi-killed steels with the rimming steel exhibiting deeper grain boundary penetration (Fig.43). In view of the grain boundary oxidation being only very slight when compared to the extent and amount of surface area covered by metal scale entanglement (compare Figs. 42 and 43) the importance of grain boundary penetration in the scale adhesion of scales formed on commercial steels such as those examined here is not thought to be very great.

Internal oxidation was also observed on all the steels examined (Fig.44). The deeper seated particles in the silicon-killed steels were silica and all the steels showed

manganese-rich globules associated with wüstite nearer the surface. The internal oxidation of iron and manganese alloys has been studied by Swisher[94] and the innermost internal oxides were found to be virtually pure manganese-oxide although there was an increasing proportion of wüstite in solution as the scale metal interface was approached. Rahmel[26] has described the internal oxidation of iron silicon alloys as outlined above but the situation is much more complex than this as the internal oxides on the silicon-killed steels probably contain quantities of manganese also and in the case of the aluminium-killed steels aluminium oxide should be present. The presence of oxygen dissolved in the metal beneath the scale-metal interface has been explained by the dissociation of the FeO into free oxygen at the voids formed at the metal surface, also discussed above, the dissociation pressure of the scale increases upon void formation to equalise the chemical potential of oxygen. Another possibility is transport of oxygen through the scale via cracks and pores as described by Rahmel[56] and by liquid phase transport in the form of the oxygen pump described by Tholander[27]. Voids at the scale metal interface were not observed in this case and the presence of liquid phases in the scale at the interface and inner wüstite region and the presence of cracks and voids in the scale layers, containing higher oxides suggests that oxygen is brought to the surface in this case by a combination of gaseous transport and liquid transport.

Several quantitative treatments of the phenomenon of

internal oxidation which are based on fundamental considerations for binary and ternary alloys have been attempted. Rhines[95] and Maak[96] have derived equations which predict the depth of internal oxidation under conditions of simulataneous internal oxidation and scale formation for a simple binary system. The method of Rhines is used in Appendix 3 to calculate the depths of internal oxidation produced on the silicon-killed and rimming steels used in this investigation assuming that silica and manganese oxides are the only oxides formed. Remarkably good correlation between the calculated and actual results were obtained. The theory predicts that the depth of internal oxidation decreases with increase in solute content. This is demonstrated by comparison of the depth of internal oxidation on the aluminium-treated steel (1.54% manganese and 0.18% silicon) and the silicon-killed steel (0.8% manganese and 0.28% silicon) and on the semi-killed steel (0.65% manganese) and the rimming steel (0.34% manganese) (Fig.44). The important feature is the amount of solute in solution in the metal and not the amount present as shown by the bulk analysis, as some is present in steel-making deoxidation products.

4.3.3 Oxidation Kinetics

From the results shown in Figs.49-52 the oxidation appears to follow an approximately parabolic rate law. If parabolic oxidation is assumed then the oxidation rate constant for each temperature and steel studied can be calculated as detailed in Appendix 2. The results are shown plotted in Fig.53 and this can be used to interpolate values of kp not experimentally determined to enable some practical

use to be made of this data, as detailed later. However the Arrhenius plot shown in Fig.53 does not obey a linear relationship with temperature, and this suggests that the mechanism of oxidation is not parabolic. In addition if the results shown in Figs.49-52 are closely examined there is a tendency for the oxidation to follow a linear relationship with time for the higher temperatures and longer times studied. This can be demonstrated by plotting the incremental parabolic rate constant kp for each five minute time interval. For example the incremental parabolic rate constant for the silicon-killed steel oxidised at 1325°C are shown in Fig.54. After the initial high value probably caused by the exothermic reaction of the oxidising gases with the bare metal surface, a rapidly increasing kp resulted. Obviously, parabolic rate laws are not obeyed in this case. If it is assumed that the oxidation follows a constant non-parabolic rate e.g. $w^n = k_n t$, the incremental k_n values can be calculated and are shown plotted on Fig.54 also. Neglecting the initial high value, the resulting rate constant is considerably more consistent than the kp values. However there is still a tendency for the value of k_n to increase with time. The value of n can be determined from the slope of a log w versus log t plot, which should produce a straight line relationship if a consistent oxidation rate is followed. If a linear oxidation rate law was obeyed the value of n would be unity, and for a parabolic rate a value of 2 would result. Such log/log plots are shown in Figs.55-58 for each five

minute time interval of each steel and temperature studied. These clearly demonstrate that not only is the parabolic rate law rarely approached but that consistent rate laws are also seldom achieved. Even with the well known characteristic of the log/log plot, which tends towards a straight line relationship because of the compression of higher numerical values on the log scale, many of the lines produced are increasing in slope at the higher temperatures, indicating an increasing oxidation rate with time. For this reason, the extrapolation of this data to longer times, for example to correlate with the oxidation obtained in soaking pits, must be suspect. For short re-heating times however, reasonable correlations can be achieved and this will be discussed later.

For fundamental consideration the log/log plots are extremely useful and may be used in conjunction with metallographic studies to investigate the mechanisms of oxidation. With the silicon-killed steels for example there is a tendency for the oxidation rate to gradually decrease with time at 950°C. Factors which may cause this decreasing rate are the build-up of fayalite particles in the scale at the metal/scale interface, restricting the diffusion of iron ions through the scale (See Figs.26 and 27). A build-up of residual elements in the metal surface layer would have a similar effect by presenting a thickening barrier to the diffusion of Fe-ions into the scale. However enrichment

effects should also occur on the other steels examined which do not show the decreasing rate, at 950°C but a reasonably constant slope which has a value of less than 2. Consequently the oxidation is not governed only by diffusion in the solid scale lattice and it is likely that the ingress of oxygen is possible through cracks in the scale. Certainly evidence of such cracks has been observed which contained the higher oxide of iron indicating that they were in existence at the oxidising temperature and were not caused by cooling or mechanical polishing stresses. These were observed to be in close proximity to the metal surface on all steels studied (Figs.20,22,26 and 27). Consequently the faster than parabolic rate observed on the rimming and balanced steels at 950°C is caused by cracking of the scale layer, allowing direct access of the oxidising gases. Although similar cracks were observed in the scales on the silicon-killed steels, these steels exhibit a gradually decreasing oxidation rate at 950°C tending towards the parabolic rate. This is thought to be caused by the build up of a layer of fayalite particles at the metal surface.

At oxidation temperatures of 1050°C and 1150°C differences were again observed in the shape of the log/log plots between the steels containing silicon and those essentially silicon-free. The rimming and semi-killed steels exhibit an initially high, gradually decreasing oxidation rate, tending towards parabolic, whereas the steels containing silicon showed gradually increasing oxidation rates faster than an initial parabolic law. The high initial oxidation rates obtained on the rimming and semi-killed steels tend

towards a linear oxidation rate indicating that non-protective scales are formed. Cracking of the scale layer both normal and parallel to the specimen surface would allow the ingress of oxidising gases and a rapid oxidation rate would ensue. As oxidation proceeded, self healing of cracks, enrichment effects at the metal surface and the build up of surface irregularity would all tend to reduce the rate of oxidation. The gradually increasing oxidation rate obtained for the rimming and semi-killed steels at 1250°C and above and for the steels containing silicon at 1050°C and above are the result of many complex mechanisms, although the temperatures at which this behaviour commences is much lower for steels containing silicon and hence liquid phases may have a pronounced effect.

4.3.3.1 Effect of Liquid Phases

Liquid phases have been observed in the metal/scale entangled layer and at the tips of the scale intrusions into the metal, and at the higher temperatures a grain boundary network of liquid phases was observed in the inner FeO layer. Tholander[27] has observed increasing oxidation rates in the presence of liquid phases in the scale layers which were postulated to act as an 'oxygen pump'. Solution of oxygen in the eutectic could occur in this case at some point between the magnetite/wüstite interface and the steel surface. This would diffuse to the metal surface more rapidly than the outward lattice diffusion of iron and hence causes

the accelerated oxidation. Similarly the liquid phase may act as a diffusion path for iron ions which would also increase the oxidation rate. In the presence of a liquid phase, iron migration into the scale could take place and the vacancies generated in the metal surface be removed by the inwards flow of the liquid thus allowing metal/scale contact to be maintained. Liquid phase flow in this manner has also been postulated to maintain metal/scale contact when irregular metal/scale interfaces are produced[51] and liquid phases at the interface may thus promote the growth of metal/scale entanglement.

4.3.3.2 Effect of Cracks and Pores

The presence of discrete porosity in the scales effectively reduces the area of scale available for lattice diffusion and should therefore reduce the oxidation rate. However, in the scales observed in this case many of the pores in the scale were seen to contain higher oxides on their inner surfaces and this would suggest the presence of oxidising gases. In many cases such porosity was seen to be connected by cracks in the scale also containing the higher oxides of iron, indicating that oxidising gases can penetrate the scale layers almost to the metal surface itself. Such cracks were observed throughout the scale layers and evidence for the healing of these cracks in the form of continuous lines of magnetite in the FeO layer was observed. It is thus likely that the formation, by growth stresses and healing of these cracks by oxidation is taking place continuously. In addition Rahmel[56] has shown that porosity can be stabilised

by gaseous mixtures of CO/CO_2 or H_2/H_2O and that oxidation can be increased by gaseous transport across pores by a reduction/oxidation reaction. Also it has been postulated[66] that the ingress of SO_2 can take place via pores in the scale and hence cracks and inter-connected porosity will increase the amount of liquid sulphur-rich phases in the scale. The amount of cracks, pores and fissures increases with time and will therefore tend to give an increasing oxidation rate at constant temperature.

To what extent the cracking observed in the scales in this investigation is caused by the geometry of the specimen is not known. Cracking of the scale has been shown to occur at the corners of rectangular specimens[2,4], and on small diameter specimens[74] oxidised in air, and a reduction in the oxidation rate resulted. With atmospheres containing CO_2 or/and H_2O however Rahmel[56] has shown that cracking of the scale on small diameter specimens is replaced by a porous adherent scale layer with an increase in oxidation rate over that obtained in an oxygen atmosphere. In addition early work by Preece and Riley[37] using cylindrical specimens with a length to diameter ratio of between 0.33 and 10 found little influence of specimen dimensions on the oxidation obtained in atmospheres containing CO_2 and H_2O. Certainly the scales formed on the specimens examined in this investigation are very similar in structure to those formed on commercial billets observed by Sachs and Tuck[39] and Moreau

and Cagnet[24], with the possible exception of the large fissures parallel to the metal surface. Ideally an infinitely flat surface is required, this is impractical and possibly the closest practical approach would be a thin sheet specimen. However for high temperature oxidation it is also necessary to consider the surface area to volume ratio (specific area)[75] which should be low if high initial specimen temperatures caused by the exothermic oxidation reaction are to be dissipated. To this end a spherical specimen is ideal but impractical as a very large sphere would be required to approach a plane surface and they are also very difficult to prepare.

The cylindrical specimens used in this investigation are thus a compromise, but the weight carrying capacity of the continuously recording balance used enabled a very large specimen to be studied (initial specimen weight approx 140 g). In addition the results are shown later to give reasonable correlation with the commercial oxidation obtained in reheating furnaces and hence specimen geometry effects are not considered to have influenced the results to a marked extent.

4.3.3.3 Effect of Enrichment

Elements more noble than iron, notably nickel and to some extent copper have been shown to concentrate in the metal surface because of the preferential oxidation of iron. Under planar interface conditions this would result in a build-up of a diffusion barrier to the outward migration of iron. However, such elements have been shown to promote the formation of irregular interfaces[51,52,54,55], which has been explained by considering the relative diffusion rates in the alloy and scale[57]. Planar metal/scale interfaces are

only stable if diffusion in the alloy is relatively rapid compared with diffusion in the oxide. In addition when very irregular interfaces are produced such as the metal scale entangled band observed here the predominant diffusion of the more noble elements take place laterally with respect to the moving interface and it was postulated[57] that the oxidation rate should be only slightly affected. Steels containing 0.4% Ni and exhibiting metal/scale entanglement have been shown to oxidise less rapidly than pure iron[52]. However, the depth of entanglement increases with time, especially in the presence of a liquid phase and the increasing surface area of specimen surface with time may result in an increasing oxidation rate at constant temperature. In addition it has been postulated[69] that liquid phases containing sulphur can attack layers of metal enriched in Cu and Ni.

Summary of 4.3.3.

The mechanisms of high temperature oxidation of commercial steels oxidised in the products of combustion of fuel oils containing sulphur are thus very complex. That the oxidation obtained can be approximated to a parabolic rate law must be largely coincidental, and the assumption that the oxidation is explained by lattice diffusion of iron through the scale layers is erroneous. An attempt has been made by careful examination of the data and detailed metallographic study of the scale and metal surface to explain the deviations from parabolic oxidation obtained in this case. From the practical point of view however, it is convenient to express the oxidation obtained in terms of the parabolic law in order that laboratory data may be used, with reservations, for commercial re-heating simulation. The

methods used for calculating the oxidation obtained under commercial conditions from the isothermal laboratory data are detailed in Appendix 4.

4.3.4 Correlation with Practice

The oxidation obtained on 230 mm square blooms of a rimming steel, a balanced (semi-killed) steel and a silicon-killed steel re-heated in a pusher type furnace heated with uncleaned coke oven gas is detailed below. The chemical analyses of these steels are given in Table 3(b). To obtain a record of the temperature achieved by each bloom during passage through the reheating furnace Pyrotenax thermocouples (Chromel-Alumel thermocouple sheathed in a stainless steel tube packed with refractory material) were peened into the surface of the blooms as shown in Fig.59. In this way the temperatures of the top and bottom surfaces and the central temperature in each bloom was determined, the results are shown in Figs.60-62. Flat bottomed holes were drilled normal to flat machined regions on the blooms on the top and bottom surfaces to determine the amount of oxidation produced by the heating. This technique uses the fact that the base of the hole does not oxidise because of poor atmosphere circulation and can thus be used as a reference point.

The three blooms were reheated separately under different furnace throughout rates. The reheating temperatures used were the same in each case, and furnace atmosphere analysis was carried out above the stock during the passage of the first trial bloom through the furnace. The results of this analysis are detailed in Table 5. The furnace used was a

conventional pusher furnace which was top fired in both the preheat and the soak zone but underfiring was also used in part of the preheat zone, the stock resting on the refractory hearth thereafter. The actual temperatures used for the trials were 1360°C for the preheat zones and 1340°C for the soaking zone. After reheating the blooms were discharged and the change in depths of the drilled holes determined after the removal of surface scale by grit blasting. Samples were also taken from each hole position for metallographic examination of the surfaces produced on both machined and as normally charged bloom surface areas. Measurement of the depth of metal scale entanglement, grain boundary penetration, and internal oxidation in each position were also taken and the results are shown in Table 6. For the purposes of the prediction, extrapolated temperatures were used for the time spent in the furnace after the thermocouples ceased to operate (see Figs.60-62) and the results of the predictions are also listed in Table 6.

Large variations were obtained in the oxidation characteristics on a given material along the length of the bloom on both top and bottom surfaces. Possible reasons for this are atmosphere and temperature variations in the furnace. The results of the atmosphere analysis carried out during the first trial shows that the atmosphere composition is not constant (see Table 5) and appears to be more oxidising on one side of the furnace. Also, temperature measurement along the length of the blooms indicates that in addition to large temperature differentials the furnace is hotter on one side in the preheat zone and on the other side in the soak zone.

In addition, in the case of the rimming and the silicon-killed steel, more oxidation occurred on one side of the furnace, and this is caused by higher temperatures and air infiltration.

The prediction techniques used have produced encouraging results in that the predicted values are comparable to the measured values obtained. However, the large variation in the measured values and the incomplete stock temperature/time record which necessitated the use of extrapolated values for the calculation have resulted in some discrepancy. Variable atmosphere conditions and steel composition would also tend to reduce the correlation. As a further verification of the prediction techniques used a specimen of the semi-killed steel as used in the laboratory isothermal treatments was subjected to a laboratory simulated reheating treatment as received by the semi-killed steel in the pusher furnace. Reasonably good correlation between the predicted and simulated results was obtained and the results are shown in Table 6.

4.4 Conclusions

The oxidation of the four steels examined in the products of combustion of uncleaned coke oven gas are very similar. They all exhibit metal scale entanglement, internal oxidation and grain boundary penetration in the metal-scale interface zone to varying degrees. Grain boundary penetration and internal oxidation effects are considered less important from the scale adhesion point of view than the metal scale

entanglement phenomena. Less metal scale entanglement was found on rimming steel and this is probably due to the lower nickel content of this steel compared to the other steels examined which were all of approximately the same nickel content. However, differences in the depths of metal scale entanglement were also obtained on the other steels and obviously other factors are involved and more work is required on this topic. The amount of oxidation which occurred on all four steels was very similar also and was found to increase rapidly with temperature and only approximately parabolically with time. The departures from ideal parabolic behaviour are thought to be caused by cracks and pores in the scale layers containing oxidising gases and liquid phases in the scales, e.g. fayalite-wüstite eutectics and FeS-FeO eutectics, and enriched layers at the metal surface. Methods of predicting the oxidation characteristics obtained under commercial reheating conditions from the isothermal data reported here show reasonably good correlation.

5. PHYSICAL ASSESSMENT OF SCALE ADHESION

The work described above provides information on the characteristics of the scale and scale/metal interface region. In this section a technique for measuring the scale metal adherence is described and the results are discussed in relation to the results of the preceeding section.

5.1 Experimental Procedure and Description of Apparatus

In essence the adherence is determined by detaching the scale on the circular end of a solid cylindrical specimen

using a stainless steel gauze embedded into the scale layer during oxidation. The original apparatus (see Fig.63) consisted of a modified Dennison creep testing machine. The load was applied by hand, by turning the handle and measured using a spring balance shown with due allowance made for the magnification ratio of the beam. This apparatus suffered from problems of specimen/gauze alignment, variable strain rate, and inaccuracies in load measurement and very variable results were obtained. Nevertheless, the technique was thought to show promise and modifications were made. The modified assembly is shown in Fig.64. The specimen and gauze rod are attached rigidly with screw threads to shafts running in linear bearings. The gauze extension rod bearing, is generously sized and of square cross section so that no torsional stresses should be transmitted to the gauze by the loading mechanism, Straining the specimen assembly was affected by a small variable speed electric motor, with a constant speed thyristor control which was geared to the large gear (gear A) causing this to rotate. The linear bearing shaft was threaded on the top portion externally and passed through internal threads on this gear. Hence, as the large gear revolved, the shaft was moved either up for testing or down for application of the gauze, depending on the direction of rotation of the motor. Thrust on the gear was taken by roller bearings as shown between the gear and machine chassis. A linear roller bearing and shaft assembly was used which

allowed the specimen/extension rod assembly to move freely in the vertical plane and to rotate and at the same time the lateral movement of the specimen was reduced to a minimum giving good alignment of specimen and gauze. The load measurement was achieved with strain gauges on a beam of alloy steel (Jethete M.152). One end of this was rigidly attached to the machine frame, the other end contacted collars on the extended linear bearing shaft. The strain gauge circuit was arranged in a full Wheatstones Bridge design, half on top of the beam and half beneath the beam, for maximum sensitivity and to give a linear output in compression and in tension. The output from the strain gauge circuit, that is the out of balance of the bridge was recorded using a mirror galvanometer and an ultra violet recorder. This was calibrated by removing the beam mounting block from the machine and holding securely in a vice, the deflection of a mirror galvanometer was then measured for different loads on the strain gauge beam and typical calibration graphs are shown in Fig.65. Calibration was checked regularly during testing as the strain gauges which were attached to the beam using epoxy resin can become detached quite easily. The compression calibration could be done in-situ by placing weights on top of the bearing shaft.

The furnace used was a platinum resistance furnace controlled by a West Guardsman controller on a maximum/minimum current principle and the temperature measurement was affected using

platinum/platinum rhodium couples in alumina sheaths in the hot zone of the furnace. The furnace gave a hot zone approximately 75 mm long with a temperature variation in this zone of plus or minus 5°C and the test surface of the specimen was placed in the middle of this zone. The top and bottom of the furnace were plugged with a refractory wool (Kaowool) and the simulated atmosphere consisting of 6% O_2, 6% CO_2, 15% H_2O, 0.125% SO_2, balance N_2, was introduced at the bottom of the furnace through an alumina tube. With a flow rate of 10 litres per minute, a slight positive pressure was maintained in the furnace and hence in-leakage of air was unlikely. The specimen used was a 19 mm dia x 50 mm long cylinder with the cylindrical end machine ground to the same surface finish as used in the oxidation tests described earlier (16 C.L.A.). This specimen size in the furnace used, gave approximately the same atmosphere velocity and also had adequate specific volume especially as the maximum temperature used was 1200°C in these tests. The gauze used was made of 18/8 stainless steel of 23 standard wire gauge, (i.e. 0.6 mm dia. with 8 wires per centimetre) and was formed into a box shape with an 18/8 stainless steel strip support to prevent collapse of the box and hold the gauze surface parallel to the specimen surface during testing. The whole assembly was held onto a screwed extension rod of 25/20 chrome-nickel steel with a stainless steel nut. The nut, gauze and support were expendable and were replaced for each test. The specimen and gauze assembly is shown in Fig.66, before and after oxidation. A platinum/rhodium thermocouple was used as shown, to check the specimen temperature during reheating

at the test temperature in nitrogen prior to oxidation. Contamination of this thermocouple occurred soon after the test commenced, probably because of iron oxide contamination at the higher temperatures. The accuracy of this couple was checked after each test by comparison with a standard thermocouple and it was remade to the original specification by discarding the contaminated zone, later a nimonic tube was fitted around part of the specimen length and the thermocouple was attached to this and contamination effects were found to be reduced. The specimen and gauze assembly were connected to the linear bearings with extension rods and put into the furnace, the test surface was placed in close proximity to the furnace control couple and the gauze was aligned with the test surface approximately 0.5 centimetres away. The top and the bottom of the furnace was packed with refractory wool, and nitrogen (white spot i.e. 'oxygen free') was introduced into the bottom of the furnace through an alumina tube. The specimen was allowed to attain the test temperature and equalise in temperature, and if necessary the furnace control setting was changed at this point to get the specimen to the correct temperature as shown by the specimen thermocouple. When the specimen was fully soaked at the correct test temperature, the atmosphere (nitrogen) was replaced by the oxidising atmosphere. After a standard time of half an hour, which was found by experience, the gauze was brought into contact with the test surface under a

constant load of 500 grams using the constant speed electric motor. At the end of the oxidation time, the refractory wool from the bottom of the furnace was removed as this had been found to interfere with the load measurement and the gauze was detached at a standard cross head velocity of 2.0 mm/min. Oxidation times of 1, $1\frac{1}{2}$ and 2 hours and temperatures of 1050, 1100, 1150 and 1200°C were used for each of the steels examined above (Table 3(a)). It was found that with lower temperatures or shorter times the gauze did not become embedded in the scale layers and hence failed to detach the scale when tested. With higher temperatures and longer times the oxidation and temperature reduced the load carrying capacity of the gauze and the gauze itself was pulled apart when the specimen was tested. The load required to detach the scale was measured, using the precalibrated strain gauge beam and ultra violet recorder as described above and after testing the gauze and specimen assembly was removed from the furnace and the detached scale inspected. Only tests which showed 100% detachment of the original scale (neglecting the scale formed by oxidation of the test surface after detachment) over the full circular face were recorded. The scaled specimen diameter was measured with a micrometer and the scale adhesion expressed as the total load divided by the total cross sectional area of the scaled specimen (i.e. the average stress in the specimen at the time of failure).

Specimens after testing always exhibited some scale on the fractured surface because of oxidation after removal of the initial scale layer. To determine the position of

fracture and thus determine whether scale cohesion or scale adhesion was being measured it was essential to prevent oxidation of the metal immediately after testing and during cooling to room temperature. It was found impossible to do this with the furnace arrangement as shown and an assembly shown in Fig.67 was devised. The specimen and gauze assembly was enclosed in a thin wall, large diameter tube of fused silica, tightly plugged at its ends with the same refractory wool used above and which could be assembled outside the furnace, inserted into the furnace for testing, and removed after testing without dismantling. The semi-transparent fused silica enabled the specimen/gauze alignment to be checked on assembly into the apparatus and the tests were carried out in the same way as before with the exception that immediately before testing, the oxidising atmosphere was replaced with commercial pure argon (99.999% pure) which was passed through a pyrex boiling tube immersed in liquid oxygen as a cooling device. The heat exchange was sufficiently efficient that some liquid argon was formed in the boiling tube. The flow rate was set at 10 litres per minute and after flushing the whole assembly for about five minutes, the gauze was detached at the same crosshead speed as used for the previous tests, no load measurements were possible in these cases because the Kaowool was not removed from the bottom of the furnace. After testing the flow rate was increased to 25 litres per minute during removal of the assembly from the furnace and after removal from the furnace the flow rate was reduced and the assembly left to cool to room temperature. The resulting

fracture surfaces were examined visually and by a stereoscan scanning electron microscope and they were also sectioned for normal optical metallographic examination as described above. Specimens from each cast (Table 3(a)) were given standard oxidation times of 1 hour at temperatures of 1050, 1100, 1150 and 1200°C to determine the position of fracture.

5.2 Results

The surfaces of the specimens after detachment of the scale appeared in most cases essentially scale free when protected from further oxidation (Fig.68). In most cases small pieces of scale from the inner FeO layer were left randomly distributed over the surface. Examination with the stereoscan revealed extensive areas on each specimen which were virtually scale free. Transverse sections through the metal surface after removal of the scale layer on the silicon-killed steel are shown in Fig.69 and the results of the Stereoscan examination on the fracture surfaces of the scale and metal are shown in Figs.70,71 and 72. On the silicon-killed steel at 1050°C the metal surface showed some protrusions of metal filaments, holes in the surface and pits containing scale (Fig.70). Some scale also adhered to the metal protrusions. Grain boundaries appeared as lines of irregular fissures and the scale was not a mirror image of the metal surface and consisted of many small rounded particles of scale. The Stereoscan results complemented the transverse microscopy. At 1100°C (Fig.71) the surfaces obtained were very similar except that they were much more irregular and the protrusions of metal were larger, the scale again, had

the appearance of boulders (Fig.72(a)). Similar results were obtained at 1150°C and 1200°C with the surfaces becoming more irregular and the general size and length of the protrusions increasing. Some geometrical shapes were found on the scale fractured surfaces on the Si-killed steel in some cases (Fig.72(c)). The surfaces found on the aluminium-treated steel at 1050°C (see Figs.73 and 74) were not as irregular as those produced on the silicon-killed steel at this temperature. In addition, there were some essentially planar areas on the metal surface which were covered with a fine angular precipitate. These areas constituted a relatively small proportion of the specimen surface and were randomly distributed over the entire specimen surface. At higher temperatures, the irregularity of the specimen surface increased and at 1100°C was similar to that found on the silicon-killed steel in some areas, but in other areas some evidence of the angular precipitate on less irregular surfaces was to be found. The metal surface increased in irregularity with reheating temperature although there was still some evidence of the angular precipitate even at 1150°C and 1200°C in small isolated areas. In no case were the angular particles found on the fractured scale surface.

The results on the balanced steel shown in Figs.78 and 79 were similar to those found on the silicon-killed steel in that the surfaces were irregular and the metal protrusions and pits increased with increasing temperature. No angular precipitates were observed on any of the specimens of balanced

steel and the scale was similar to that found on the fractured surfaces of the silicon-killed steel, The results of the rimming steel are shown in Figs.80 and 81 and the surfaces produced at 1050°C were extremely planar and contained much more oxide than the specimen examined at 1100°C, the metal surface was again essentially planar with small protrusions and pits with less scale on the surface and at 1150°C the irregularity increased, but it was not until a temperature of 1200°C was reached, that the fractured metal surface took on the appearance of marked protrusions and pits similar to that found on the other steels examined.

The results of the scale adhesion measurement tests are shown in Figs.82-85. For all specimens examined the results were found to be of the same order of magnitude. The adhesion appeared to increase with time although no clear trend in this respect was found in the case of the aluminium-treated steel at all temperatures and times studied and with the silicon-killed steel at temperatures below 1100°C. The results plotted are the average of four tests at each temperature and time showing full scale detachment and the variation in the results were approximately $\pm$ 25% of the load measured for the silicon-killed steels at temperatures less than 1100°C and the aluminium-killed steel at all test conditions, to approximately $\pm$ 10% in the other cases. The adhesion increased rapidly with temperature above 1100°C and the highest adhesion of all was found at 1200°C with the silicon-killed steel. The aluminium-treated steel results were erratic and showed no clear trend with temperature.

The balanced steel results showed a steadily increasing adherence with temperature and the rimming steel had a very high adhesion at the low temperature 1050°C, the highest in fact of all the steels studied, but this decreased at 1100°C and increased thereafter similarly to the balanced steel quality.

5.3 Discussion

5.3.1 The Influence of the Gauze on the Oxidation Produced

The gauze element was found embedded in the outer FeO layer, and it is important for the method of assessing the scale adhesion that the gauze should not influence the natural scale adhesion of the specimen. The gauze may influence the adhesion in two ways, firstly by affecting the oxidation produced and hence the characteristics of the scale and scale metal interface which could have a pronounced effect on the scale adherence, and secondly, by maintaining the adhesion because of the compressive force applied to the scale by the preload on the gauze which is found to be necessary in order that the gauze should be well embedded into the scale.

5.3.1.1 Influence on Oxidation

Considerable oxidation of the 18/8 stainless steel gauze occurred in the FeO layer (see Fig.86), and evidence of spinel formation was observed in the scale immediately surrounding each wire element. The iron ion mobility in iron chromium spinel lattice is considerably less than that in the iron oxide lattice and in compact scales this would result in a restriction in the iron ion movement in the scale. [N.B. A Platinum gauze was tried to minimise this effect but this was not strong enough and was destroyed on testing]

In addition considerable reduction in the effective cross sectional area of the scale available for diffusion would be expected by the presence of the wire gauze element. Accordingly, measurements of the depth of grain boundary penetration and internal oxidation were made on the specimens used to determine the position of fracture of the scale and these results were found to compare favourably with those measured earlier. The results obtained indicate that the amount of oxidation and metal scale interface characteristics were not affected by the presence of the gauze. This is probably because of a marked gas phase transport and liquid phase transport down cracks in the outer scale layers as discussed above.

5.3.1.2 Maintenance of Adhesion

This was not a problem as the scales did not tend to become detached at the metal scale interface, however the fissures parallel to the metal surface in the scale were not as apparent on the scale adhesion specimens as on the specimens used for oxidation previously and this could be because of the pressure on the scale by the gauze increased the creep rate and consequently the fissures were not formed, and the coherency of the scale was maintained. Mackenzie and Birchenall[14] have shown that the creep of polycrystalline iron oxide can occur under the action of an applied stress and hence it is quite likely that this has occurred. It is also probable that because the planar interface was examined

in the scale adhesion test and not the cylindrical face as with the oxidation specimens examined previously, and the tendency to form this striated scale layer is less in the case of flat surfaces. However, one should still get the mutual support of the scales at the edges of the specimen which tends to form laminated scales on small specimens even on a planar surface as used here. In practice however, with large areas of billet or slab a laminated scale is not formed and hence the scale adhesion specimens simulate practical conditions more closely than the oxidation specimens used previously. In general similar types of porosity were observed in the scale layers as on the oxidation specimens, with the exception of the fissures parallel to the metal scale surface and hence this is further evidence that the gauze and the preload had very little effect on the oxidation. In earlier work the scales on specimens heated in air have been shown to have magnetite wedges growing along the scale metal interfaces at cracks in the scale at the specimen corners. This effect of cracking and magnetite formation has been observed by other workers[4], and its formation is described as being caused by the mutual support that the scale on each perpendicular surface affords for the other. This results in the scale being unable to follow the receding metal scale surface and loss of contact at the edges results, growth of magnetite along the metal surface takes place by the ingress of the oxidising atmosphere. Cracks and magnetite seams around the edges of the specimen are undesirable in this case as they will affect the scale adhesion results. An example of the type of scale found at the edges of the

specimens in this case shows that the edges remain essentially rectangular, (see Fig.87) with no magnetite formation and although there is a crack in the scale at the specimen corner, it does not contain magnetite and was probably formed during cooling because of thermal stresses. The metal surface also remained essentially level with no sign of concavity. The absence of cracks containing magnetite and magnetite wedges along the specimen surface in this case is probably related to the presence of water vapour and CO_2 in the atmosphere[56] which maintained oxidation at the metal surface, even with gap formation, by a gas phase transport as discussed earlier.

5.3.2 Analysis of Load Curve

The initial preload on the specimen assembly appears as a negative deflection of the strain gauge beam and consequently at the start of the test the removal of this preload appears as an increase in load. Further movement of the cross head picks the specimen assembly off the strain gauge beam and a flat portion BC (Fig.88) of the curve results until the bottom collar on the extended linear bearing shaft contacts the beam assembly and thereafter a steadily increasing load is applied to the scale metal surface as shown by line CD. Fracture occurred at point D with an instantaneous fall in load to a low point E, which was caused by bounce of the specimen and gauze on the beam, and recovery to point F with the specimen and extension rod and the linear bearing shaft resting on the strain gauge beam which was again under compression. The load was measured between point D and point F which consisted of the total tensile force on the specimen at the time of fracture. In certain instances when higher

temperature tests were attempted, for example 1250°C, curve CD', resulted, which was the steady fall in load caused by necking down of the gauze wires by plastic failure. The rapid decrease in load is evidence for the very rapid propagation of the crack and consequently crack initiation is thought to be the difficult stage in scale adhesion at these temperatures and not crack propagation. It is possible however that the plastic deformation of the scale at the interface is confined to a very small layer of material and small plastic deformations would not be detectable by this technique because of the deflection of the strain gauge beam. The figure presented for the scale adhesion assumes that the critical failure always occurs at the metal scale interface and not in the scale surrounding the edge of the specimen. This is reasonable in view of the tensile strength of the scale which is excessively greater than the loads measured in this case and by the fact that the scale cohesion has been found to be much greater than scale adhesion by Hulley and Rolls[80] although the figures quoted are not of the same order as those found here. The calculation of the load divided by the total specimen-plus-scale area assumes that the stress is evenly distributed over the whole cross section of the specimen scale composite at the point of fracture, this is obviously very difficult to achieve in practice because of stress concentration effects and misalignment, but these effects cannot be compensated for.

5.3.4 Analysis of Scale Adhesion Results

5.3.4.1 Silicon-Killed Steel

The relatively low adhesion at temperatures less than 1150°C and no clear trend with time at 1050°C are difficult to explain. However, in view of the scatter obtained at these temperatures with this test, which was of the order of ± 25% more testing is probably required to establish the trend in this case. However, similar results were obtained by Peters and Engell[23,76] on material cooled to room temperature in which no clear trend with reheating temperature was found and they attributed this to the presence of the solid fayalite in the scale at the metal scale interface. Solid fayalite particles have been observed in the scale layer on these steels at the metal scale interface on samples previously examined, reheated under identical conditions. However, at 1050°C evidence of melting of this phase and the presence of sulphur rich liquid was also observed and it is unlikely therefore that the fayalite particles behaved in a brittle manner under these conditions. At 1100°C the fayalite even if present as solid fayalite and not in conjunction with sulphur and therefore liquid, would have fairly high plasticity as the melting point of this phase is of the order of 1140°C. Consequently, brittle behaviour would not be expected and the scatter in the results cannot be attributed to a brittle behaviour of constituents in the scale at temperatures of 1050 and 1100°C. However, there is a clear trend with time at temperatures of 1100°C and above, the scale adhesion increasing with time

and this is probably because of the increasing amount of liquid phase formed at the metal scale interface with time and the increase in surface irregularity. The increase in scale adhesion with temperature was very marked above 1150°C and this also coincided with a marked increase in the metal scale entanglement and the amount of liquid phases in the scale layer.

5.3.4.2 Aluminium-Treated Steel

This steel which was silicon-killed with an aluminium addition did not show any clear relationship with time or temperature over the temperature and time conditions studied. Angular particles were observed on the metal surface after the detachment of the scale and protection from further oxidation in this case, at all the temperatures examined. The erratic results are thought to be caused by the presence of these particles leading to crack initiation in the scale at the interface at low stresses. This is a further indication that crack initiation is the controlling factor in scale adhesion at the heating temperatures and not crack propagation. The particles were analysed by an Ortec analyser (an attachment which can be used on a stereoscan to give a qualitative analysis of the field of view) and found to be aluminium rich. Similar results have been found by Bateman and Rolls[33] on steels containing more than 0.045% aluminium. They concluded that these were hircenite particles ($FeO.Al_2O_3$) and loss of adhesion was probably due to an increased creep resistance of the wüstite/Al_2O_3 solid solution layer and by enhanced crack propagation tendencies because of localised stress concentration

within the scale and because of the brittle nature of the particles relative to the scale. Under the conditions of the test reported here the particles were not found in the fractured scale layer and the failure appeared to have occurred at the particle scale surface and not within the particle or at the metal particle boundary. Consequently the particles were not brittle in this case and it is possible that growth of the particles at the interface resulted in stress in the FeO which tended to push the scale from the metal surface. The fact that these particles were found in small areas randomly distributed over the specimen surface and the total area of the specimen surface which contained particles was very small indeed, is further evidence to suggest that crack initiation is the main criterion in scale adhesion.

5.3.4.3 Rimming Steel

The very high scale adhesion obtained on rimming steel at the low temperature compared with the two silicon steels examined above indicated that the iron oxide bond is greater than the iron-silicon rich phase bond or the iron-sulphur rich bond. The presence of large areas of metal and scale on the stereoscan results shown in Fig.81(a) indicates that scale cohesion and scale adhesion is measured in this case and this probably explains the high results obtained in view of the high tensile strength of scale at these temperatures. Sulphur-rich phases were observed in the scale at the scale metal interface at 1100°C and this resulted in a decrease in the scale adhesion. The adhesion increased

with time with an increase in surface roughness at 1100°C. Increasing amounts of metal/scale entanglement at 1150 and 1200°C resulted in a steady increase in the scale adhesion. The increase in adhesion with temperature and time was not as marked in the case of rimming steel as with the silicon-killed steel examined above and this is probably because the metal scale entanglement was much less in the case of the rimming steel, and liquid phases which were sulphur-rich and probably of lower viscosity than the silicon-rich liquid phases, were not as extensive.

5.2.4.4 Balanced Steel

Similar results were obtained for the balanced steel as with the rimming steel with the exception of the low temperature (1050°C) results which were not as high in the case of the balanced steel as on the rimming steel. Metallographic examination of scales found on this steel under identical reheating conditions has been carried out earlier, and it is interesting to note that more sulphur-rich phase was found on the balanced steel at these temperatures, than on the rimming steel in the metal scale interface regions. The greater amounts of liquid sulphur phase found at 1050°C on the balanced steel probably explains the low scale adhesion obtained.

5.3.5 Mechanism of Adhesion

5.3.5.1 Metal/Scale Entanglement

The adhesion increases markedly with the depth of metal scale entanglement. This is most clearly demonstrated in the case of the silicon-killed steel, although liquid

phases also influence the adhesion for a given surface roughness as discussed later. The mechanism by which metal scale entanglement may increase the adhesion may include:

(a) a mechanical keying on effect,

(b) an increase in the surface area, and

(c) by its influence on the crack nucleation and propagation in the metal scale interface region.

For the mechanical keying on effect either the scale metal interface bond is separated or the metal filaments and scale in the entangled layer are ruptured. This does not show up on the load curve as plastic deformation as it is confined to a very small layer of material and the technique used for measuring the change in load during the test would not be sensitive enough to detect such very small plastic deformations. On examination of the stereoscan pictures it can be seen that there is some oxide still in the intrusions into the metal, the surfaces of the oxide are rounded and it is possible that these were liquid or at least very plastic at the temperature of testing and surface tension effects would tend to round any fracture surfaces. It is not considered that these would be very strong at the temperature of testing, especially at the higher temperatures. The metal filaments do not appear as long as one would have expected from the measurements taken of metal scale entanglement depths on transverse metallographic samples in a previous report. However, it is difficult to make accurate measurements on the stereoscan pictures because the angle of view is not known, also it is not known whether the filaments are

continuous as suggested by Brown[55], or whether they break up into discrete particles further out into the scale layer as proposed by Sachs[51]. Consequently the filaments may have been ruptured but the fractured ends of the filaments always appeared rounded on the stereoscan pictures, this could have been caused either by oxidation in the scale or by surface tension effects which may be sufficient to cause rounding of the drawn out fractured filament ends. It is difficult to see in many cases how the scale has been removed from beneath the filaments on the stereoscan photographs as there is often an interwoven effect. This may be caused by collapse of the filaments after removal of the scale as the test surface was in the horizontal plane, with the filaments pointing upwards and they would therefore tend to collapse under their own weight. The scale did not appear as a mirror image of the metal surface at the high temperatures and this was again probably caused by surface tension effects and liquid phases in the scale. There was very little scale left on the metal in most cases except the protrusions into the metal and consequently the strength of the metal scale bond at the high temperatures was not very great and is not as high for example as on the rimming steel at 1050°C when a considerable amount of scale was seen to be adhering to the metal surface. Consequently, it is concluded that the increase in adhesion must be caused by a keying on effect of the filaments coupled with a low scale metal bond but a very high specimen surface area. Because of the importance of metal scale entanglement in scale adhesion, the mechanisms of formation of the entangled layer will be considered in a later section . The effect of metal scale entanglement on

increasing scale adhesion has also been indicated by the examination of a pitted plate sample, (see Fig.90) the metal scale interface region from a transverse metallographic sample taken from the pitted area has the appearance of a deformed entangled structure, there is however, very little liquid phase present and this would not have been expected from the results of a previous report and this matter will be discussed later.

5.3.5.2 Effect of Liquid Phases

At low temperatures, the liquid phases formed on the rimming steel and the silicon-killed steels appeared to have decreased the adhesion. The adhesion being high for example at 1050°C on the rimming steel compared to the balanced steel or the silicon-killed steel and this is probably because there is very little liquid phase present at the metal scale interface region on the rimming steel at this temperature. A decrease in adhesion on the rimming and silicon-killed steels may have been caused by an increase in the amount of liquid phase and an increase in plasticity of the scale at the interface because of the exothermic oxidation reaction[27]. Evidence of melting of the silicon-rich phase at 1050°C for example would indicate that the interface region temperature is considerably higher than the furnace temperature, although this phase did contain some sulphur which would have also lowered its melting point[92]. At the high temperatures it is very difficult to separate the effects of liquid phases and metal scale entanglement. Comparing the balanced steel, Fig.85 and the rimming steel,

Fig.89 the same liquid phase is present in both these cases, (sulphur-rich), and very similar results were obtained at 1100°C and above although the balanced steel has considerably more entanglement and more liquid phases than the rimming steel in all cases. Consequently, it is likely that the sulphur-rich liquid phases decrease the adherence for a given surface roughness. Silicon- killed steels have the greatest scale metal entanglement and also the greatest high temperature adhesion and it is likely that the liquid phase especially if silicon-rich increases the depth of metal scale entanglement.

The results of the metallographic examination of the pitted sample is puzzling, as from the metallographic examination of reheated specimens of the silicon-killed steel it would be expected that there should be large amounts of liquid phases present in the interface region. However, no liquid phase was observed in the oxide metal compacted zone. Consequently a sample of silicon-killed steel (Table 3(c)) was given a simulated reheating treatment in the laboratory, which consisted of reheating for five hours at 1250°C in a furnace fired with towns gas. Subsequently, this was rolled down by 75% with every effort being made to maintain the scale on the material before it entered the roll gap. The resulting scale metal interface is shown in Fig.91 and it is similar to the one found on the pitted plate sample shown in Fig.90 with due allowance for the differing amounts of deformation. Examination of the outer scale layers from the material rolled in the laboratory indicates that the liquid phases have been forced from the interface region into cracks in the outer layer. This is very important in practice as

the method used for scale removal is often high pressure water. The actual action of the high pressure water is not clear[87] but the scale may be removed by a penetration of water down the cracks where steam is generated explosively leading to removal of the scale. Consequently, if the material is rolled before the high pressure water is applied the liquid from the interface region will be forced into cracks in the outer scale layer and penetration of the water down the cracks would therefore be impossible. It is also possible that scale cohesion would be improved by the presence of the liquid and consequently removal of the scale by the kinetic energy of the water which has also been suggested as the mechanism of high pressure water descaling[87] would be difficult. A further consideration is that the iron scale bond is very strong as shown by the low temperature rimming steel results and if all the liquid phases were moved from the interface region, the adhesion may be considerably increased, especially with an entangled interface structure. Consequently it is imperative that the scale is removed from the material prior to it being passed into the roll gap.

5.3.5.3 The Effect of Crystalline Phases at the Metal Scale Interface

The case of the silicon-killed steel containing aluminium deserves special mention as very low and erratic results were produced by the presence of aluminium rich particles at the scale metal interface. These particles were most probably formed by an internal oxidation mechanism, and

the random and infrequent location of these particles on the metal surface may have been caused by segregation effects in the steel. From the stereoscan photographs they appear to have a very crystalline morphology and appear on the metal surface and not on the scale surface. Consequently they have a higher affinity for the metal than for the scale, very low solubility in the scale and a high melting point. The growth of these particles may tend to push the scale away from the metal surface and lead to crack nucleation. They did not appear to have been fractured and it is also likely that these particles can act as stress raisers at the metal scale interface and separation of the scale from the particle may be easy, consequently cracks nucleate and propagate along the particle scale interface. It was not possible to positively identify the chemical composition of these particles and consequently their melting temperature is not known. It is therefore possible that they may not be effective in reducing the scale adhesion and reheating temperatures in excess of 1200^{o}C because of liquefaction.

5.3.6 Comparison with Other Workers

It should be noted that in this section although the results referred to in this exercise have been shown to be a measurement of scale adhesion this is not true in all other cases mentioned and it is possible that scale cohesion was being measured. In general, scale adhesion was found to increase with time in this exercise and this is in agreement with the qualitative methods which express the 'adhesion' as the amount of adherent scale remaining after the test.

This parameter is used in the quench test[58] and in the hammer test[64] and in addition the hot detachment test of Hulley and Rolls[80] indicates that 'adhesion' increases with time to a maximum of $4\frac{1}{2}$ hours and thereafter decreases with time. The other methods of testing for example, the bend[33,63], and the impact test[28] give opposing results in that the 'adhesion' was found to decrease with the time of reheating and this is probably caused by the use of a parameter which does not effectively reflect the scale adhesion.

Adhesion was found to decrease in general with temperature at temperatures less than 1100°C and this is in agreement with work by Hulley and Rolls[80] who found that in the temperature range 850-1050°C adhesion decreased with temperature although there is considerable discrepancy between the value of the actual adhesion force measured using Hulley and Rolls' test and the tests referred to here. The results of Bruce and Hancock[74] for the temperature range 850-1050°C do not agree with either of these results as they indicate that the 'adhesion' increased with temperature in this range, However the method of calculating 'adhesion' is rather empirical. This method is however in agreement with other methods of measuring scale 'adhesion' for example, the bend tests[33,63] and the impact testing[28].

The effect of liquid phases is not clear from the present work and it appears that below temperatures of 1100°C liquid phases appear to decrease the adhesion and above 1100°C an increase in adhesion results but it is not clear whether this is due partly to the liquid phase or wholly to the

metal scale entanglement. It is possible of course that liquid phases increase the metal scale entanglement and therefore increases adhesion in that way. Several other workers have found an influence of liquid phases on scale adhesion, for example with the quench test[58], sulphur dioxide pick-up from the atmosphere was found to increase the 'adhesion', with the impact test[28], liquid phases were also found to increase the 'adhesion' but this probably increased the cohesion of the scale, because in this case the parameter was the ratio of the amount of adherent scale to the total scale formed and this test failed to show the increase in 'adhesion' with temperature and time. The ha mmer test[64] found that 'adhesion' increased with low excess air values with a sulphur-rich fuel and this is obviously caused by liquid sulphur pick-up in the scale. The influence of the solid aluminium rich phases at the metal surface which were found to decrease the adhesion confirmed the work of Bateman and Rolls[33] using a bend test and the parameter used in this case was again a ratio of the adherent scale to the non-adherent scale and this indicates that aluminium additions probably have a similar effect on the scale adhesion as on the scale cohesion in that Rolls found a decrease in 'adhesion' as measured by his parameter because of the aluminium particles. However, it is also confirmed by work done by Peters and Engell[23] on the room temperature tensile strength of the metal scale bond in which aluminium was found to decrease the load required to detach the scale.

The mechanical keying on effect of the metal scale

entanglement has been suggested by Sachs at et[51] based on metallographic observation of nickel steels and rolled in scale defects and also by Hough and Rolls using the impact test[63] in which it was found that scale 'adhesion' was increased by a mechanical keying on effect of the metal scale surface. This test again failed to show up many of the effects of time and temperature and it is therefore likely that the effect of the mechanical keying on was very marked for this test to be able to show an influence of this factor on scale 'adhesion'.

5.3.7 Practical Consideration

The object of this study was to provide information on scale adhesion so that the adherences of scale to steel may be more effectively controlled during reheating and hot working operations. The results of this investigation have shown that with the exception of the aluminium-treated steels and the rimming steel at 1050°C the adhesion increases with temperature in the range 1050-1200°C because of the increase in the metal scale entanglement and the presence of liquid phases in the scale at the metal scale interface region. Consequently, if the materials examined in this report could be reheated and hot worked below 1150°C with short reheating times, the results indicate that there would be very little difficulty in removing the scale. However, it is often the case that the material is reheated at temperatures in excess of 1300°C and a simple extrapolation of the data presented here leads to the obvious conclusion that the effect of such practice is very detrimental to scale

adhesion. Nevertheless it is impossible to roll material at low temperatures in many instances, large thin plates for example invariably are produced from thick slabs which require long reheating times and high initial rolling temperatures in order that the final rolling pass is performed above the minimum rolling temperature for these particular steels. Within such limitations anything which can be done to reduce the depth of metal scale entanglement and the amount of liquid phases in the scale layer will be beneficial. It has been shown that the depth of metal scale entanglement is directly related to the nickel content of the steel and consequently, steels should be manufactured with as low a nickel content as possible. In addition the amount of liquid phase in the scale can be reduced by maintaining the sulphur and silicon levels in the steel at as low a value as possible. High aluminium figures are beneficial if it is possible to include these in the steel during manufacture or other systems which would produce a second phase particle at the metal scale interface with a low solubility in iron oxide and a high melting point. It is difficult to envisage such a system which could be used for unkilled or balanced steels as it appears that these particles are produced in the metal surface by an internal oxidation mechanism and this implies that they have a higher affinity for oxygen than iron. Any addition of such elements would therefore tend to kill the steel. Even in fully killed steels a high aluminium in solution is detrimental in many instances because of the precipitation of aluminium nitride particles which considerably

lower the plasticity of the metal during hot working operations. Aluminium is also very detrimental to the free machining properties of steels and it is therefore obvious that there are many instances where such a technique as the introduction of aluminium to a steel to minimise scale adhesion would results in drawbacks in the fabrication of the product. During reheating, liquid phases can be introduced into the scale from the furnace atmosphere in sulphur bearing furnace atmospheres, especially if low oxygen contents in the furnace are used. With sulphur bearing fuels it is therefore important that high excess air values are used to give oxygen contents well in excess of about 4%. A reduction in the amount of oxidation would also lead to a reduction in the scale thickness and therefore a reduction in the amount of liquid phases and metal scale entanglement. Such a reduction can be brought about by reheating under controlled atmosphere conditions but this is usually rather expensive. Having reheated the material under the most favourable conditions and with the most favourable steel composition it is imperative to remove the scale before it enters the roll gap as discussed above.

5.4 Conclusions

A method has been developed to study the scale adhesion of mild steels under simulated reheating conditions at temperatures in the range 1050°C to 1200°C and a direct value of the adhesion is obtained.

The location of fracture was shown to be the scale metal interface in all cases and consequently the technique can be used for the measurement of scale adhesion as opposed to scale cohesion.

With silicon-killed steels the adhesion was found to increase markedly with temperature and time above 1150°C because of the increase in the depth of metal scale entanglement which resulted in an increase in surface area and a mechanical keying on effect.

A silicon-killed steel containing aluminium gave no clear trend with temperature or time over the conditions studied because of the presence of aluminium rich crystalline phases in discrete randomly distributed areas on the specimen surface leading to crack initiation at low stresses.

The adhesion on rimming steel increased with time and a high scale adhesion resulted at 1050°C in spite of a relatively planar metal surface, probably because there was very little liquid phase present in the scale at this temperature. The adhesion decreased at 1100°C because of the presence of liquid sulphur-rich phases and thereafter there was a steady increase in adhesion with temperature because of an increase in surface irregularity.

The scale adhesion was found to increase with temperature and time on balanced steel at a similar rate to that of the rimming steel. The scale on the balanced steel contained more liquid sulphur phase than the rimming steel and also considerably more metal scale entanglement and it is probable

that the liquid sulphur phase decreased the adhesion at these temperatures for a given surface roughness. However, liquid phases most probably increase the depth of metal/scale entanglement also and this will be examined in a later section .

Scale adhesion may be reduced in practice by limiting the temperature to 1150°C having a short reheating time and with low silicon, sulphur, manganese and nickel in the steel. Furnace atmospheres should preferably not contain any sulphur, but if sulphur bearing constituents are present a high oxygen content in excess of 4% should be used.

It is imperative that all scale is removed before the material enters the roll gap otherwise it is very difficult to remove.

6. INVESTIGATION INTO THE MECHANISMS OF FORMATION AND GROWTH OF METAL SCALE ENTANGLEMENT

In the preceding section it has been demonstrated that the phenomenon of metal/scale entanglement plays a significant role in scale adhesion. In an effort to reduce the metal/scale entanglement and therefore reduce scale adhesion it is useful to understand the mechanism of formation and growth of the entanglement. The current theories have been reviewed in detail in Section (1).

6.1 Summary of Theories

The presence of nickel in steels is undoubtedly the major factor influencing the formation of entangled layers.

However, as the above work shows, the depth of metal/scale entanglement can vary considerably on steels with identical nickel contents oxidised under identical conditions, and obviously other factors are influencing the depth of entanglement. The mechanisms to date may be summarised as follows, the initiation of the entanglement by nickel steels is thought by Sachs[49-51] and by Brown et al[52,54,55] to be internal oxidation mechanism, entrappment of nickel-rich metal occurring in the inner oxide layer. Growth of this oxide into the metal and therefore the increase in the length of the filigree or depth of the metal/scale entangled zone is accomplished by plastic flow of the oxide or by gaseous oxygen flow across pores, either by a redox reaction or by dissociation of the oxide. The growth of the particle (or filigree) size with distance from the advancing oxide surface has been suggested to be either because of the diffusion of nickel in the scale, (which is unlikely), or by compaction because of the inward creep of the bulk scale layer. These proposals only partially explain the observations of the various depths of metal/scale entanglements found in this study . In particular internal oxide particles have not been seen to coalesce to the rod-like form suggested by Sachs nor do the filaments appear as cylindrical sheaths surrounding oxides when the scales are detached which would also support this theory. A further factor is the precipitate free nature of the metal in the entangled zone which has also been observed by Moreau and

Cagnet but which so far has not been explained.

In order to achieve an understanding of these points the initiation of the entanglement was studied using short time experiments as detailed below and in addition the influence of internal oxidation, liquid phases, and nickel enrichment was studied using a factorial experiment.

6.2 Experimental Procedure and Results

To investigate the initiation of the metal/scale entanglement, cylindrical specimens from a silicon-killed steel (for analysis see Table 3(d)) prepared as described were heated to 1200°C in commercial oxygen-free nitrogen for 15 minutes and then oxidised in an atmosphere simulating the products of combustion of uncleaned coke oven gas burnt to give 6% oxygen in the furnace atmosphere for periods of time between one and five minutes. The specimens were water quenched after this time and prepared for metallographic examination as described above. The metal/scale interfaces produced by these short time treatments are shown in Fig.94. After 15 minutes in commercial oxygen-free nitrogen a considerable amount of internal oxidation had occurred and an irregular interface was produced. On introducing the oxidising atmospheres the growth of oxide into the metal took place rapidly with liquid sulphur-rich and silicon-rich phases at the tips of the penetration into the metal. Irregularity of the interface increased with time and after five minutes at this temperature well defined metal/scale entanglement was observed.

The separate and combined effects of nickel enrichment, liquid phases and internal oxidation were examined using a factorial experiment. A base cast of iron was made as pure as possible with commercially available material in a basic lined high frequency vacuum furnace and the effect of nickel was examined by the addition of 1% pure nickel to this cast, the effect of internal oxidation was examined by the addition of 1% manganese and the combined effect of enrichment and internal oxidation by an alloy containing the addition of 1% nickel and 1% manganese. The chemical analyses of these casts are shown in Table 3(e). The effect of liquid phases was to be studied using sulphur bearing and sulphur free low oxygen atmospheres based on the products of combustion of sulphur containing and sulphur-free coke oven gas.

The 1.2 in diameter by 1 in high solid cylinders were prepared for oxidation as described above, and oxidised at 1200°C for 1 h in the atmosphere composition given in Table 4(b) after heating to temperature for 15 minutes in commercial oxygen free nitrogen. After testing, the specimens were air cooled and prepared for transverse metallography as described earlier. The results are shown in Figs.95 and 96. Unfortunately no sulphur-rich liquid phase could be found in the scales or at the scale/metal interface and consequently the effect of the liquid phases in the scale layer could not be studied using these steels. It was suggested[97] that the addition of some carbon to the iron would probably assist sulphur pick up into the scale and consequently the experiment was repeated with higher C steels. The resultings alloy compositions are shown in Table 1.

The full factorial experiment was repeated and the results are shown in Figs.97-99. With the base composition irregular metal/scale interfaces were produced in the sulphur-free atmosphere. The addition of sulphur to the atmosphere resulted in some liquid sulphur phases in the scale but a very similar interface was produced to those produced without sulphur. Similar results were obtained also with the material containing 1% manganese except that internal oxidation was more extensive in this case. With 1% nickel in the base material metal particles appeared in the inner scale layer in the sulphur-free atmosphere but with the sulphur bearing atmosphere however, extensive penetration of liquid sulphur-rich phases occurred into the metal, and scale/metal entanglement and grain boundary oxide penetration was very marked. There was much more liquid sulphur found in the scales than in the scales on the base cast or the 1% manganese steel in the sulphur bearing atmospheres. Very similar results to the nickel steel were found on the cast containing manganese and nickel and in order to quantify the effect of the variables the depth of metal/scale entanglement and internal oxidation were measured. The separate and combined effects of liquid phases, nickel enrichment and internal oxidation were determined using the factorial analysis shown in the Appendix 5.

6.3 Discussion

6.3.1 Short Time Testing

The large number of internal oxide particles formed in the oxygen-free nitrogen used after 15 minutes oxidation

at 1200°C is not surprising as the gas used was only of commercial purity. In no case have the internal oxides appeared to coalesce to form rod like oxides as produced by Sachs and only when the advancing oxide front reaches the internal oxide particle does oxidation grow slightly into the metal. The very rapid preferential growth of some of the small surface irregularities from the introduction of the sulphur bearing atmospheres may be caused by the point of contact of the liquid phases in the scale grain boundaries which resulted in more oxidation because of an oxygen pump mechanism as suggested by Tholander[27]. Alternatively this may result from the penetration of the sulphur bearing gases through cracks in the scale layer formed by gaseous evolution of carbon oxidation products and this factor will be discussed later.

After two minutes the whole of the interface consisted of the growths of oxides containing liquid phases into the metal , and filaments of precipitate-free metal were observed between the oxide intrusions. The size of the advancing oxides compared with the internal oxides indicates that the entrappment mechanisms proposed for the high nickel steels cannot be operating with these short time conditions because the internal oxides were very small. With longer time tests, e.g. 3 hours at 1350°C (see Fig.93) although apparent islands of oxides appeared to be forming beneath the metal surface the presence of liquid sulphur phases indicates that these are contiguous with the outer scale layer and are not in fact internal oxide particles and only appear as internal oxide particles because of a sectioning

effect. It is thus considered more likely that the theory of Wagner[56] is in operation and that the irregular interface is stabilised by the enrichment of nickel and the growth of the oxide takes place into the metal.

6.3.2 The Factorial Experiment

The results of the factorial experiment analysis are shown in the Appendix[5]. With the alloy series containing no carbon the absence of the liquid phase limited the conclusions which could be made, however the presence of manganese has resulted in some internal oxidation, and the presence of nickel in the appearance of metal particles in the scales. The presence of both manganese plus nickel did slightly reduce the extent of internal oxidation compared with manganese alone and had very little effect on the metal/scale entanglement compared with the effect of nickel alone. Consequently it would appear that internal oxidation does not influence the effect of metal/scale entanglement. The introduction of carbon has allowed the penetration of the sulphur liquid phase to the metal/scale interface and therefore the second experiment was successful in this respect. The results of the factorial analysis of the experiment in terms of the effect of each variable and the combined effects of variables on the metal/scale entanglement, internal oxidation are shown in the Appendix. It is sufficient to note here that the presence of liquid phases or internal oxidation did not lead to metal/scale entanglement in the absence of nickel. Nickel on its own resulted in some metal/scale entanglement but in the presence of a liquid phase a very marked increase

in metal/scale entanglement and grain boundary penetration resulted. In the presence of nickel, manganese increased the amount of metal/scale entanglement slightly but in the presence of sulphur and nickel, manganese decreased the metal/scale entanglement slightly. Consequently manganese and therefore internal oxidation has no significant effect on the depth of metal/scale entanglement. Sulphur on its own or in the presence of manganese had no effect but the presence of sulphur increased markedly the amount of the metal/scale entanglement in the presence of nickel. Consequently for the phenomenon of metal/scale entanglement the presence of an enriching element is required and the presence of a liquid phase markedly increases the depth of metal/scale entanglement. These results have not taken into account the effect of these variations on the oxidation rate as no measurement of the oxidation rates were recorded but from the scale thicknesses obtained it was seen that the oxidation rates varied widely especially in the presence of liquid phases.

The effect of carbon in producing liquid sulphur phases in the scale layer indicates that under these reheating conditions sulphur has been transported to the metal/scale interface via cracks in the scale layer formed by the gaseous evolution of carbon oxidation products. The evolution of carbon oxides may also take place through small pores as suggested by Engel and Bohnenkamp[38] and hence the ingress of sulphur dioxide could take place via this porosity. In addition nickel appears to have in some way catalysed the reaction to produce the liquid sulphides which are assumed

in this case to be iron sulphides/iron oxide eutectics. This assumption is made on the basis that if nickel sulphide were produced the liquid phases would be able to attack the enriched areas resulting in a reduction in the amount of metal/scale entanglement. This point could be clarified by a microprobe analysis but nickel was not found in the liquid phases formed on commercial steels oxidised under similar conditions examined earlier, and this indicates that liquid nickel sulphides were probably not formed.

6.3.3 The Mechanism of Formation of Metal/Scale Entanglement (see Fig.100)

It is proposed that the metal/scale entanglement initiates at some instability in the initial planar metal/scale interface. This instability could be an internal oxide particle or a steelmaking oxide or sulphide inclusion in steel. In the absence of a liquid phase the growth of the embryo oxide inclusion is dependent on the creep rate of the scale which would increase with temperature. The presence of water vapour or CO_2 in the furnace atmosphere may also maintain oxidation at the base of the growing oxide because of a 'redox' type reaction. In the presence of a liquid scale the creep rate is high and the liquid may act as an oxygen pump resulting in an increase in the penetration rate. The presence of nickel stabilises the metal protrusions into the scale layer by enrichment effects because of the preferential solution of iron as proposed by Wagner and

hence a stable irregular interface results which grows into the steel at a rate which is commensurate with the creep rate of the scale. The metal particles in the scale are most likely part of a metal filigree which appears as particles because of a sectioning effect and the particles appeared to grow in size with distance from the oxidation interface. This growth is most likely caused by compaction effects because of the inward creep of the inner scale layer, the liquid or very plastic scale is exuded from between two metal filigrees which are being compacted. Evidence for this mechanism can be seen in Fig.93 (top left-hand side) where part of the metal filigree has become folded over.

The space between the compacting metal surfaces is filled with a liquid sulphur phase which would presumably be exuded as the compaction continued and re-crystallisation of the metal could then take place to form a larger discrete particle observed on the transverse metallographic section. The metal filigree may, in fact, break up into discrete particles in the outer scale layers because of oxidation but this was not shown by the experiments of Brown and therefore is not considered likely. It would be necessary to undertake a similar technique as used by Brown of successive polishing and examination to determine this. It is considered that the oxide penetrations into the metal also often appear as discrete 'internal oxide particles' but many of these can be seen to include liquid sulphur phases. Some of this liquid phase may have resulted from the manganese sulphides in the metal, but the deeper seated particles can be seen to contain no sulphur rich phase and in any case the small amounts of

sulphur formed in this way would probably be dissolved in the oxide complexes formed in these internal particles and not present as a discrete sulphur rich phase. It is concluded that the presence of sulphur liquid phases in the 'internal oxide particles' indicates that these are, in fact contiguous with the outer scale layer. Consequently the metal/scale entanglement actually exists as an oxide filigree penetrating the metal. The oxide metal entangled zone, therefore, exists in a form shown schematically in Fig.100(d) where the meandering of the metal into the scale and the scale into the metal has been neglected. The effects of the liquid phases are to increase the flow of the scale and therefore allow the growth of the oxide protrusions into the metal and also to increase the oxidation rate at the tips of the growing oxide intrusions because of a mechanism similar to the oxygen pump described by Tholander.

However, this does not explain why there are no internal oxide particles in the metal in the filaments in the entangled zone. It is possible that solution of the internal oxide particles could occur in the enriched alloy in the entangled zone, but this would require a higher oxygen solubility in the enriched zone than in the underlaying metal and higher diffusion rates in this metal also. To investigate this, two steels were made, a base cast containing only residual nickel and copper levels and an alloy cast containing nickel plus copper and tin (for analysis see Table 3(f)). These were oxidised under an atmosphere consisting of carbon monoxide/carbon dioxide mixture in argon at 1200°C (Table 4(c)) in which it was anticipated that minimal scaling

would occur. The alloy composition contained much more internal oxide than the base cast, after this treatment, as shown in Fig.101. Hence, the oxygen solubility in the alloy composition had increased but had also resulted in a very extensive internal oxidation which was most probably iron oxide. Menzies and Tomlinson[44] found nickel enrichment at the metal/scale interface and considerable internal oxidation behind the metal/scale interface which they attributed to a higher oxygen solubility in nickel rich layers. This has also been demonstrated by Fisher[45] who found that the effect of small additions of nickel on the entrappment of harmful liquid copper rich phases in the inner FeO layer could be explained by the formation of iron oxide internal oxide particles. The presence of sufficient free oxygen at the scale/metal interface to form iron oxide in the presence of an iron oxide scale was explained by the dissociation mechanism put forward by Dravnieks and Mcdonald[7]. However, though it appears that the solubility of oxygen is increased by the enrichment of nickel, it is unlikely that solution of the internal oxides takes place as the presence of the enriched layer has resulted in more internal oxidation in the case of the alloy mentioned above. In addition an increase in the size of the particles is observed and they get fewer in number as the metal surface is approached. This preferential growth of some particles at the expense of smaller particles is termed 'over ageing' or 'Ostwald ripening'[98]. This is demonstrated by observations made on the oxidation obtained in a billet containing a hacksaw cut which was approximately 2 inches deep, the oxidation of this

commercial mild steel billet in a furnace fired with towns gas at 1250°C for one hour resulted in a scale which completely sealed the top of the saw cut and the structures shown in Fig.102. Near the top of the cut some oxidation had taken place and the typical metal/scale entangled layer with normal internal oxide particles resulted, (Fig.102(a)). Near the base of the cut, where the oxygen partial pressure was very low and very little scaling on the metal occurred which was indicated by an extremely thin scale layer, the structure shown in Fig.102(b) resulted. Deeper into the metal, typical internal oxide particles were formed but nearer the surface ripening has occurred and only very few large oxide particles are present indicating that the ripening effect can be very marked. However, with an advancing oxide metal interface the ripening would not be fast enough to explain the absence of particles, in the metal in the entangled layer, and the largest particles can be seen to be quite small compared with the oxide intrusions in the entangled layer in Figs.94,98,99.

If we consider a planar metal oxide interface growing into a nickel containing steel, nickel is enriched ahead of the interface. Neglecting for the moment that such an interface is unstable, the schematic representation is shown in Fig.103(a). Oxidation proceeds by diffusion of iron through the nickel enriched layer of metal at the metal surface and transfer of iron to the oxide takes place. In order to do this there must be a vacancy produced at the nickel rich/steel boundary. In order for continued oxidation without gross void formation in the metal, these vacancies must be

annihilated by the diffusion of nickel inwards in order that contact is maintained between the nickel rich layer and the iron layer and that transfer of iron into the enriched layer is still possible. This results in a bulk inward movement of the nickel enriched layer. When this moving nickel/iron interface encounters an internal oxide particle formed in the iron layer ahead of the enriched layer, it is proposed that the vacancies produced in the vicinity of the internal oxide condenses on the internal oxide particle at the particle iron boundary, thus resulting in the bulk inwards movement of this oxide with the enriched layer (Fig. 103(b)). Consequently, internal oxide particles would never appear in the enriched metal. The possibility of vacancy precipitation on internal oxides has been proposed by Stringer[81] and has been demonstrated by Tien and Pettit[18] who showed that adherence was maintained on scaled specimens containing internal oxides, because the vacancies produced at the metal /scale interface condensed on the internal oxide particles and not at the metal/scale interface, thus promoting good adhesion. The interfaces considered here are not planar, but this mechanism is still valid for the entangled layer at the base of the filaments which protrude into the oxide. In this case, the bulk inwards movement of the whole metal scale entangled layer will be necessary. Such movement has been shown by the compaction theory which explains the growth in size of the outer metal 'particles' and thus the necessary compressive stress for the bulk inwards movement of the whole enriched layer is demonstrated. For this mechanism to be valid, one would expect that the internal particles should

align themselves along the interface between the enriched metal and the base composition. In addition they should increase in size and get fewer in number by the ripening effect. Such behaviour is observed in Fig.99(b) where the oxide particles can be seen to be lining up in the metal ahead of the oxide metal interface and increasing quite markedly in size. In addition under conditions of very little prior oxidation, and therefore little prior enrichment, for example in the grain boundary penetration by liquid phases, one would expect to find the internal oxides very close to the oxide metal interface, because of the absence of the enriched layer. Such behaviour is again demonstrated in Fig.99(b), where internal oxides can be seen to be in very close proximity to the advancing liquid phase in the grain boundary penetration.

Consequently, the absence of internal oxide particles in the enriched metal in the entangled zone can be explained by considering that the bulk inwards movement of the enriched metal at least at the base of the filaments results in the internal oxides being swept ahead of the advancing enriched metal. This is aided by the condensation of vacancies which are formed by the transfer of iron from the base alloy composition to the enriched layer on the internal oxide particles. Ostwald ripening of the internal oxide particles can then occur with time until the particles are big enough to be encountered by the meandering liquid oxide intrusions into the metal.

6.3.4 Correlation with Practical Results

Using this hypothesis it is possible to explain the difference in metal/scale entanglement found in the mild steels examined previously which had varying amounts of entanglement, although all had ostensibly the same nickel content. The rimming steel had, in fact, the lowest nickel content (0.03%) and also the smallest amount of liquid phases in the scale layer. Both of these features will tend to reduce the depth of metal/scale entanglement produced according to the above hypothesis. In addition, the results of the factorial experiment indicate that the probable reason for the lower sulphur content on the rimming steel compared to the balanced steel examined previously is the very low carbon content of the rimming steel which resulted in much less sulphur pickup in the scale. The balanced steel (semi-killed) which had a greater depth of metal/scale entanglement than the rimming steel also contained more nickel and more liquid sulphur phases. The two silicon-killed steels both of which had 0.05% nickel also exhibited different depths of metal/scale entanglements for the same oxidation treatments. This can also be explained by the differences in the amount of liquid phase present in the inner scale layer. The steel exhibiting the greatest amount of metal/scale entanglement also contained the largest amount of liquid phase. It is also possible that with silicon-killed steels the internal oxide particles which would contain large proportions of silicon also influenced the depth of metal/scale entanglement as the liquid fayalite-iron oxide eutectics would be produced by the internal oxidation mechanism at the metal/scale

interface and therefore the bulk of the liquid phase would not have to penetrate the scale layer as is the case with sulphur rich phases produced by contamination from the atmosphere. This effect was not examined in the factorial experiment as it was necessary to separate the effects of the liquid phases and the internal oxide particles which cannot be done in the case of silicon. The presence of sulphur in the inner scale layer on the silicon-killed steels would be detrimental as it lowers the melting point of the liquid scale layer.

6.4 Conclusions

The phenomenon of metal/scale entanglement found on mild steels oxidised under conventional reheating conditions is formed by the enrichment of nickel in the metal surface, which leads to the instability of a planar metal/scale interface. The initiation of the irregular interface may be caused by internal oxide particles or steelmaking inclusions which the initial oxide layer encounters as it grows into the metal. The irregular oxide metal interface produced is stabilised by the diffusion of nickel, and the oxide intrusions grow into the metal. The rate of growth of the intrusions in the metal surface is dependent on the creep rate of the scale and the depth of the entanglement increases with time and temperature. The presence of liquid phases in the scale layer increased the rate of growth markedly. Bulk inwards movement of the inner scale layer takes place leading to compaction of the outer metal in the entangled zone and the internal oxides in the metal are swept ahead of the advancing alloy enrichment at the base of the metal filaments

by the bulk inwards movement of the enriched layer.

The differences in depths of metal/scale entanglement found on commercial steels, previously examined with similar nickel contents, have been explained using this theory and have been found to result mainly from the amount and possibly the composition of the liquid phases present in the inner scale layers.

7. SUGGESTIONS FOR FURTHER WORK

This work could be extended in three major areas, these are:

(i) Extending the study to other variables using the existing equipment.

(ii) Further development of the technique.

(iii) Investigations into the fundamentals of oxidation.

7.1 Study of Other Variables

These could include steel composition (i.e. high Ni steels or Si/Mn steels for example); furnace atmosphere (high and low sulphur fuel for example) and the use of non-isothermal conditions more closely simulating practical reheating. In addition the technique could be used to assess the effectiveness of surface coatings/furnace atmosphere additions (e.g. Alkyl Borates) claimed to reduce scale adhesion.

7.2 Further Development of the Technique

It would be an advantage to increase the testing temperature to examine the effect of high reheating temperatures often used in practice. Alternative gauze material may

allow this. It may also be possible to adapt the technique for use on thinner scale formed for example under heat treating or 'service' conditions. Adaption for use on material (e.g. billets) reheated in commercial furnaces would yield useful information and overcome the difficulties inherent with simulation in the laboratory.

7.3 Fundamental Studies

Methods of reducing the growth of the metal/scale entanglement should be studied, by a more comprehensive study of the effects of, for example, furnace atmosphere and of additions to the steel or surface coatings designed to increase the melting point of the liquid phases formed.

In addition possible systems which could generate brittle particles at the metal/scale interface should be investigated.

The technique of hot scale removal under a controlled atmosphere combined with stereoscan techniques could also be used to study the initial stages of oxidation under isothermal conditions.

8. REFERENCES

1. J. Paidassi, Acta Met. March 1958, pp. 184-194
2. J. Coq et al, Paper presented to the Technical Association of the French Gas Industry Congress, 1962
3. R. Collangues et al, Rev. de Met. No. 10, 1953, pp 727-736
4. H. Engel and F. Wever, Acta Met. Vol. 5, December 1957, pp. 695-702
5. R. F. Tylecote and T. E. Mitchell, JISI Vol. 196 4 December 1960, pp. 445-453
6. S. Mrowec, Corr. Science Vol. 7, No. 9, September 1967, pp. 563-578
7. A. Dravnieks and H. J. McDonald - J. Electrochem Soc. 1948, 94, pp. 139-151
8. M. H. Davies, M. T. Simnad and C. E. Birchenall, Trans. AIME J. Met., October 1951, pp. 889-896
9. K. Hauffe Metalloberflache (A) 8 97, 1954
10. C. Wagner, Z. Phys. Chem (B) 21 25, 1933
11. E. A. Gulbransen et al., Trans AIME J. Met, September 1954 pp. 1027-1053
12. C. W. Tuck, M. Odgers and K. Sachs, Anti Corrosion, June 1966 pp. 14-26 and July 1966 pp. 17-21
13. L. Himmel, R. F. Mehl and C. E. Birchenall, Trans. AIME J. Met., June 1953, pp. 827-843
14. J. D. Mackenzie and C. E. Birchenall, Corrosion, Vol. 13, No. 12, December 1957, pp. 17-19
15. P. Hancock, Work referred to in Lecture at Sheffield Polytechnic 1969
16. B. W. Dunnington et al, Corrosion, Vol. 8 1952
17. R. F. Tylecote, The Metallurgist Vol. 2 No. 2 March 1962 pp. 32-40

18. J. K. Tien and F. S. Pettit, Met. Trans. 1972 Vol. 3 pp. 1587-1599

19. P. D. Dankov and P. V. Churaev Dock. Akad. Nauk. SSSR 73, 1950, pp. 1221-1224

20. J. Maldy, Mem. Sci. Rev. Met., May 1965

21. Chaudron and Forestier, Comptes Rendus, 178, No. 2, 1924 p. 173

22. W. A. Fischer et al, Arch Eisenhutte, August 1956 pp. 521-529 and February 1958, pp. 107-113

23. F. K. Peters and H. Engell, Arch f.d. Eisenhutte, 30, 1959, pp. 272-282

24. J. Moreau and M. Cagnet, Metal Treatment, September 1957, pp. 362-376, October 1957, pp. 407-415 and November 1957, pp. 456-458

25. H. Schenck et al, Arch F.D. Eisenhutte, 31, February 1960, pp. 121-128

26. A. Rahmel, Z Electrochem 66, 1962, p. 363

27. E. Tholander and S. Blomgren, Jerkon. Ann. 151, January 1967 pp. 16-61

28. A. K. Ghosh and R. Rolls, Iron and Steel, June 1969, 42 (3) pp. 151-157

29. G. C. Wood and D. A. Melford, JISI 198, 2, June 1961, pp. 142-148

30. J. Moreau, Comptes Rendus, 236, 85, 1953

31. D. Lai et al, Corrosion, 17 July, 1961, pp. 109-116

32. E. Scheil and K. Kiwit, Arch f.d. Eisenhutte, February 1936 pp. 405-416

33. G. J. Bateman and R. Rolls, Br. Corrosion J, 5th May 1970, pp. 122-127

34. J. H. Andrew et al, JISI, 124, 1931, p. 283

35. Ch de Beaulieu et al, Rev. de Met. 57, (11), 1960, pp. 863-875

36. J. H. Swisher, Trans. AIME 242, June 1968, pp. 1035-1038

37. A. Preece and R. V. Riley, JISI 1944, pp. 253-273

38. K. Bohnenkamp and H. J. Engel , Arch. f.d. Eisenhutte 33, June 1962, pp. 359-367

39. K. Sachs and C. W. Tuck, Paper given at Reheating for Hot Working Conference ISI Publication, 111, 1968, pp. 1-17

40. W. W. Webb, J. Electrochem. Soc. 103, 1956, p. 112

41. K. Sachs and J. R. Brown, JISI, October 1958, pp. 169-170

42. D. A. Melford and P. A. Duncumb, Metallurgia 1958 57 pp. 159-161

43. T. J. Carter, G. L. Wulf and G. R. Wallwork, Corrosion Science 9, 1969, pp. 471-478

44. P. A. Menzies and W. J. Tomlinson JISI 1966 Vol. 204 pp. 1239-1252.

45. G. L. Fisher JISI 1969 Vol. 207 pp. 1010-1016

46. G. L. Wulf, T. J. Carter and G. R. Wallwork, Corrosion Science 9, 1969, pp. 639-701

47. J. E. Stead, JISI 1916, Vol. 94, p. 243

48. L. B. Pfeil, JISI 1929, Vol. 119, pp. 501-560

49. K. Sachs, JISI 1957, Vol. 185, pp. 348-357

50. K. Sachs, JISI 1957, Vol. 187, pp. 93-104

51. K. Sachs, C. W. Tuck and J. Barlow. Anti-Corrosion Part 1 April 1966 pp. 20-26 Part 2 May 1966 pp. 33-36

52. G. G. Brown, J. Australian Inst. Metals, Vol. 7, No. 2 pp. 85-93

53. D. A. Melford and P. Duncumb Metallurgia 1960 61 pp. 205

54. G. G. Brown and D. C. Mears, Australian Corrosion Engineering Sept. 1964, pp. 23-28

55. G. G. Brown and K. G. Wold, JISI, Vol. 207, pp. 1457-1462

56. A. Rahmel, Werkstoffe u Corrosion, Oct. 1965, pp. 837-843

57. C. Wagner, J. Electrochem Soc. Oct. 1956, pp. 571-580

58. A. Nicholson and J. D. Murray, JISI 203, October 1965, pp. 1007-1018

59. R. C. Willingham and J. Williams, BISRA Rep. No. DIS/18/65, 1965

60. D. A. Melford, JISI 200, 1962, pp. 290-299

61. G. L. Fisher, JISI, July 1969 pp. 1010-1016

62. A. Rahmel and H. Engell, Arch. f.d. Eisenhutte, 1959, 30 (12), p. 743

63. R. R. Hough and R. Rolls, Metal Forming, November 1969, pp. 307-315

64. E. A. K. Patrick and N. G. Patel. Paper presented at the Autumn Meeting of the Inst. of Gas Engineers, November 1960, Gas Council Research Communication GC67

65. R. Rolls, Metal Treatment, November 1963, pp. 423-436

66. C. W. Tuck, Anti-Corrosion, July 1968, pp. 4-7

67. R. Rolls, Metal Treatment, April 1960, pp. 139-147

68. K. Born, Stahl und Eisen, Vol. 73, 1953, No. 20

69. F. D. Richardson and J. H. E. Jeffes - JISI 1952, 171, p. 165

70. D. W. Murphy and W. E. Jominy, University of Michigan Eng. Res. Bulletin, No. 21, 1931, pp. 96-148.

71. C. W. Tuck and D. W. Down, JISI 205, September 1967, p. 972

72. W. J. Tomlinson and S. Catchpole, Corrosion Science 8, 1968 pp. 845-849

73. U. R. Evans, Symp. on Internal Stresses in Metals and Alloys 1948, London Inst. Metals, pp. 295-310

74. D. Bruce and P. Hancock, J. Inst. Metals 97, 1969, pp. 140-155

75. J. Romanski, Corr. Science 8, 1968, pp. 67-87

76. H. Engel and F. K. Peters, Arch. Eisenhutten, 28, 1957 pp. 567-574

77. V. N. Culiaev, Zavodskaya Lab. 24, 1958, Pt. 10, pp. 1375-6

78. K. Sachs and T. Pitt, JISI, January 1961, pp. 1-8

79. S. Modin and E. Tholander, Metal Treat. July 1961, pp. 261-270

80. J. M. Hulley and R. Rolls Technical Note JISI November 1970 pp. 1029-1030

81. J. Stringer, Met. Reviews 11, 1966, pp. 113-128

82. R. F. Tylecote, JISI August 1960, pp. 380-385

83. N. B. Pilling and R. E. Bedworth, Paper presented to the Annual General Meeting, London March 1923

84. G. Vagnard and J. Manenc, Rev. Met. November 1964, pp. 768-776

85. R. F. Tylecote, JISI, October 1960, pp. 135-141

86. V. I. Rospasienko and V. S. Chernitisyn, Stal in English, May 1969, pp. 480-482

87. T. Sheppard and W. M. Steen, JISI 208, September 1970, pp. 797-805

88. G. M. Palin, Stal, 8, August 1965, pp. 677-679

89. L. Kidman - BISRA Report. No. MS/DB/238/63, 1963

90. G. V. Beaton - Journal of Scientific Instruments,1969, Series 2 Vol. 2 pp. 252-256

91. J. I. Olsanskij - Dok. Akad. Nauk. USSR 59, 1948, p. 513

92. R. Vogel - Archiv. f.d. Eisenhutt. July 1965, Vol. 36, No. 7 pp. 481-484

93. D. C. Hilty and W. Crafts Trans AIME J. Metals December 1952 pp. 1307-1312

94. J. H. Swisher and E. T. Turkdogan - Trans. Met. Soc. AIME 239, April 1967, p. 426

95. F. N. Rhines, W. A. Johnson and W. A. Anderson - AIMME, Trans. 147, 1942, p. 205

96. F. Maak - Z. Metallkde, 1961, 52, pp. 545-6

97. Private communication N. Birks Sheffield University

98. R. A. Rapp, Corrosion, Dec. 1965, pp. 382-401

TABLE 1 ADHERENCE INDEX DATA (BATEMAN AND ROLLS) (HOT BEND)

Material	Atmosphere	Oxidation Temperature			
		950°C Time - h		1050°C Time - h	
		0.5	1	0.5	1
Pure Fe	A	1.00	1.00	0.96	0.96
	B	1.00	1.00	0.88	0.88
Fe + 0.005% Al	A	1.00	1.00	1.00	0.92
	B	1.00	1.00	0.92	0.83
Fe + 0.045% Al	A	1.00	1.00	0.92	0.92
	B	1.00	1.00	0.88	0.88
Fe + 0.1% Al	A	1.00	1.00	0.92	0.67
	B	-	-	-	-
Fe + 0.2% Al	A	1.00	0.79	0.79	0.50
	B	0.88	0.71	0.58	0.33

All scales were completely adherent (Index = 1.00) at 850°C.

A = Low oxygen potential atmosphere. B = High oxygen potential atmosphere.

TABLE 2 ADHERENCE INDEX DATA (GHOSH AND ROLLS - HOT IMPACT)

Alloy	Composition Weight %			Oxidation Conditions											
				Low Oxygen Potential Atmosphere						High Oxygen Potential Atmosphere					
				Temperature °C						Temperature °C					
				1050			1250			1050			1250		
				Time - h			Time - h			Time - h			Time - h		
	C	Si	S	1	2	4	1	2	4	1	2	4	1	2	4
A	0.74	3.15	0.069	94	95	83	91	88	81	100	99	99	75	51	42
B	0.55	0.32	0.076	100	99	100	97	99	100	100	98	100	88	83	87
C	1.02	2.90	0.019	99	91	84	86	30	0	95	60	21	95	0	0
D	1.03	0.25	0.006	97	95	96	98	89	99	98	99	48	90	100	89
E	0.13	2.60	0.074	95	98	98	92	96	88	97	98	99	97	67	93
F	0.063	0.05	0.099	94	90	98	100	98	100	100	99	99	97	84	98
G	0.10	2.60	0.010	98	100	99	93	91	83	98	98	95	99	90	39
H	0.077	0.18	0.014	99	100	97	100	99	78	97	99	88	97	100	70

TABLE 3 CHEMICAL ANALYSIS OF STEELS EXAMINED (% BY WEIGHT)

	Quality	Cast Number	C	Mn	Si	S	P	Ni	Cr	Mo	Cu	Sn	Al Sol/Insol
(a) Isothermal Laboratory Oxidation and Scale Adhesion Testing.	Rimming	15460	0.049	0.34	Nil	0.023	0.012	0.03	0.02	0.02	0.05	<.01	Nil/Nil
	Si-Killed	50442	0.18	0.78	0.26	0.035	0.047	0.05	0.02	0.02	0.04	<.01	Nil/Nil
	Si-Killed + Al	52279	0.183	0.54	0.18	0.039	0.037	0.05	0.03	0.02	0.04	<.01	0.034/.002
	Semi-Killed	51375	0.194	0.65	0.03	0.060	0.033	0.05	0.01	0.02	0.05	<.01	Nil/Nil
(b) Commercially reheated blooms.	Rimming	61949	0.07	0.38	-	0.025	0.017	-	0.02	-	0.047	-	-
	Si-Killed	61643	0.14	0.61	0.26	0.032	0.026	-	0.03	-	0.04	-	-
	Semi-Killed	16158	0.07	0.43	-	0.027	0.033	-	0.01	-	0.039	-	-
(c) Rolling sumulation	Si-Killed	-	0.23	0.60	0.175	0.030	0.051	- Not Determined -					-
(d) Short time tests		50442	- See above -										
(e) Factorial Experiment (i) Low Carbon		1235	0.004	0.02	0.08	0.006	0.001	<0.01	<0.01	<0.01	0.003	<0.001	< 0.004
		1236	0.008	0.98	0.04	0.005	0.003	<0.01	<0.01	<0.01	0.003	0.003	< 0.004
		1237	0.008	0.06	0.06	0.005	0.001	0.93	<0.01	<0.01	<0.001	<0.001	< 0.004
		1238	0.009	0.88	0.04	0.005	0.003	0.95	<0.01	<0.01	0.005	<0.001	< 0.004
(ii) High Carbon		1287	0.44	0.01	0.02	0.008	0.001	<0.01	<0.01	<0.01	0.004	<0.001	< 0.01
		1288	0.45	1.06	<0.01	0.007	0.001	<0.01	<0.01	<0.01	<0.001	<0.001	< 0.01
		1289	0.43	0.02	<0.01	0.008	0.002	0.95	<0.01	<0.01	<0.001	<0.001	< 0.01
		1290	0.43	0.89	<0.01	0.006	0.001	1.0	<0.01	<0.01	<0.001	<0.001	< 0.01
(f) Effect of enrichment on internal oxidation		Base	0.003	0.03	0.07	0.005	0.003	0.05	<0.01	<0.01	0.05	0.02	-
		Alloy	0.004	0.02	0.04	0.005	0.001	6.2	<0.01	<0.01	5.6	0.5	-

TABLE 4 ATMOSPHERES USED (Volume %)

	Composition				
	O_2	SO_2	H_2O	CO_2	N_2
(a) Short time tests and Isothermal laboratory simulation	6.0	0.125	15.0	6.0	Balance
(b) Factorial Experiment					
Without sulphur	1.5	Nil	15.0	6.0	Balance
With sulphur	1.5	0.25	15.0	6.0	Balance
(c) Atmosphere used to study the internal oxides produced in the enriched zone. 4% CO, 1% CO_2, balanced high purity argon					

TABLE 5 FURNACE ATMOSPHERE SURVEY (Commercial Furnace)

Conditions of Sample		CO_2 %	H_2O %	SO_2 %	O_2 %	N_2 %
Doors shut between bloom discharge:	right-hand zone	6.70	18.05	0.15	3.60	71.50
	left-hand zone	7.70	20.70	0.17	1.12	70.30
Doors open on bloom discharge:	right-hand zone	6.10	16.30	0.13	5.28	72.20
	left-hand zone	6.62	17.74	0.14	3.90	71.60
Doors open for extended period:	right-hand zone	4.49	12.04	0.10	9.37	74.00
	left-hand zone	5.75	15.40	0.13	6.13	72.60
Doors shut during meal-break:	right-hand zone	4.80	12.90	0.10	8.60	73.60
	left-hand zone	6.25	16.75	0.14	4.86	72.00
Doors shut during rolling:	Upper tonnage zone	7.22	19.38	0.16	2.34	70.90
Average Atmosphere		6.2	16.5	0.13	5.0	BAL.
Atmosphere Used For Prediction		6	15	0.125	6	BAL.

NOTE: Coke oven gas was the only fuel used during the trials.

TABLE 6 COMPARISON OF OXIDATION CHARACTERISTICS OBTAINED IN PRACTICE WITH LABORATORY VALUES

Quality	Position	Oxidation Characteristics (mm x 10^2)											
		Entanglement			Grain Boundary Penetration			Internal Oxidation			Metal Consumed		
		M*	C*	T*	M	C	T	M	C	T	M	C	T
Rimming	1	8.56			13.36			-			104.9		
	2	14.40	8.4	N.D.	18.56	11.5	N.D.	-	13.3	N.D.	121.9	90.4	NOT
	3	6.08			12.0			9.68			96.52		DONE
	4	5.44			9.68			-			60.96		
Si-Killed	1	12.72			16.08			-			104.1		
	2	N.D.	15.3	14.1	-	21.0	19	-	7.9	8.9	111.7		
	3	5.60			10.40			14.16			83.82	56.9	50.6
	4	8.64			15.20			13.04			81.28		
Balanced	1	4.16			8.64			13.28			81.28		
	2	23.68	15.4	13.7	28.16	21.4	22.4	8.88	13.7	14.2	81.28	73.4	72.5
	3	3.92			8.08			8.72			88.90		
	4	15.54			21.12			9.61			86.36		

M = Measured Values - Furnace Trial
C = Calculated Values from Isothermal Laboratory Data
T = Measured Values from Simulated Laboratory Specimen

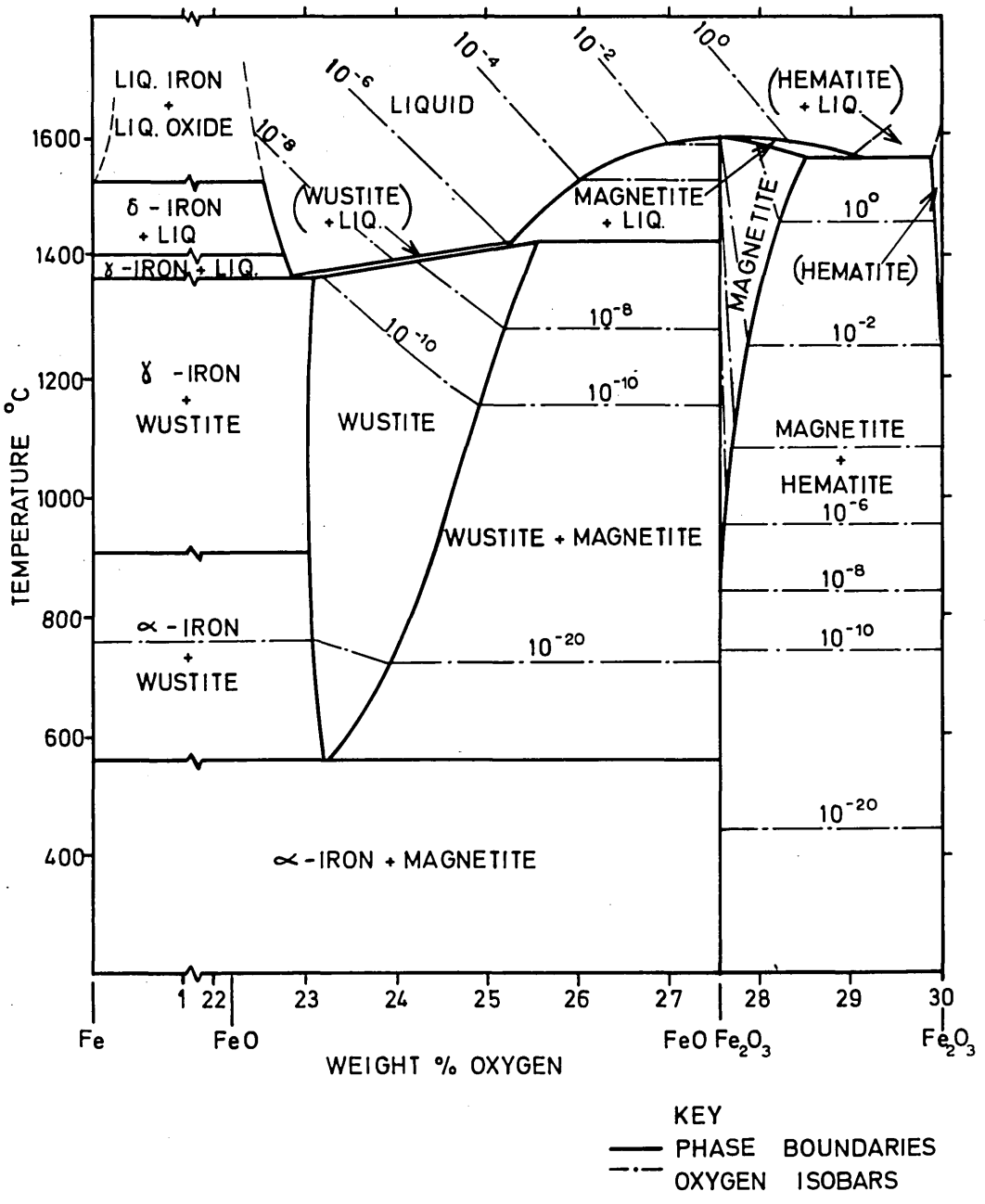

IRON-OXYGEN EQUILIBRIUM DIAGRAM

(FROM PHASE DIAGRAMS FOR CERAMISISTS 1969)

FIG. 1

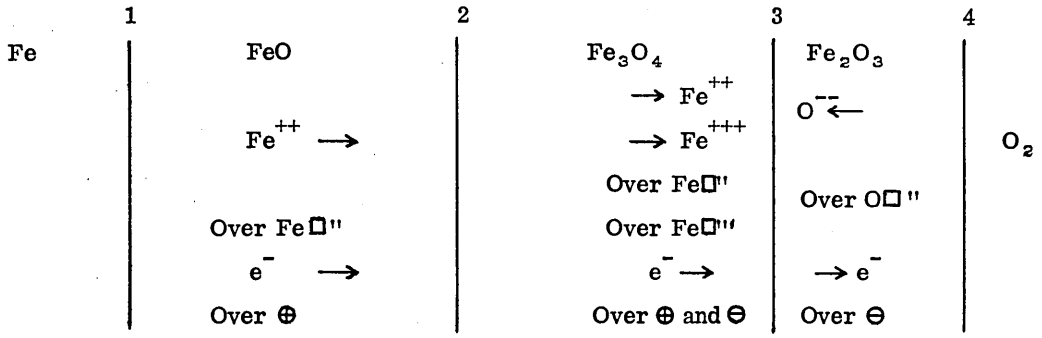

Phase Boundary Reactions

1. $Fe_{(Metal)} + (Fe\square'' + 2\oplus)_{\text{in FeO}} \rightleftharpoons$ Null

2. $Fe_3O_4 \rightleftharpoons (4\,FeO + Fe\square'' + 2\oplus)_{\text{in FeO}}$ (Fe_3O_4 Decomposition)

   Some of the Fe^{++} ions arriving through the FeO and the Fe^{+++} ions arriving at the FeO/Fe_3O_4 phase boundary pass over into the Fe_3O_4

   $\oplus_{\text{in FeO}} + (Fe\square'' + Fe\square''')$ vacant tetrahedral position in Fe_3O_4
   $\rightleftharpoons$ Filled lattice position + $(2Fe\square'')_{\text{in FeO}}$

3. $12\,Fe_2O_3 \rightleftharpoons 9\,Fe_3O_4 + (Fe\square'' + 2\,Fe\square''' + 8\oplus)_{\text{in } Fe_3O_4}$ (Fe_2O_3 Decomposition)

   $2\,Fe_3O_4 \rightleftharpoons 3\,Fe_2O_3 + (0\square'' + 2\ominus)_{\text{in } Fe_2O_3}$ (Fe_2O_3 Formation)

4. $\frac{1}{2}O_{2\,(gas)} + (0\square'' + 2\ominus)_{\text{in } Fe_2O_3} \rightleftharpoons$ Null

SCHEMATIC REPRESENTATION OF THE OXIDATION OF IRON (HAUFFE)

FIG. 2

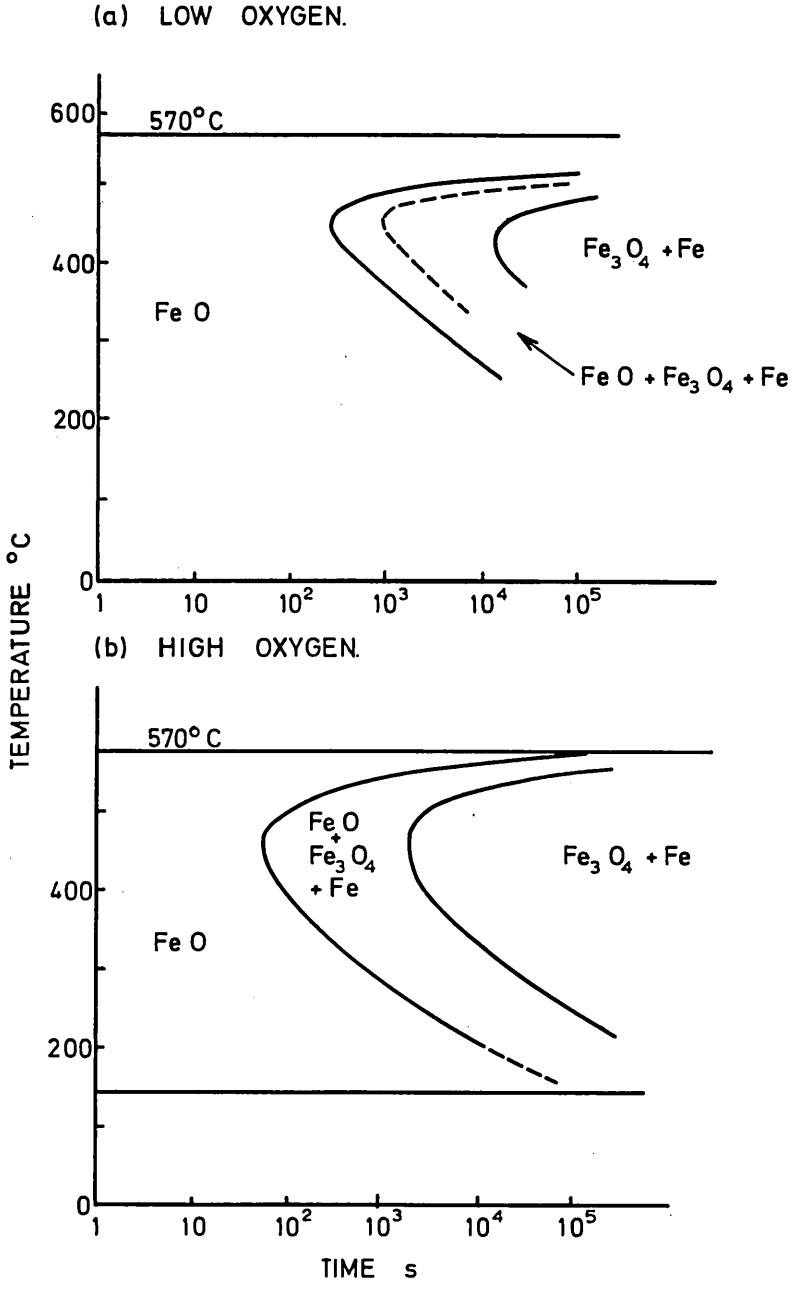

ISOTHERMAL TRANSFORMATION OF WÜSTITE. (COLLONGUES)

FIG. 3

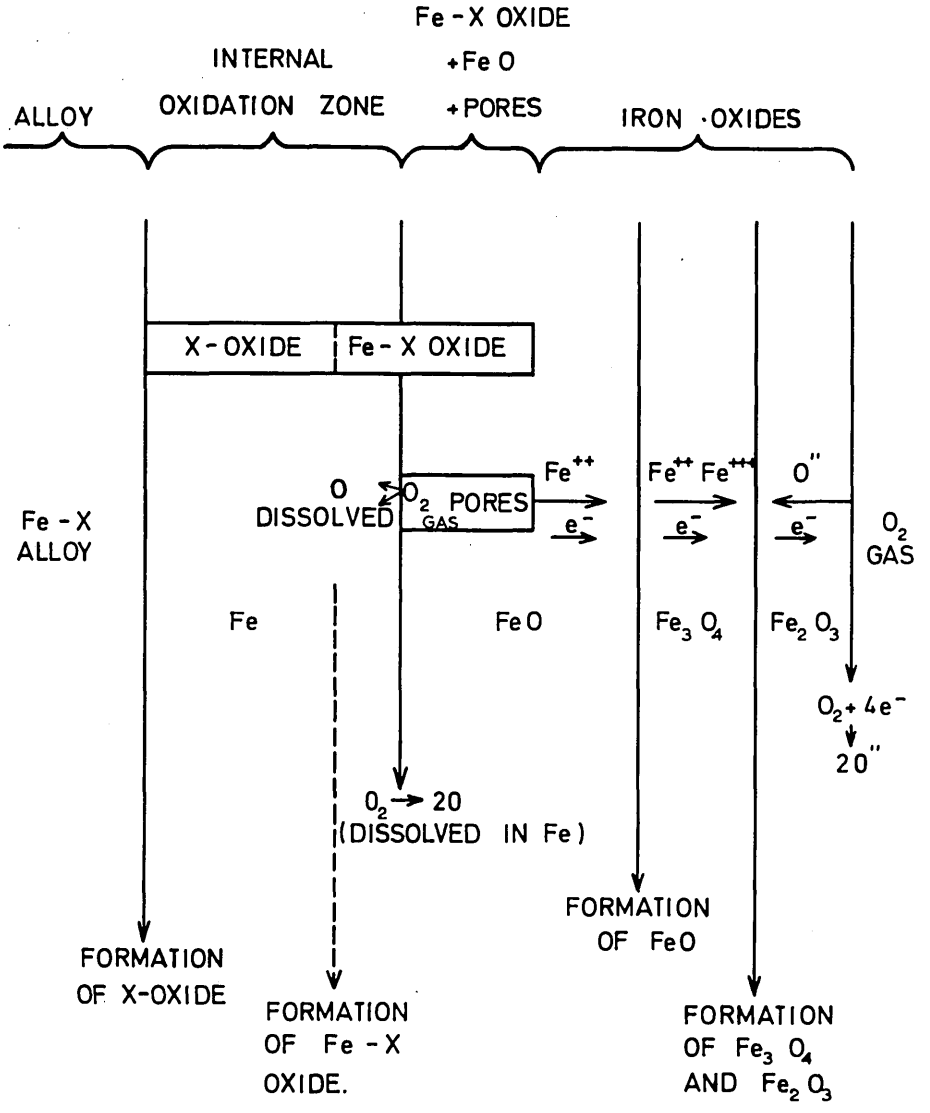

SCHEMATIC REPRESENTATION OF THE OXIDATION OF IRON ALLOYS. (RAHMEL)

FIG. 4

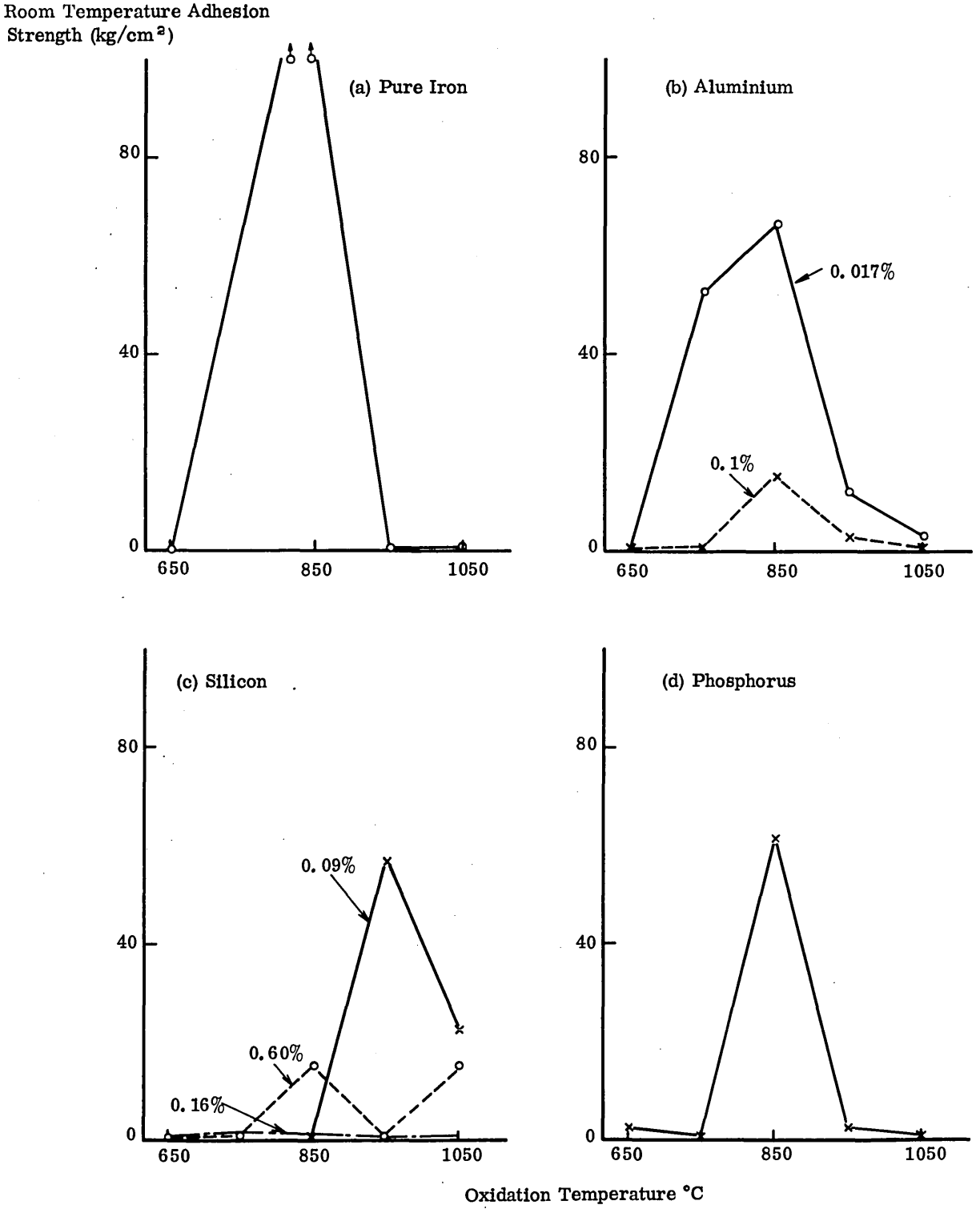

THE EFFECT OF ALLOY ADDITIONS ON THE ROOM TEMPERATURE ADHESION OF SCALES ON PURE IRON

(CONSTANT SCALE THICKNESS - 200 μ - PETERS AND ENGELL)

FIG. 5

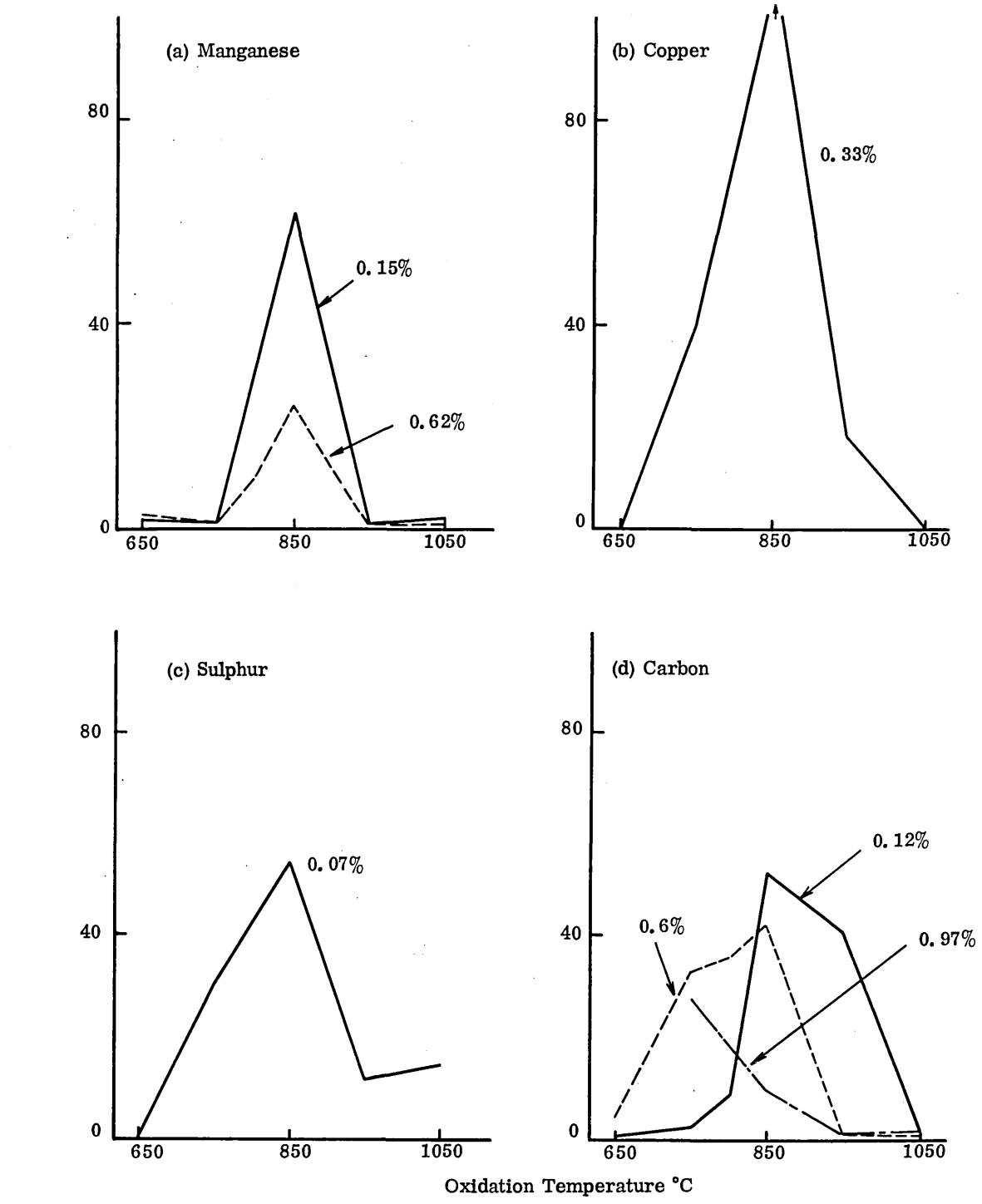

THE EFFECT OF ALLOY ADDITIONS ON THE ROOM TEMPERATURE ADHESION OF SCALES ON PURE IRON (CONSTANT SCALE THICKNESS - 200 μ - PETERS AND ENGELL)

FIG. 6

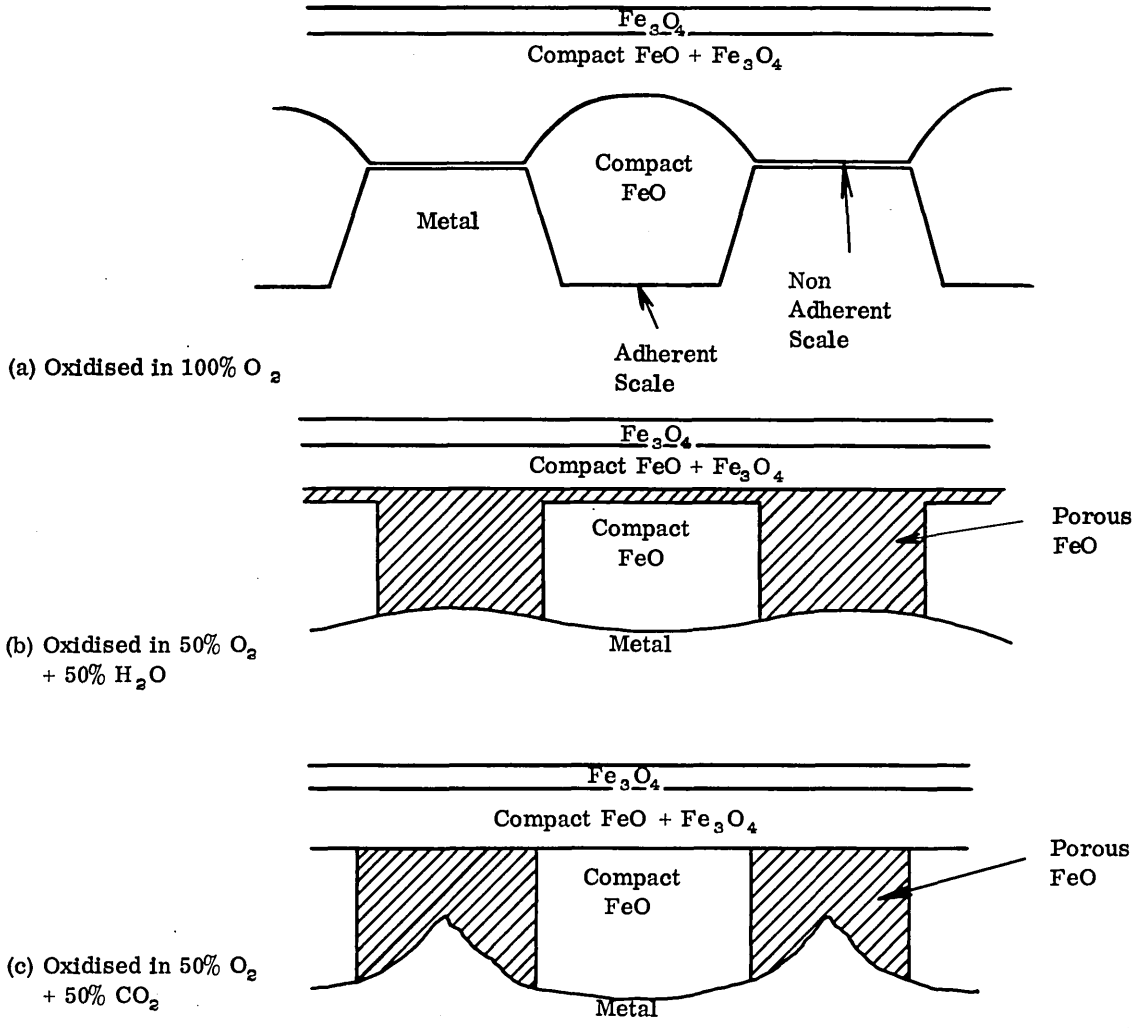

THE INFLUENCE OF WATER VAPOUR OR CARBON DIOXIDE IN THE FURNACE ATMOSPHERE ON THE OXIDATION OF IRON. (RAHMEL)[57]

FIG. 7 (5882)

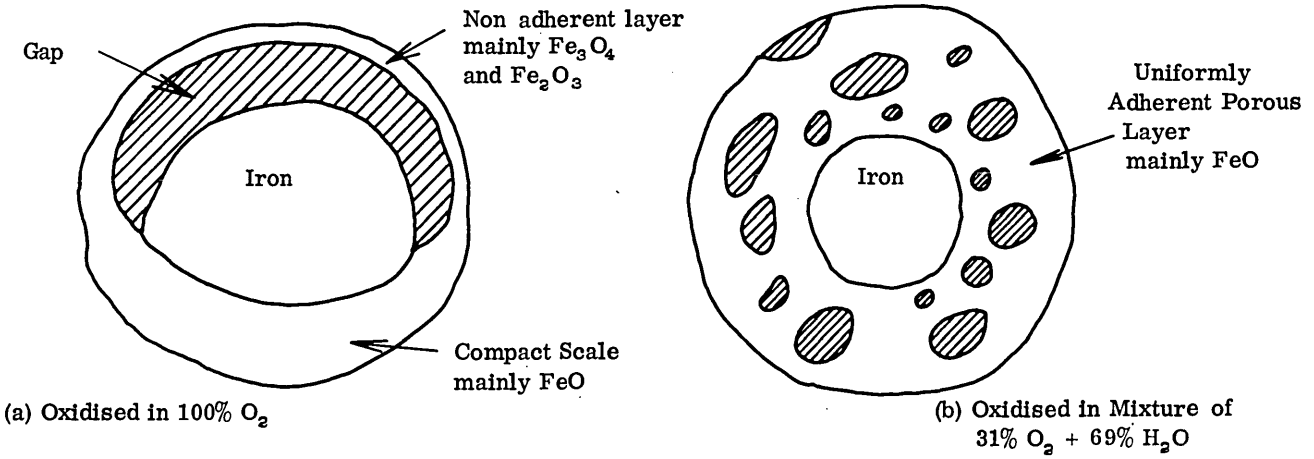

SCHEMATIC REPRESENTATION OF THE OXIDATION OF CYLINDRICAL SPECIMENS OF IRON (RAHMEL)[57]

FIG. 8

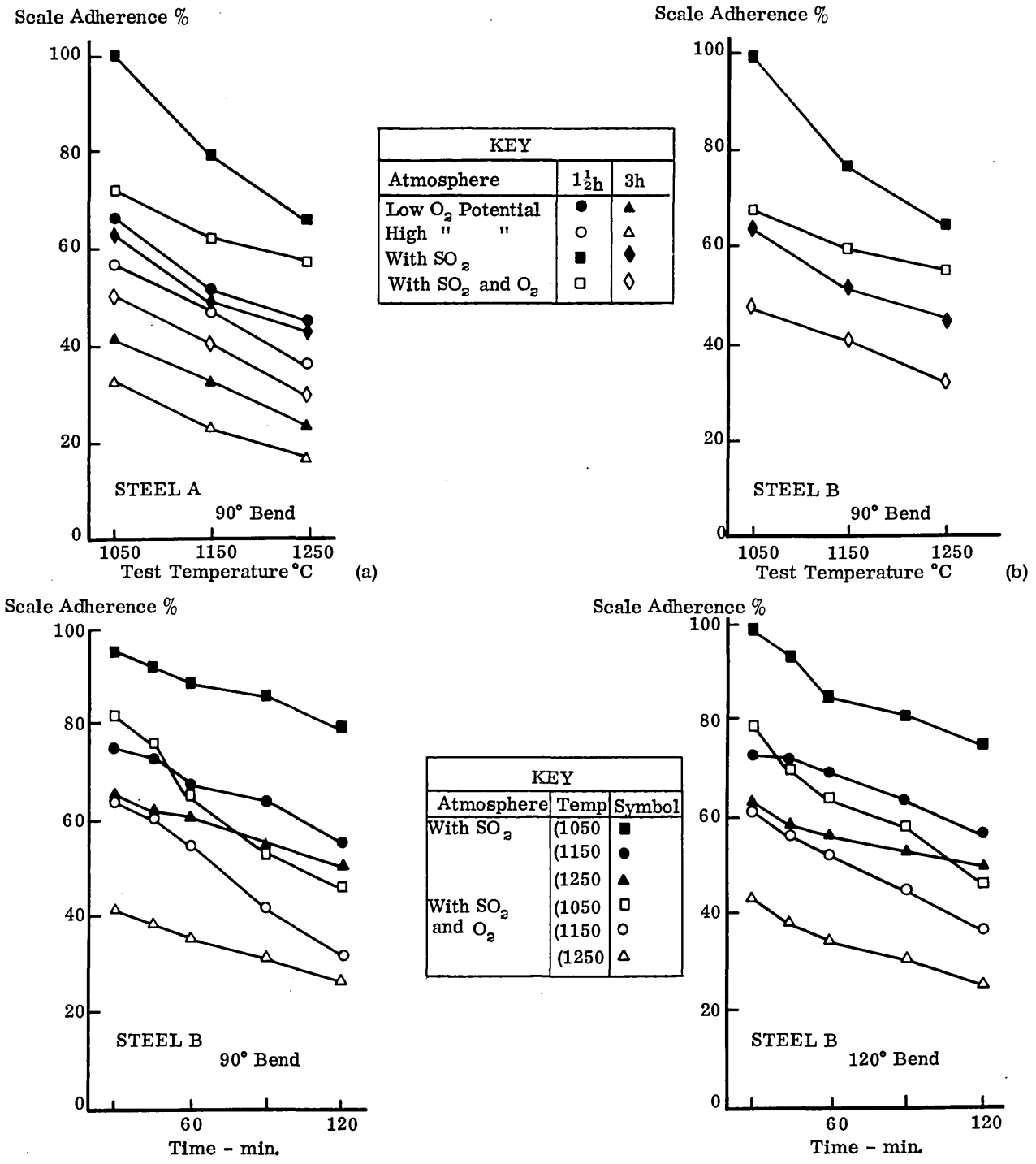

THE EFFECT OF OXIDATION CONDITIONS AND STRAIN RATE ON SCALE ADHERENCE (% ADHERENT SCALE) (HOUGH AND ROLLS - HOT BENDING)

0.7% C Si-KILLED STEEL WITH LOW (A) AND VERY LOW (B) RESIDUAL ELEMENTS

FIG. 9

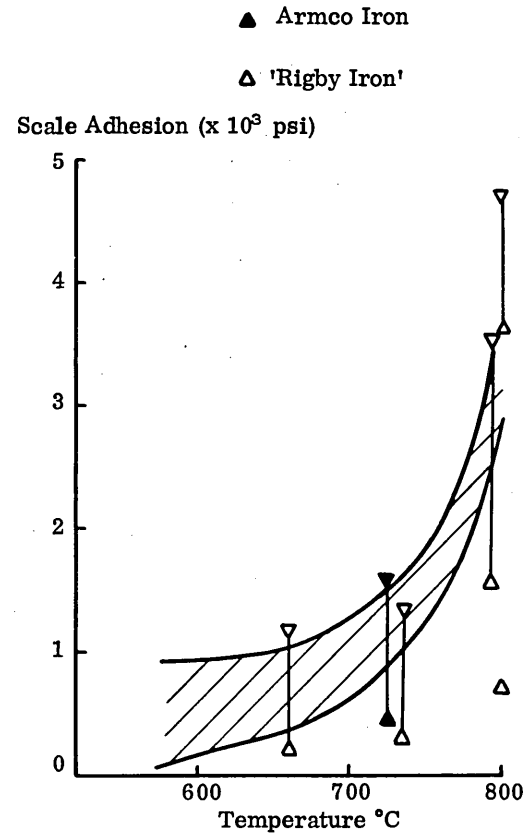

CALCULATED RESULTS OF BRUCE AND HANCOCK - VIBRATION TECHNIQUE FIG. 10

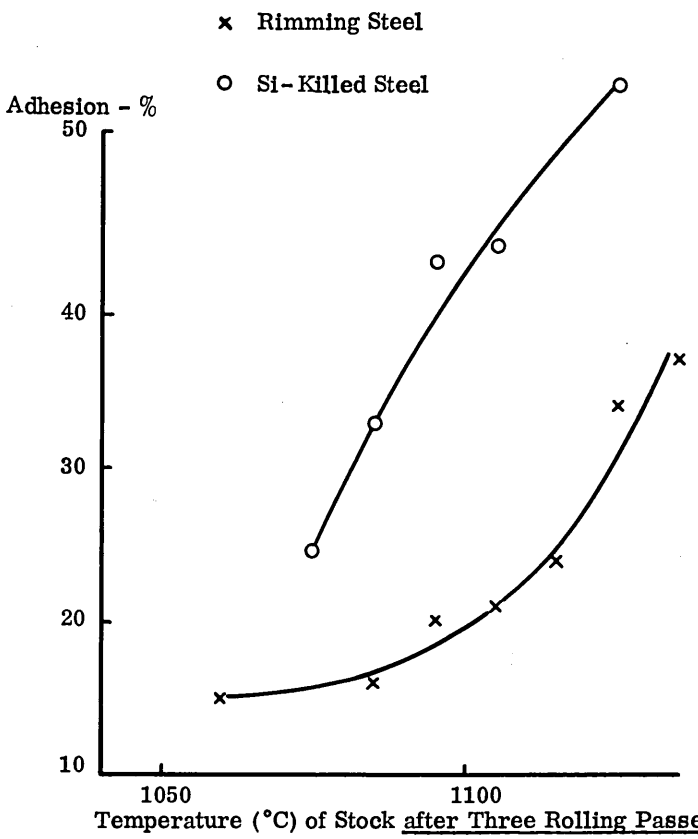

THE EFFECT OF REHEATING TEMPERATURE* ON THE AMOUNT OF FURNACE SCALE FOUND ON SLABS AFTER ROLLING (PALIN) FIG. 12

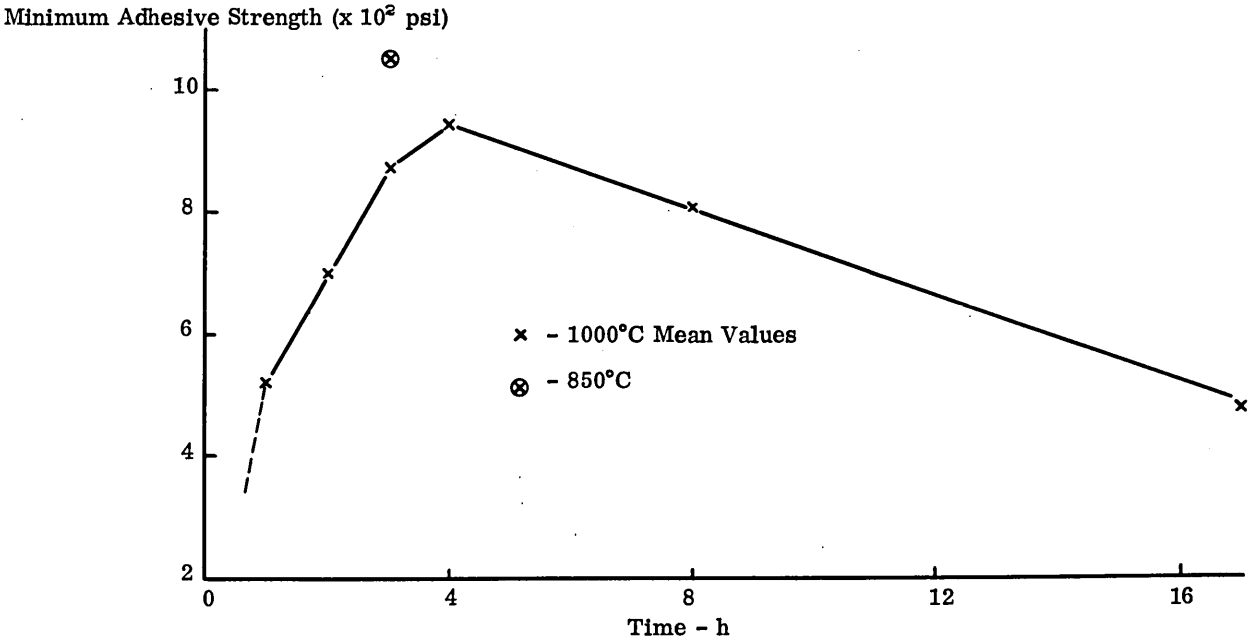

HOT DETACHMENT MEASUREMENTS OF HULLEY AND ROLLS

FIG. 11

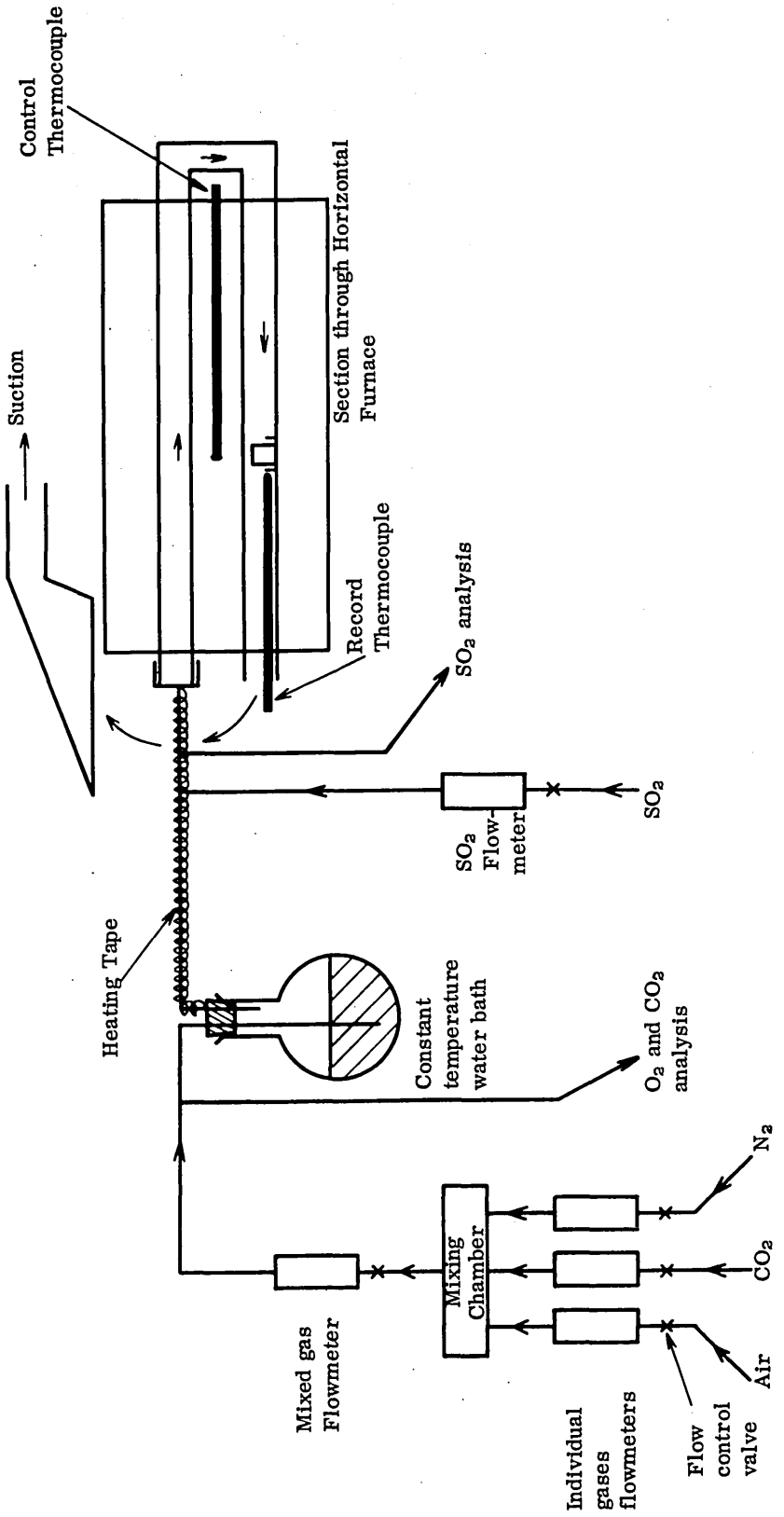

ARRANGEMENT OF APPARATUS (DIAGRAMMATIC)

FIG. 13

$\frac{1}{4}$ hour Unetched (a)

$\frac{1}{2}$ hour Unetched (b)

THE EFFECT OF REHEATING TIME ON THE SCALES FORMED
(SILICON KILLED STEEL 1050°C)

x200

FIG. 14

Unetched

THE EFFECT OF REHEATING TIME ON THE SCALES FORMED
(SILICON KILLED STEEL $1\frac{1}{2}$ HOURS AT 1050°C)

x200

FIG. 15

Unetched

THE EFFECT OF REHEATING TIME ON THE SCALES FORMED
(SILICON KILLED STEEL 3 HOURS AT 1050°C)

x200

FIG. 16

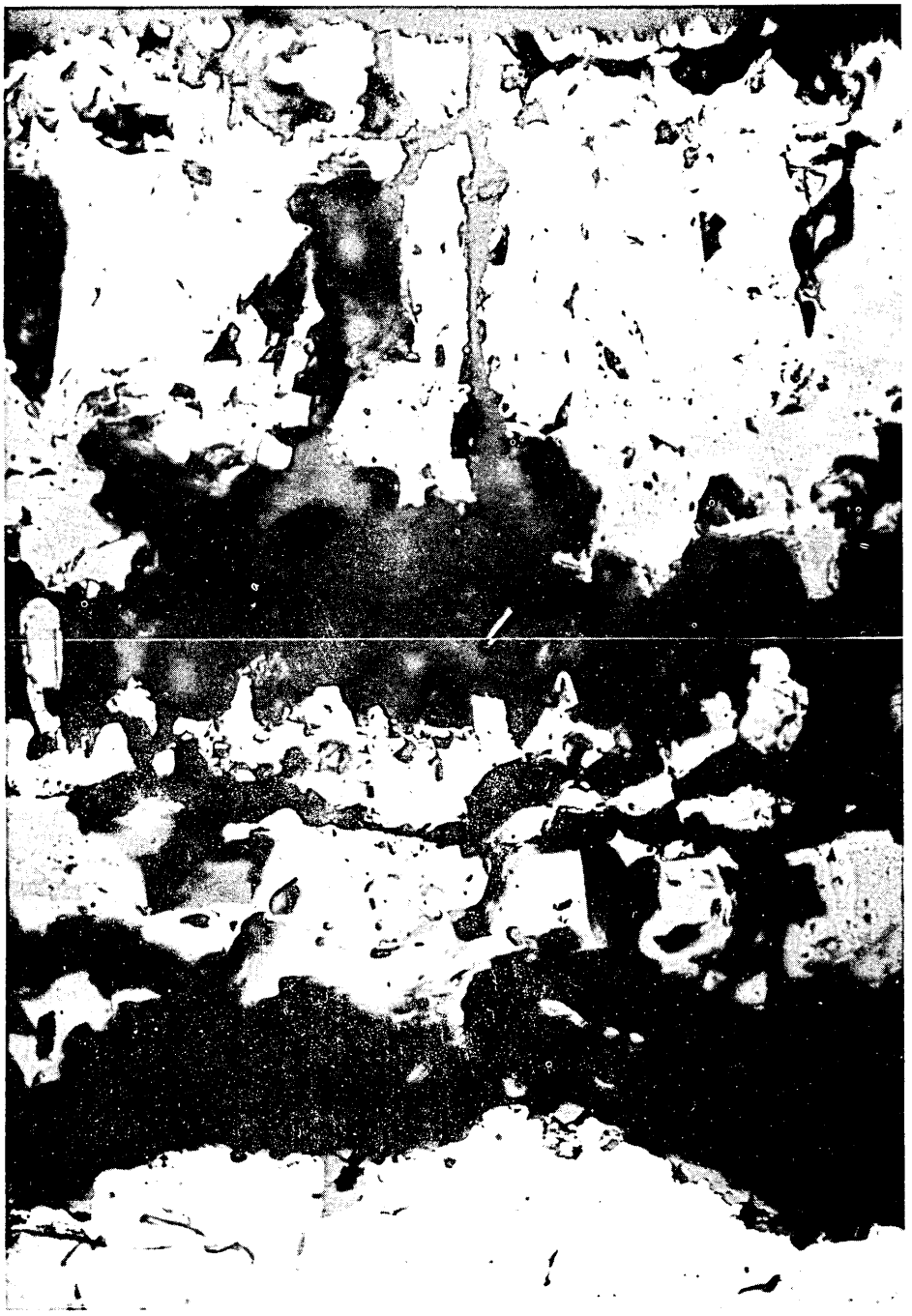

Unetched

THE EFFECT OF REHEATING TEMPERATURE ON THE SCALES FORMED
(SILICON KILLED STEEL 1½ HOURS AT 950°C)

x500

FIG. 17

Unetched

THE EFFECT OF REHEATING TEMPERATURE ON THE SCALES FORMED
(SILICON KILLED STEEL 1½ HOURS AT 1150°C)

x100

FIG. 18

Unetched

THE EFFECT OF REHEATING TEMPERATURE ON THE SCALE
(SILICON KILLED STEEL 1½ HOURS AT 1325°C)

x50

FIG. 19

← Thin layer of Fe_2O_3

Fe_3O_4

FeO containing Fe_3O_4 precipitates

FeO

Etched

TYPICAL SCALE PRODUCED (SEMI KILLED STEEL $1\frac{1}{2}$ HOURS AT 1250°C)

x200

FIG. 20

Unetched

EXAMPLE OF LENTICULAR POROSITY
(SILICON KILLED STEEL 3 HOURS AT 1150°C)
x200

FIG. 21

(a) $\frac{1}{2}$ hour at 950°C

Etched

x500

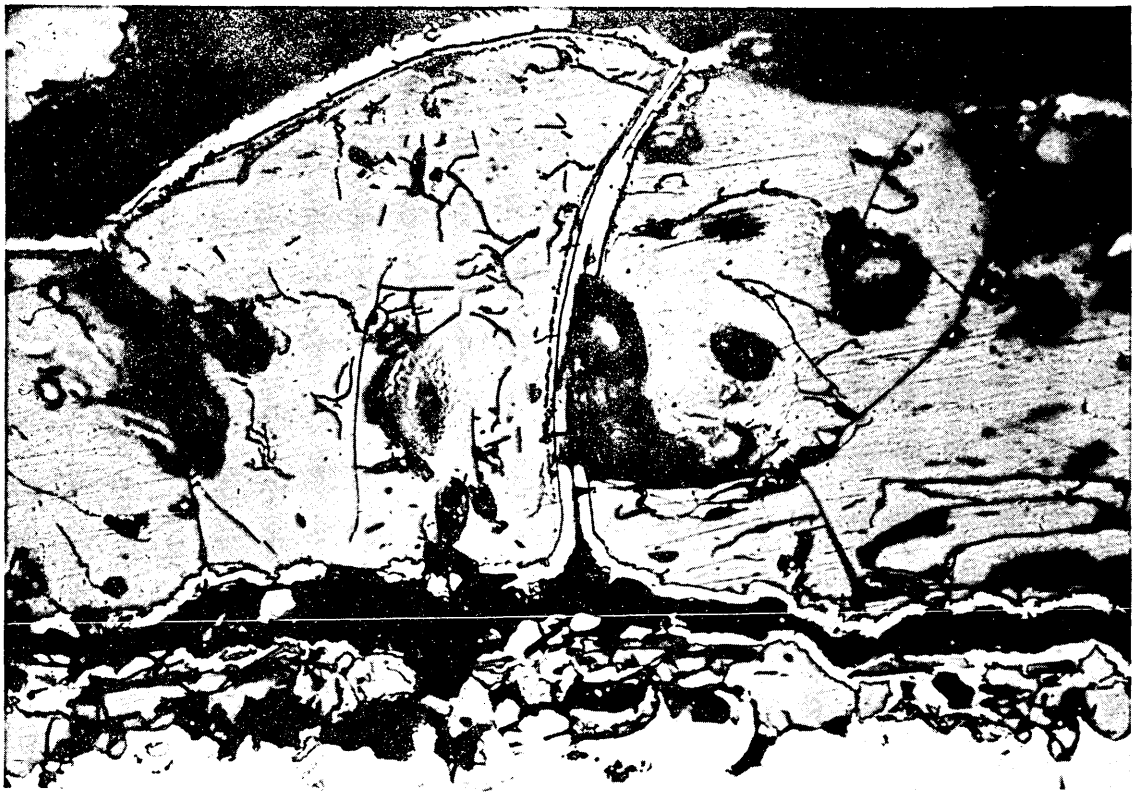

x750 3 hours at 950°C Etched (b)

EXAMPLES OF CRACKS IN THE WUSTITE LAYER ADJACENT TO THE METAL SURFACE CONTAINING MAGNETITE

FIG. 22

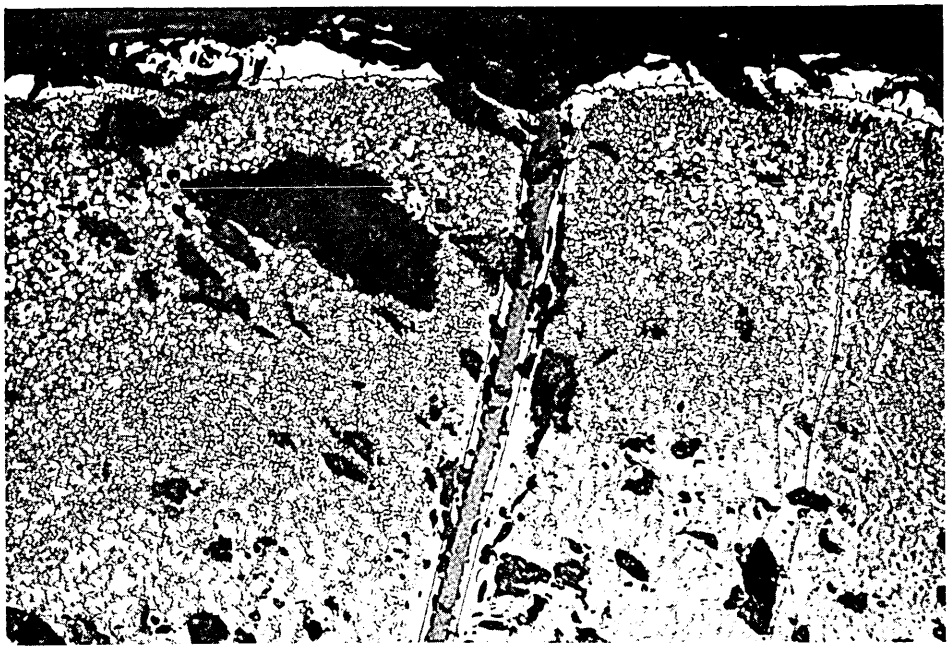

x150

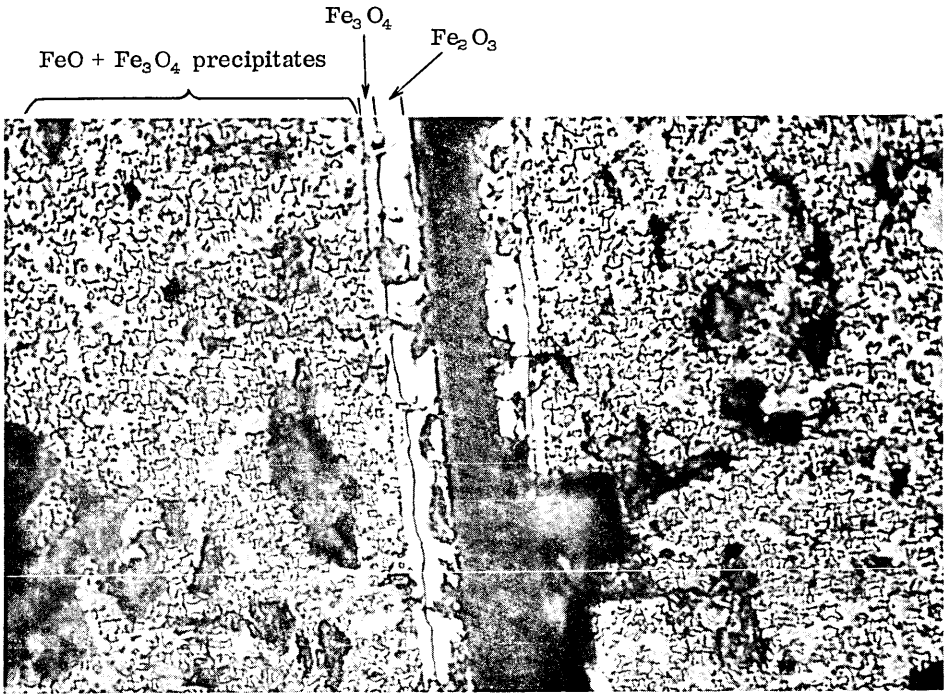

x500

EXAMPLES OF A CRACK FORMED THROUGH THE SCALE LAYERS CONTAINING THE HIGHER OXIDES OF IRON (SEMI KILLED STEEL $1\frac{1}{2}$ HOURS AT 1050°C)

FIG. 23

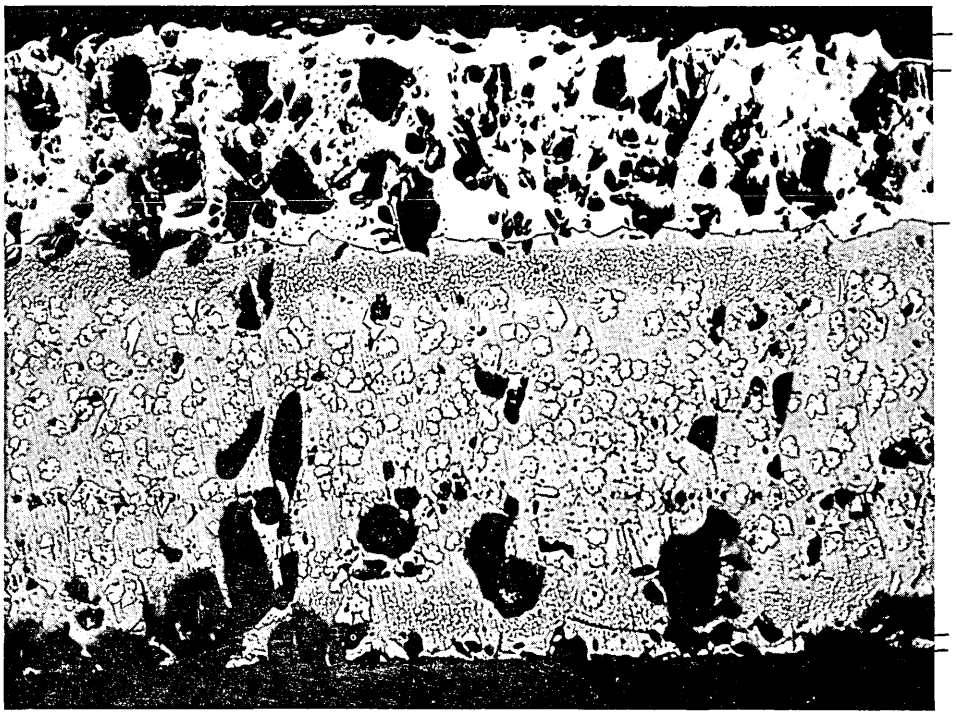

Etched

EXAMPLE OF SCALE STRUCTURE OF NON-ADHERENT SCALE
(RIMMING STEEL 1½ HOURS AT 950°C)

x100

FIG. 24

Etched

EXAMPLE OF DISCONTINUOUS LINE OF Fe_3O_4 IN THE FeO LAYER
(SEMI KILLED STEEL 1½ HOURS AT 1150°C)

x750

FIG. 25

EXAMPLE OF THE DARK PHASE FORMED AT THE METAL SURFACE
(SILICON KILLED STEEL 950°C FOR 3 HOURS)

x500

FIG. 26

EXAMPLE OF THE DARK PHASE FORMED AT THE METAL SURFACE
(ALUMINIUM TREATED STEEL 950°C FOR 3 HOURS)

x750

FIG. 27

LIQUID PHASES IN THE FeO GRAIN BOUNDARIES (SILICON KILLED STEEL 1150°C ½ HOUR)

FIG. 28

Unetched

x150

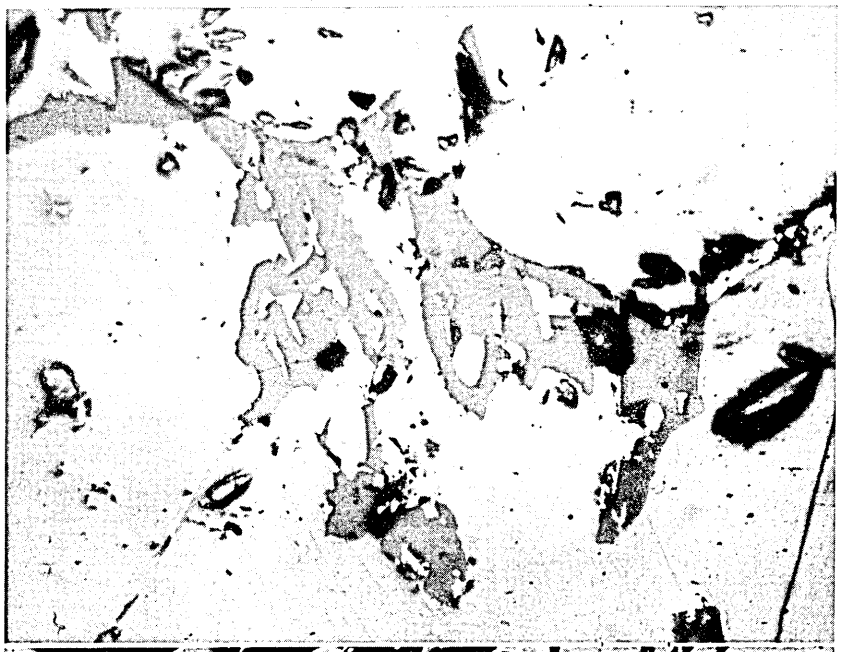

(a) Silicon killed steel 1250°C 1½ hours.

Unetched

x500

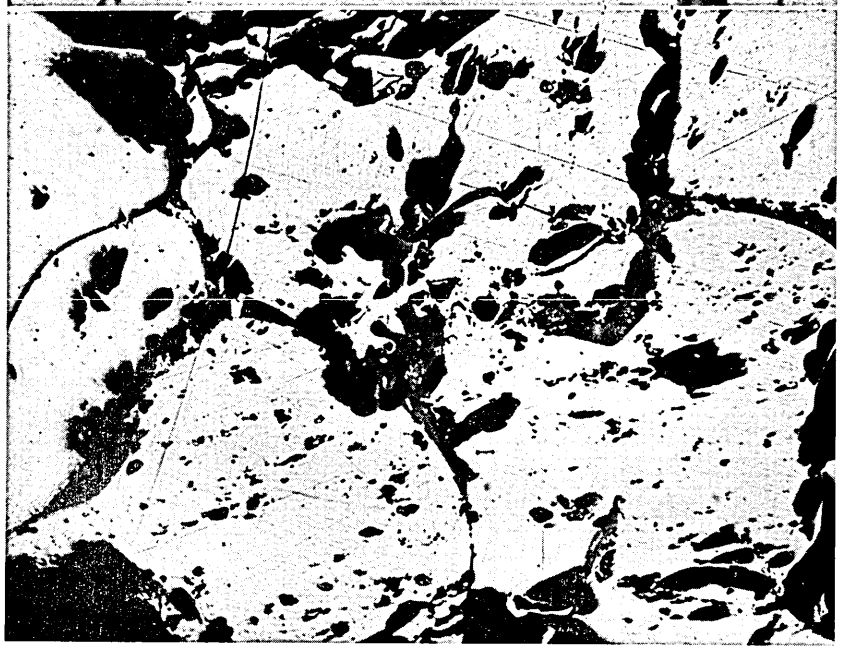

(b) Al treated steel 1350°C 3 hours.

Unetched

x500

EXAMPLES OF LIQUID PHASES IN THE FeO LAYER - STEELS CONTAINING SILICON

FIG. 29

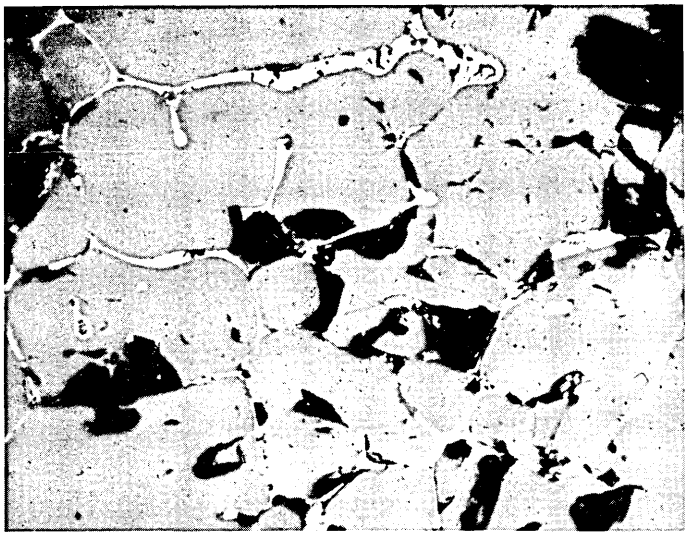

Unetched

LIQUID PHASES FORMED IN THE FeO LAYER ON RIMMING STEEL AFTER $1\frac{1}{2}$ HOURS AT 1325°C
x500

FIG. 30

Unetched

LIQUID PHASES FORMED IN THE FeO LAYER IN THE SEMI KILLED STEEL AFTER $1\frac{1}{2}$ HOURS AT 1350°C
x50

FIG. 31

(a) 950°C

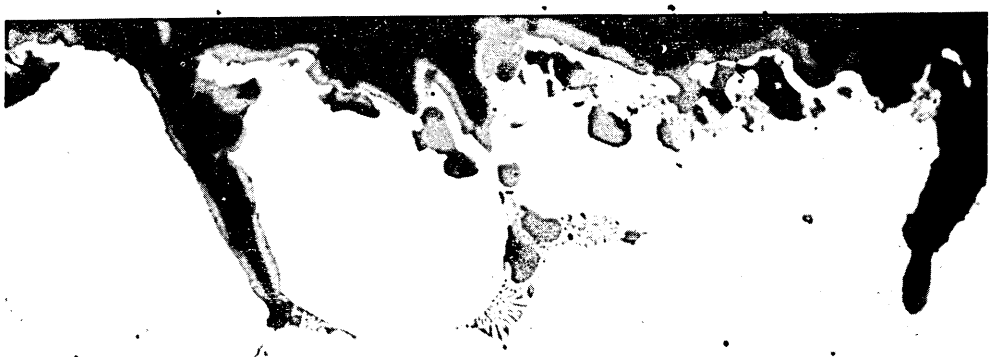

(b) 1050°C

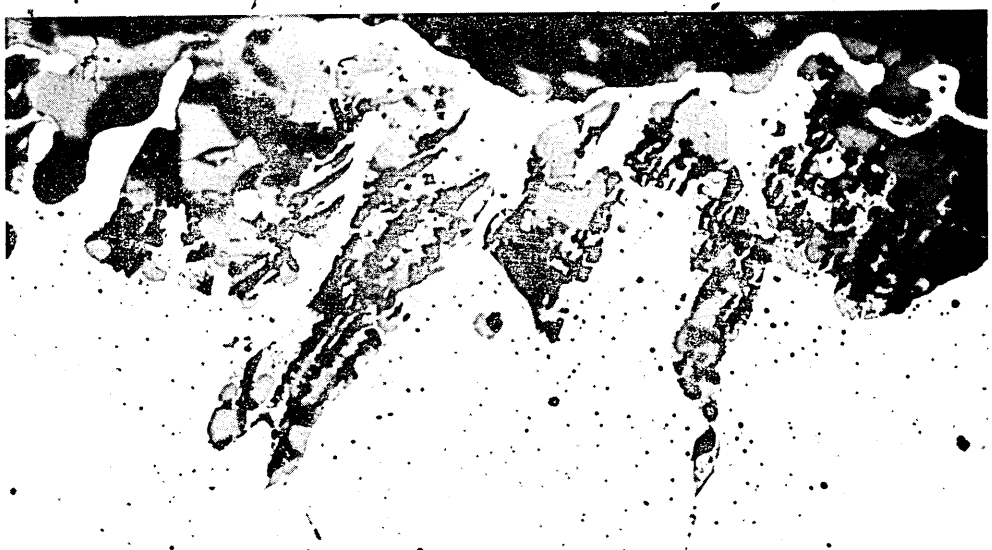

(c) 1150°C

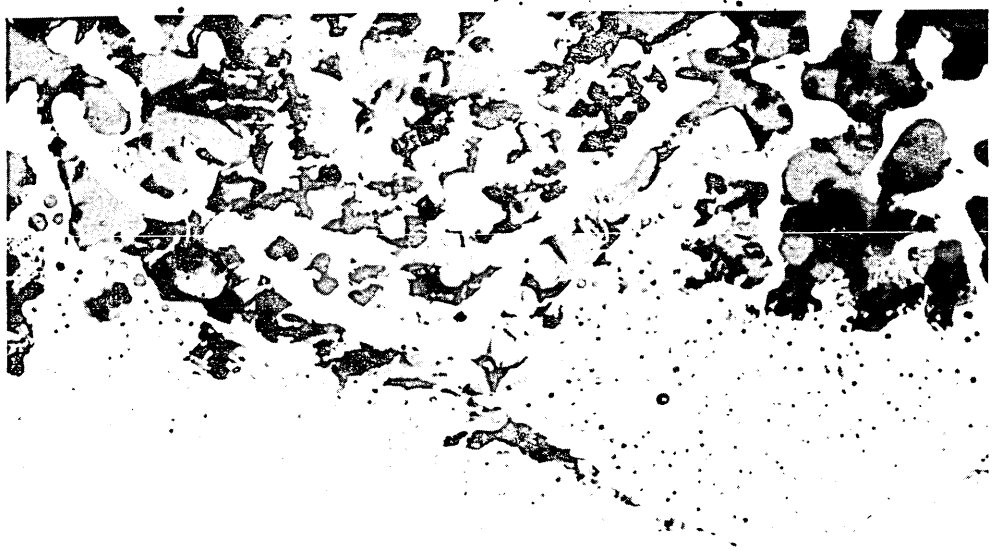

(d) 1250°C

Unetched

THE EFFECT OF TEMPERATURE ON THE METAL/SCALE INTERFACE FORMED IN THE SILICON KILLED STEEL AFTER ½ HOUR

x500

FIG. 32

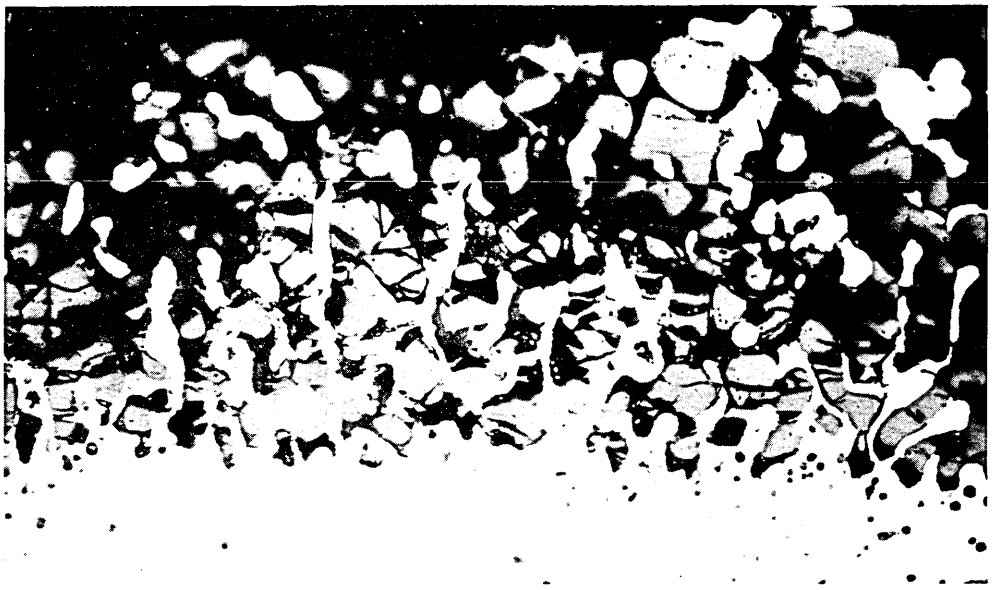

$\frac{1}{4}$ hour Unetched (a)

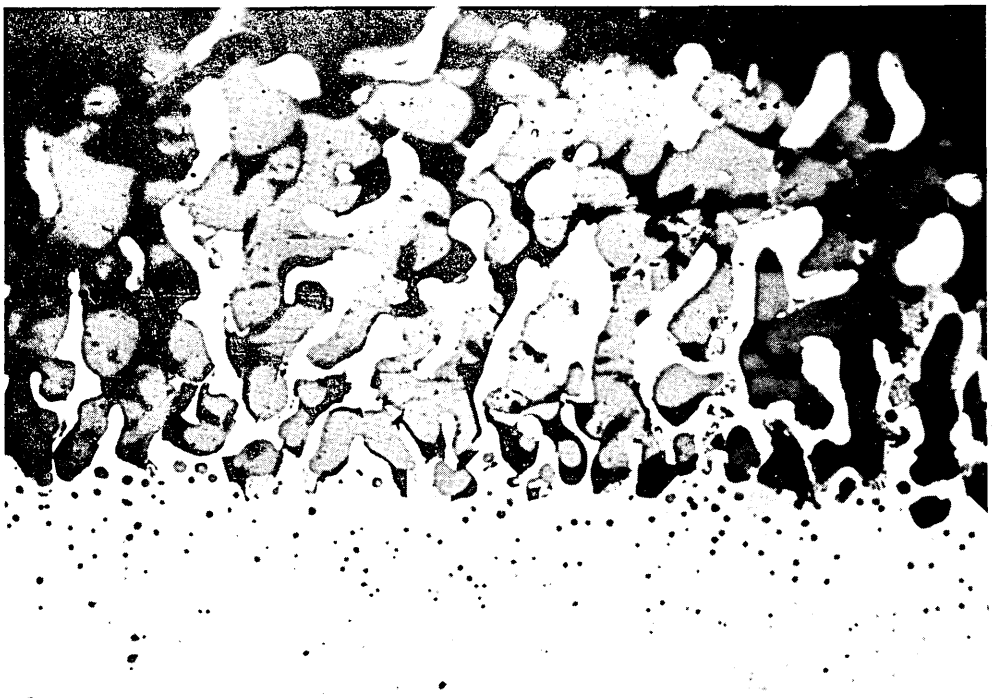

$\frac{1}{2}$ hour Unetched (b)

THE EFFECT OF TIME ON THE METAL/SCALE INTERFACE PRODUCED AT 1350°C ON THE SILICON KILLED STEEL

x500

FIG. 33

/\ hours Unetched (a)

Unetched

THE EFFECT OF TIME ON THE METAL/SCALE INTERFACE PRODUCED ON THE SILICON KILLED STEEL AT 1350°C

x500

PIG. 3U

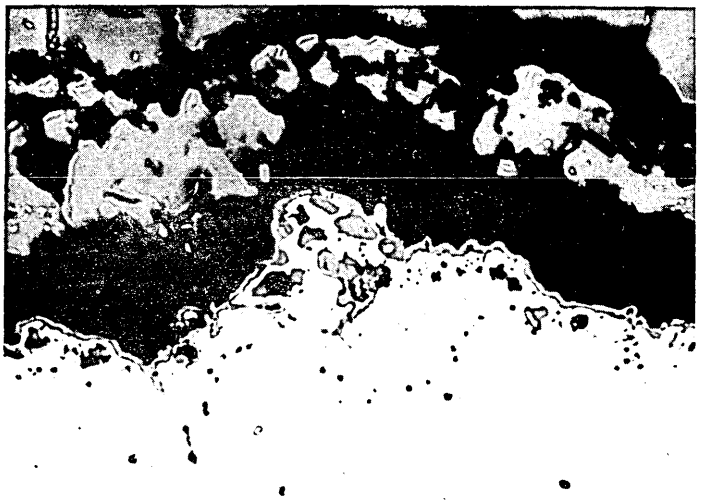

(a) 1050°C

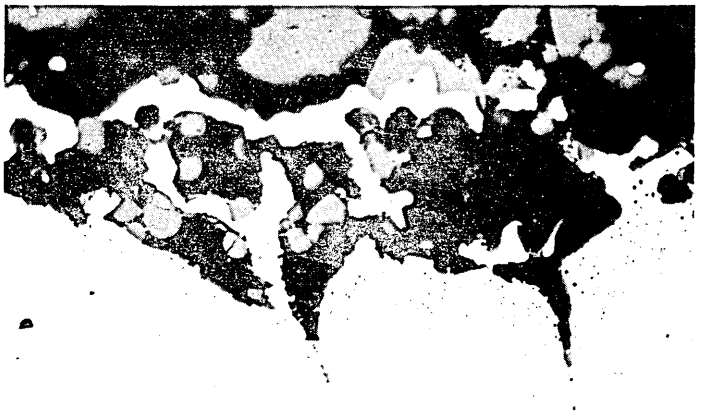

(b) 1150°C

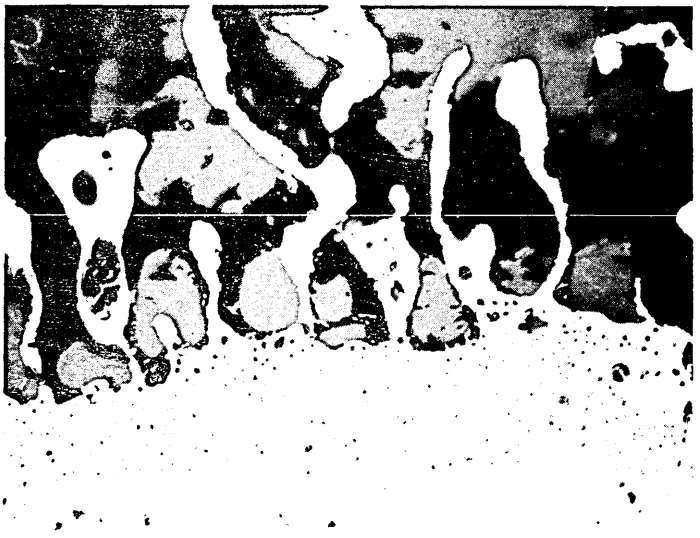

(c) 1250°C

Unetched

THE EFFECT OF TEMPERATURE ON THE METAL/SCALE INTERFACE PRODUCED ON THE Al TREATED STEEL AFTER $\frac{1}{2}$ HOUR

x500

FIG. 35

(a) $\frac{1}{4}$ hour

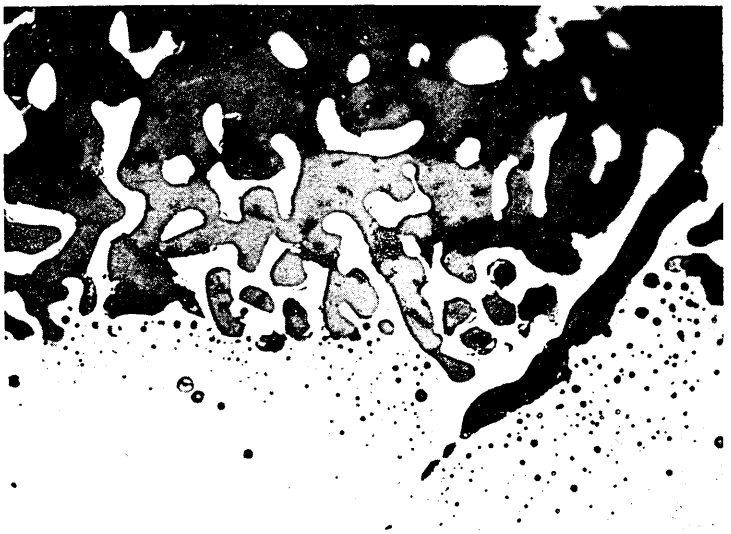

(b) $\frac{1}{2}$ hour

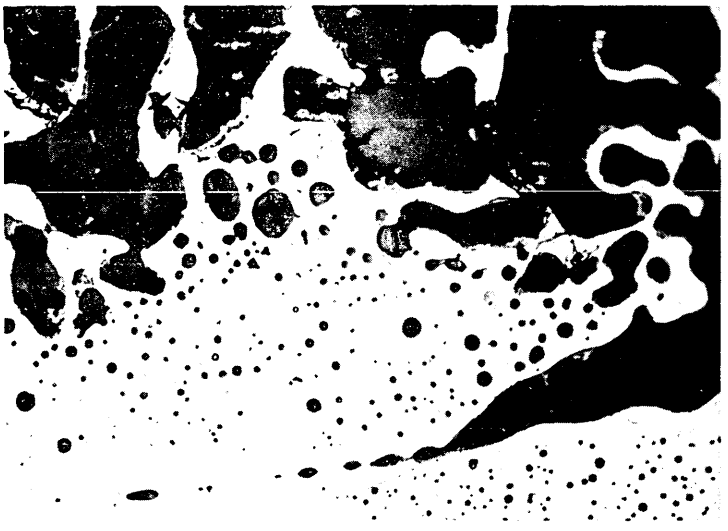

(c) $1\frac{1}{2}$ hours

Unetched

THE EFFECT OF TIME ON THE METAL/SCALE INTERFACE PRODUCED ON THE Al TREATED STEEL AT 1340°C

x500

FIG. 36

(a) 1050°C

(b) 1150°C

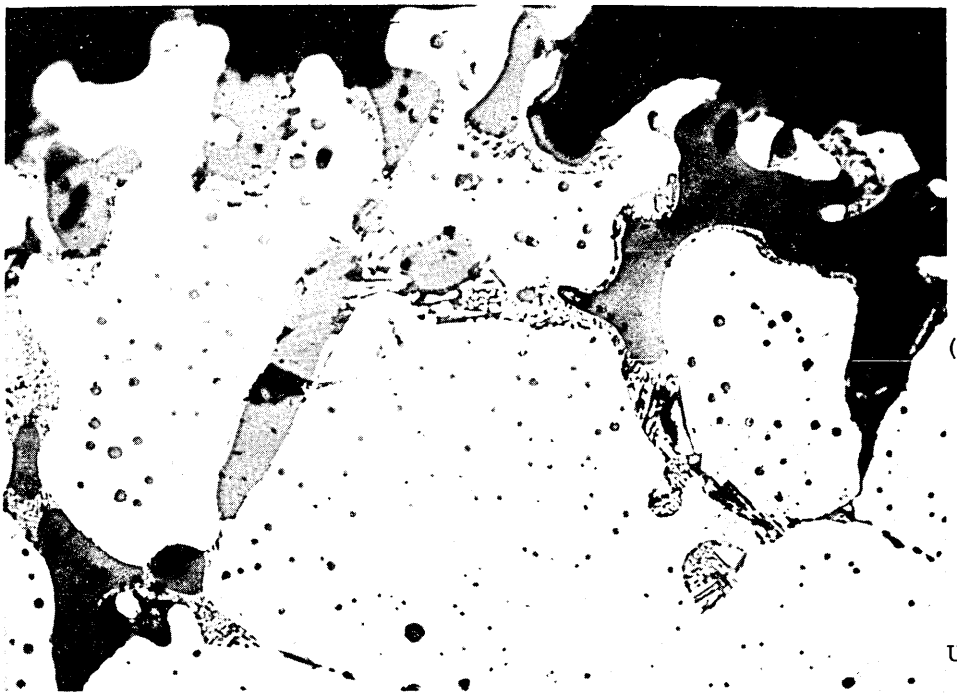

(c) 1250°C

Unetched

THE EFFECT OF TEMPERATURE ON THE METAL/SCALE INTERFACE PRODUCED ON THE SEMI KILLED STEEL AFTER $\frac{1}{2}$ HOUR

x500

FIG. 37

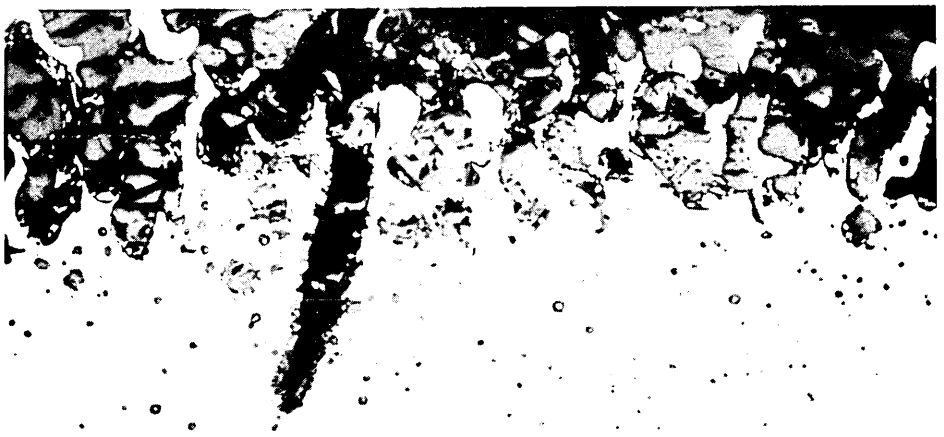

(a) $\frac{1}{4}$ hour

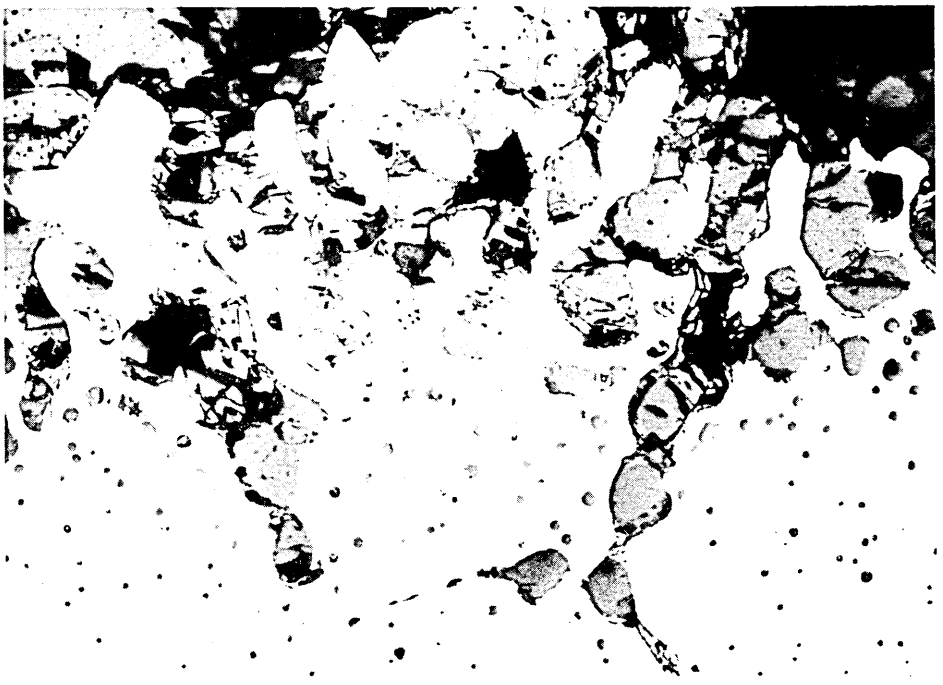

(b) $\frac{1}{2}$ hour

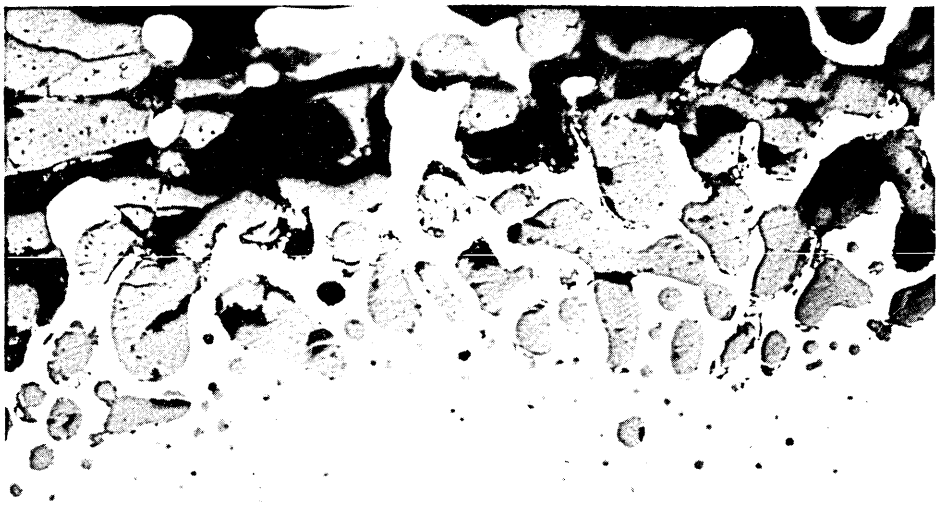

(c) $1\frac{1}{2}$ hours

Unetched

THE EFFECT OF TIME ON THE METAL/SCALE INTERFACE PRODUCED ON THE SEMI KILLED STEEL AT 1350°C

x500

FIG. 38

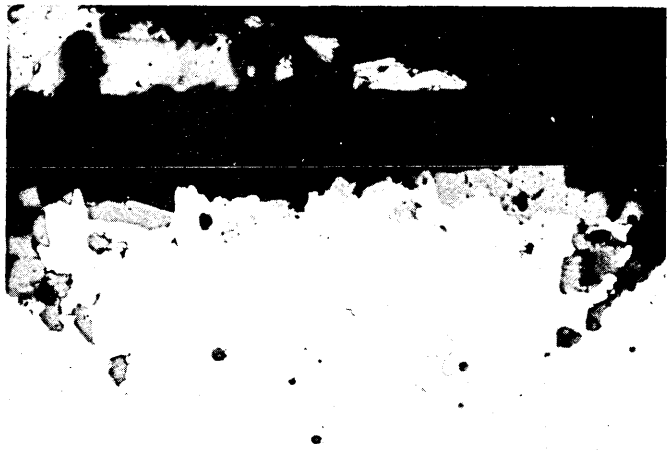

(a) 1050°C

(b) 1150°C

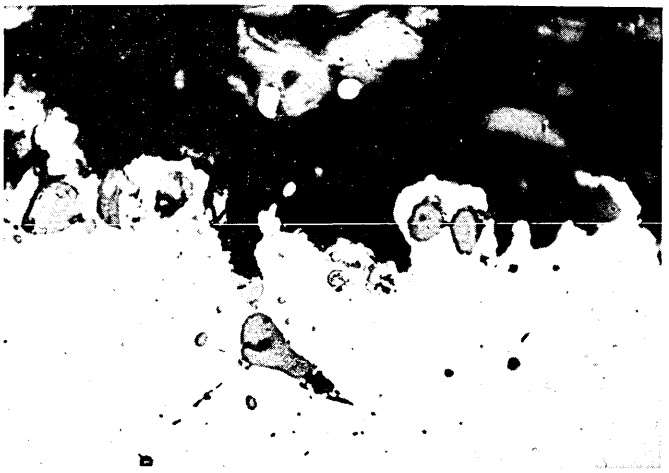

(c) 1250°C

Unetched

THE EFFECT OF TEMPERATURE ON THE METAL/SCALE INTERFACE PRODUCED ON THE RIMMING STEEL AFTER $\frac{1}{2}$ HOUR

x500

FIG. 39

(a) $\frac{1}{4}$ hour

(b) $\frac{1}{2}$ hour

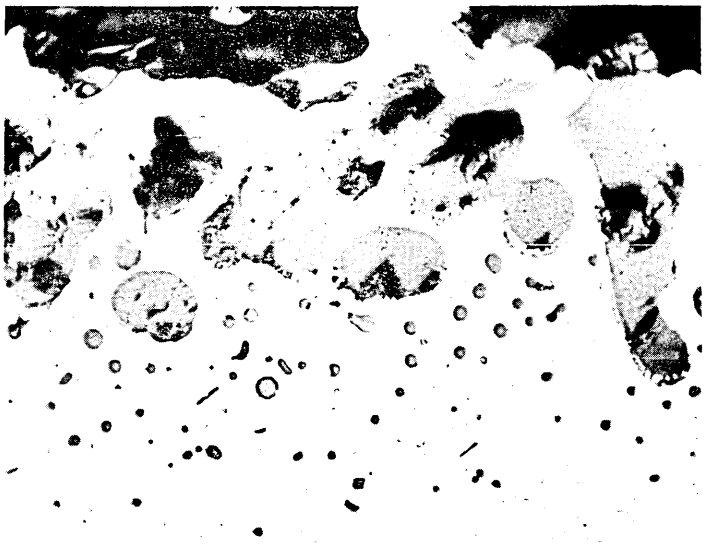

(c) $1\frac{1}{2}$ hours

Unetched

THE EFFECT OF TIME ON THE METAL/SCALE INTERFACE PRODUCED AT 1325°C ON THE RIMMING STEEL

x500

FIG. 40

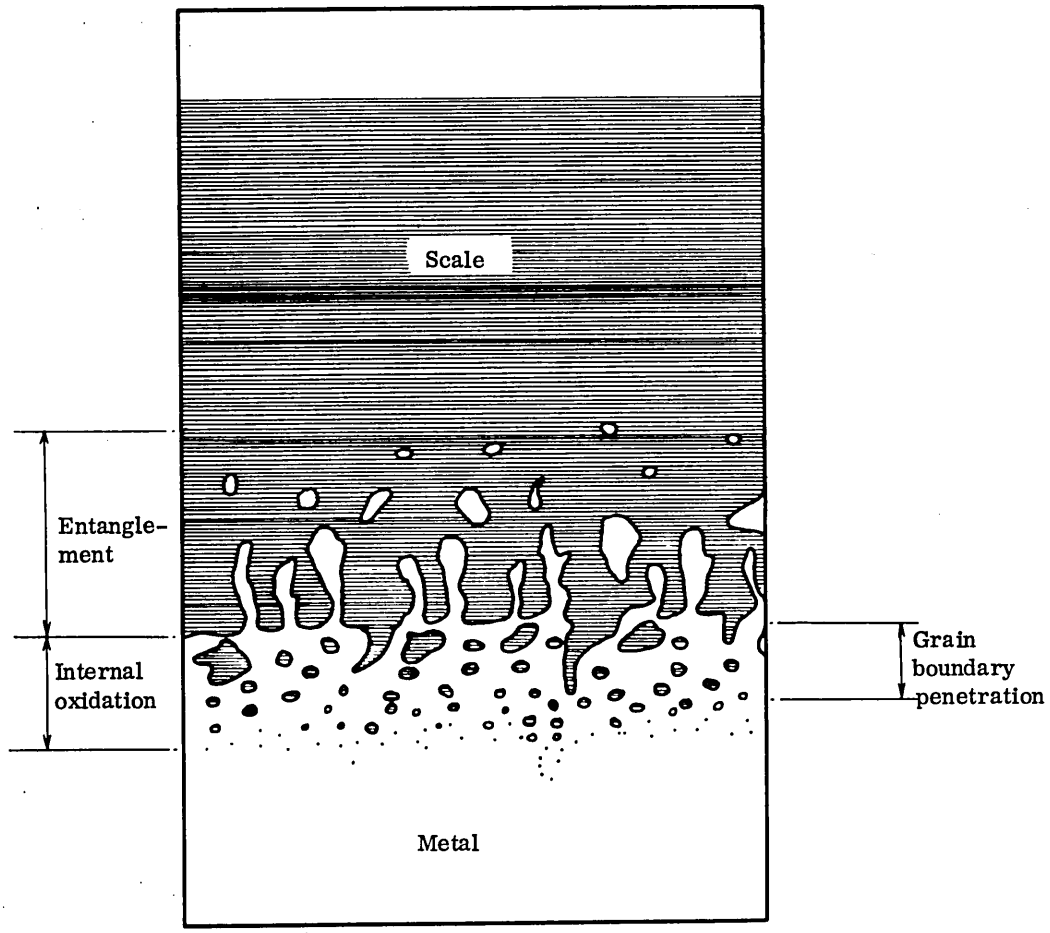

ILLUSTRATION OF METALLOGRAPHIC MEASUREMENTS MADE

FIG. 41

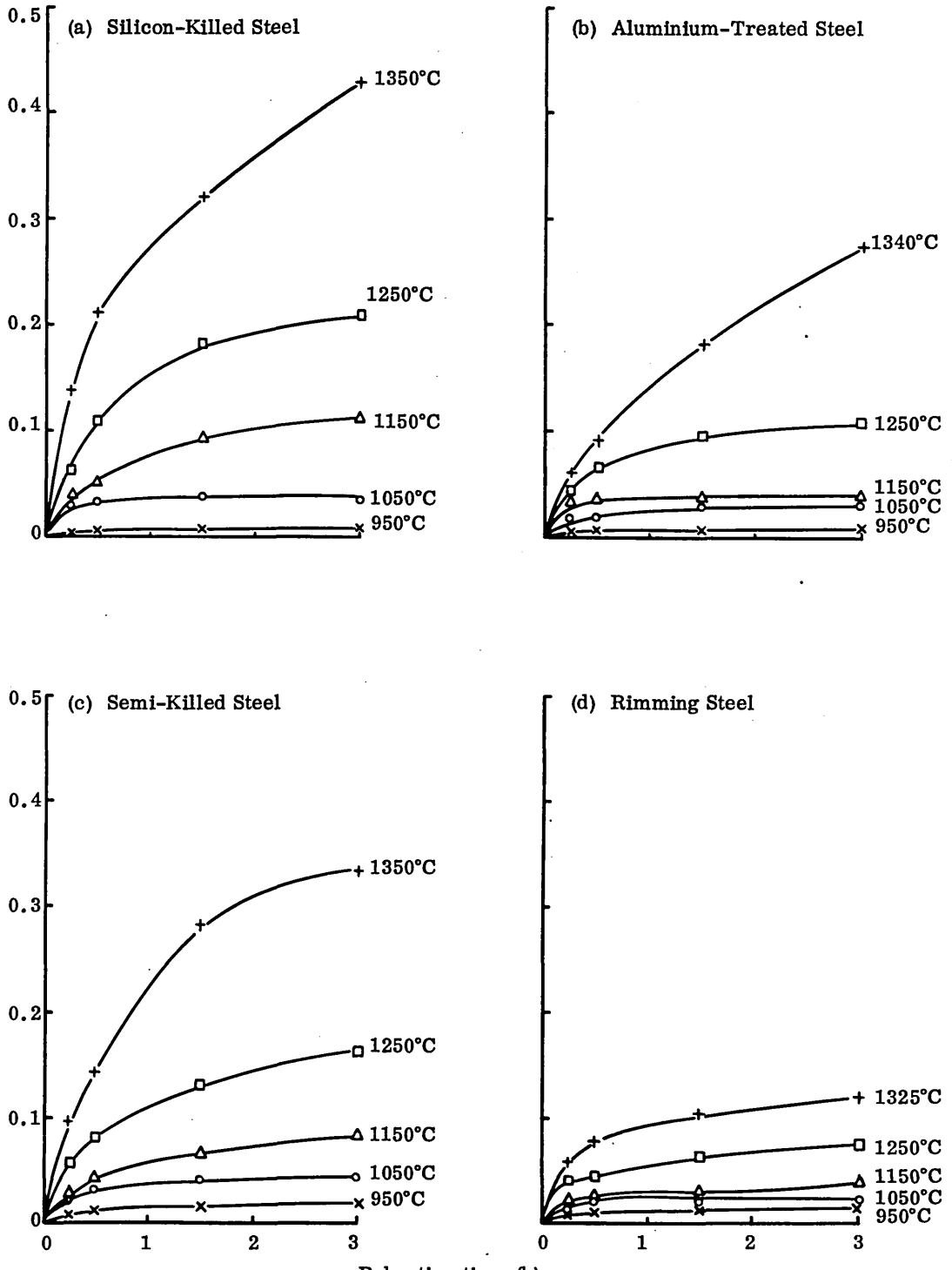

THE EFFECTS OF REHEATING TIME AND TEMPERATURE ON THE DEPTH OF METAL-SCALE ENTANGLEMENT

FIG. 42

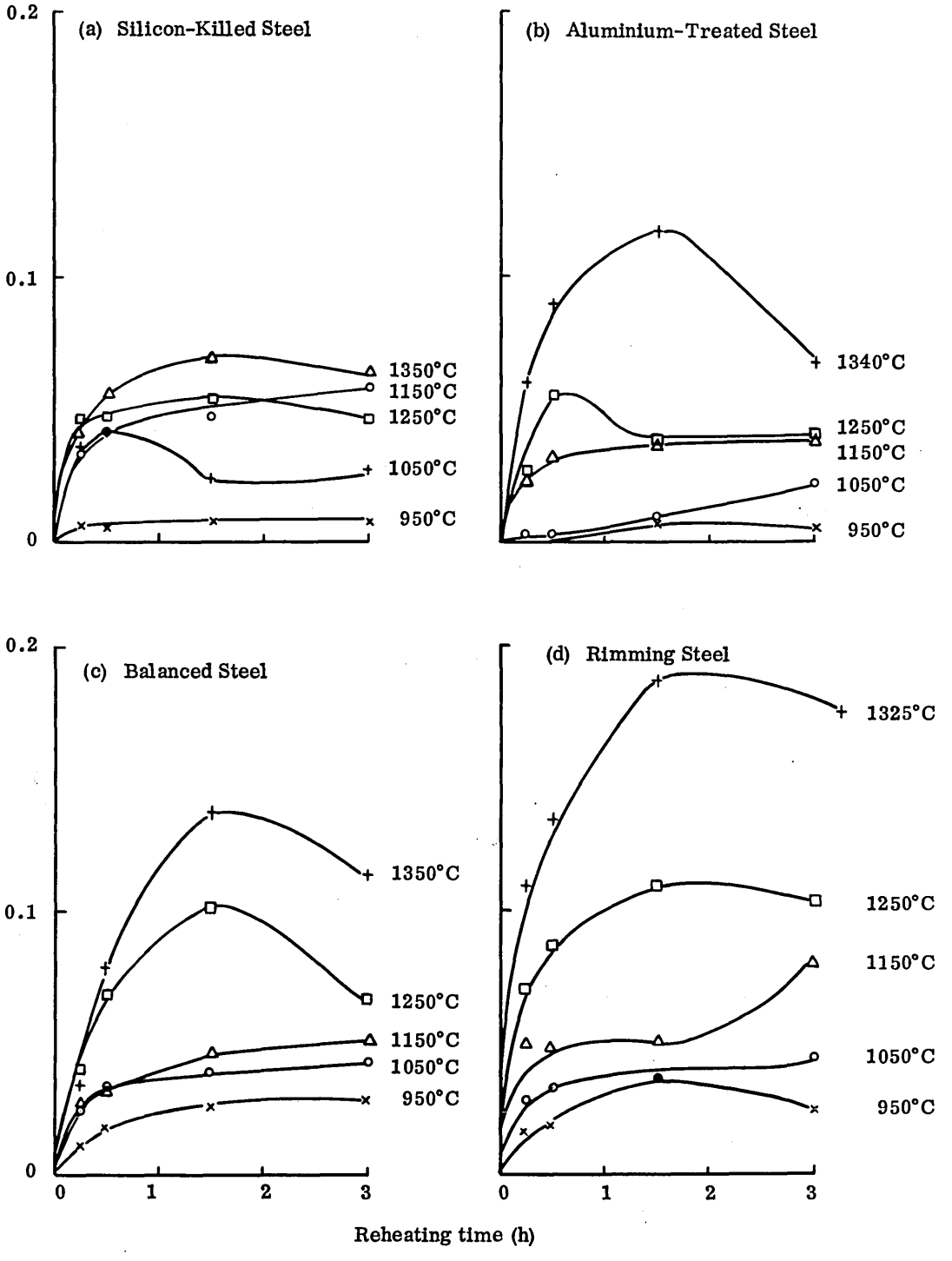

THE EFFECTS OF REHEATING TIME AND TEMPERTURE ON THE DEPTH OF GRAIN BOUNDARY OXIDE PENETRATION

FIG. 43

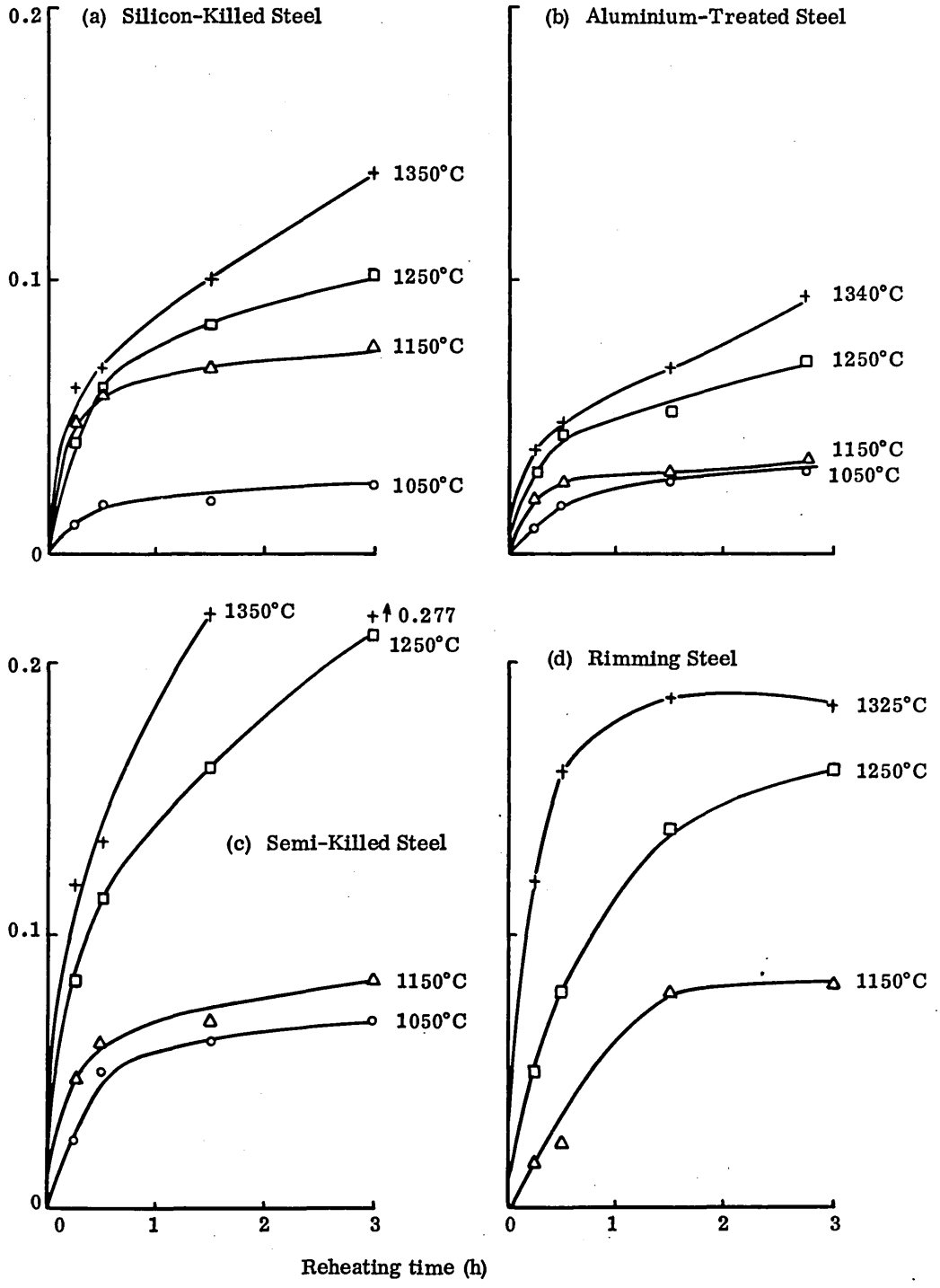

THE EFFECTS OF REHEATING TEMPERATURE AND TIME ON THE DEPTH OF INTERNAL OXIDATION

FIG. 44

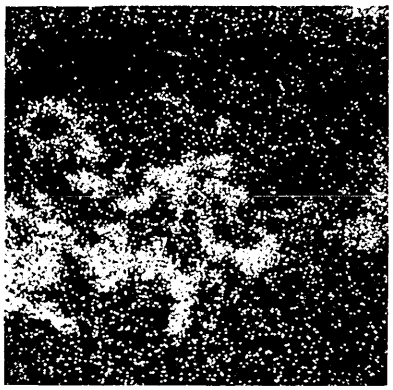

Silicon (a)

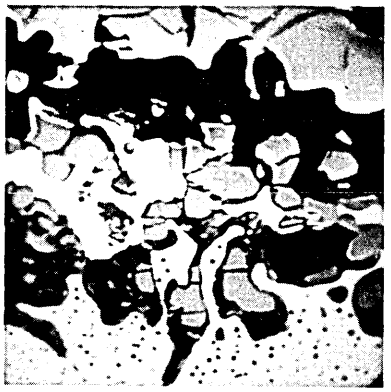

Electron image (b)

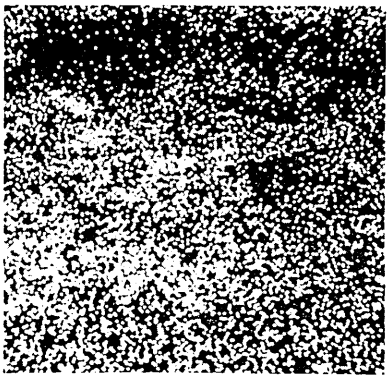

Sulphur (c)

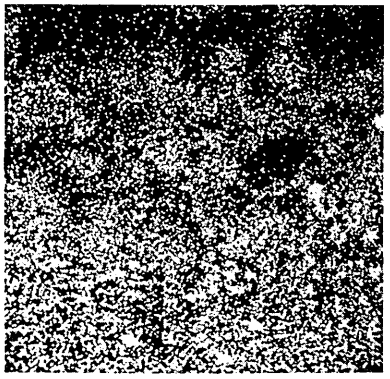

Manganese (d)

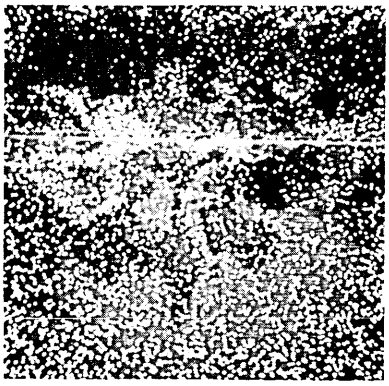

Nickel (1.2%) (e)

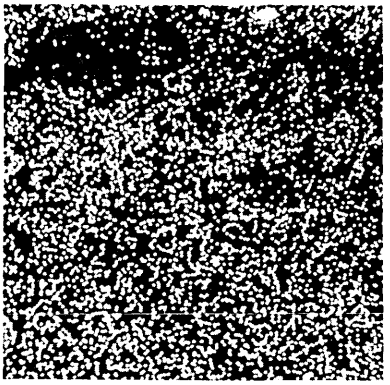

Copper (f)

ELECTRON-PROBE ANALYSIS RESULTS
SILICON KILLED STEEL 1150°C 1½ HOURS

FIG. 45

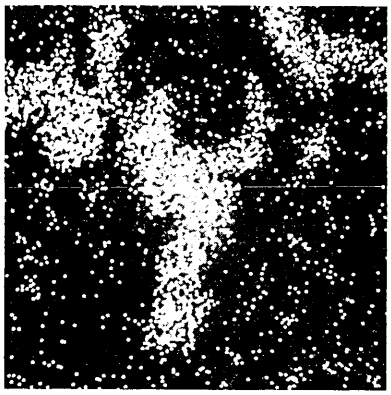

Silicon (20% Si) (a)

Electron image (b)

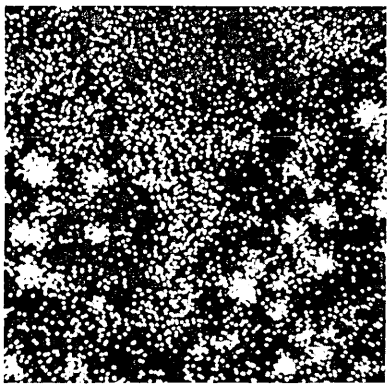

Manganese (c)

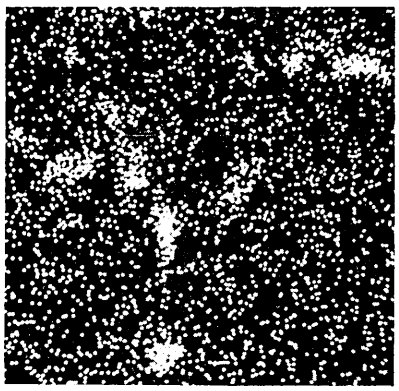

Sulphur (30% S) (d)

ELECTRON-PROBE ANALYSIS RESULTS
SILICON KILLED STEEL 1150°C 1½ HOURS (ANOTHER AREA)

FIG. 46

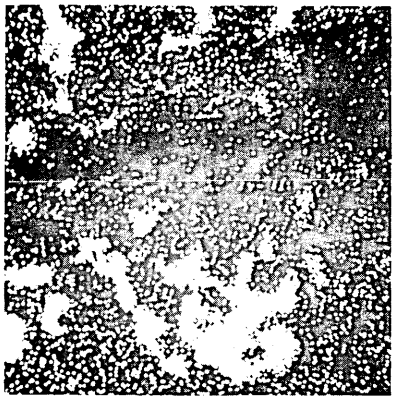

Silicon (24% Si) (a)

Electron image (b)

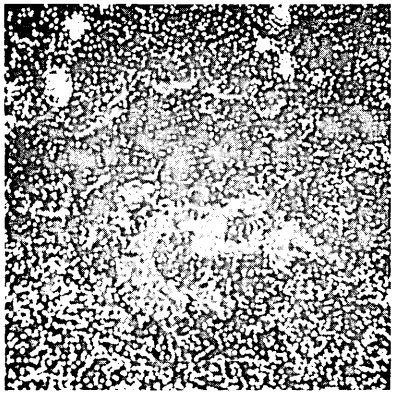

Nickel (1.7%) (c)

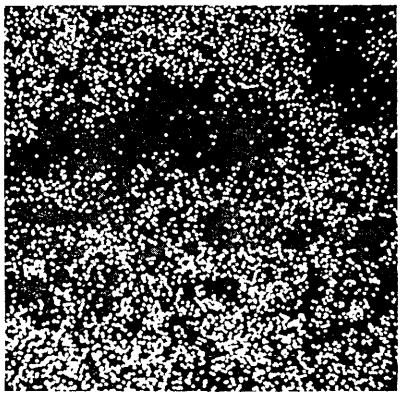

Manganese (d)

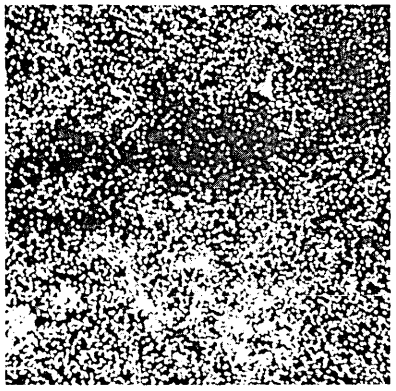

Sulphur (e)

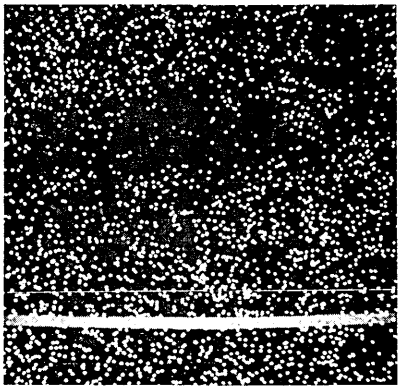

Aluminium (f)

ELECTRON-PROBE RESULTS
ALUMINIUM TREATED STEEL 1150°C 1½ HOURS

FIG. 47

Electron Image (a) Sulphur (30% S) (b)

Nickel (c) Silicon (d) Manganese (e)

ELECTRON-PROBE RESULTS
SEMI-KILLED STEEL 1150°C *1j* HOURS

PIG. 1^8

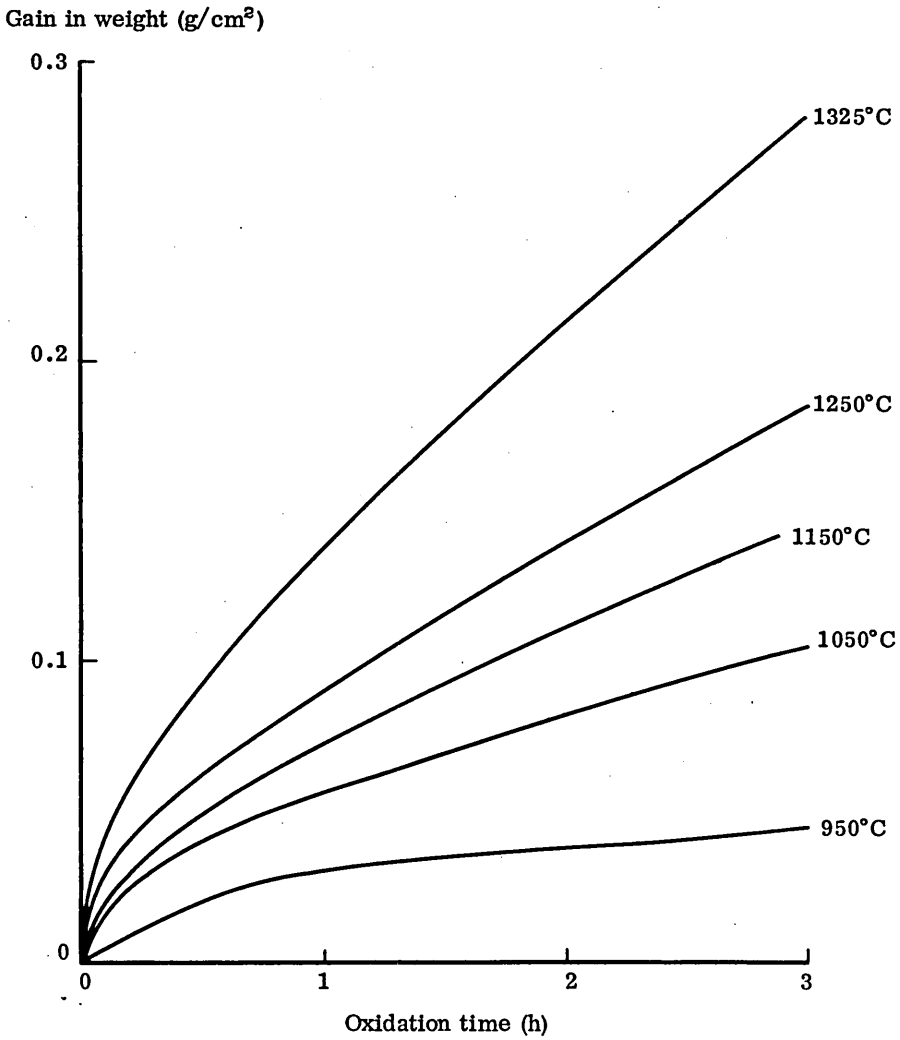

GRAVIMETRIC OXIDATION DATA
SILICON-KILLED STEEL

FIG. 49

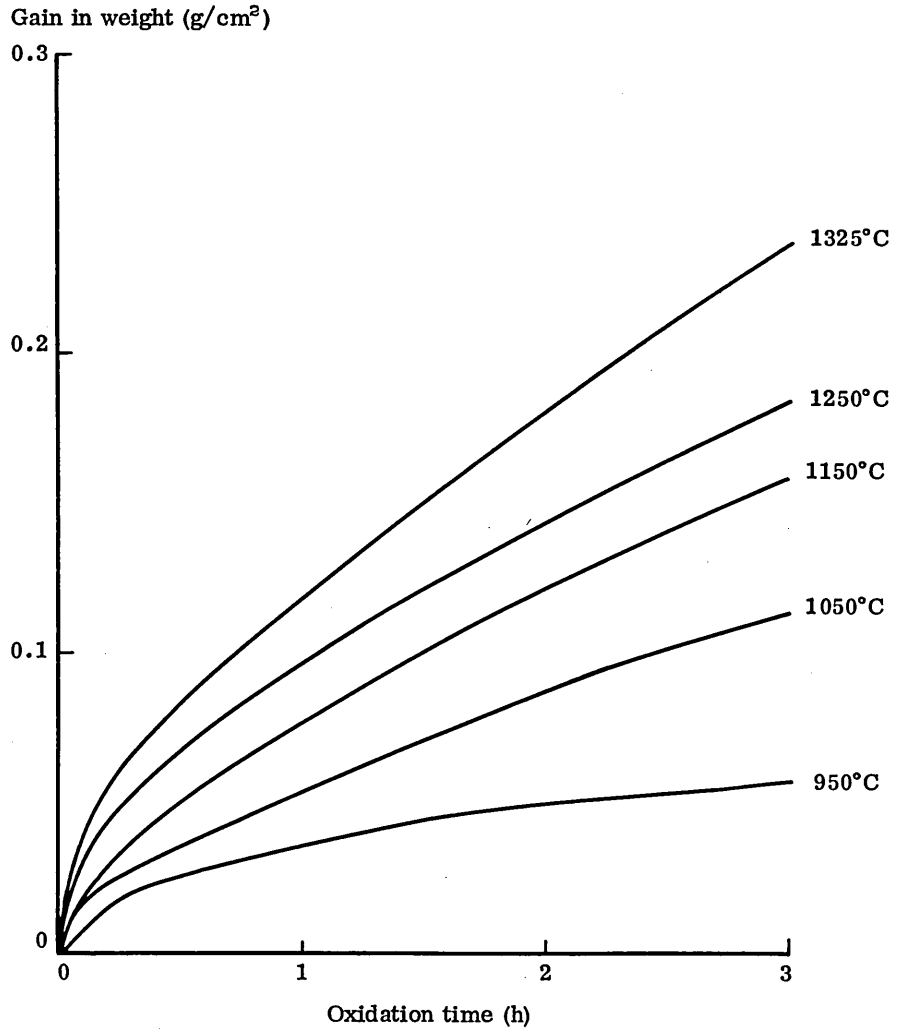

GRAVIMETRIC OXIDATION DATA
ALUMINIUM-TREATED STEEL

FIG. 50

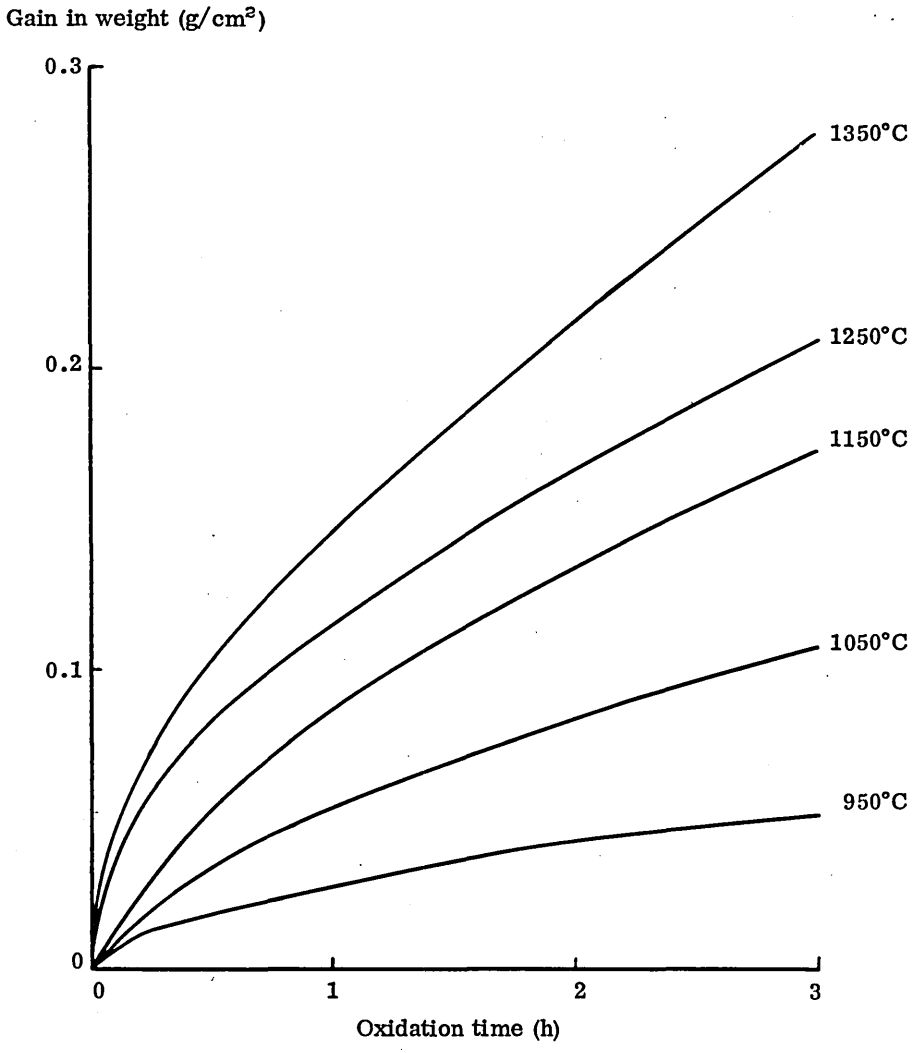

GRAVIMETRIC OXIDATION DATA
SEMI-KILLED STEEL

FIG. 51

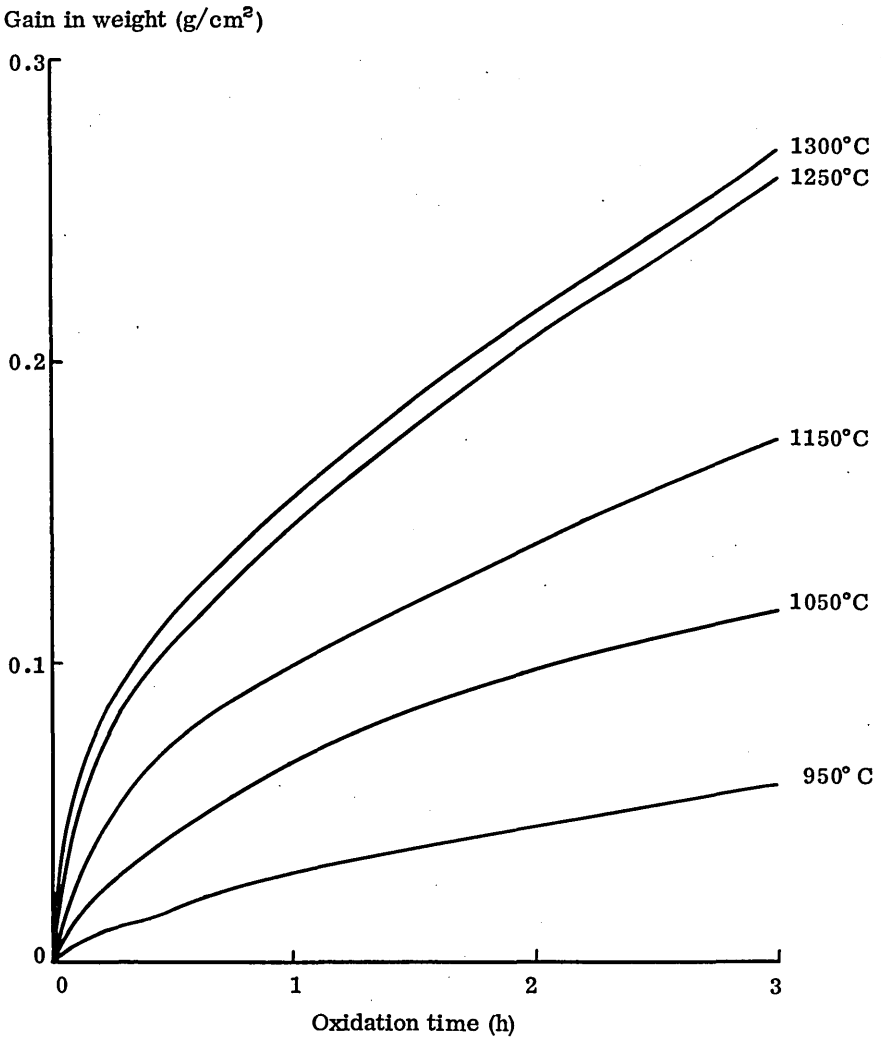

GRAVIMETRIC OXIDATION DATA
RIMMING STEEL

FIG. 52

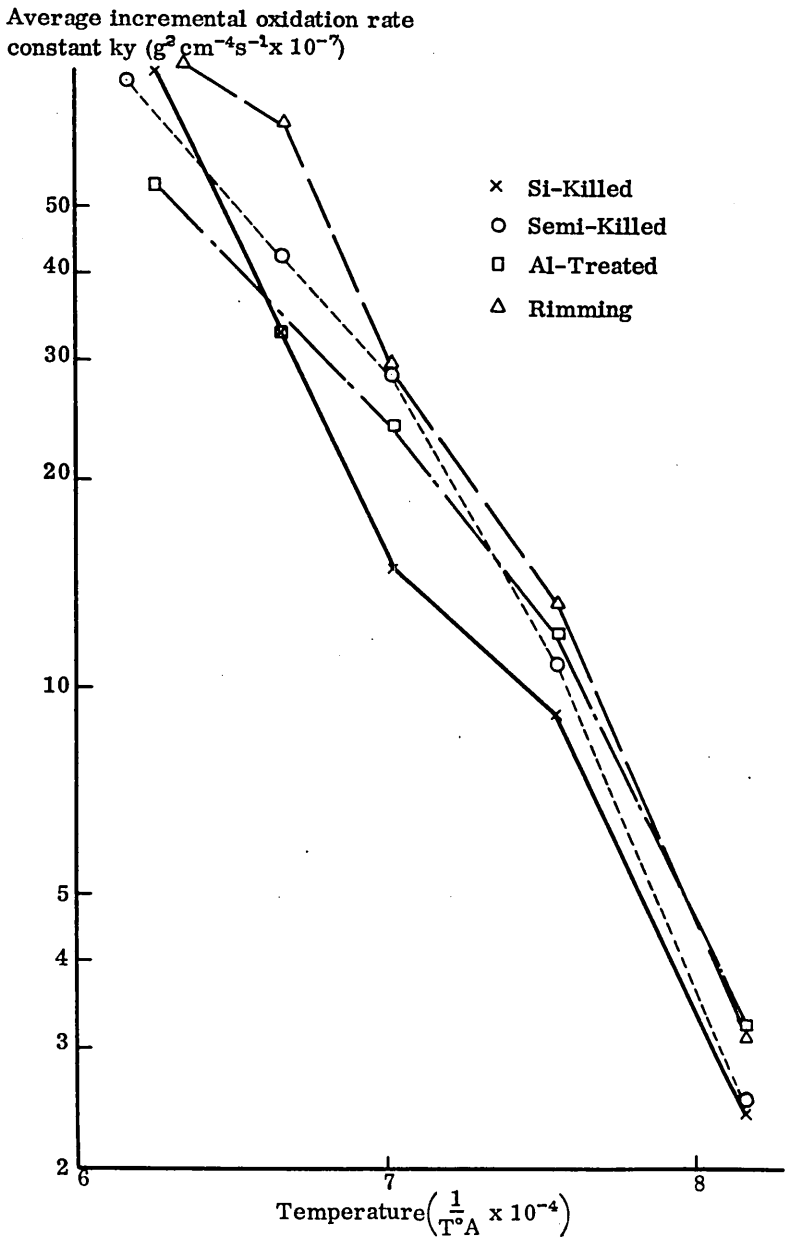

THE EFFECT OF TEMPERATURE ON THE APPROXIMATE PARABOLIC RATE CONSTANT

FIG. 53

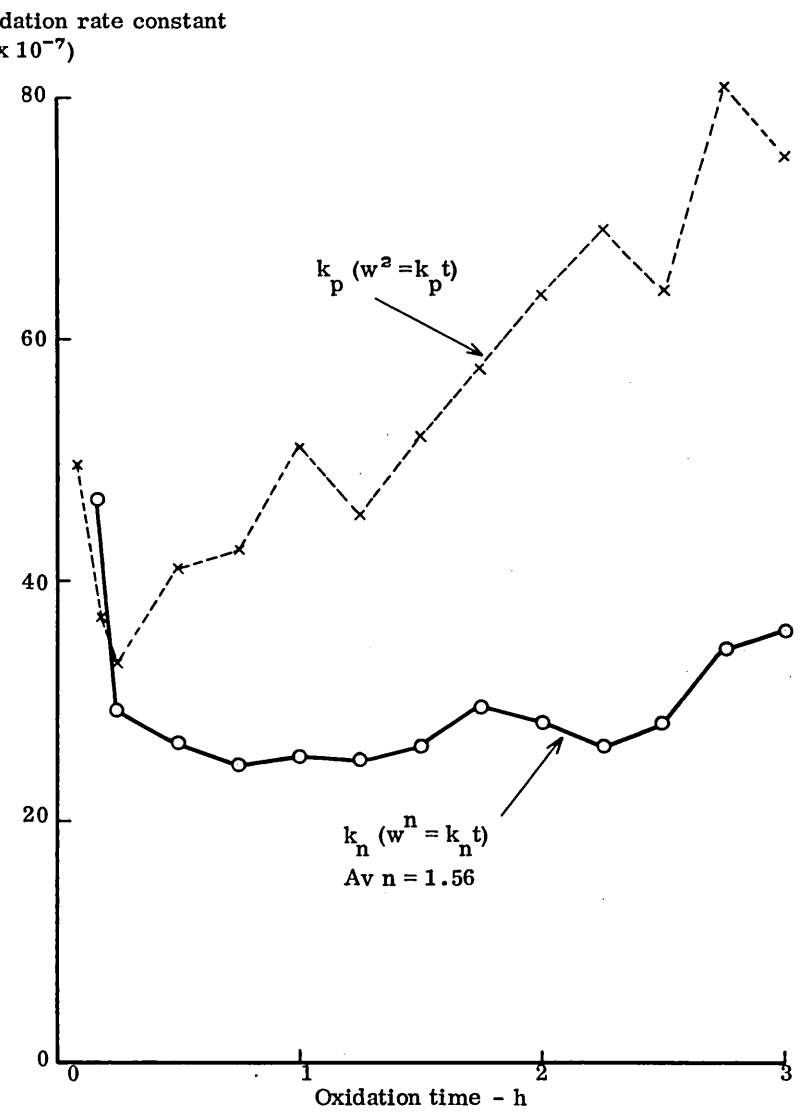

EXAMPLES OF DEVIATION FROM CONSTANT OXIDATION RATES WITH TIME (SILICON-KILLED STEEL 1325°C)

FIG. 54

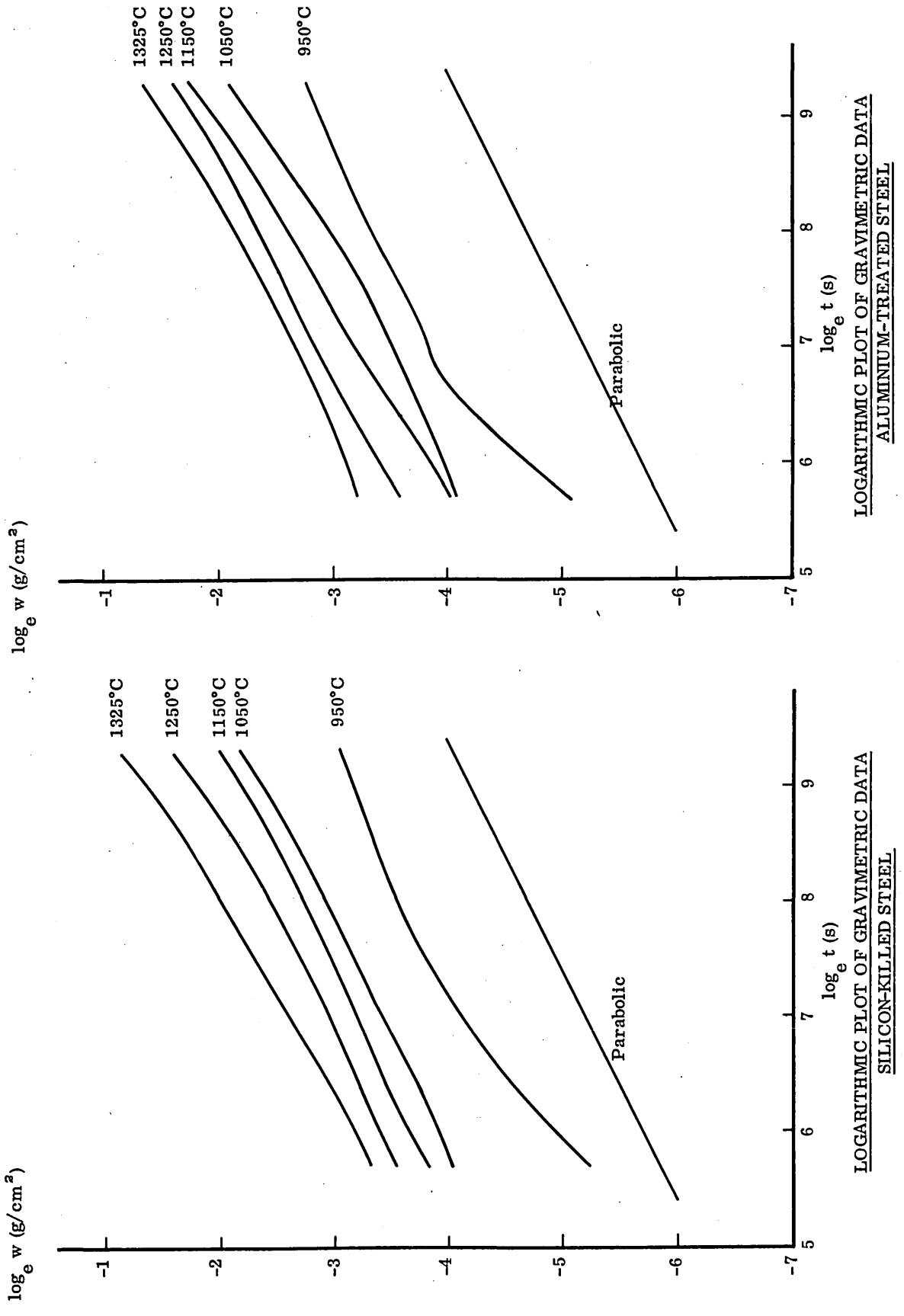

LOGARITHMIC PLOT OF GRAVIMETRIC DATA
SILICON-KILLED STEEL

FIG. 55

LOGARITHMIC PLOT OF GRAVIMETRIC DATA
ALUMINIUM-TREATED STEEL

FIG. 56

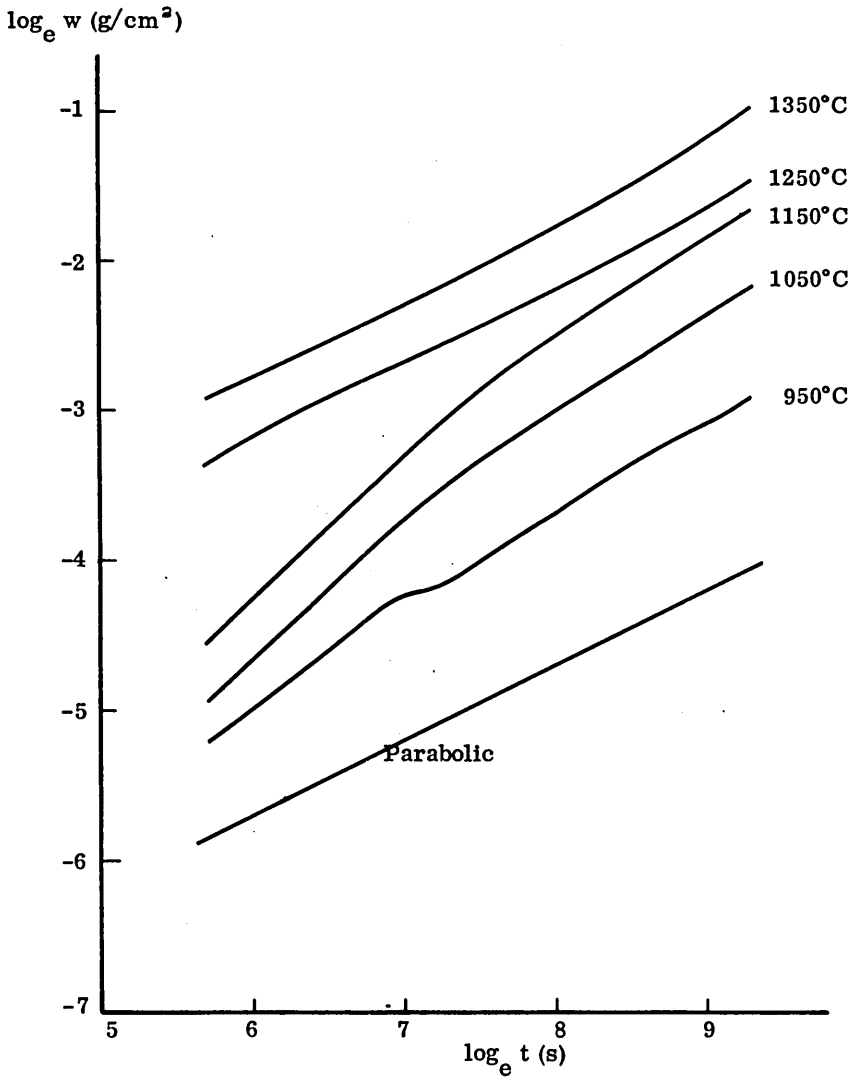

LOGARITHMIC PLOT OF GRAVIMETRIC DATA
SEMI-KILLED STEEL

FIG. 57

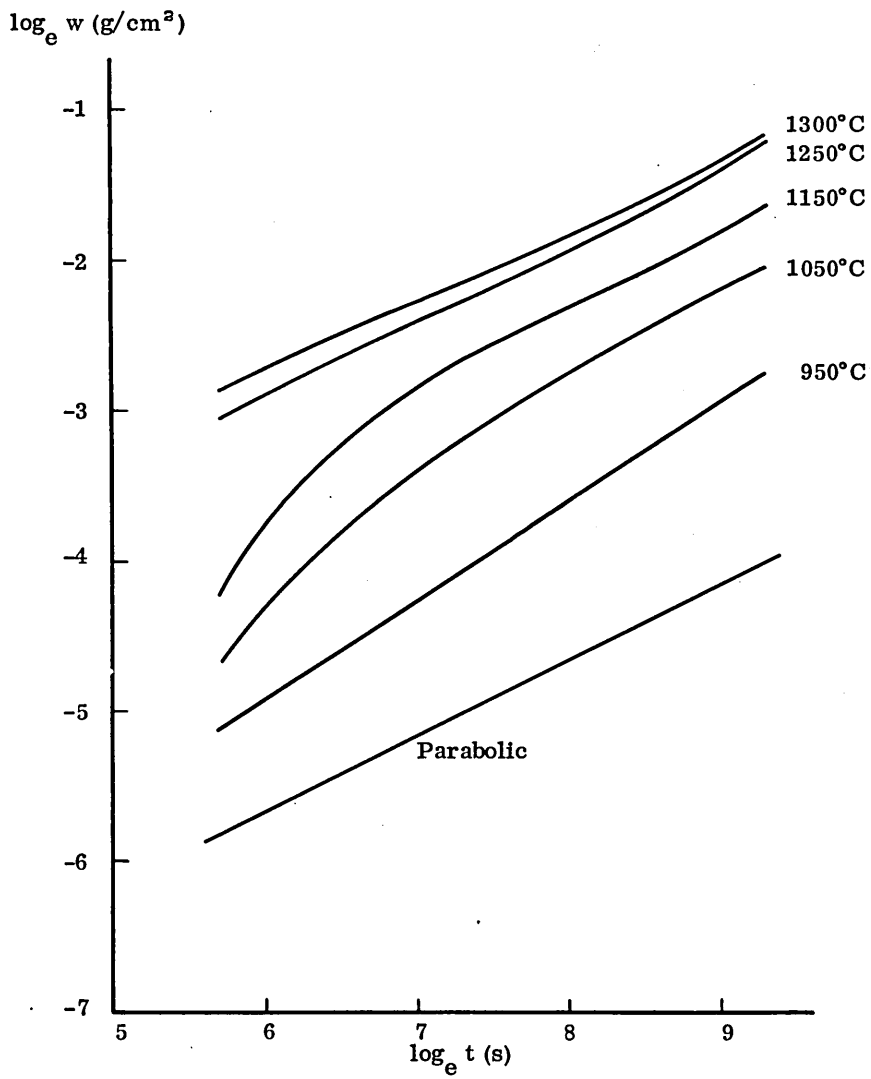

LOGARITHMIC PLOT OF GRAVIMETRIC DATA
RIMMING STEEL

FIG. 58

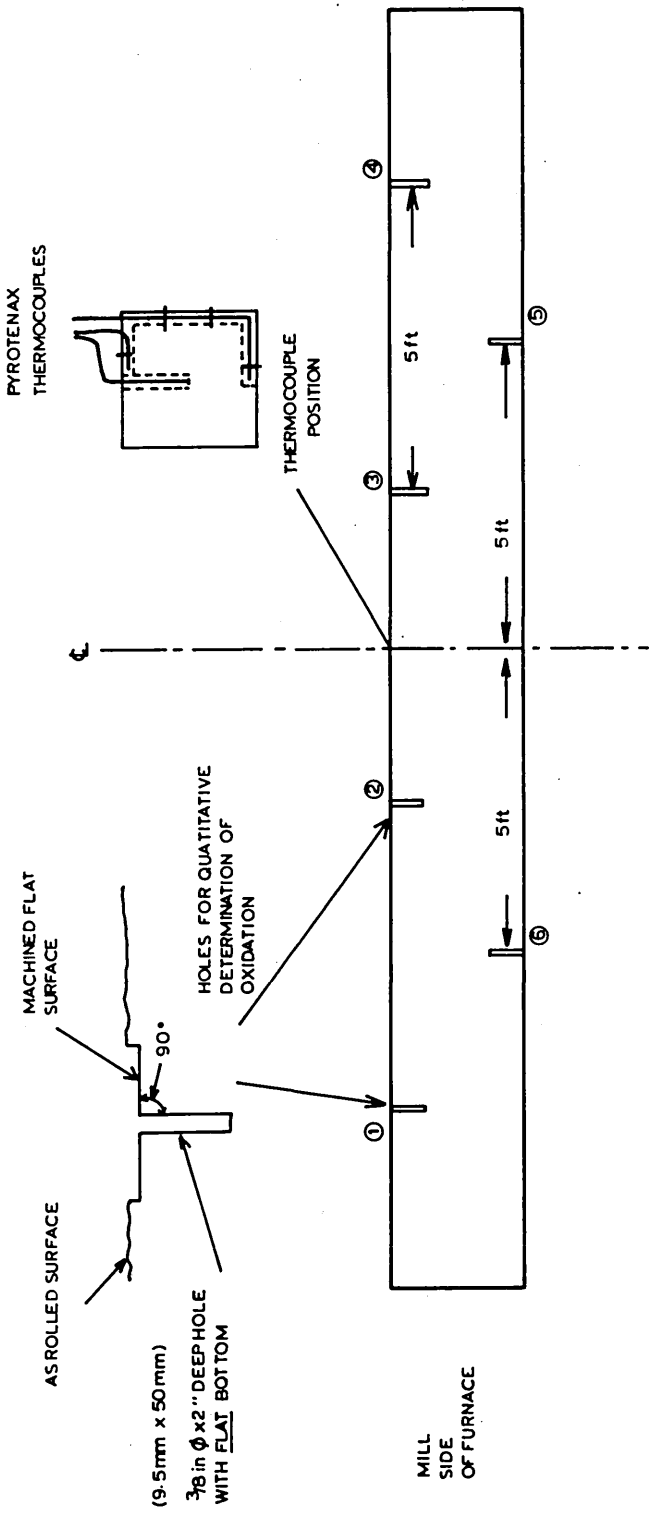

DETAILS OF THERMOCOUPLES AND DRILLED HOLES IN INSTRUMENTED BLOOMS

FIG. 59

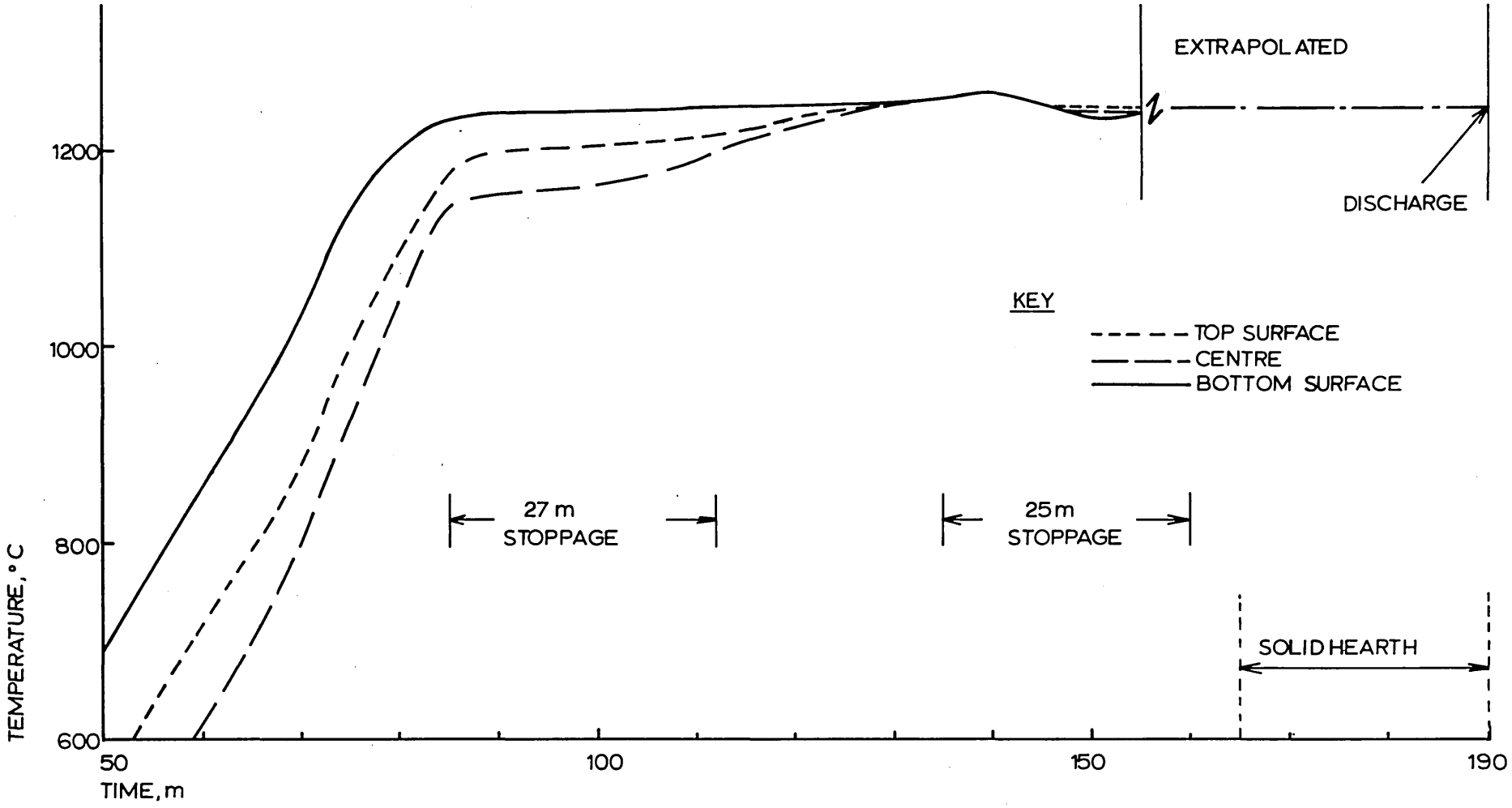

REHEATING TEMPERATURE/TIME PROFILE. Si-KILLED BLOOM FROM CAST NO. 61648

FIG. 60

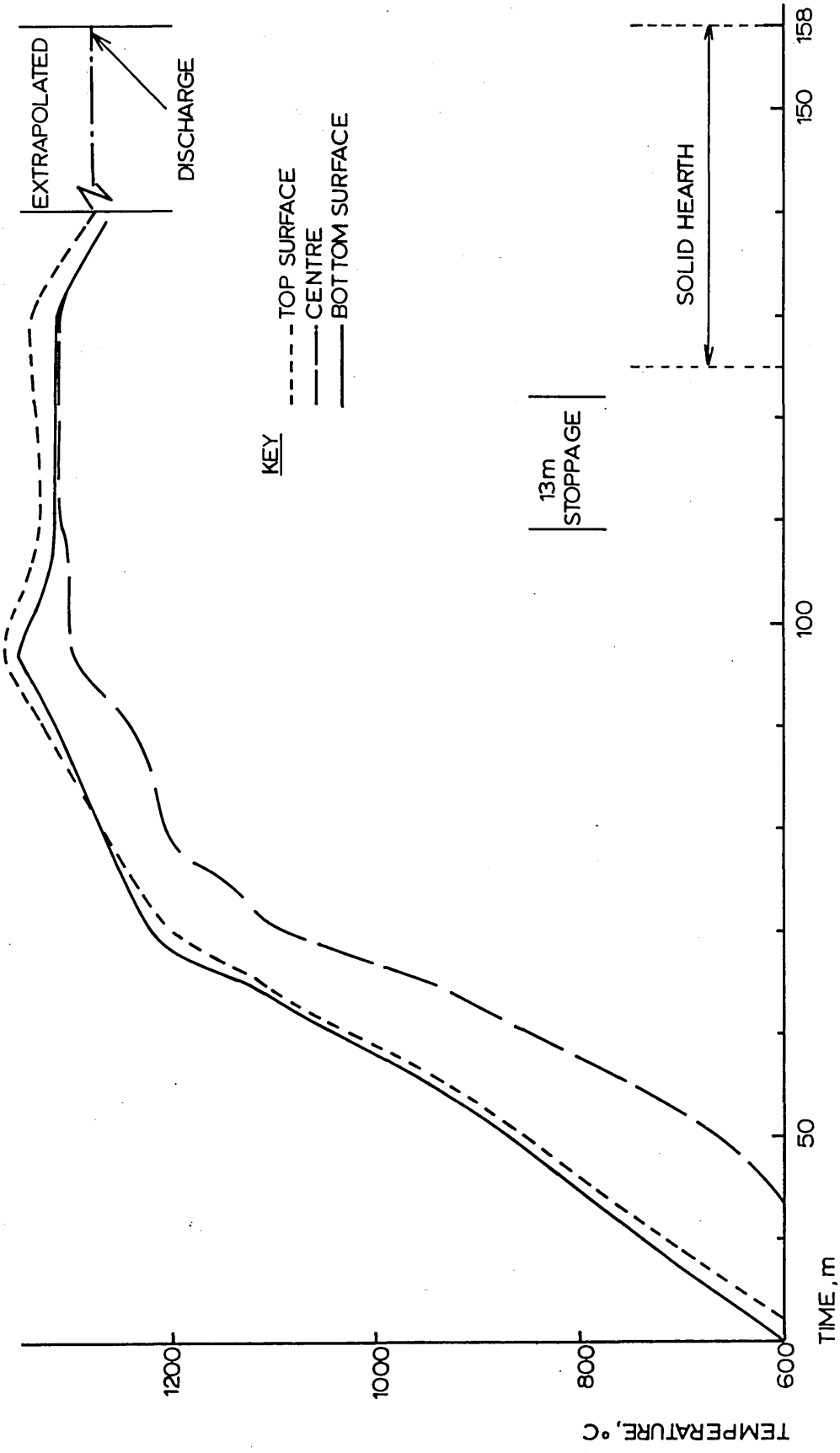

REHEATING TEMPERATURE/TIME PROFILE RIMMING STEEL BLOOM FROM CAST NO. 61949

FIG. 61

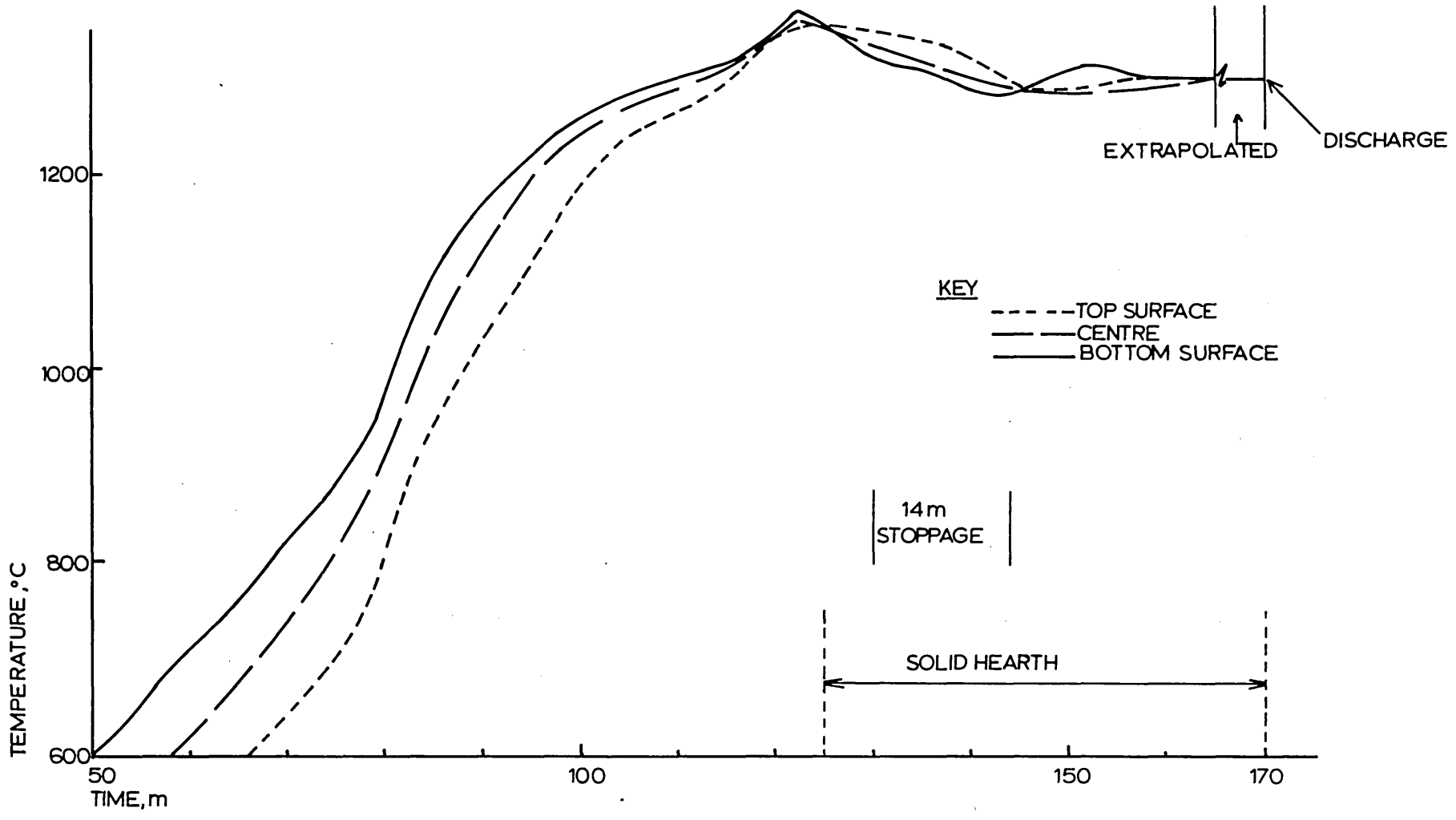

REHEATING TEMPERATURE/TIME PROFILE BALANCED STEEL BLOOM FROM CAST NO. 16158

FIG. 62

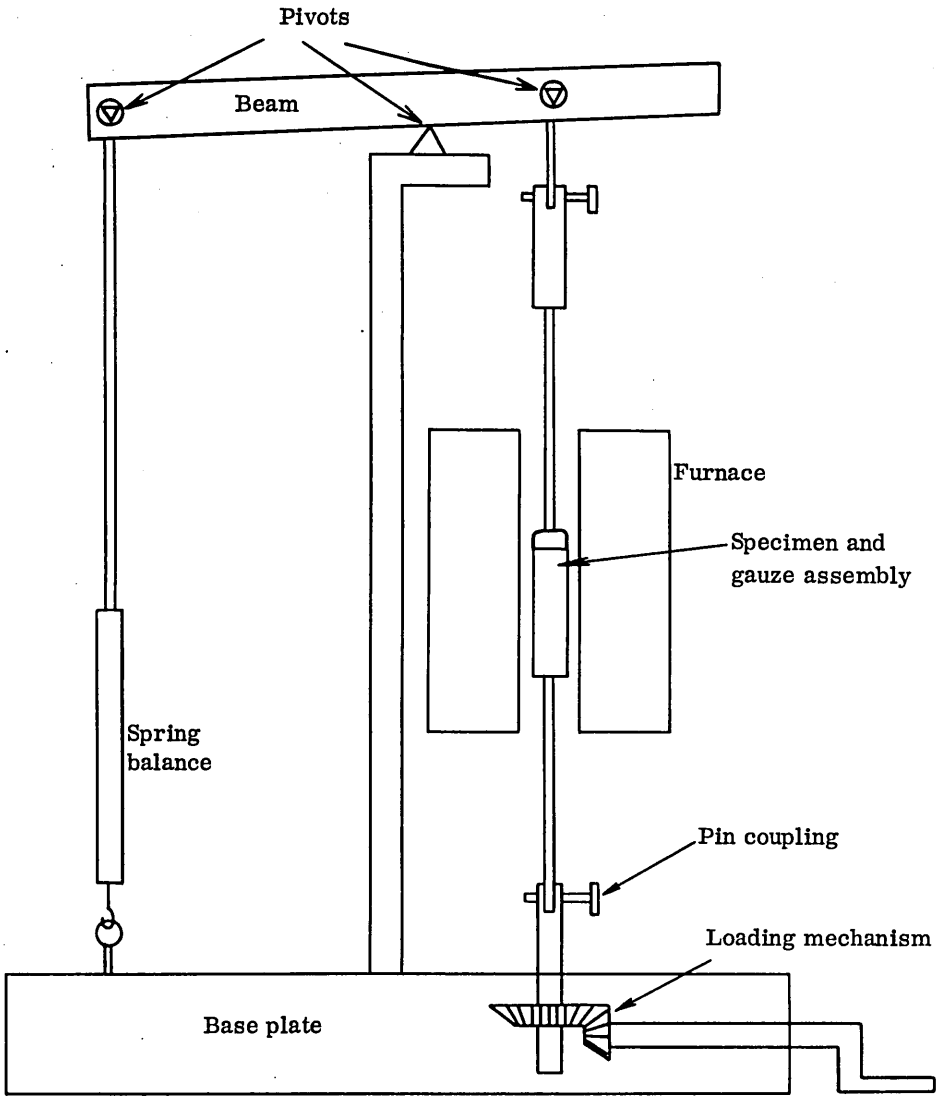

SCHEMATIC DIAGRAM OF ORIGINAL SCALE ADHESION EQUIPMENT

FIG. 63

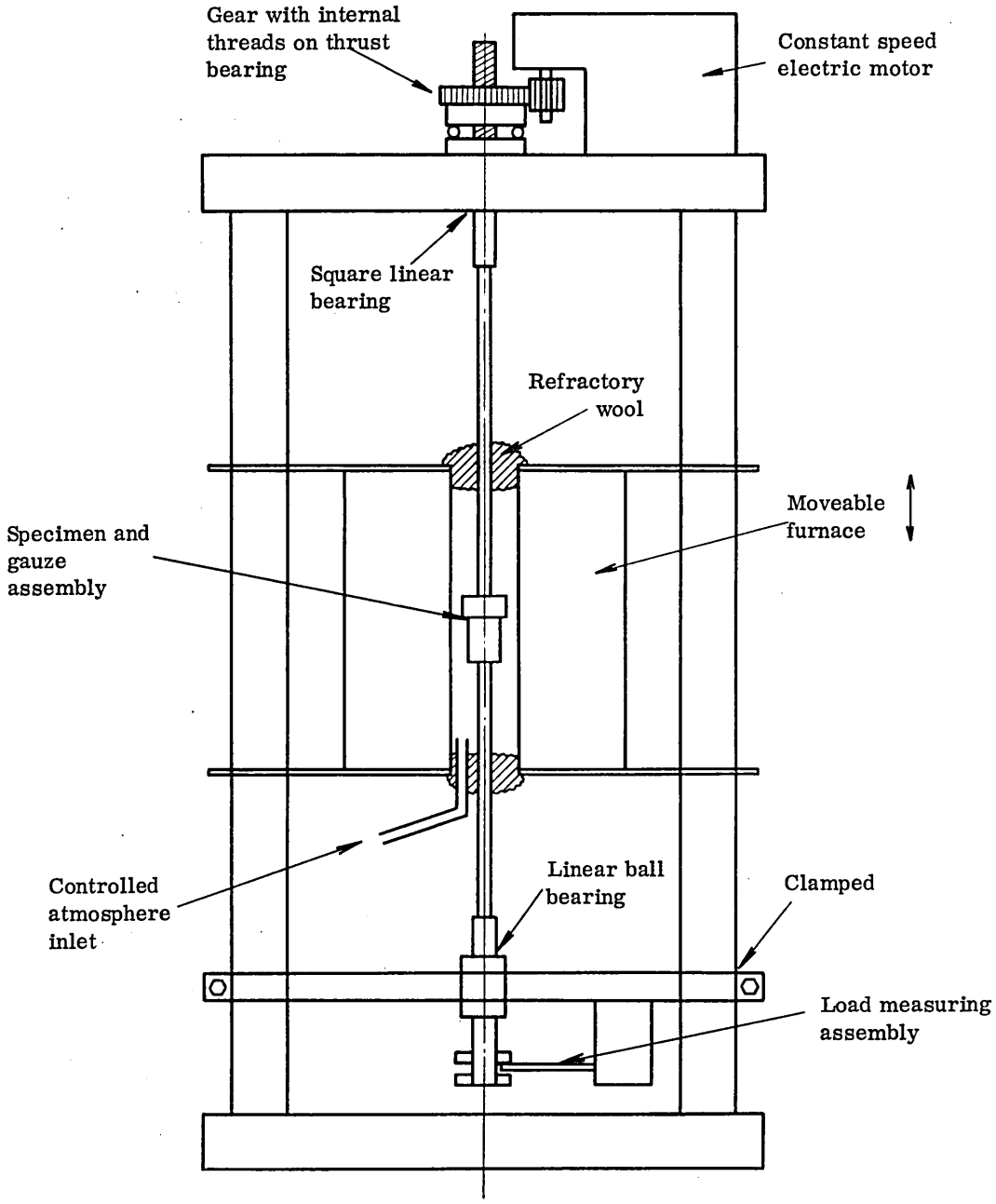

RE-DESIGNED SCALE ADHESION APPARATUS

FIG. 64

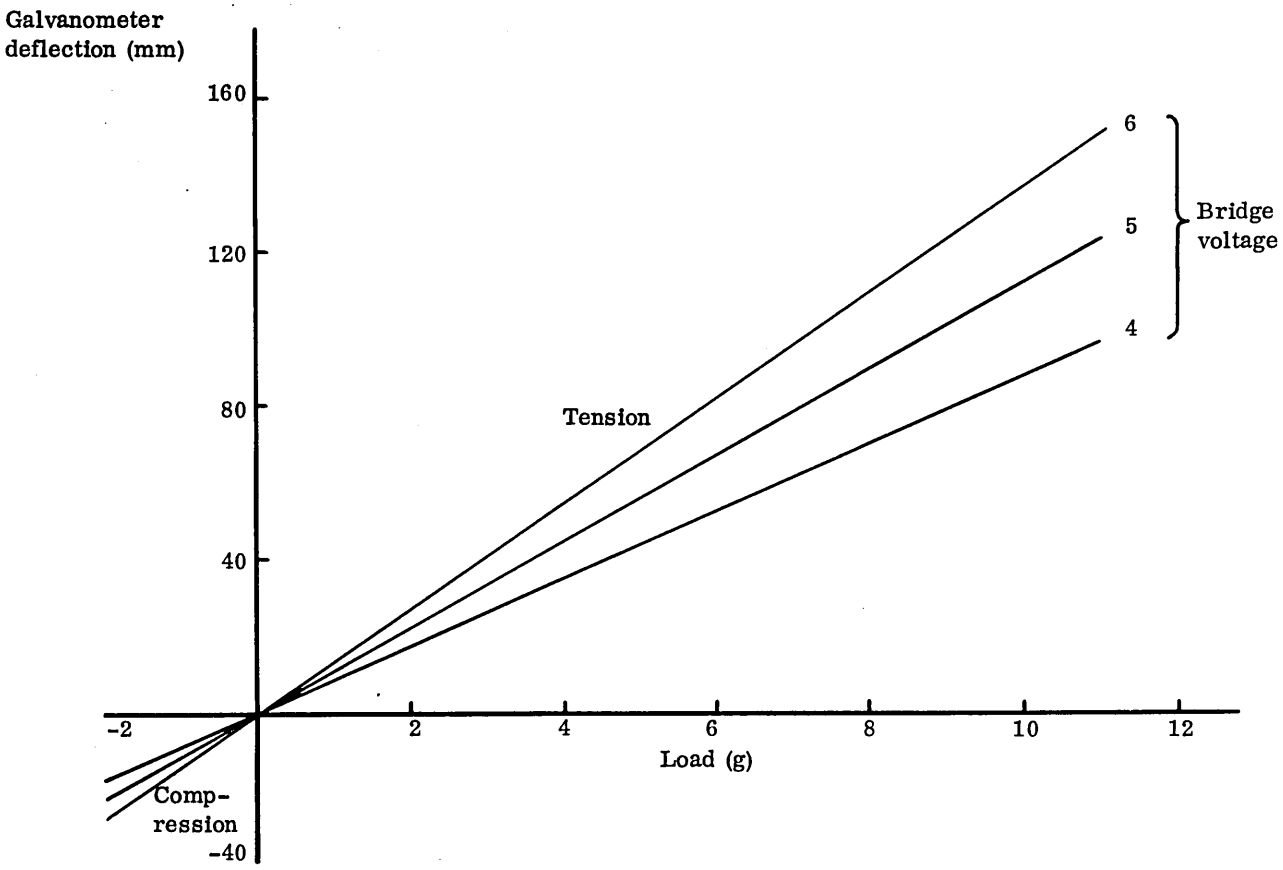

STRAIN GAUGE CALIBRATION

FIG. 65

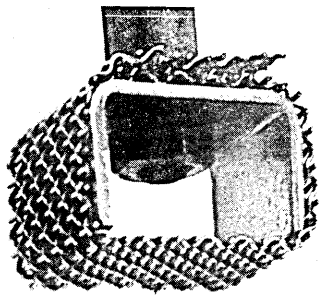

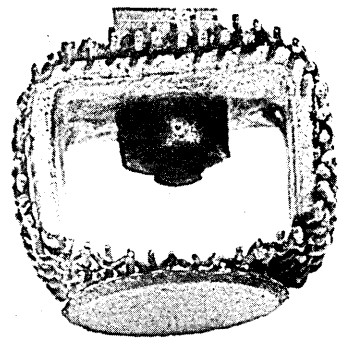

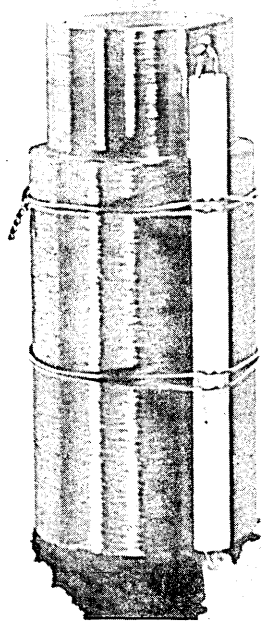

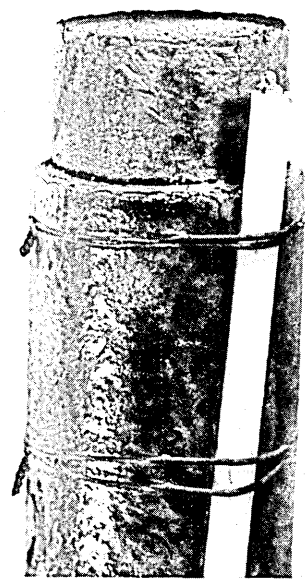

Before oxidation (a)

After oxidation and testing (b)

SPECIMEN AND GAUZE ASSEMBLY
x 1.3

FIG. 66

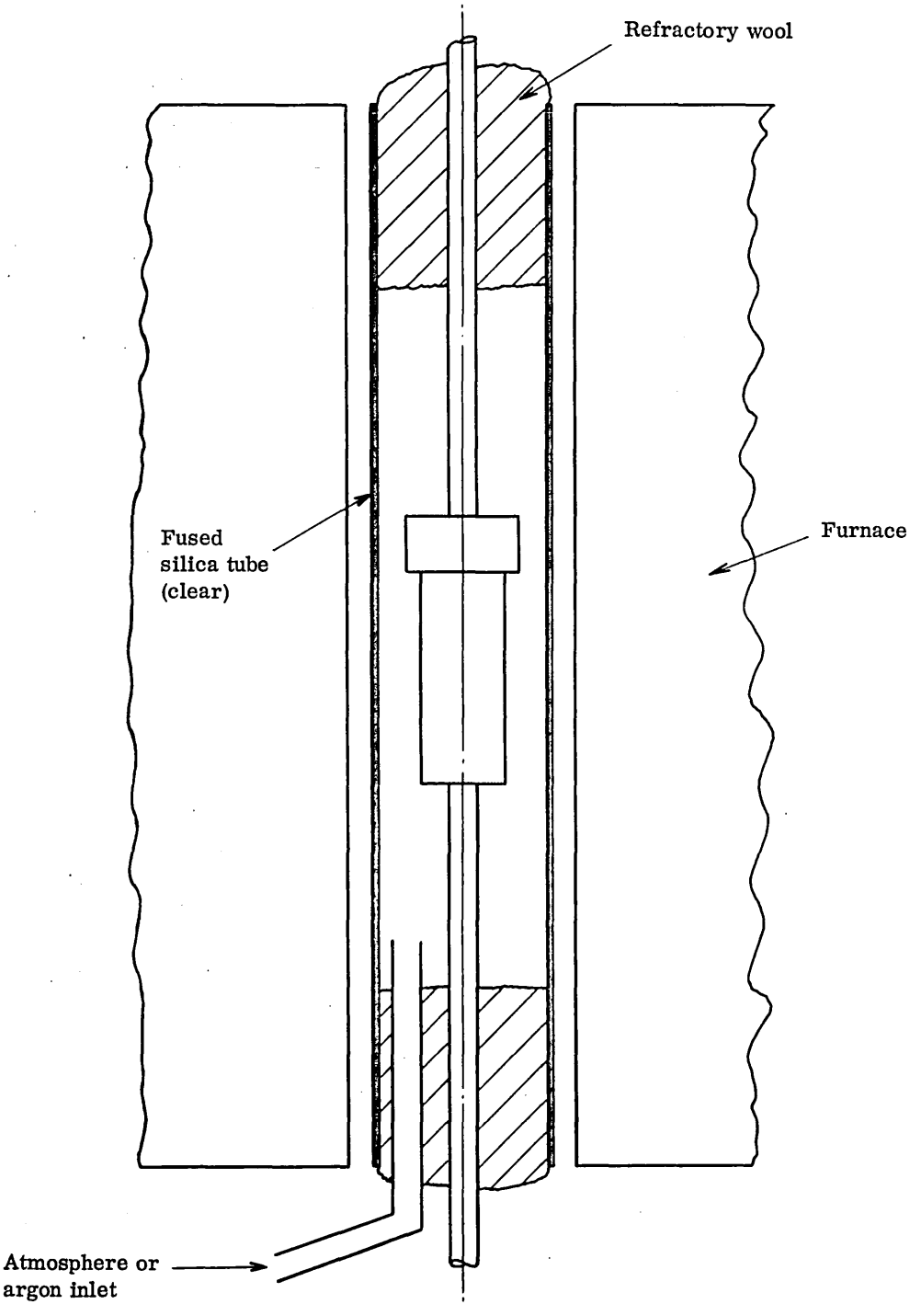

MODIFICATION TO PREVENT OXIDATION AFTER TESTING

FIG. 67

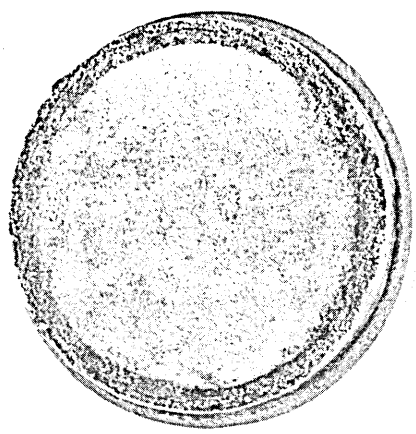

Si-killed steel 1200°C 1 h (a)

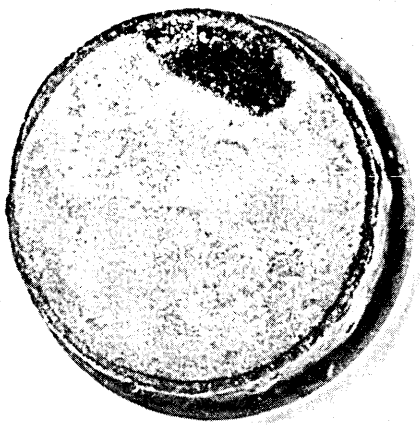

Rimming steel 1100°C 1 h (b)

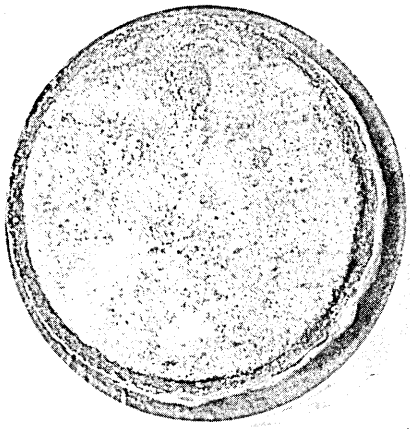

Al-treated steel 1150°C 1 h (c)

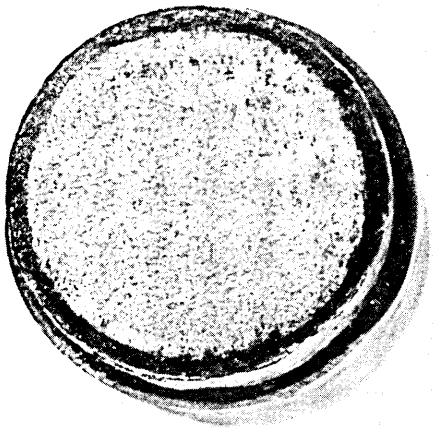

Balanced steel 1200°C 1 h (d)

SURFACES PRODUCED ON DETACHING SCALE
x 2 approx

FIG. 68

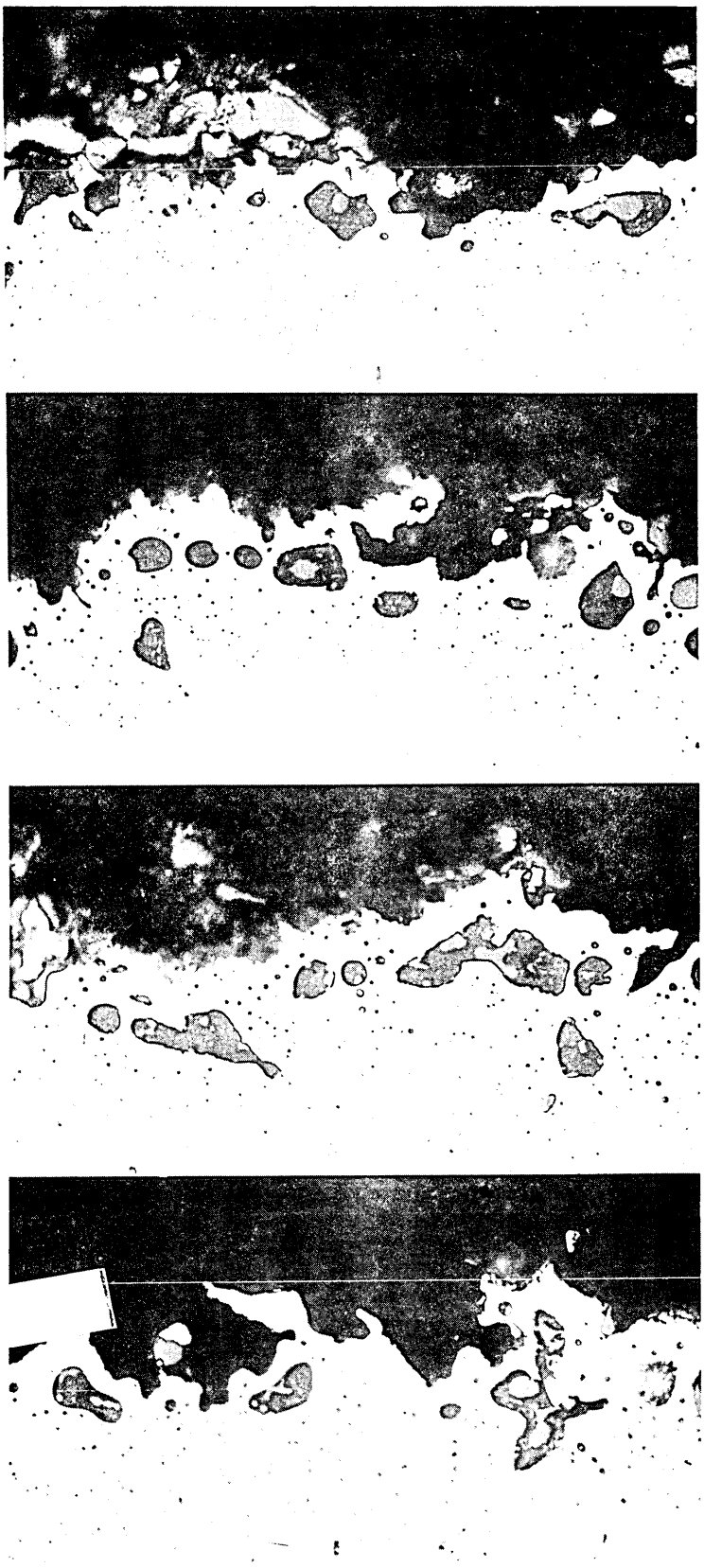

(a) 1050°C, 1 h

(b) 1100°C, 1 h

(c) 1150°C, 1 h

(d) 1200°C, 1 h

FRACTURED SURFACE PRODUCED ON Si-KILLED STEEL
(Transverse metallography)

x 500

FIG. 69

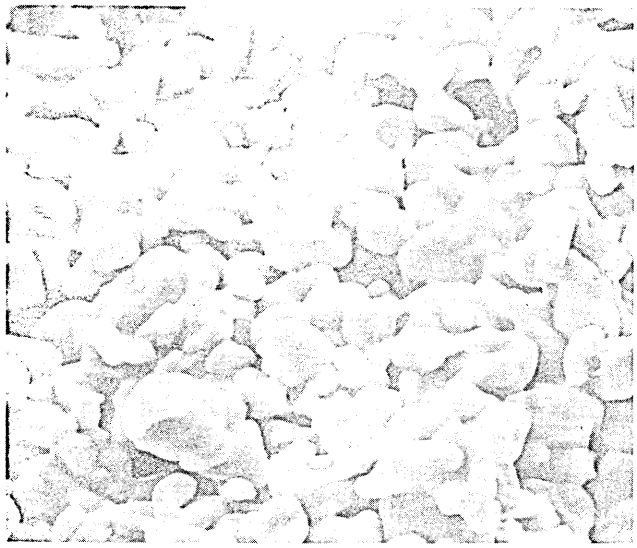

x 1000 Scale surface (a)

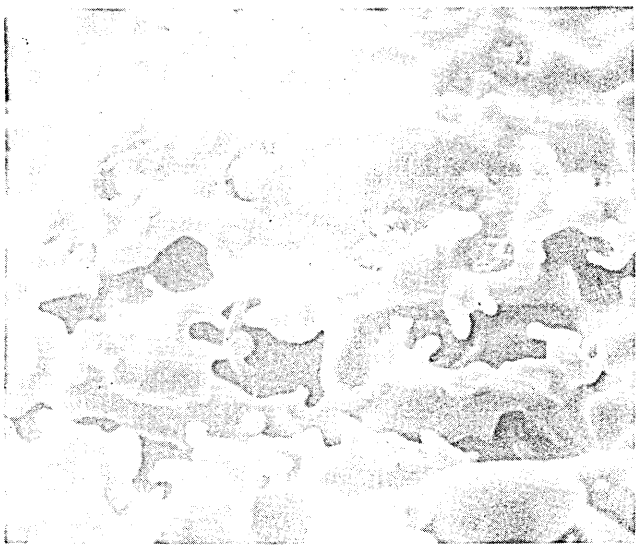

x 1100 Metal surface showing grain boundary (b)

x 2300 Metal surface (c)

FRACTURED SURFACES PRODUCED AFTER 1 HOUR AT 1050°C ON Si-KILLED STEEL
(Stereoscan electron images)

FIG. 70

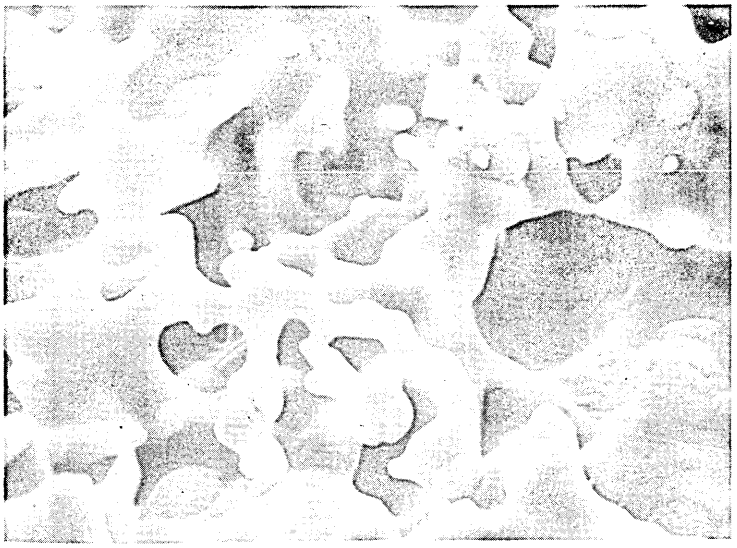

(a) 1100°C, 1 h

(b) 1150°C, 1 h

(c) 1200°C, 1 h

METAL SURFACE PRODUCED ON REMOVING SCALE ON Si-KILLED STEEL
(Stereoscan electron images)

(a) and (c) x 2200
(b) x 2300

FIG. 71

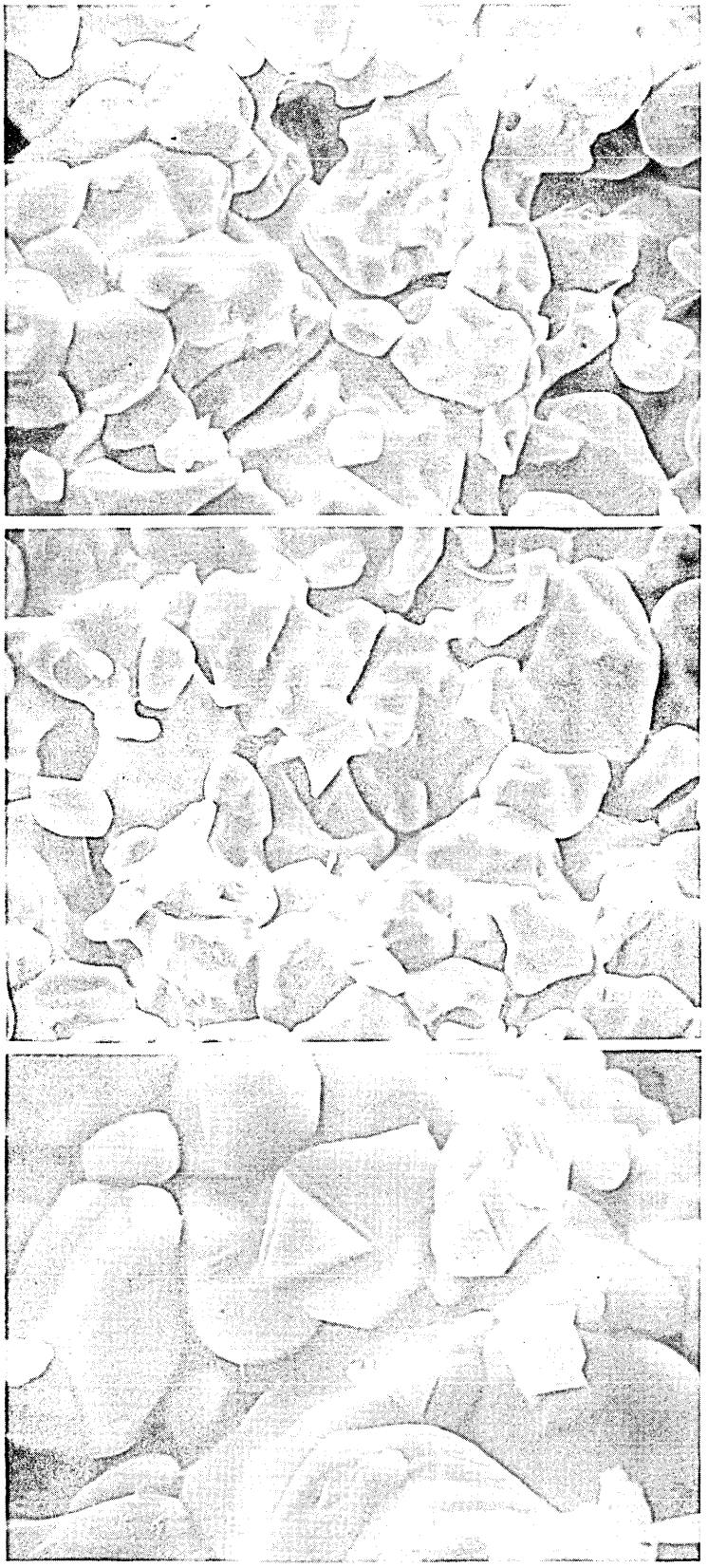

(a) 1100°C, 1 h

(b) 1150°C, 1 h

(c) 1200°C, 1 h

SCALE SURFACES PRODUCED ON REMOVAL FROM METAL ON Si-KILLED STEEL
(Stereoscan electron images)

(a) and (c) x 2200
(b) x 2300

FIG. 72

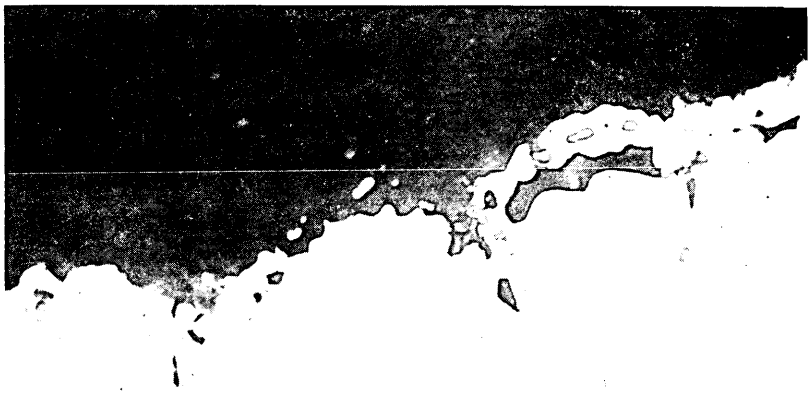

(a) 1050°C, 1 h

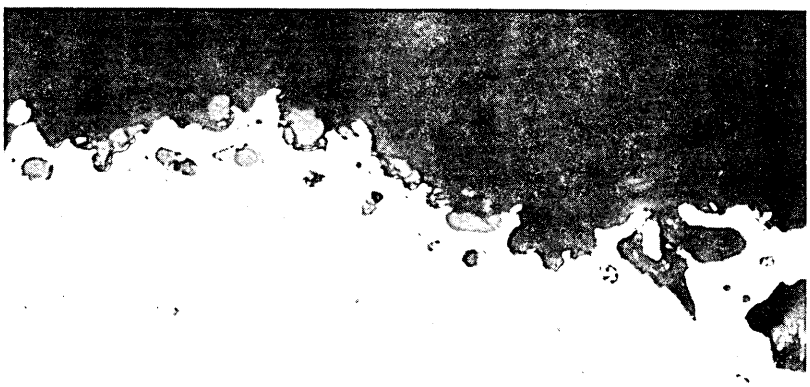

(b) 1100°C, 1 h

(c) 1150°C, 1 h

(d) 1200°C, 1 h

FRACTURED SURFACES PRODUCED ON Al-TREATED STEEL
(Transverse metallography)

x 500

FIG. 73

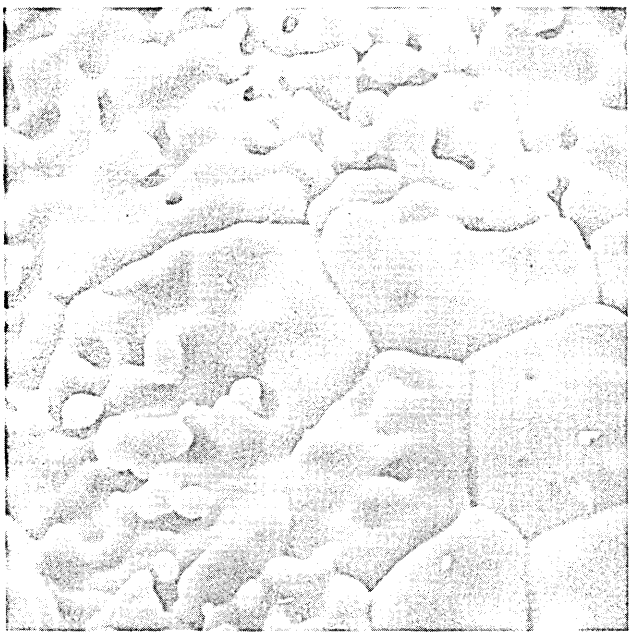

x 1000 Scale surface (a)

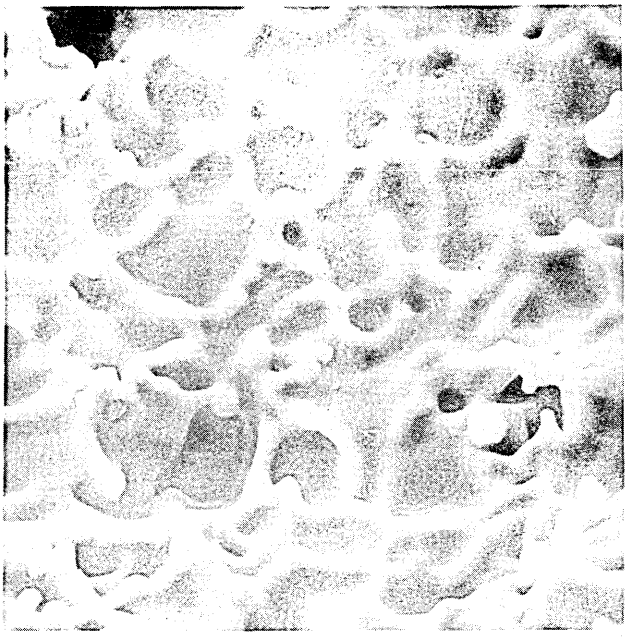

x 1200 Metal surface (b)

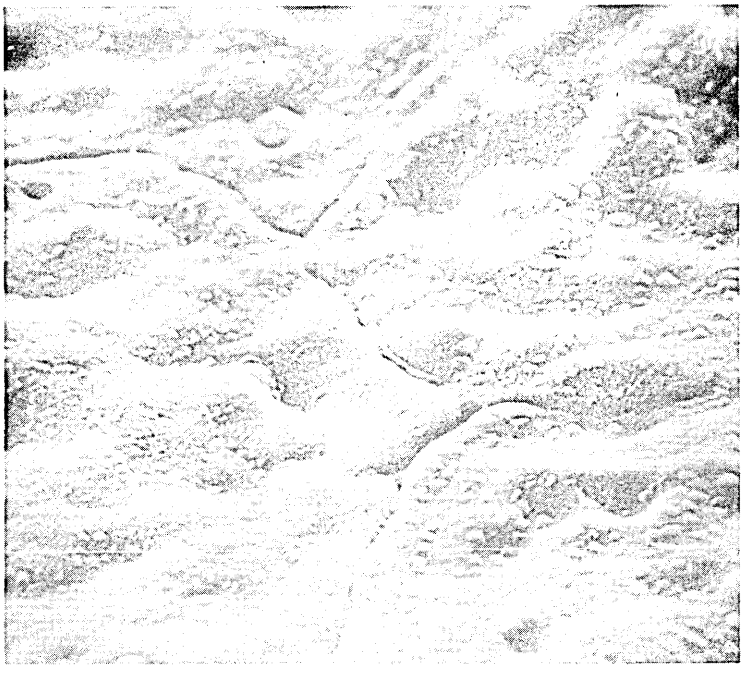

x 1400 Metal surface (c)

FRACTURED SURFACES PRODUCED AFTER 1 HOUR AT 1050°C ON Al-TREATED STEEL
(Stereoscan electron images)

FIG. 74

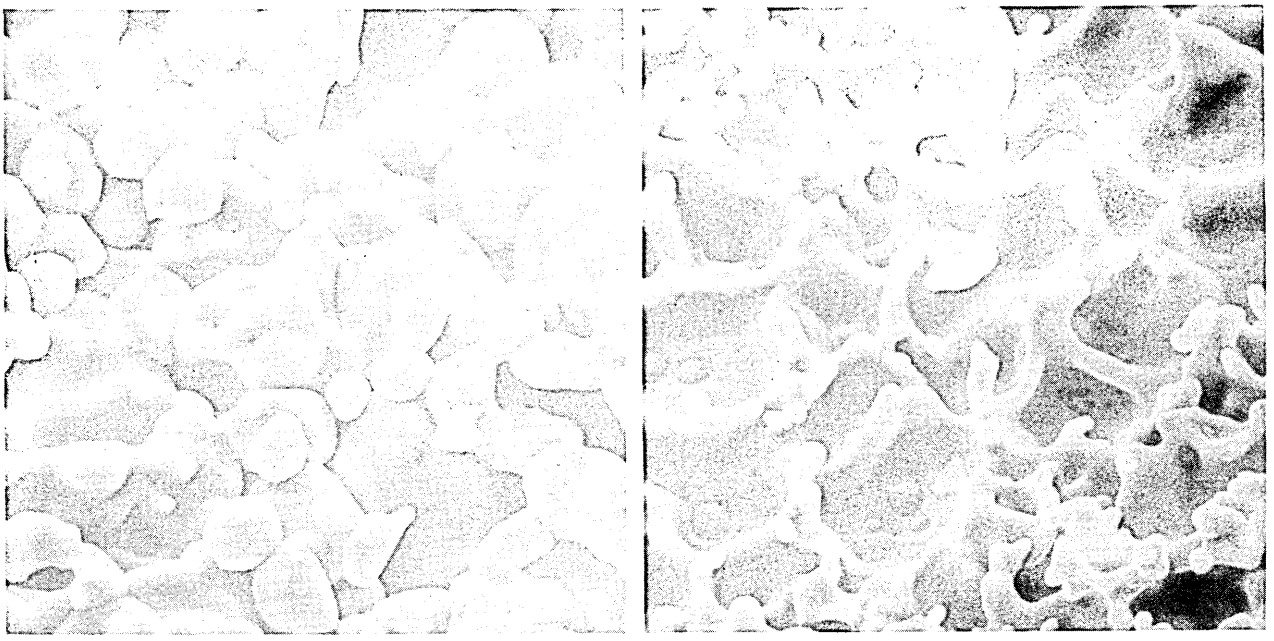

x 1100 Scale surface (a) x 1200 Metal surface (b)

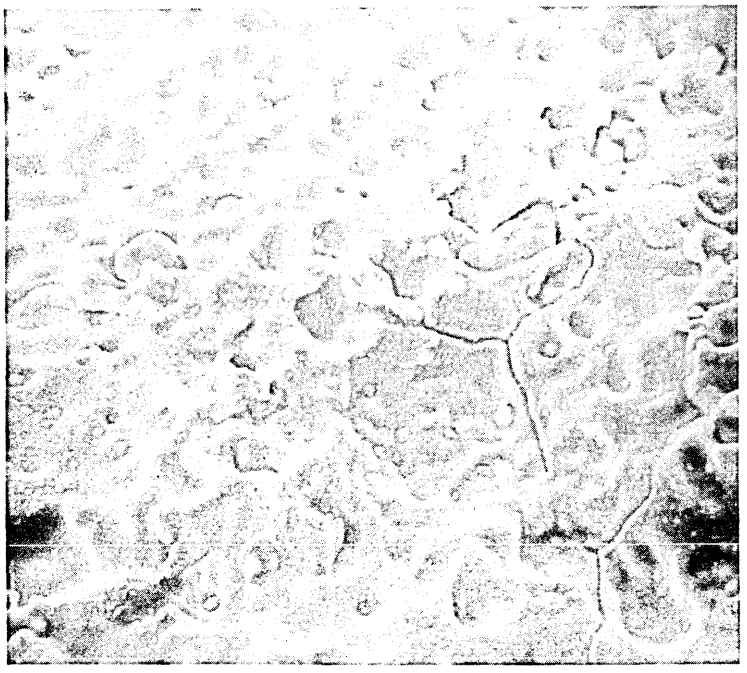

x 1200 Metal surface (c)

FRACTURED SURFACES PRODUCED AFTER 1 HOUR AT 1100°C ON Al-TREATED STEEL
(Stereoscan electron images)

FIG. 75

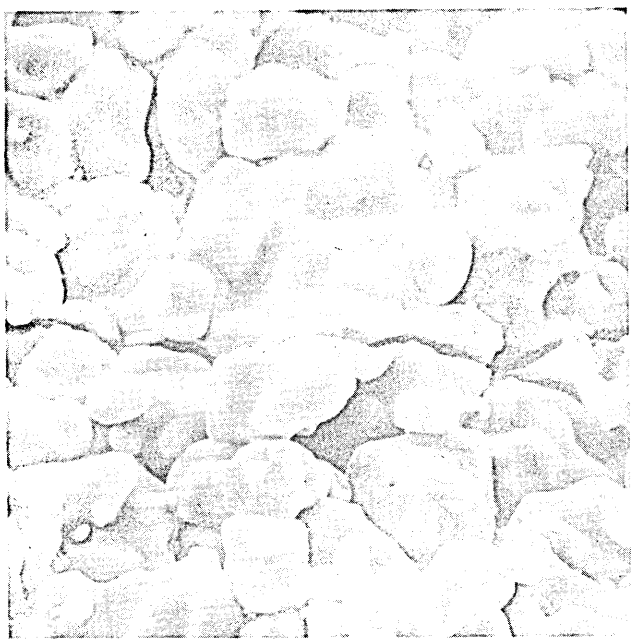

x 1100 Scale surface showing crack (a)

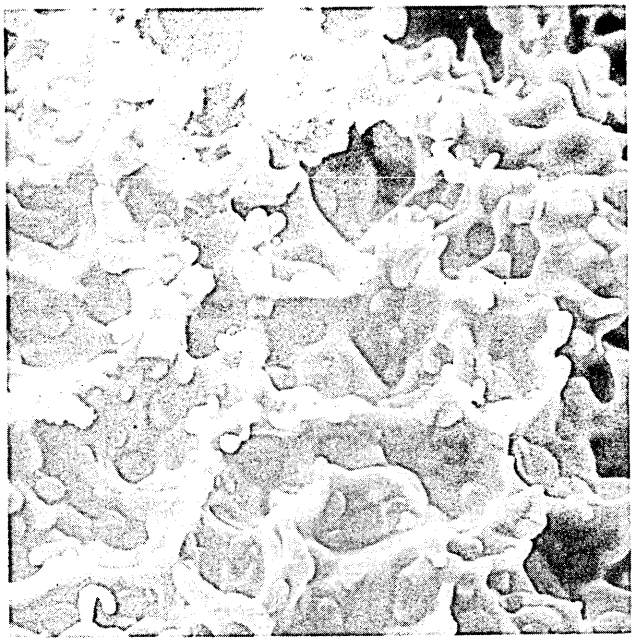

x 1100 Metal surface (b)

x 2200 Metal surface - note angular particles (c)

FRACTURED SURFACES PRODUCED AFTER 1 HOUR AT 1150°C ON Al-TREATED STEEL
(Stereoscan electron images)

FIG. 76

x 1400 Scale surface (a)

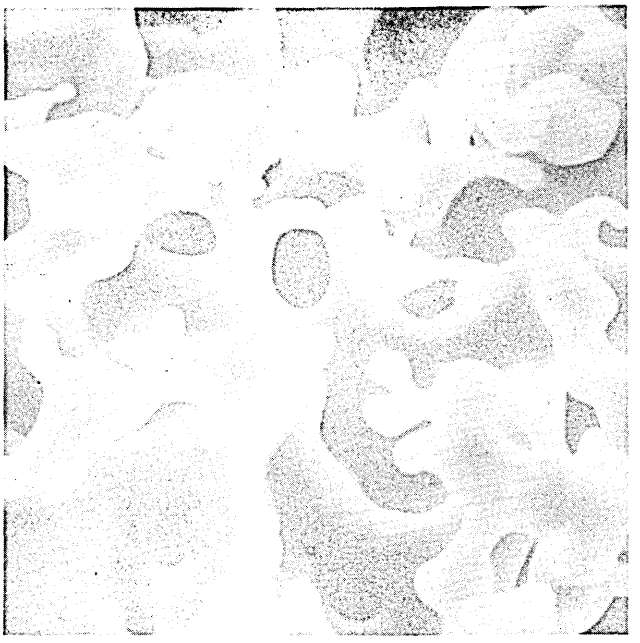

x 2400 Metal surface (b)

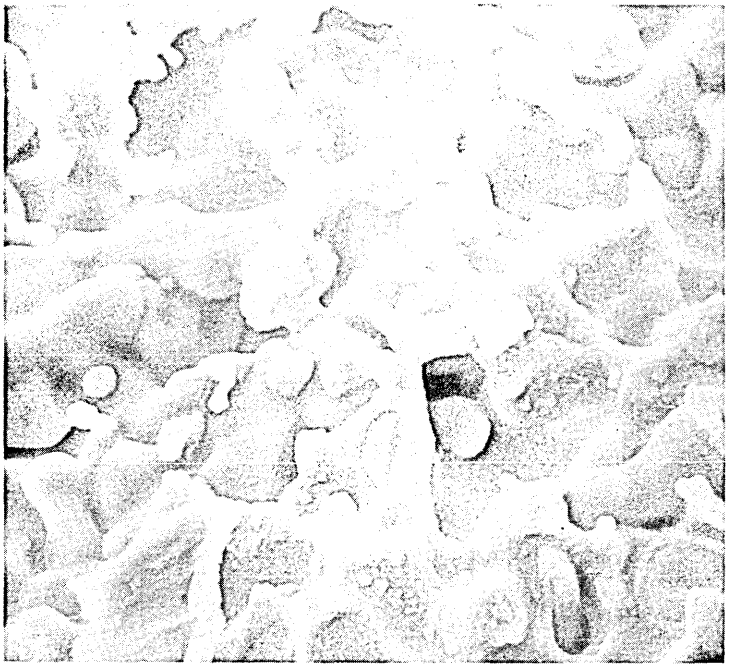

x 1300 Metal surface showing angular phase (c)

FRACTURED SURFACES PRODUCED AFTER 1 HOUR AT 1200°C ON Al-TREATED STEEL
(Stereoscan electron images)

FIG. 77

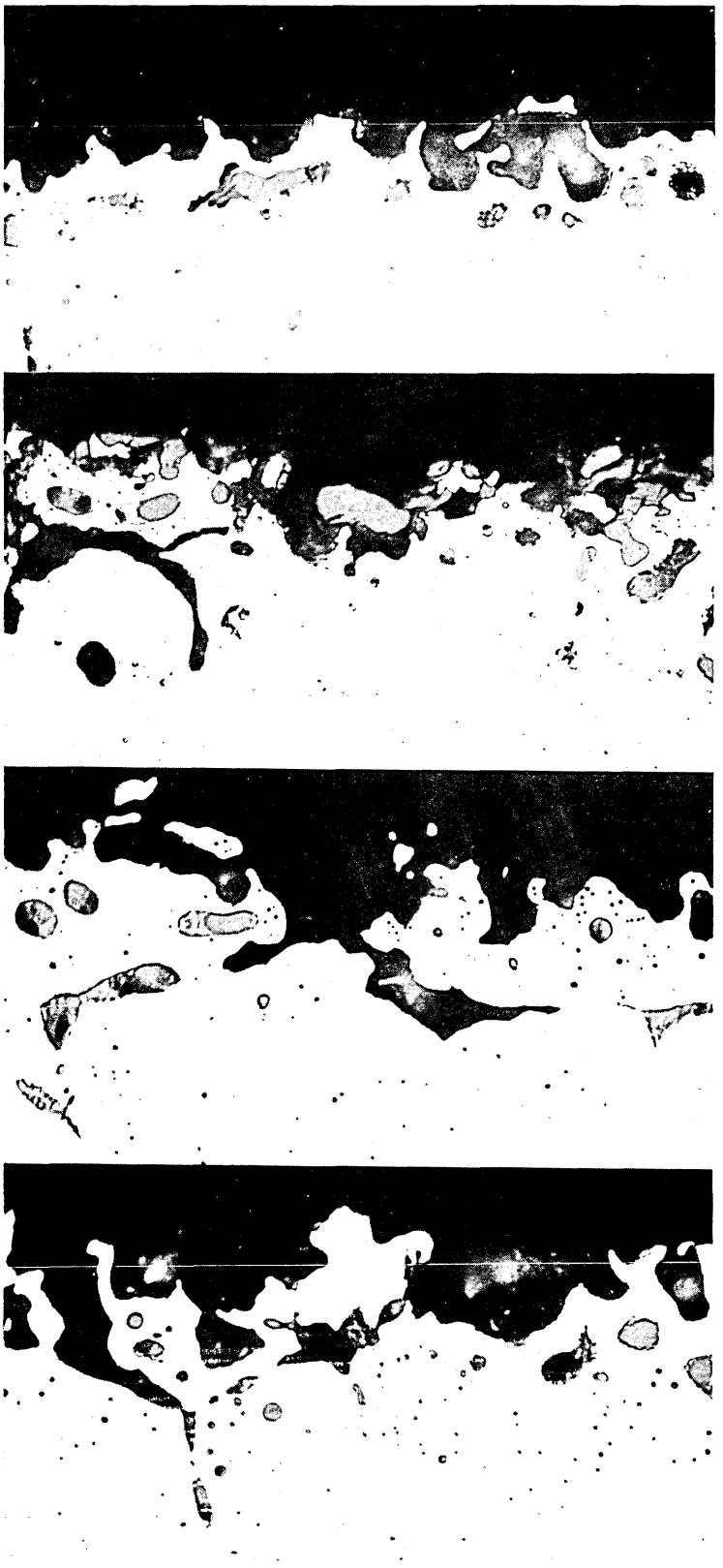

(a) 1050°C, 1 h

(b) 1100°C, 1 h

(c) 1150°C, 1 h

(d) 1200°C, 1 h

FRACTURED SURFACES PRODUCED ON SEMI-KILLED STEEL
(Transverse metallography)

x 500

FIG. 78

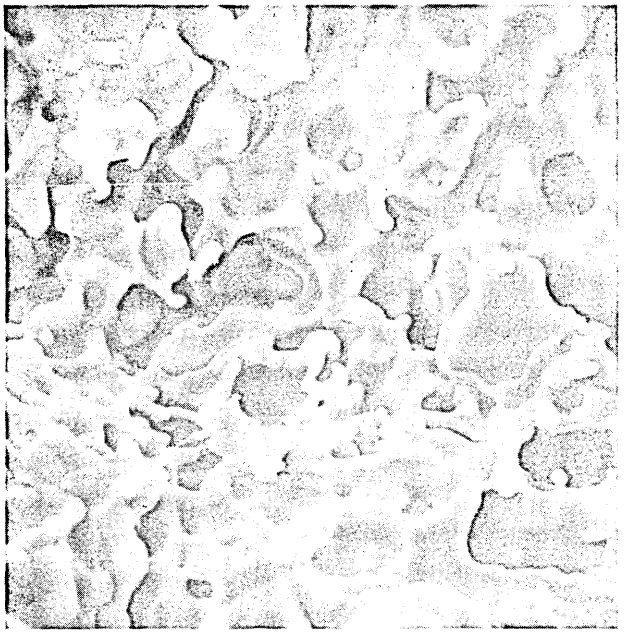

x 1200 1050°C, 1 h (a)

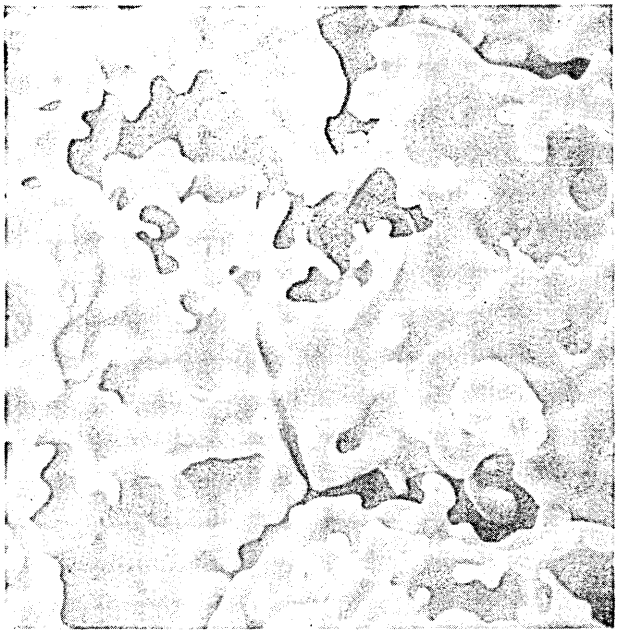

x 1200 1100°C, 1 h (b)

x 1400 1150°C, 1 h (c)

x 1300 1200°C, 1 h (d)

METAL SURFACES PRODUCED ON REMOVAL OF SCALE LAYER ON SEMI-KILLED STEEL
(Stereoscan electron images)

FIG. 79

(a) 1050°C, 1 h

(b) 1100°C, 1 h

(c) 1150°C, 1 h

(d) 1200°C, 1 h

FRACTURED SURFACE PRODUCED ON RIMMING STEEL
(Transverse metallography)
x 500

PIG. 80

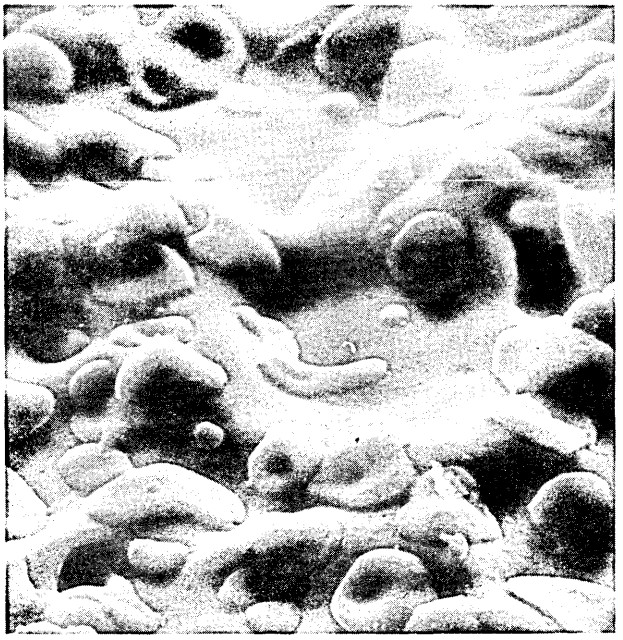

x 1100 1050°C, 1 h (a)

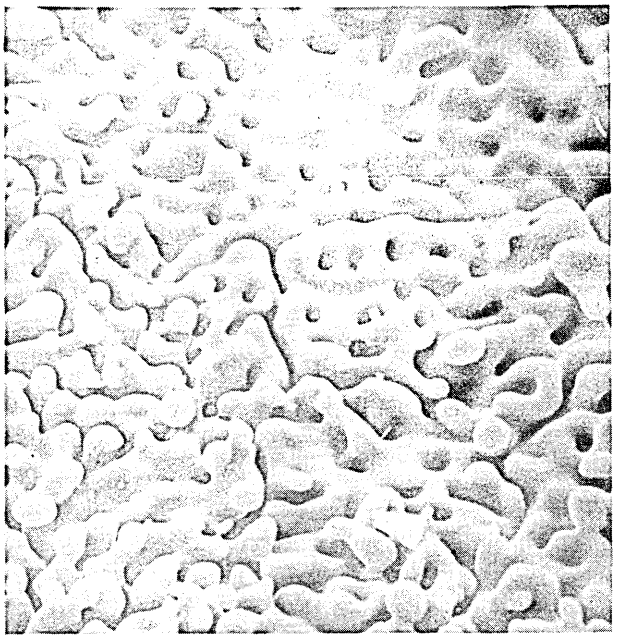

x 1200 1100°C, 1 h (b)

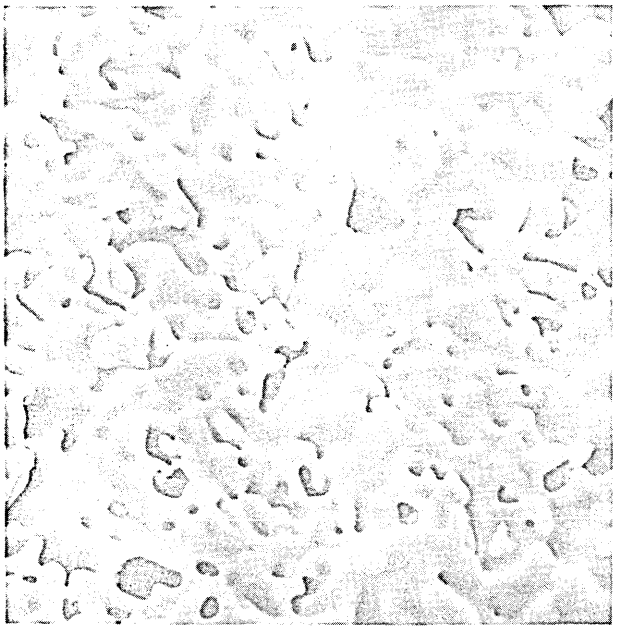

x 1000 1150°C, 1 h (c)

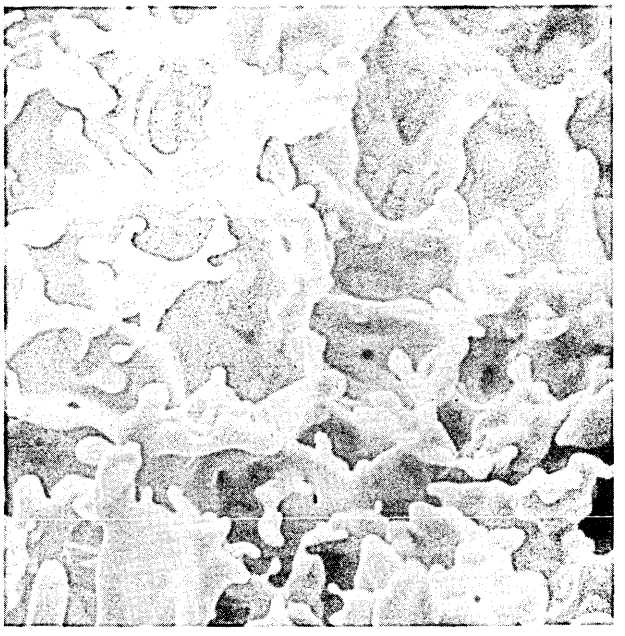

x 1150 1200°C, 1 h (d)

METAL SURFACE REVEALED ON REMOVAL OF SCALE LAYER ON RIMMING STEEL
(Stereoscan electron images)

FIG. 81

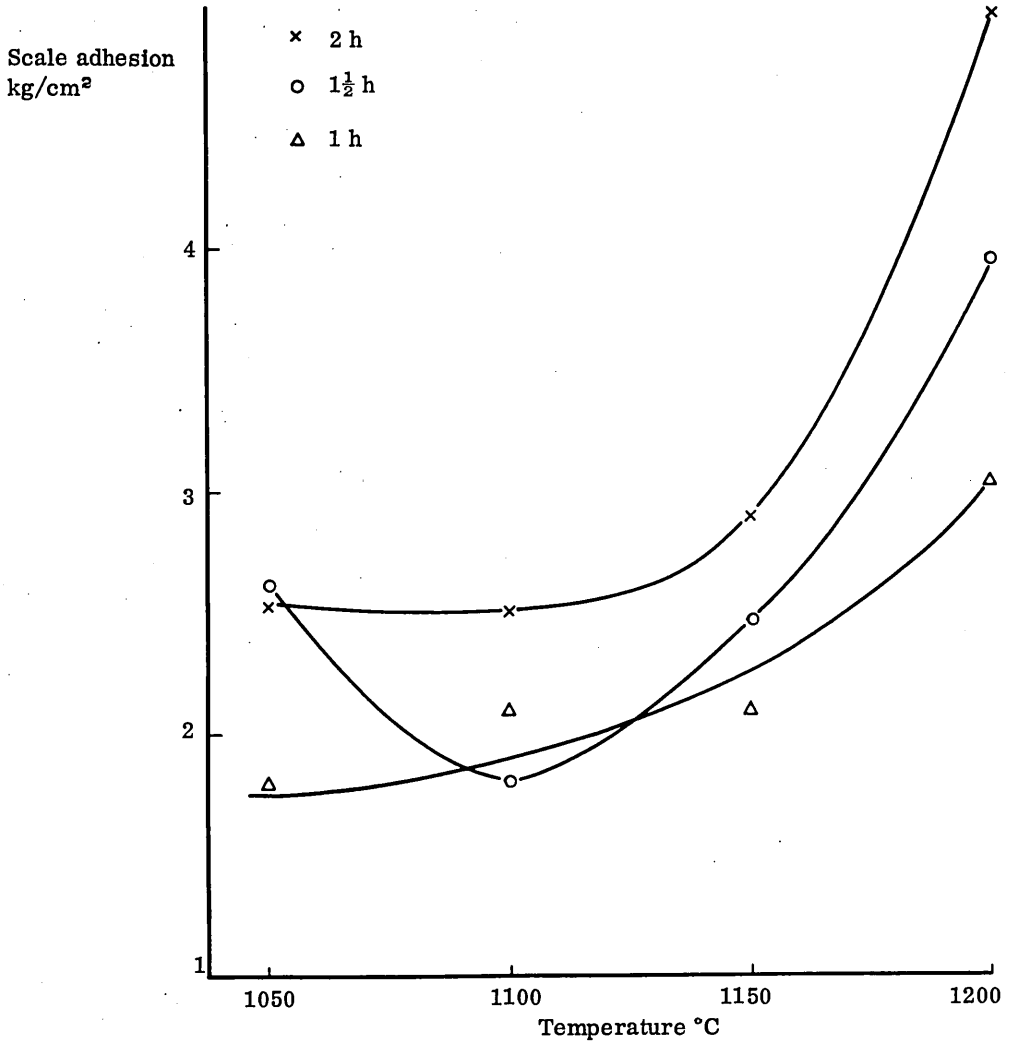

THE EFFECT OF REHEATING TEMPERATURE AND TIME ON THE SCALE ADHESION ON Si-KILLED STEEL EXX. 20 FIG. 82

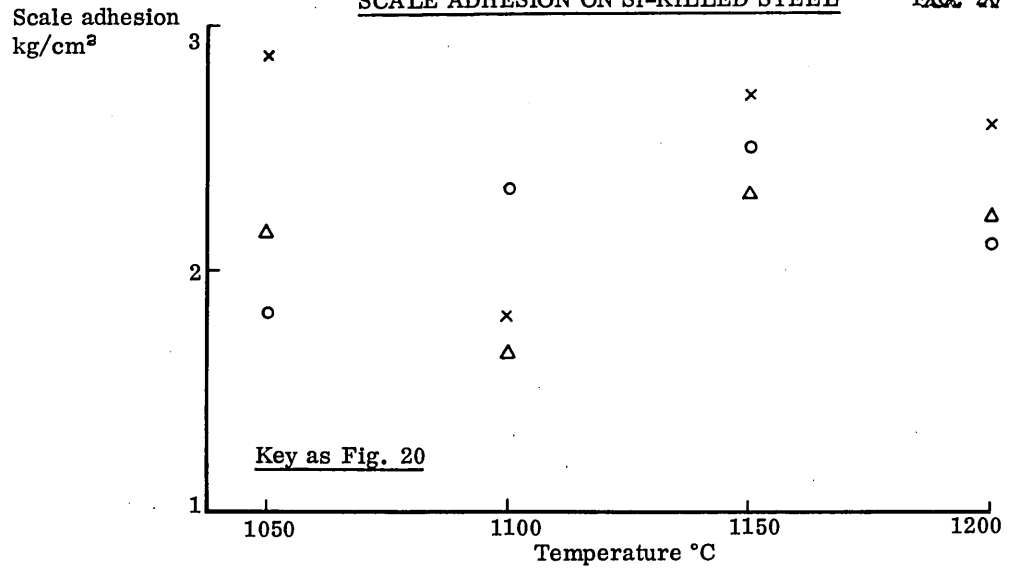

THE EFFECT OF REHEATING TIME AND TEMPERATURE ON THE SCALE ADHESION ON Al-TREATED STEEL

FIG. 83

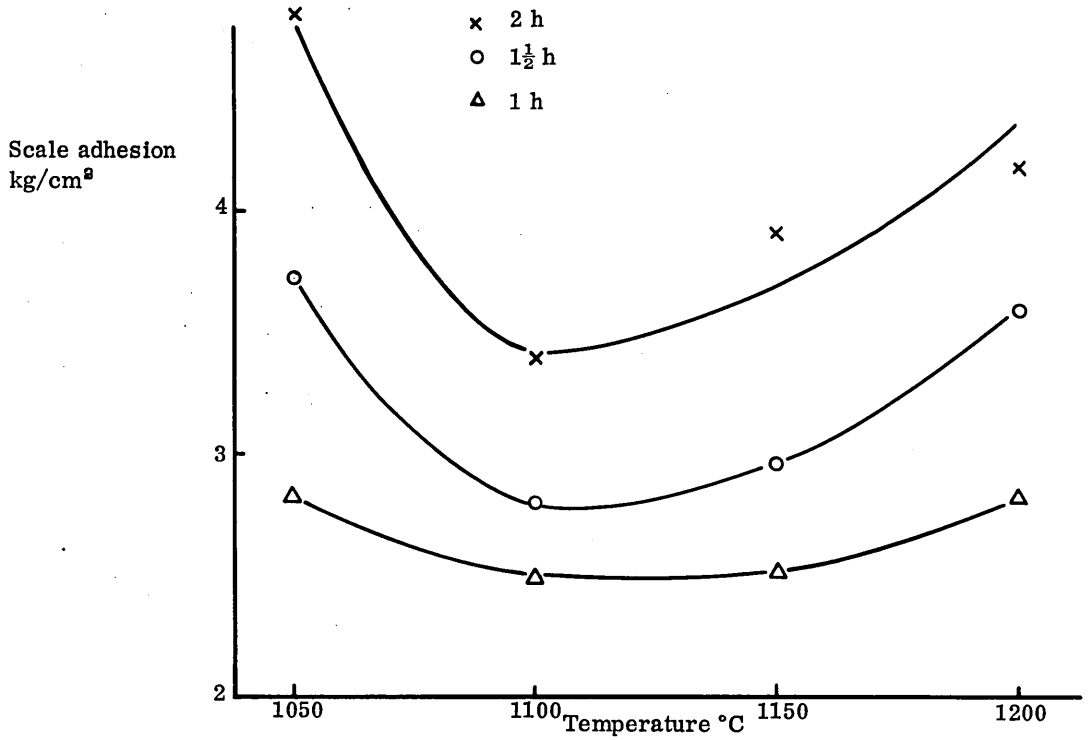

THE EFFECT OF REHEATING TEMPERATURE AND TIME ON THE SCALE ADHESION ON RIMMING STEEL

FIG. 84

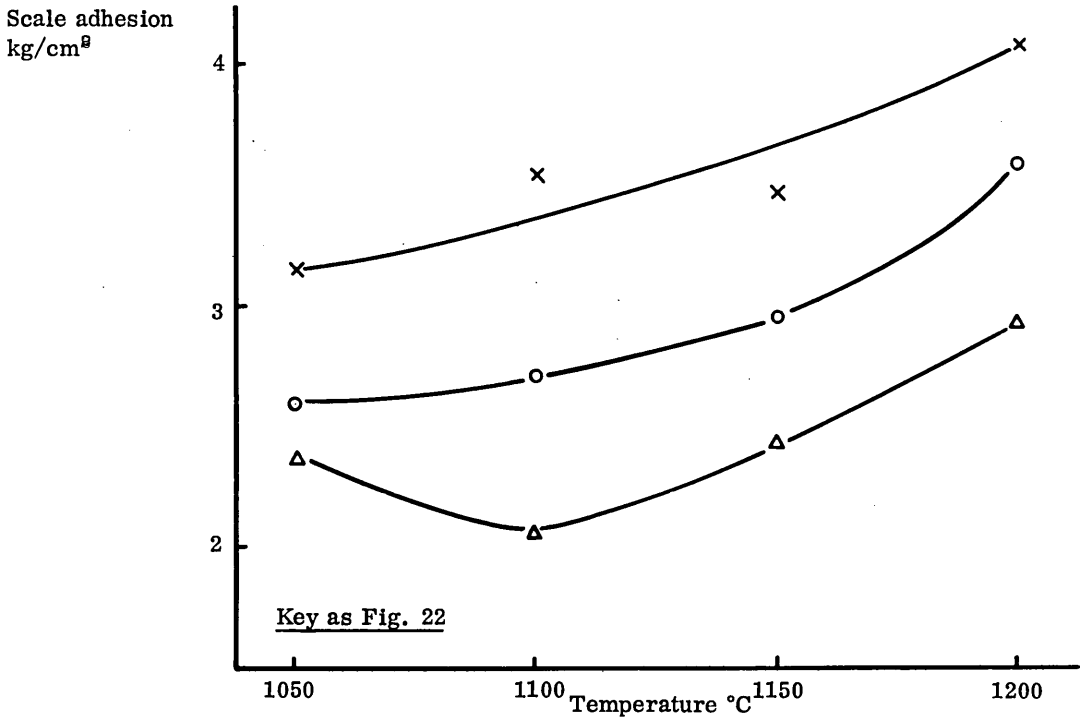

THE EFFECT OF REHEATING TEMPERATURE AND TIME ON THE SCALE ADHESION OF SEMI-KILLED STEEL

FIG. 85

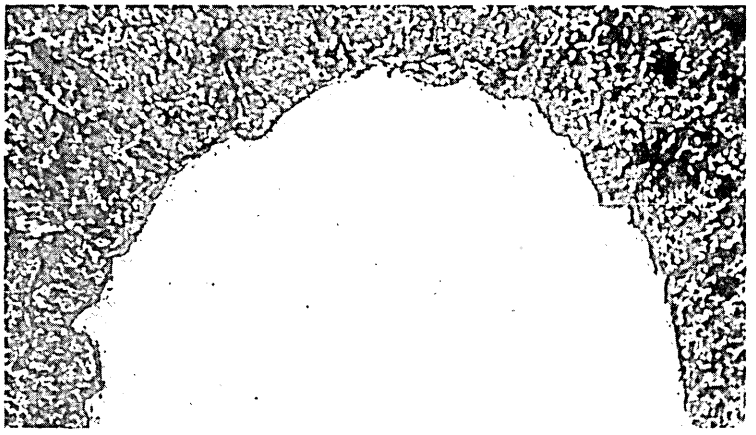

OXIDATION OF GAUZE WIRE IN SCALE
x 500

FIG. 86

x 25 Scaled specimen showing corner crack (a)

x 500 Scale at crack (FeO) - etched (b)

STRUCTURE OF SCALE AT SPECIMEN CORNER

FIG. 87

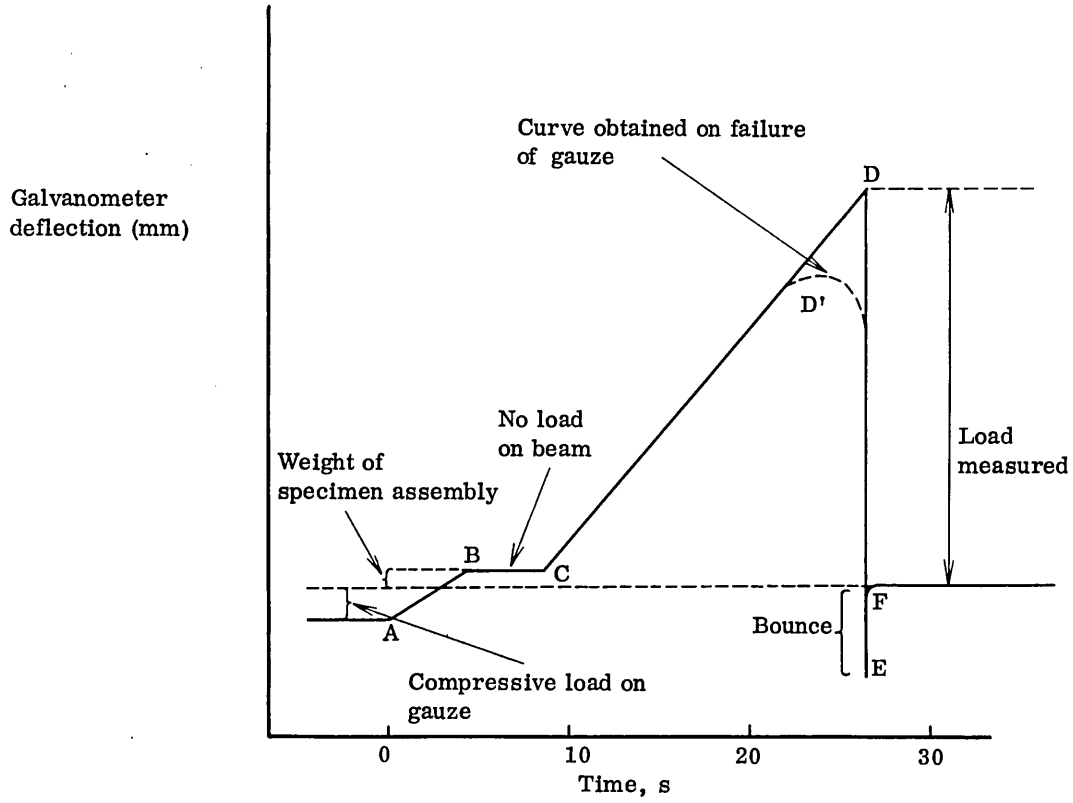

TYPICAL TRACE FROM ULTRA-VIOLET RECORDER

FIG. 88

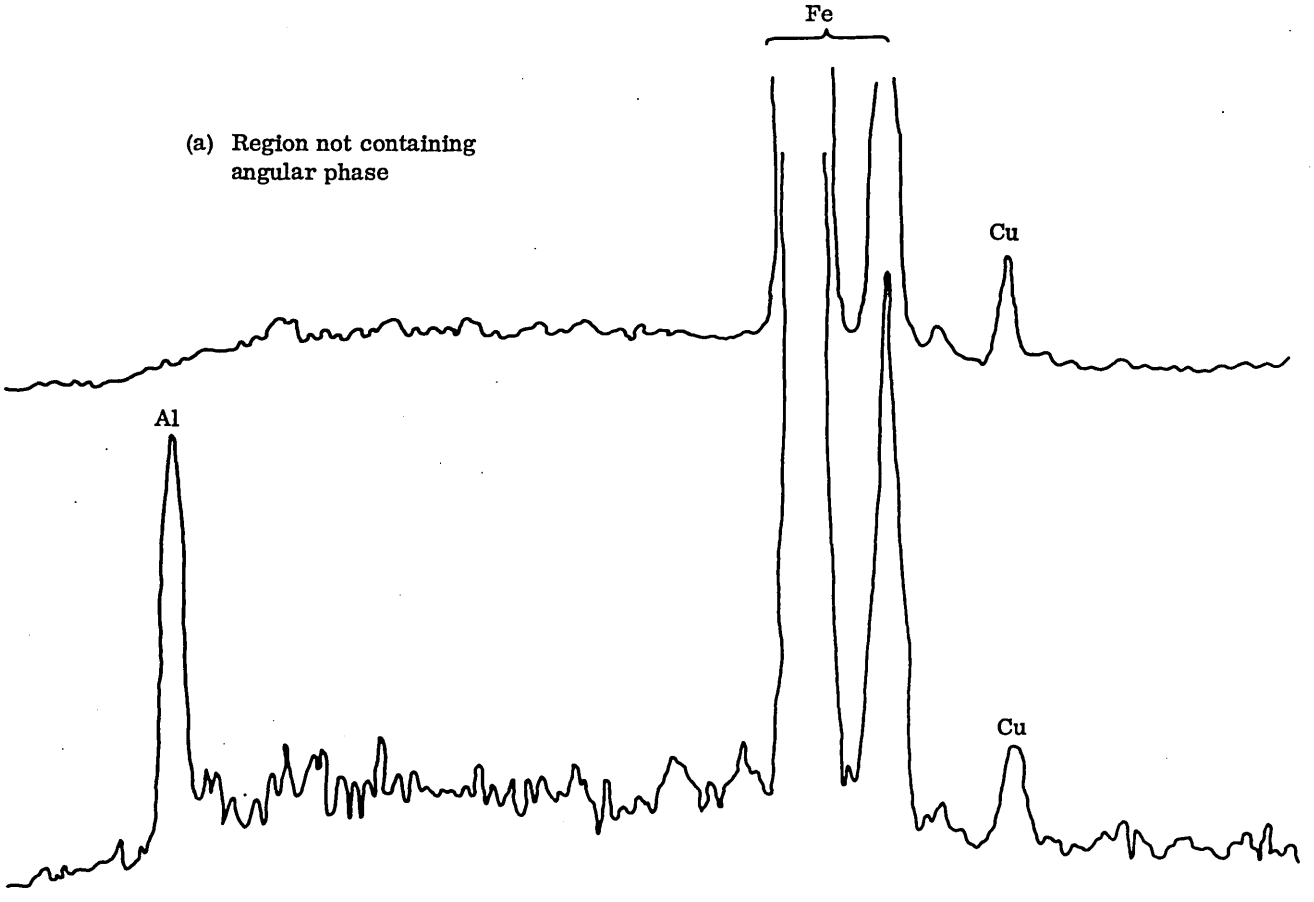

ORTEC NON-DISPERSIVE ANALYSER RESULTS

FIG. 89

x $\frac{1}{2}$ Example of Pitted Plate
(Note the pits may appear as blisters due to an optical effect)

x 500 Section through Base of Pits - unetched

SCALE PITTING SURFACE DEFECT ON Si-KILLED STEEL

FIG. 90

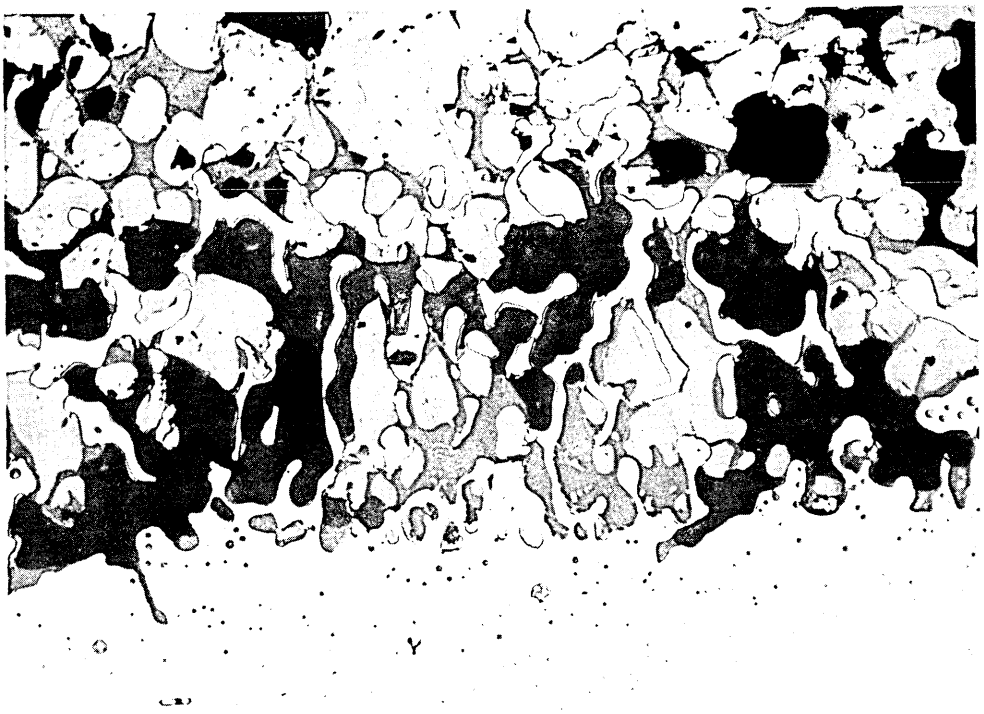

Reheated at 1250°C, 3 h - unetched
(Towns gas furnace ~4% O_2) (a)

As above + 75% rolling reduction - unetched (b)

LABORATORY ROLLING TRIAL METAL/SCALE INTERFACE
STRUCTURES PRODUCED BY REHEATING AND ROLLING ON Si-KILLED STEEL
x 250

FIG. 91

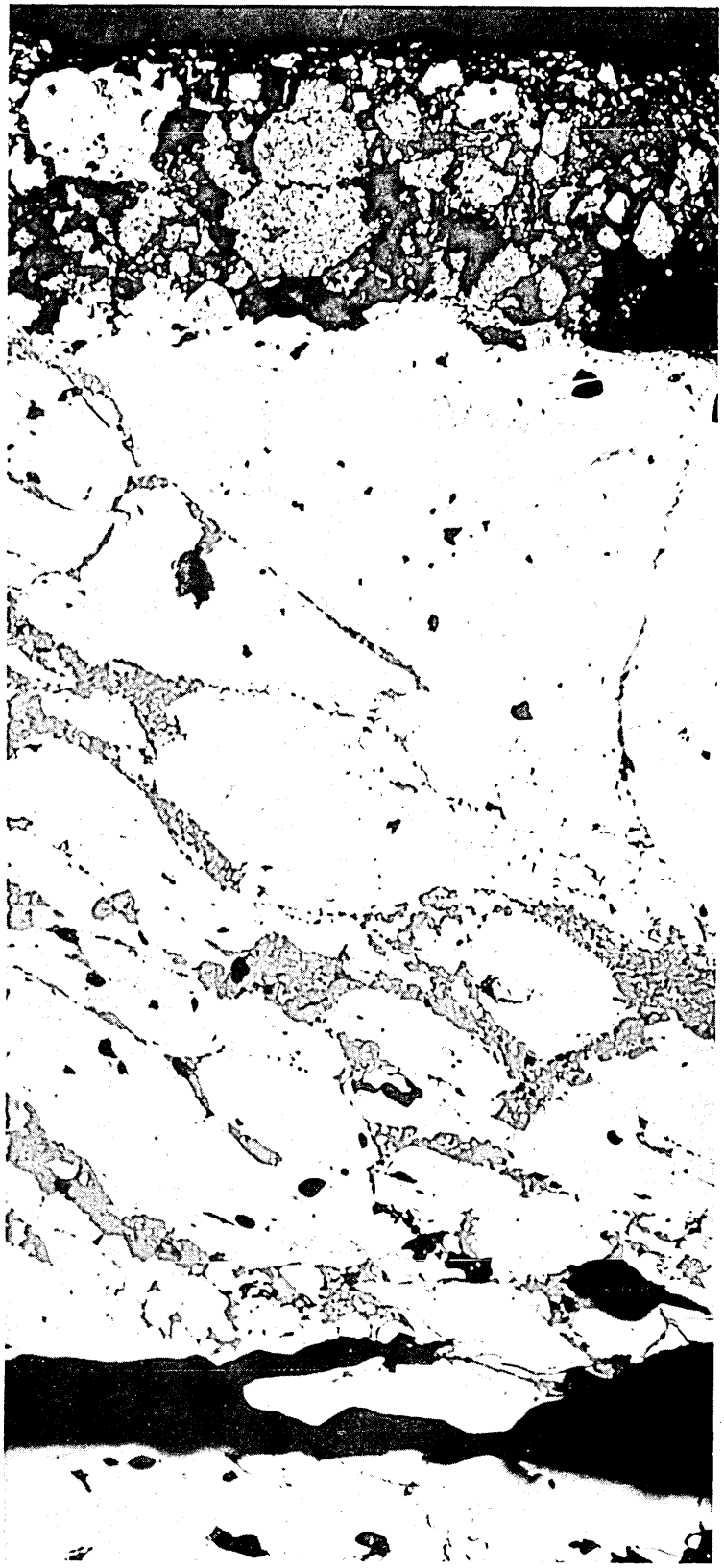

SCALE LAYER FROM FIG. 30(b) SHOWING LIQUID SHAPE FORCED INTO CRACKS IN THE OUTER FeO LAYER

x 250 unetched

FIG. 92

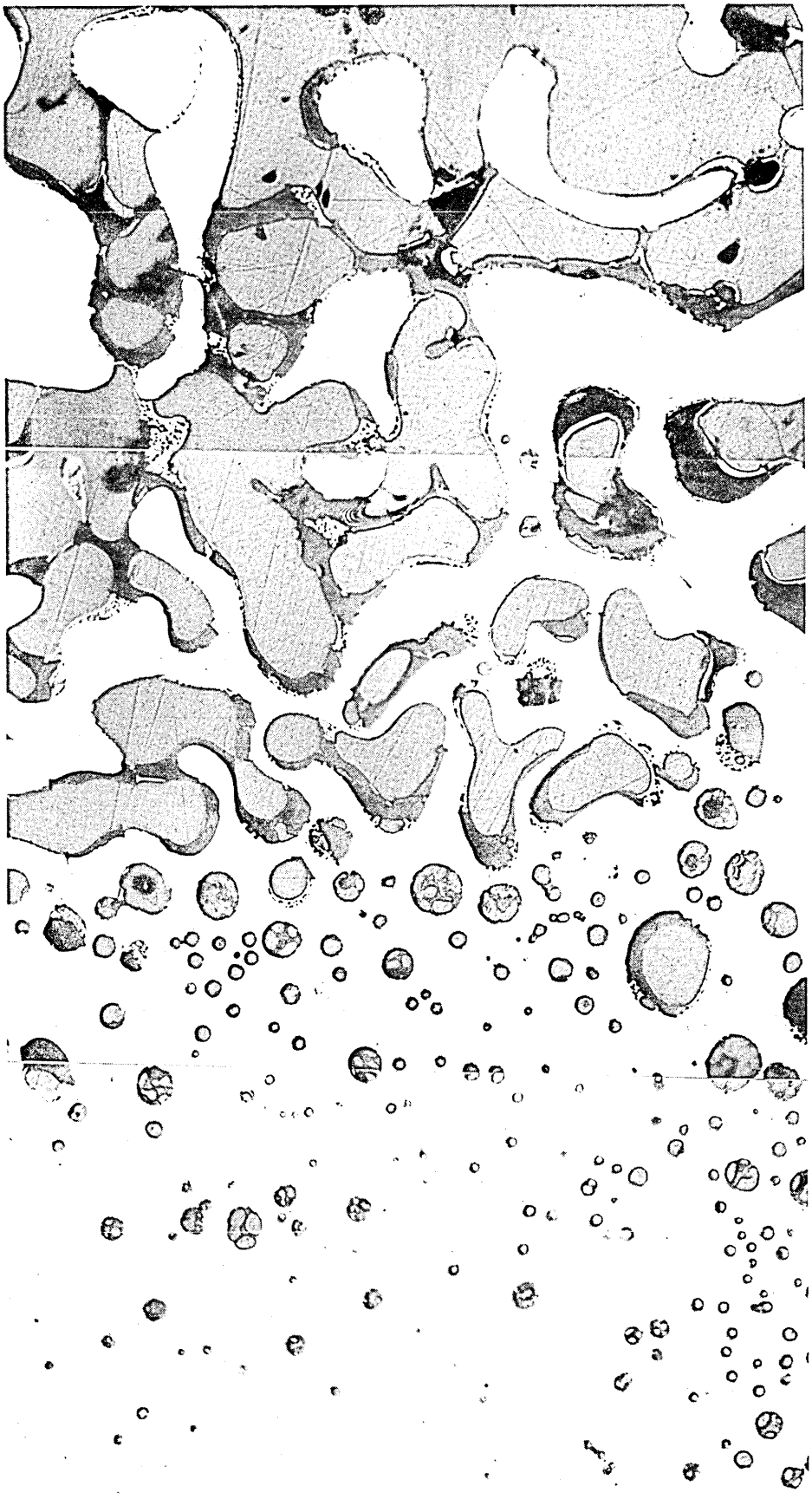

COMMERCIAL SILICON-KILLED STEEL (Cast 50442) 1340°C, 3 h, COMBUSTED COKE OVEN GAS (6.0% O_2) x 750

FIG. 93

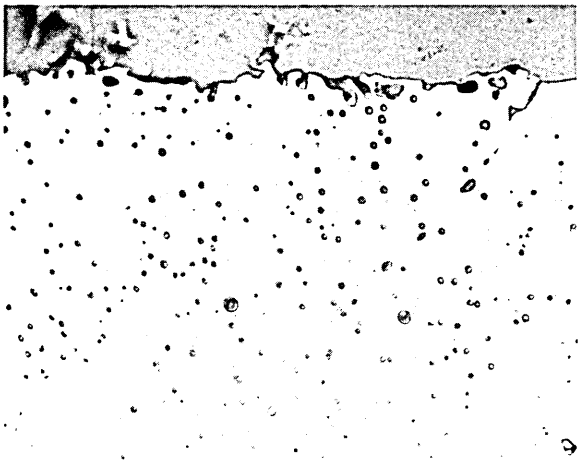

15 min N_2 (a)

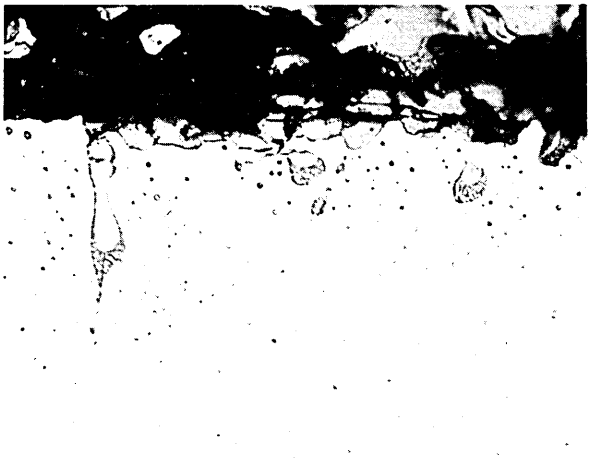

1 min oxidising atmosphere (b)

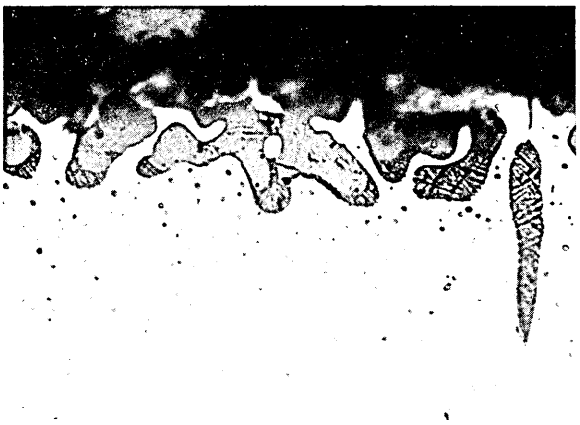

2 min oxidising atmosphere (c)

5 min oxidising atmosphere (d)

SHORT TIME TESTS (Cast 50442) 1200°C
x 750

FIG. 94

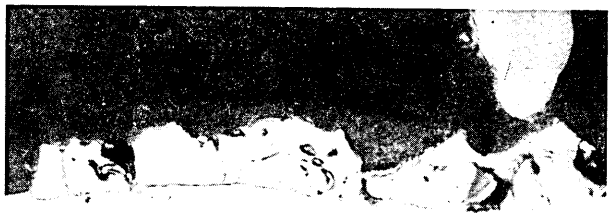

Nil SO_2 (a) Plus SO_2 (b)

Base Cast

Nil SO_2 (c) Plus SO_2 (d)

Base Cast plus 1% Mn

FACTORIAL EXPERIMENT (LOW CARBON SERIES)
x 500

FIG. 95

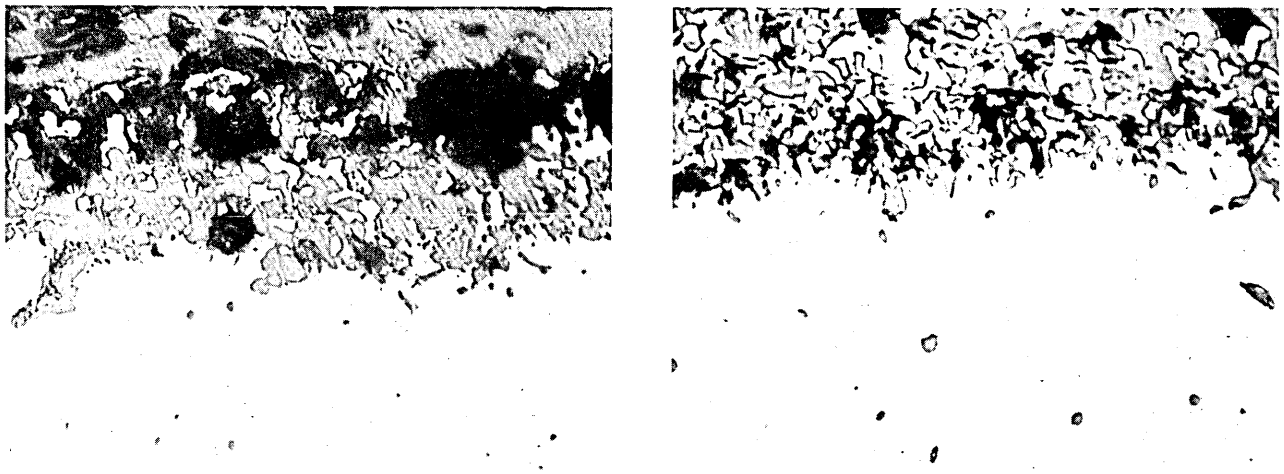

Nil SO_2 (a) Plus SO_2 (b)

Base plus 1% Ni

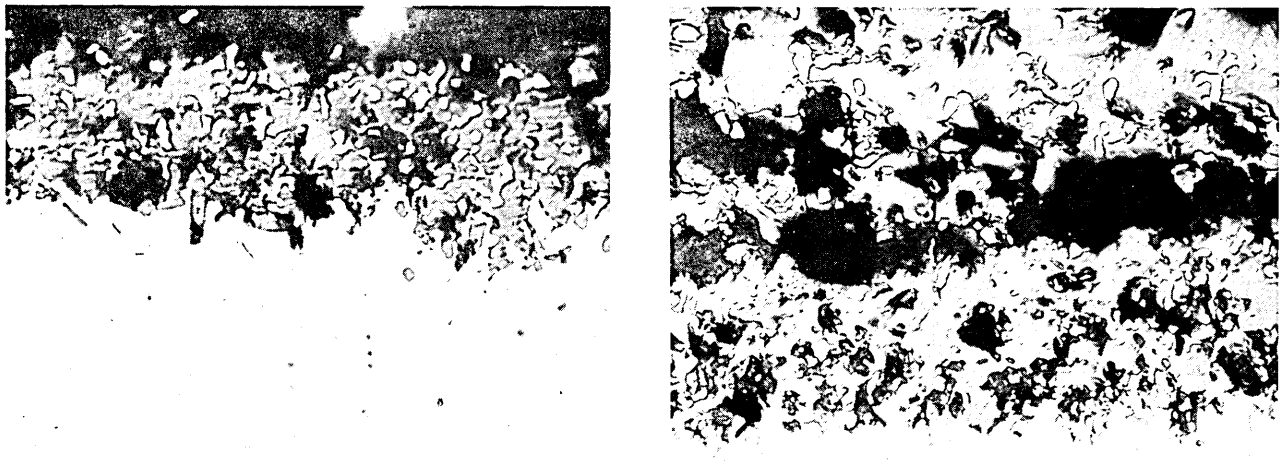

Nil SO_2 (c) Plus SO_2 (d)

Base plus 1% Mn 1% Ni

FACTORIAL EXPERIMENT (LOW CARBON SERIES)
x 500

FIG. 96

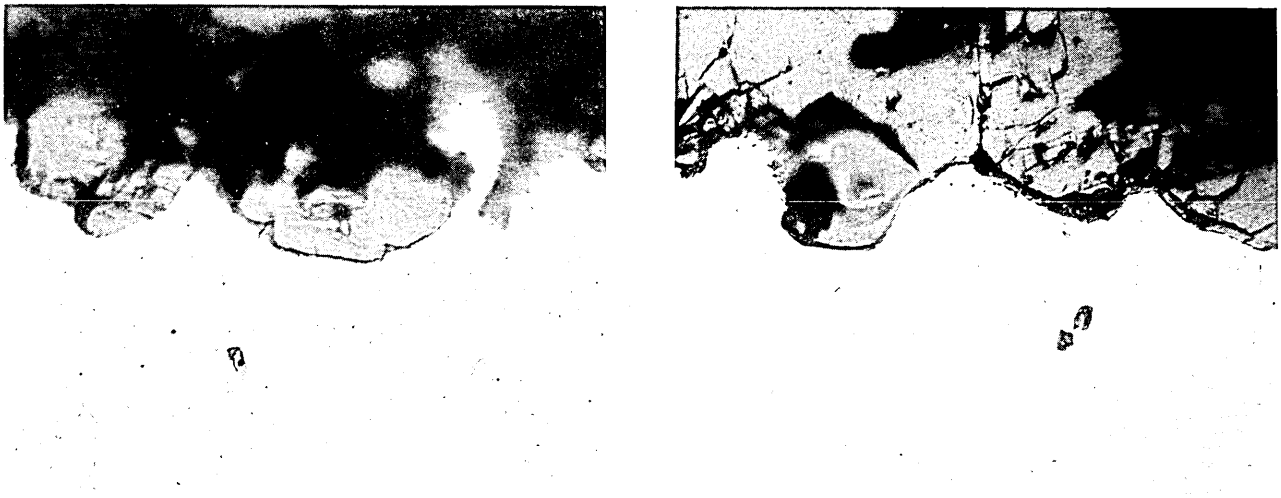

Nil SO_2 (a) Plus SO_2 (b)

Base cast

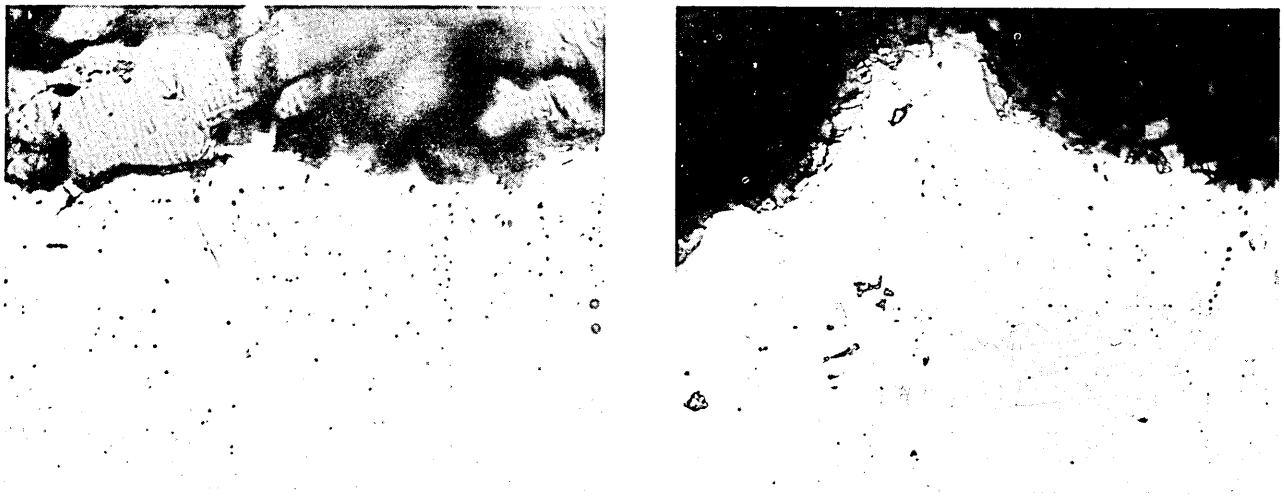

Nil SO_2 (c) Plus SO_2 (d)

Base cast plus 1% Mn

FACTORIAL EXPERIMENT (HIGH CARBON SERIES)
x 500

FIG. 97

Nil SO_2 (a)

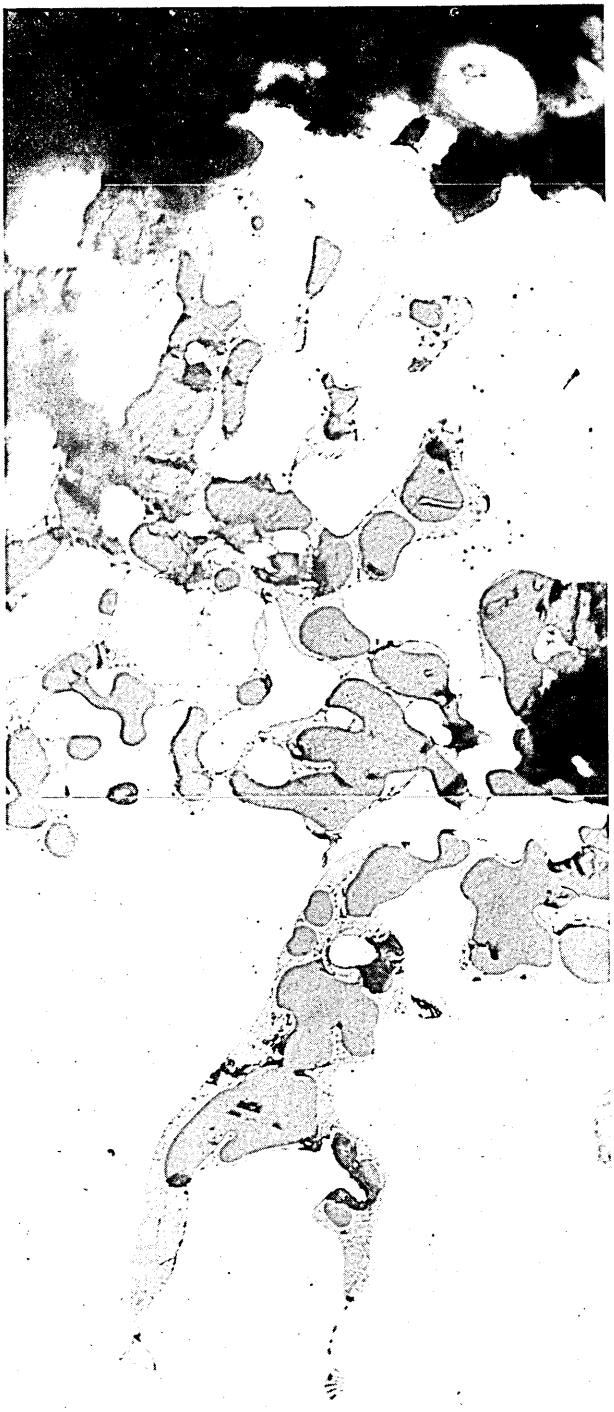

Plus SO_2 (b)

Base plus 1% Ni

FACTORIAL EXPERIMENT (HIGH CARBON SERIES)
x 500

FIG. 98

Nil SO_2 (a)

Plus SO_2 (b)

Base plus 1% Mn, 1% Ni

FACTORIAL EXPERIMENT (HIGH CARBON SERIES)
x 500

FIG. 99

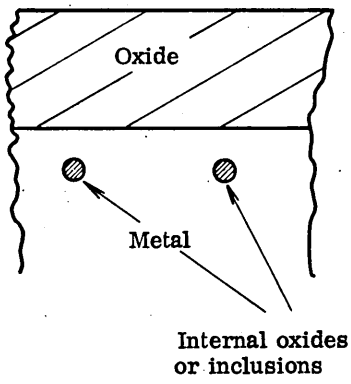

(a) Initial stages of oxidation

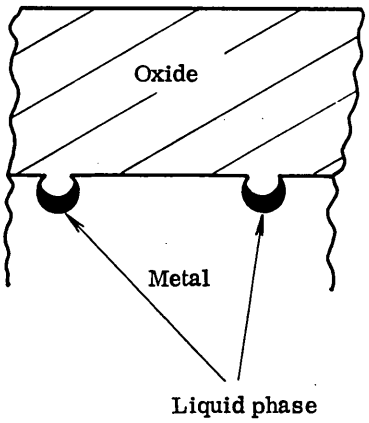

(b) Initiation of surface irregularity

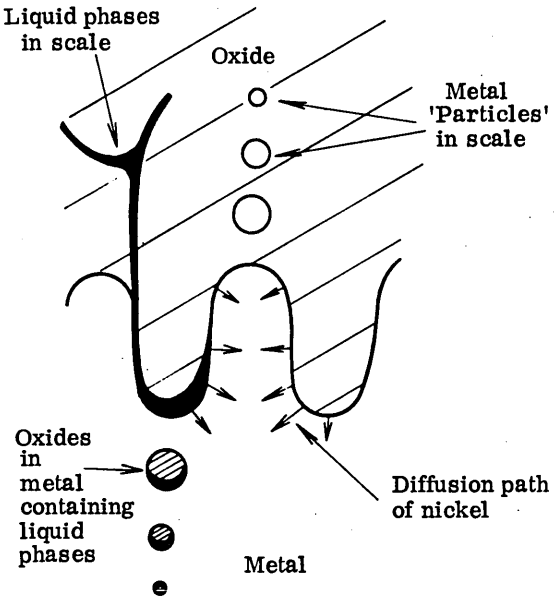

(c) Development of entanglement

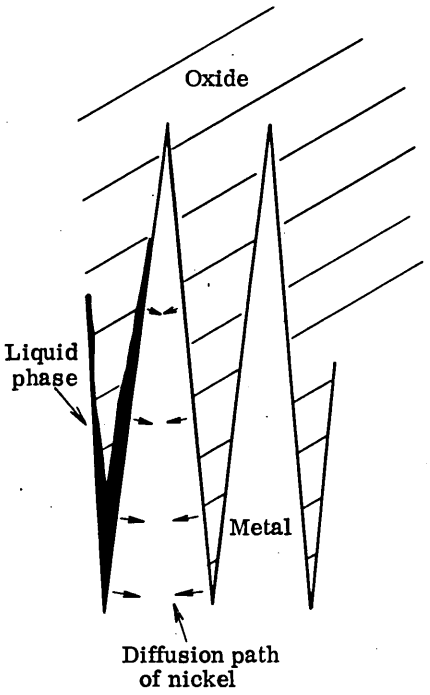

(d) Entanglement neglecting the meandering effect

SCHEMATIC REPRESENTATION OF THE MECHANISM OF METAL/SCALE ENTANGLEMENT

FIG. 100

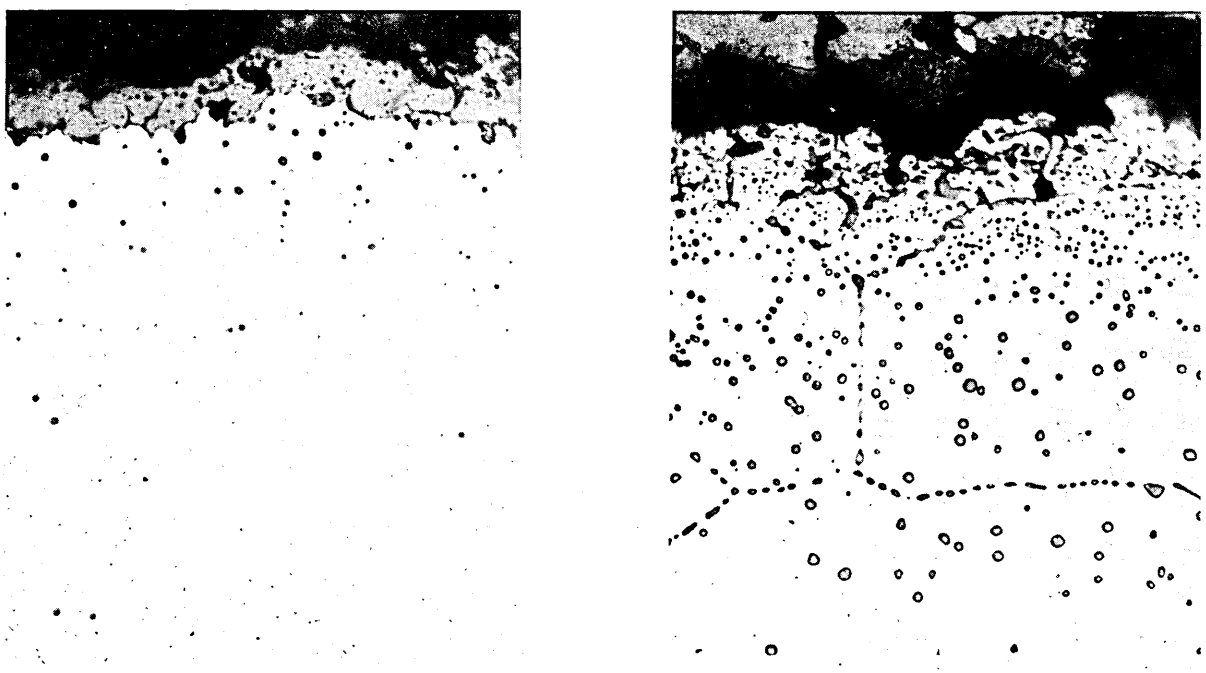

Base cast (a) Alloy composition + Cu + Ni + Sn (b)

EFFECT OF ENRICHMENT ON INTERNAL OXIDATION
x 250

FIG. 101

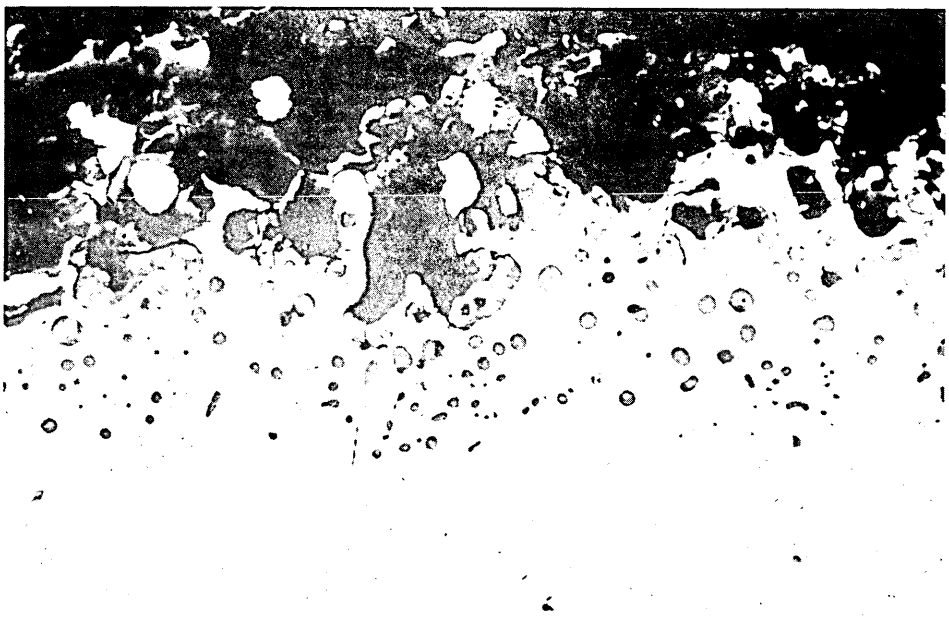

Near surface of cut (a)

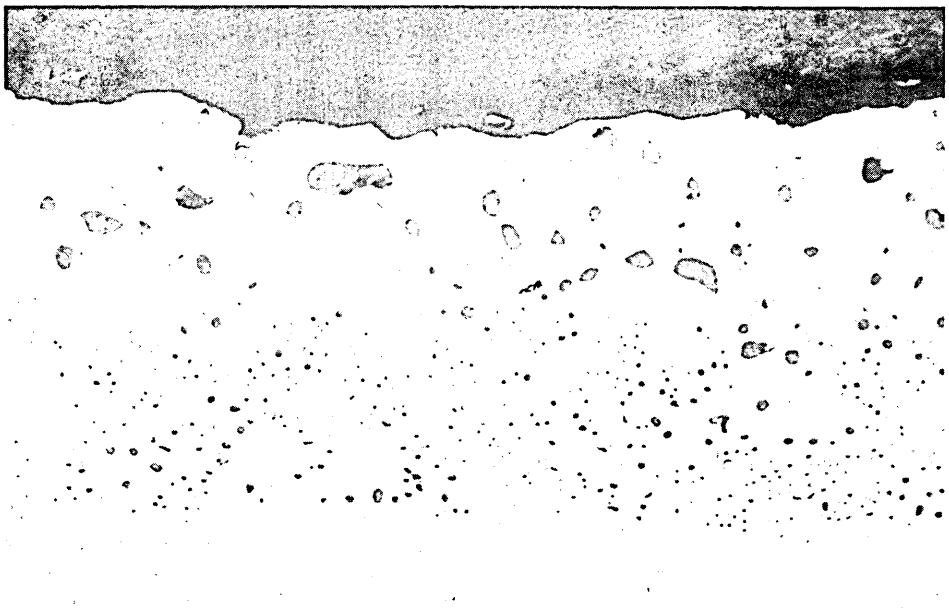

Near bottom of cut (b)

EXAMPLE OF 'OSTWALD RIPENING'
x 250

FIG. 102

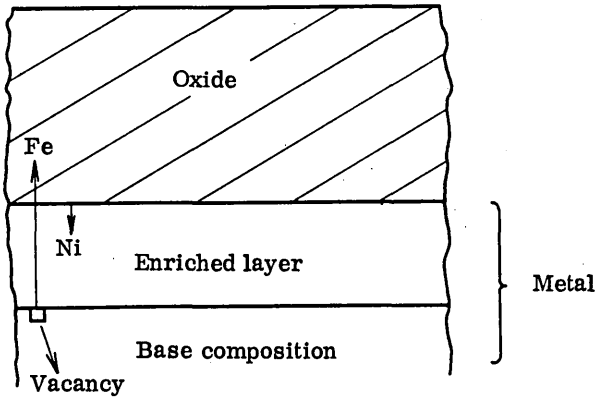

(a) Mechanism of oxidation with an enriched layer present and assuming planar interface conditions

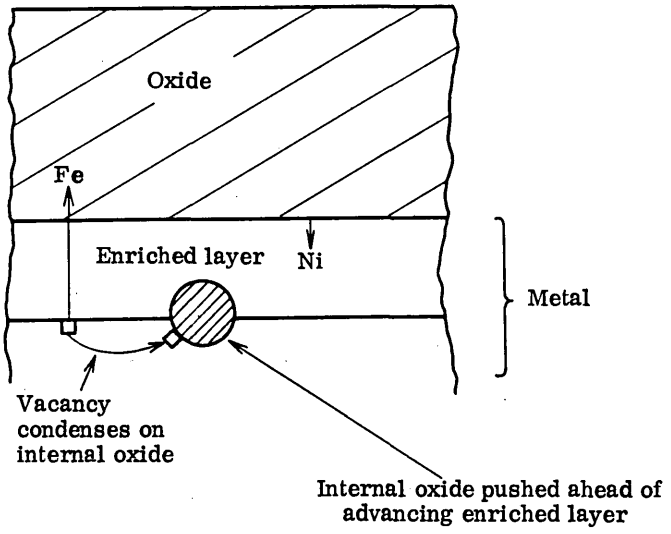

(b) Behaviour of internal oxide particles with an enriched layer present

FIG. 103

APPENDIX 1

DETERMINATION OF THE SO_2 CONTENT OF THE ATMOSPHERE USED (89)

The addition of potassium iodate to an acid solution of potassium iodide liberates iodine, which in the presence of starch gives a blue colouration. Sulphur dioxide reduces the iodine formed and decolourises the starch complex until the addition of more potassium iodate restores the blue colour.

Thus if a known volume of the furnace atmosphere is passed through acidified potassium iodide and the amount of potassium iodate which has to be added during the absorption to maintain a blue colouration is determined, the amount of SO_2 in the atmosphere can be calculated.

Solutions Required

Standard Potassium Iodate:- Dissolve 0.223 g of KIO_3 in water and dilute to 1 litre. (1 ml KIO_3 ≡ 0.0001 g S)

Solution A:- Hydrochloric acid 1.5%, Dilute 15 ml conc. HCl to 1 litre with water.

Solution B:- Potassium iodide 3%, Dissolve 3 g KI in 100 ml water.

Solution C:- Starch solution 2%, Dissolve 2 g starch in 100 ml water.

Solution for absorption:- Immediately before use mix 80 ml of A, 1 ml of B and 1 ml of C.

Pass a known volume of the synthetic atmosphere into the absorption solution and titrate with the standard potassium iodate, i.e. just before absorption the solution is made just blue by the addition of a few drops of potassium iodate, and thence maintained blue during absorption by the constant addition drop-wise of KIO_3 until the blue colour remains stable for a few minutes. This is the end point of the titration.

$$6HCl + KIO_3 + 5KI = 3I_2 + 6KCl + 3H_2O$$

Addition of SO_2

$$SO_2 + I_2 + 2H_2O = H_2SO_4 + 2HI$$

With more KIO_3

$$KIO_3 + 3H_2SO_4 + 6HI + 6KCl = 3K_2SO_4 + KI + 3I_2 + 6HCl + 3H_2O$$

As 1 ml $KIO_3 \equiv 0.0001$ g S the volume of SO_2 in the furnace atmosphere can be calculated.

METHODS OF CALCULATING THE OXIDATION KINETICS

It is usual to express gravimetric oxidation data in terms of the gain in weight per unit area of the oxidising metal (g/cm^2). If the assumption is made that the surface area of the specimen does not change during oxidation a typical oxidation/time curve results (A.2 Fig. 1 (a). Oxidation theory predicts a parabolic rate law.

$$w^2 = k_p t$$

Where:-

w = gain in weight/unit area (g/cm^2)

t = oxidation time (seconds)

kp = parabolic oxidation rate constant.

The silicon killed steel in the example does not obey the parabolic time law and the deviation increases with time (A.2. Fig.1(b). However the surface area of the specimen does change as the oxidation proceeds because of the transfer of metal ions into the scale.

Consequently the cylinder dimensions decrease and in order that the oxidation kinetics may be studied accurately it is necessary to establish the rate of change of the surface area of the specimen used. If it is assumed that the scale consists of stoichiometric FeO only the oxidation reaction may be written.

$$Fe + O \rightarrow FeO$$

The atomic weight of iron and oxygen are 56 and 16 respectively and hence 1 g of oxygen combines with $\frac{56}{16}$ (i.e. 3.5) g of iron to form FeO. Therefore the net transfer of iron into the scale is equal to 3.5 x (gain in weight of the specimen). The volume of metal lost from the culinder is given by:

$$\text{Vol. lost } (cm^3) = \frac{3.5 \times \text{gain in weight (g)}}{\text{Density of iron (i.e. 8)}}$$

At any time (t) after the start of oxidation the volume of the cylinder may thus be found if the original volume is known, and the area at time (t) may be calculated from the volume as follows.

To determine the surface area of a cylinder from its volume it is necessary to have a relationship connecting cylinder length and cylinder radius.

An iron cylinder is assumed to oxidise at equal rates on both the curved surface and the flat ends. For a cylinder of length x and radius r this implies that $\delta x = 2\delta r$.

Hence, $x = 2r + \text{constant}$.

If initially the radius is a and the length is 1, then when $x = 1$, $r = a$. Hence,

$$x = 2r - b \qquad (1)$$

where $b = 2a - 1$. If the cylinder volume is denoted by V then,

$V = \pi r^2 x$. Using equation 1,

$$V = \pi r^2 (2r - b) \qquad (2)$$

If the surface area of the cylinder is denoted by S, then,

$$S = 2\pi r^2 + 2\pi rx$$

Using equation 1,

$$S = 2\pi r^2 + 2\pi r (2r - b) \qquad (3)$$

Thus S and V are in terms of r alone.

It is required to find the radius, r, from equation 2 given the volume, V, and hence to substitute this radius into equation 3 to determine the surface area, S. Equation 2 may be rewritten as the cubic equation in r,

$$2\pi r^3 - \pi br^2 - V = 0$$

which must be solved for r, assuming the required value to be the one real root. In accordance with the theory on cubic equations let

$$G = -4\pi^2 V - 2\left(\frac{\pi b}{3}\right)^3$$

$$H = -\left(\frac{\pi b}{3}\right)^2$$

$$p = \left(\frac{-G + \sqrt{G^2 + 4H^3}}{2}\right)^{1/3}$$

then,

$$r = \frac{3p^2 + \pi bp - 3H}{6\pi p}$$

Substituting this value into equation 3 yields the value of surface area, S, corresponding to the volume, V, of the cylinder.

Using this method the specimen area for a cylindrical specimen can be calculated as the oxidation proceeds and in the example a decrease in area was obtained of 8% after three hours (A.2 Fig. 1(a). If the actual surface area of the specimen at any instant in time is used to calculate w an increase in w results and still further deviation from the parabolic time law is observed. In addition in this case, linear oxidation tendencies are observed for the longer times when the decreasing area of the specimen is allowed for.

The Incremental oxidation rate constant may be calculated from the weight gain/unit area data (corrected for diminishing surface area) for each five minute time interval as follows:

$$k_{p1} = \frac{w_1^2}{300},\ k_{p2} = \frac{w_2^2 - w_1^2}{300},\ \ldots\ k_{p36} = \frac{w_{36}^2 - w_{35}^2}{300}$$

Where w = weight gain/unit area (g/cm^2)

300 = time interval (s)

Then the units of k_p the incremental oxidation rate constant are

$$g^2 cm^{-4} s^{-1}$$

Additional deviations from the parabolic law are demonstrated by the fact that the value of k_p increases with time (Fig. 2)

A closer approximation to the rate laws governing the oxidation process may be obtained by considering the general equation.

$$w^n = k_{(n)} t.$$

Values of n may be determined from the slope of a log w versus log t plot and incremental k_n values determined in a similar way to that above. A more consistent rate constant results (Fig. 54), but there is still a tendency for k_n to increase with time in the example. This is because the log w versus log t plot is not straight line in this case and an average value of n is used.

For practical use, however, it is more useful to assume that parabolic rate laws are followed for the calculation of the oxidation obtained under non-isothermal heating conditions (see Appendix 4).

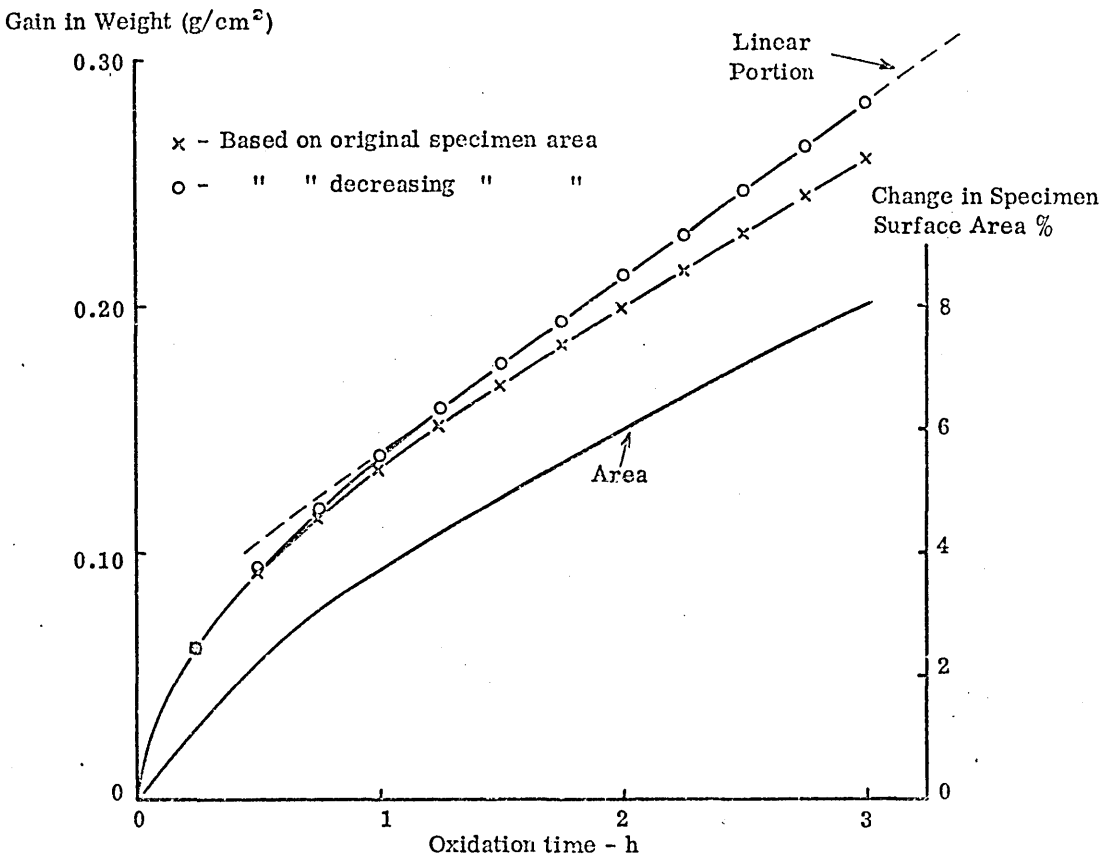

a) EFFECT OF DECREASING SURFACE AREA OF SPECIMEN

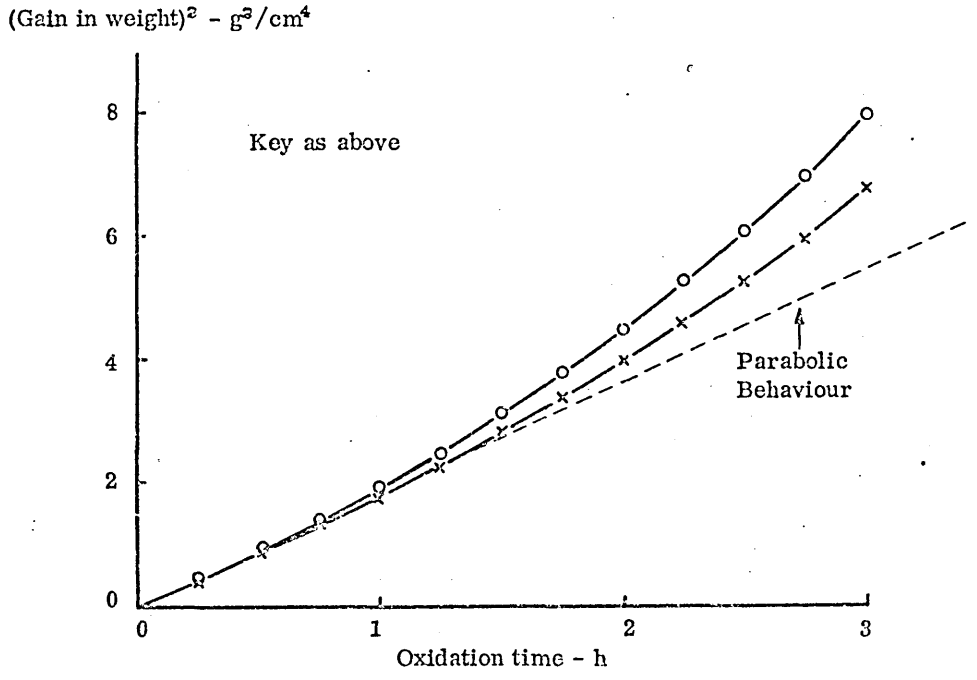

b) NON-PARABOLIC BEHAVIOUR
(Si-KILLED STEEL OXIDISED AT 1325°C)

Appendix 2 Fig. 1

CALCULATION OF THE DEPTH OF INTERNAL OXIDATION FOR ISOTHERMAL OXIDATION

Several quantitative treatments have been made of the problem of internal oxidation based on fundamental considerations for binary and ternary alloys. Rhines et alia [95] and Maak [96] have derived equations which predict the depth of internal oxidation under conditions of simultaneous internal and external oxidation for a simple binary system. A.3 Fig. 1 represents the distribution of dissolved oxygen and solute metal (having greater affinity for oxygen than iron) at some stage in the oxidation process. The oxygen is imagined to be supplied at the outside surface at a rate sufficient to maintain saturation of the surface iron. At the interface between the subscale and the alloy, oxygen meets the solute and reacts to precipitate its oxide. Since the solute metal is removed from solution by this process its concentration is reduced in the neighbourhood of the subscale/alloy interface to some limiting value, C_L. This provides a concentration gradient in the alloy, and diffusion of the solute towards the interface occurs along the gradient $C_M - C_L$. As oxidation proceeds the alloy becomes impoverished, thus reducing the rate of delivery of solute metal and the interface moves inwards.

In both Rhines et alia and Maak's treatment a number of simplifying assumptions are made in deriving their equations. For instance C_L and C_P are taken as zero, which is reasonable for cases where very stable oxides are formed. Also the precipitated oxide particles are assumed not to impede the inward deffusion of oxygen, and the diffusivities of oxygen and solute are regarded as independent of concentration.

Rhines et alia derive the following expression:-

$$S^2 = \frac{2\,C_O\,D_O\,t}{C_M\,O/_M \left(1 + \sigma\sqrt{\frac{K_E}{K_S}}\right)\left(1 + \frac{1.68 D_M}{(\sigma\sqrt{K_E} + \sqrt{K_S})^2}\right)} \qquad \ldots\ldots\ldots (1)$$

Where S = Depth of internal oxide penetration (cm)

Co = Solubility of oxygen (in iron) (weight %)

Do = Diffusivity of oxygen (cm^2/S)

C_M = Initial solute content (weight %)

$^o/_M$ = Weight ratio of oxygen to metal in the oxide formed = 1.14

K_E = (Depth alloy oxidised)^2 ÷ oxidation time, t (cm^2/S)

$K_S = S^2 \div t$

D_M = Diffusivity of solute (cm^2/S)

$$\delta = \frac{\text{density FeO x 2 At. Wt. Fe}}{\text{Density Fe x Mol. Wt. FeO}} = 1.17$$

Equation (a) has been used to predict the depth of internal oxidation in the Si-killed steel specimens tested in these experiments making a further simplifying assumption that the oxide formed at the reaction interface is SiO_2 and that the subsequent conversion to more complex oxides nearer the metal surface does not markedly affect the process.

Values of Co, So, K_E and D_M are given in Table A.3. 1, K_E being obtained from the thermobalance data in Fig, 41. The value of $^o/_M$ is taken as 1.14 and δ is taken as equal to 1.17 and insensitive to temperature changes.

From Table A.3. it can be seen that:

$$\left(\delta\sqrt{K_E} + \sqrt{K_S}\right)^2 \gg 1.68\, D_M$$

Therefore equation (1) can be simplified:-

$$S^2 = \frac{2\, Co\, Do\, t}{C_M\ ^o/_M \left(1 + \delta\sqrt{\frac{K_E}{K_S}}\right)} \qquad \text{.....(2)}$$

The values for depth of internal oxidation calculated from equation (2) are compared with measured values in A.3. Table 2. The agreement is reasonably good in view of the assumptions made and warrants a more detailed study. Swisher and Turkdogan [94] point out that their oxygen solubility data (and therefore their diffusivity data) is inaccurate at

Temperatures below 1200°C and this may explain the relatively poor correlation between theory and experiment at 1050°C and 1150°C. A further reason is that at these temperatures the measured values of S are very small and therefore the experimental error in measurement is likely to be appreciable. If it is accepted that equations (1) and (2) are based on a reasonably accurate model, it is possible to make a number of predictions from it. For example, the depth of internal oxidation will decrease with increasing Si contents in the steel, and increasing the rate of oxidation at a given temperature will minimise the extent of internal oxidation. Also in ferritic structures D_M is increased by almost two orders of magnitude compared with austenitic structures. Thus D_M in equation (1) becomes significant and this should lead to a reduced depth of internal oxidation in steels that are ferritic at oxidation temperatures.

No attempt has been made to predict the size of internal oxide particles from diffusivity data but this may be considered worthwhile studying in future work.

A.3 TABLE 1

Oxidation Temperature °C	Co (weight %)	Do (cm^2/s)	K_E (cm^2/s)	D_M (cm^2/s)
1050	5×10^{-4}	1.26×10^{-6}	1.7×10^{-7}	5×10^{-11}
1150	9.5×10^{-4}	3.72×10^{-6}	3.2×10^{-7}	2×10^{-10}
1250	16×10^{-4}	9.44×10^{-6}	5.6×10^{-7}	8×10^{-10}
1325	22×10^{-4}	1.78×10^{-5}	1.2×10^{-6}	1.79×10^{-9}
1350	25×10^{-4}	2.29×10^{-5}	3.5×10^{-6}	2.3×10^{-9}

Values of Co, Do from reference 94

Values of D_M from Bohnenkamp & Engle Arch f.d. Eisenhutte

Values of K_E from thermobalance data, this report. 35 Oct 1964 pp 1011-1018

A.3 TABLE 2 INTERNAL OXIDATION OF LABORATORY OXIDISED SPECIMENS – COMPARISON OF PREDICTED AND MEASURED VALUES (CAST 50442)

Oxidation Temperature °C	Oxidation Time h	Measured Internal Oxtn. Depth mm	Calculated Internal Oxtn. Depth mm
1050	¼	0.011	0.002
	½	0.018	0.004
	1½	0.018	0.006
	3	0.024	0.010
1150	¼	0.05	0.01
	½	0.06	0.02
	1½	0.07	0.03
	3	0.08	0.04
1250	¼	0.04	0.04
	½	0.06	0.05
	1½	0.08	0.09
	3	0.10	0.12
1325	3	0.16	0.18
1350	¼	0.06	0.06
	½	0.07	0.08
	1½	0.10	0.14
	3	0.14	0.19

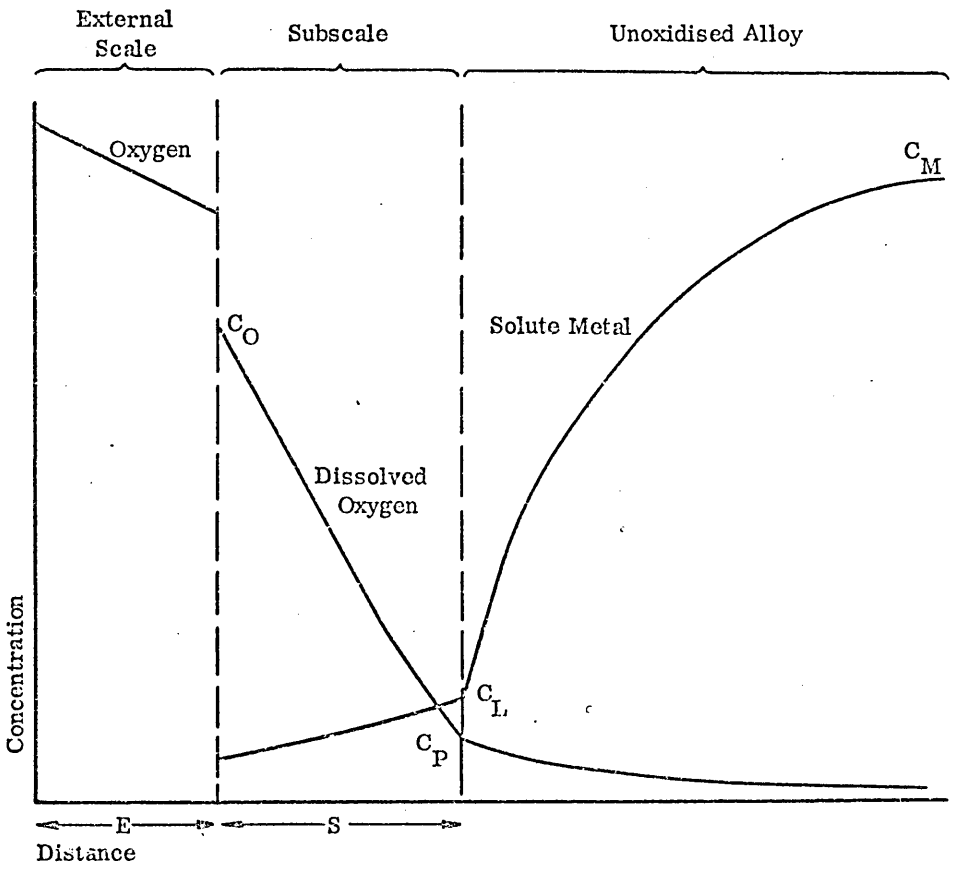

IDEAL DISTRIBUTION OF DIFFUSING ELEMENTS DURING COURSE OF COMBINED INTERNAL AND EXTERNAL OXIDATION (RHINES)[27]

Appendix 3 Fig. 1

METHODS OF CALCULATING THE OXIDATION CHARACTERISTICS OBTAINED UNDER NON-ISOTHERMAL CONDITIONS

Each method uses the assumption that a non-isothermal case such as that shown in A.4 Fig. 1 (a) can be considered as a finite number of isothermal treatments. The average temperature and the time spent at that temperature for each step is determined for as many steps as possible. The oxidation characteristic i.e. amount of oxidation (weight gain), depths of metal/scale entanglement, internal oxidation, and grain boundry oxidation, can be claculated in several ways.

Oxidation characteristics which do not obey a simple rate law may be determined using a graphical method (see A.4. Fig. 1(b)). The amount of, for example, internal oxidation after time t_1 at temperature T_1 is read from the graph. This amount (X_1) would have been formed at some time less than t_1 at a higher temperature T_2 and the additional internal oxidation formed at T_2 is found by projecting horizontally X_1 onto curve T_2 and progressing up curve T_2 for time t_2. This is repeated for each interval until the final value X is obtained.

Oxidation characteristics which do obey approximate rate laws can be determined by calculation:- For example if a parabolic law is followed.

$$w = \sqrt{kt} = \sqrt{k_1t_1 + k_2t_2 + k_3t_3} \quad \text{etc}$$

Where k_1k_2 etc. are the parabolic rate constant for the particular characteristic at temperatures T_1T_2 etc.,

Irregularly shaped non-isothermal curves may be accommodated using Simpsons Rule. In this case the curve is divided into strips of equal time. Then if the rate constant is superimposed on the temperature axis:-

$$w = \sqrt{\text{Area under curve}}$$

$$= \sqrt{\text{Width of strip} \times 1/3 \left[(\text{sum of end ordinates}) + 2 \ (\text{sum of other 'odd' ordinates}) + 4 \ (\text{sum of 'even' ordinates}) \right]}$$

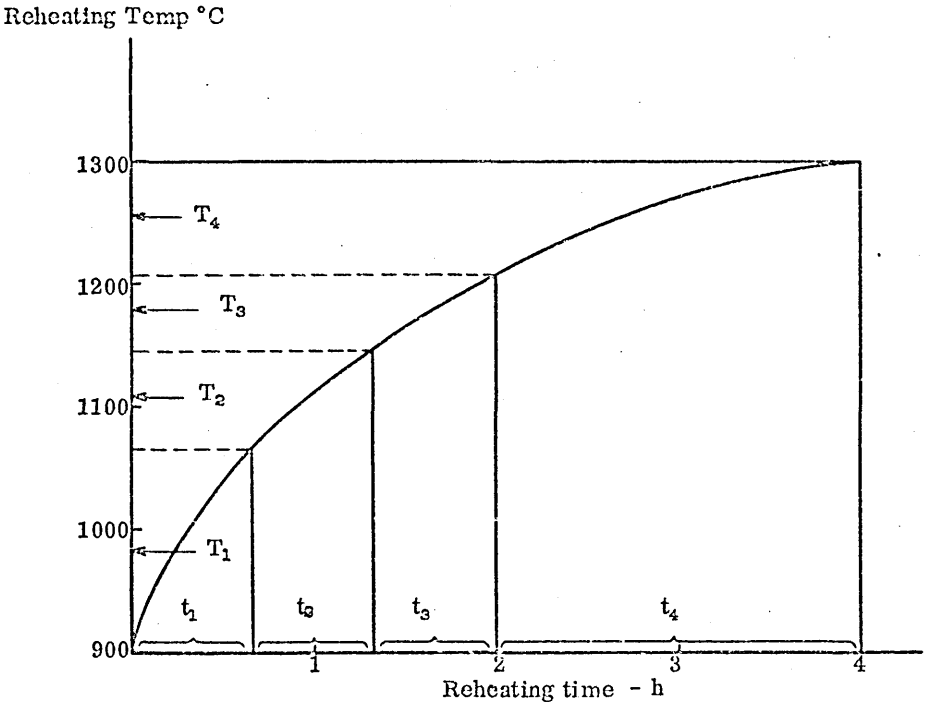

(a) Typical reheating time/temp curve

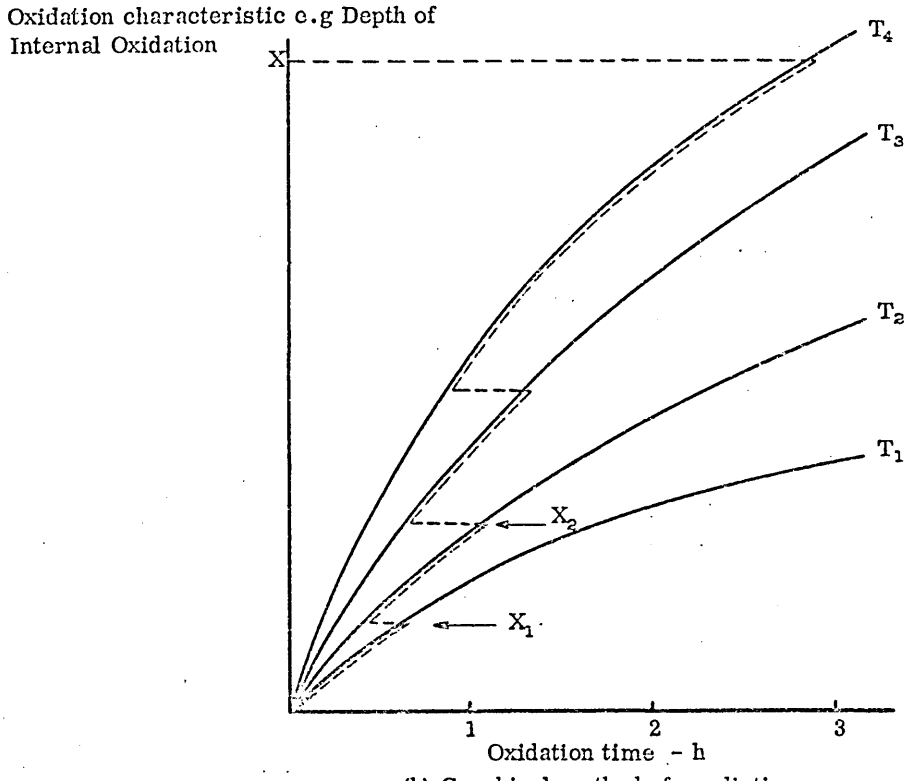

(b) Graphical method of prediction

GRAPHICAL METHOD OF PREDICTING OXIDATION IN COMMERCIAL FURNACES FROM LABORATORY DATA

Appendix 4 Fig. 1

ANALYSIS OF FACTORIAL DATA

The results of the factorial experiment are shown in Table A5/1 and the analysis of these data in A5 Table 2.

1. Low Carbon Steels

In these steels the experiment failed to introduce sulphur as a variable and therefore all considerations with sulphur as a variable either by itself or as a secondary element will not be dealt with.

Nevertheless, from the results it can be seen that nickel when present on its own leads to extensive metal/scale entanglement but has no effect on internal oxidation. The addition of manganese to a steel containing nickel increases the depth of metal/scale entanglement and also introduces internal oxidation.

Manganese on its own has no effect on metal/scale entanglement but leads to the presence of internal oxidation. The addition of nickel decreases the extent of internal oxidation and introduces metal/scale entanglement.

2. High Carbon Steels

Similar effects of Ni and Mn were noted in the steels containing carbon additions as for the low carbon series discussed above. The effect of each element was greater in the high carbon series with more extensive metal/scale entanglements and internal oxidation being produced with similar levels of nickel and manganese.

(a) Metal/Scale Entanglement

Sulphur had no effect on the depth of metal/scale entanglement by itself of in the presence of manganese. In the presence of nickel, metal/scale entanglement was increased by the addition of sulphur. In the presence of both manganese and nickel the effect of sulphur was less marked.

Manganese had no effect on the extent of metal/scale entanglement by itself or in the presence of sulphur. A slight increase was observed in the presence of nickel and a slight decrease in the presence of both nickel and sulphur. Nickel produced extensive entanglement on its own, and the extent of entanglement increased markedly in the presenceof sulphur. There was also a slight increase in entanglement with nickel and manganese present but the effect of nickel and sulphur and manganese was slightly less that the effect of nickel and sulphur together.

(b) Internal Oxidation

Sulphur had no effect on internal oxidation on its own or in the presence of nickel. In the presence of manganese the depth of internal oxidation was increased by the addition of sulphur and in the presence of both nickel and manganese the extent of internal oxidation was decreased by the addition of sulphur. Manganese produced internal oxidation on its own. The effect was reduced in the presenceof nickel and sulphur but increased by the presence of both nickel and sulphur. The very rough interface produced by the presence of nickel and sulphur, however, made measurement of the depth of internal oxidation difficult. Nickel had no effect on internal oxidation on its own or in the presence of sulphur. With manganese present, nickel reduced the extent of internal oxidation and with both manganese and sulphur present nickel increased the extent of internal oxidation.

A5 TABLE 1 RESULTS OF FACTORIAL EXPERIMENT

Condition	Material	Atmosphere	Depth of Penetration (mm at x 500)			
			Metal/Scale Entanglement		Internal Oxidation	
			Low Carbon	High Carbon	Low Carbon	High Carbon
1	Base cast	Nil SO_2	Nil	Nil	Nil	Nil
2		Plus SO_2	Nil	Nil	Nil	Nil
3	Base plus 1% Ni	Nil SO_2	35	48	Nil	Nil
4		Plus SO_2	39	103	Nil	Nil
5	Base plus 1% Mn	Nil SO_2	Nil	Nil	40	43
6		Plus SO_2	Nil	Nil	37	38
7	Base plus 1% Ni, 1% Mn	Nil SO_2	50	56	30	20
8		Plus SO_2	45	97	20	55

A5 TABLE 2 ANALYSIS OF FACTORIAL EXPERIMENTS

Calculation	Effect of Element	In Presence of Element/s	Metal/Scale Entanglement		Internal Oxidation	
			Low Carbon	High Carbon	Low Carbon	High Carbon
2-1	S	-	0	0	0	0
3-1	Ni	-	+35	+48	0	0
5-1	Mn	-	0	0	+40	+43
4-1	Ni + S	-	+39	+103	0	0
6-1	Mn + S	-	0	0	+37	+38
7-1	Mn + Ni	-	+50	+56	+30	+20
8-1	Mn + Ni + S	-	+45	+97	+20	+55
4-3	S	Ni	+4	+55	0	0
6-5	S	Mn	0	0	-3	-5
8-7	S	Ni + Mn	-5	+41	-10	+35
4-2	Ni	S	+39	+103	0	0
7-5	Ni	Mn	+50	+56	-10	-23
8-6	Ni	S + Mn	+45	+97	-17	+17
7-3	Mn	Ni	+15	+8	+30	+20
6-2	Mn	S	0	0	+37	+38
8-4	Mn	Ni + S	+6	-6	+20	+55
8-2	Mn + Ni	S	+45	+97	+20	+55
8-5	Ni + S	Mn	+45	+97	-20	+12